PHYS

Volume 62

THE PHYSICAL REVIEW

A journal of experimental and theoretical physics established by E. L. Nichols in 1893

Published by the American Institute of Physics
for the
AMERICAN PHYSICAL SOCIETY

Officers

President

C. C. LAURITSEN
California Institute of Technology
Pasadena, California

Vice-President

J. H. VAN VLECK
Harvard University
Cambridge, Massachusetts

Secretary

K. K. DARROW
Bell Telephone Laboratories
Office:
Columbia University
New York 27, New York

Treasurer

G. B. PEGRAM
Columbia University
New York 27, New York

Local Secretary
for the Pacific Coast

J. KAPLAN
University of California at Los Angeles
Los Angeles, California

Managing Editor

S. A. GOUDSMIT
Brookhaven National Laboratory
Upton, Long Island
New York

BOARD OF EDITORS

Editor

S. A. GOUDSMIT

Assistant Editor

S. PASTERNACK

Associate Editors

J. BARDEEN — HARVEY BROOKS — M. GOLDHABER
T. BONNER — R. F. CHRISTY — E. HOFSTADTER
R. G. HERB — C. L. CRITCHFIELD — A. W. LAWSON
W. E. LAMB, JR. — M. DEUTSCH — A. PAIS
A. J. F. SIEGERT — T. H. JOHNSON — R. SERBER
W. E. STEPHENS — BRUNO ROSSI — C. H. TOWNES

Manuscripts for publication should be submitted to S. A. Goudsmit, Brookhaven National Laboratory, Upton, Long Island, New York. The authors' institutions are requested to pay a publication charge of $8 per page which, if honored, entitles them to 100 free reprints. Instructions will be sent with galley proofs.

Proof and all correspondence concerning papers in the process of publication should be addressed to the Publication Manager, American Institute of Physics, 57 East 55 Street, New York 22, New York.

Subscription Price

United States and Canada $25.00
Elsewhere $27.00

Back Numbers[1]

Yearly back number rate when complete year is available:
Prior to 1949: $20.00
Thereafter: $27.00
Single copies: $2.00 each, prior to July, 1929;
$1.00 each, July, 1929–December, 1941;
$2.00 each, January, 1942–December, 1946;
$1.00 each, January, 1947–December, 1948;
$1.25 each, thereafter.
General Index, 1893–1920: $4.00.

Subscriptions, renewals, and orders for back numbers should be addressed to the American Institute of Physics, 57 East 55 Street, New York 22, New York.

Changes of address in the case of members of the American Physical Society should be addressed to the Treasurer; in the case of other subscribers to the American Institute of Physics.

[1] For Series I Inquire of Physics Department, Cornell University, Ithaca, New York.

The Physical Review is published semi-monthly at Prince and Lemon Streets, Lancaster, Pennsylvania.

Entered as second-class matter March 6, 1947, at the Post Office at Lancaster, Pennsylvania, under the Act of March 3, 1879.

Acceptance for mailing at special rate of postage provided for in paragraph (d-2), section 34.40, P. L. & R. of 1948, authorized January

THE
PHYSICAL REVIEW

A journal of experimental and theoretical physics established by E. L. Nichols in 1893

SECOND SERIES, VOL. 82, NO. 4 MAY 15, 1951

Angular Yield of Protons, Tritons, and Alphas from the Deuteron Bombardment of Beryllium

I. RESNICK* AND S. S. HANNA
Department of Physics, The Johns Hopkins University, Baltimore, Maryland†
(Received January 15, 1951)

The photographic target chamber incorporating limited magnetic deflection of product particles, which was used to investigate the beryllium plus proton reactions, has been applied to the beryllium plus deuteron reactions. Angular yields of the long and the short range protons, the tritons, and the unresolved alphas were obtained at bombarding energies below 1 Mev. Most of the distributions are fairly complex and energy dependent. The 90° yield of the long range protons increases rapidly with energy up to 900 kev, except for an anomaly at 700 kev. Tritons having a continuous distribution in energy, resulting from the three-particle disintegration $Be^9(d,t)2\alpha$, were observed. Range measurements on the mono-energetic triton group give a $Q=4.61\pm0.04$ Mev for the $Be^9(d,t)Be^8$ reaction.

I. INTRODUCTION

THE bombardment of beryllium by deuterons in the low energy region is of interest in that the compound nucleus formed disintegrates in a relatively large number of ways:[1]

$Be^9(d,p)Be^{10}$, Be^{10*}	$Q=4.58$, 1.20 Mev
$Be^9(d,t)Be^8$	$Q=4.59$ Mev
$Be^9(d,\alpha)Li^7$, Li^{7*}	$Q=7.15$, 6.67 Mev
$Be^9(d,n)B^{10}$, B^{10*}, ⋯	$Q=4.31$, 3.60, ⋯ Mev
$Be^9(d,t)2\alpha$	$Q=4.68$ Mev.

The present investigation is part of a study of the angular distributions of these reaction products. The nature of these distributions should reveal properties of the participating states of the compound nucleus. It is noteworthy also that in at least three cases the final nucleus may be left in one of its excited states. The angular distributions of this investigation do not directly give information on these states, but it is possible that a careful comparison of the behavior of the long and short range particles, leading, respectively, to the ground and excited states of a nucleus, might uncover pertinent differences between the states. A more direct approach to the problem of the excited states of a residual nucleus is the study of the radiation that is emitted. Such an investigation will be aided, however, by a knowledge of the behavior of the reaction as a whole.

II. METHOD AND PROCEDURE

The photographic method, which was described in connection with the investigation of the proton bombardment of beryllium,[2] is ideally suited to the study of both ranges of protons and the tritons in this experiment. The photographic plate easily resolves these groups of particles from each other and from the other particles of the reaction by the difference in their ranges in the emulsion. Because of the great variety of particles, including the scattered deuterons, however, it is highly desirable, if not essential, actually to separate the groups from each other on the plate. This is accomplished by means of the limited magnetic deflection which is provided in the method. Particles from the target are collimated into narrow beams as they pass through seven radial gaps in a semicircular ring of iron mounted within the target chamber. The internal iron constitutes the yoke of an external electromagnet which produces a magnetic field in the particle gaps. After deflection in the magnetic field, the particles are recorded on the photographic plates mounted in the vacuum behind each gap.

* Now at Columbia University, New York, New York.
† Assisted by a contract with the AEC.
[1] Oliphant, Kempton, and Rutherford, Proc. Roy. Soc. (London) A150, 241 (1935); Lattes, Fowler, and Cuer, Proc. Phys. Soc. (London) 59, 883 (1947); Williams, Haxby, and Shepherd, Phys. Rev. 52, 1031 (1937); E. R. Graves, Phys. Rev. 57, 855 (1940); T. W. Bonner and G. Brubaker, Phys. Rev. 50, 308 (1936).
[2] Neuendorffer, Inglis, and Hanna, Phys. Rev. 82, 75 (1951).

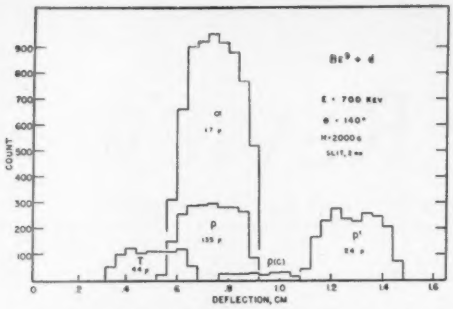

FIG. 1. Typical plate analysis, showing number of particles of each type per microscope swath *vs* deflection along plate. Approximate range in emulsion for each group is recorded.

The experimental detail was similar to that described in reference 2. The Be foil,[3] used as a target for most of the work, was 30 micro-inches thick. The plate emulsions were 100 microns thick. As this was one of the first experiments performed with the apparatus, care was taken to insure satisfactory alignment. The arrangement in the target chamber was adjusted by optical means, and the final alignment tested by exposing plates to the scattering of a beam of protons by a silver foil. A comparison of the results with the Rutherford scattering law showed that the alignment was satisfactory within the statistics of the experiment.

Plates exposed to the bombardment of beryllium by a beam of deuterons were obtained for several deuteron energies. The magnetic spectrum of the reaction is spread lengthwise along each plate, particles having a given momentum and charge appearing in a rather well-defined rectangular area at the appropriate place in the spectrum. The plates were counted in a microscope using a swath method. A record was made of the number of tracks passing a fiducial line in the eyepiece

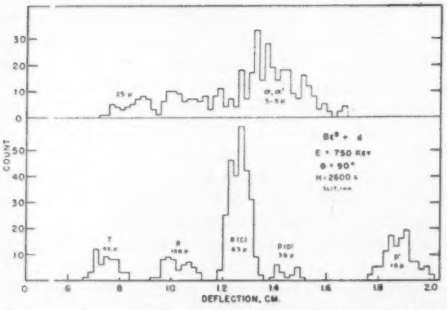

FIG. 2. Plate analysis with apparatus modified to give higher resolution. Background tracks and the alpha-groups are plotted separately from the well resolved groups.

[3] These foils were generously supplied to us by Dr. Hugh Bradner of the University of California at Berkeley.

of the microscope as the photographic plate was moved along. The plates were first scanned lengthwise, and the number of tracks in each swath was tabulated. An inspection of these numbers enabled one to select a region of constant particle density across the plate. The plates were then scanned systematically in a transverse direction, the length of each swath being such as to keep within the region of constant density. These data were tabulated (and plotted), and only those swaths which obviously were part of a plateau were used to compute the final yield for each group of product

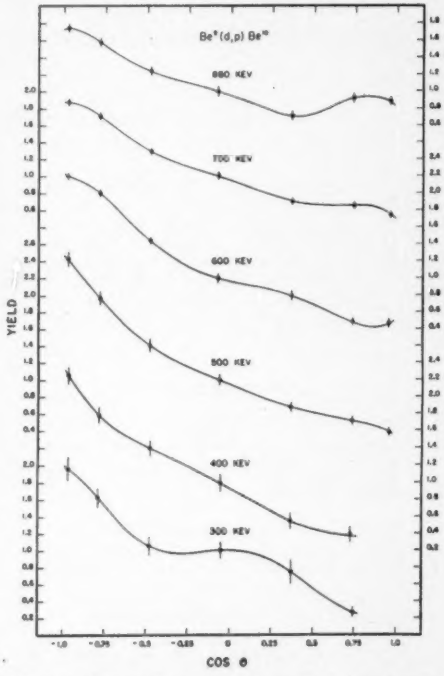

FIG. 3. Angular distributions in the center-of-mass system of the reaction $Be^9(d,p)Be^{10}$. Yields are normalized to unity at the 90° angle of the laboratory system. The curves are sixth-power polynomials having the coefficients given in Table I.

particles. To illustrate the method Figs. 1 and 2 are presented, showing results from two runs under different conditions.

A plate analysis of this type was made at each angle and energy. The number of particles per unit area of plate was computed for each particle group, and these data were used to compute the angular distributions in the center-of-mass coordinate system. Included in the results were small geometrical factors, which corrected for irregularities in the plate distance and inclination in the target chamber. The results are presented in Figs. 3–7.

III. DISCUSSION

In Fig. 1, which is representative of most of the runs, it is apparent that the two ranges of alpha-particles were not resolved. The curves in Fig. 6, therefore, give the total alpha-yields, and, for reasons that appear below, are somewhat approximate. An effort to separate the alpha-groups was made in the run illustrated in Fig. 2. The collimating slits were narrowed considerably, a higher magnetic field was used, and 0.2 mil of nickel foil was interposed between the target and the magnetic field. The foil served to decrease the alpha-energies from 4.85 and 4.55 Mev to approximately 2.0 and 1.5 Mev, respectively. It is seen that for the triton group and the various proton groups, shown in the lower part of Fig. 2, the plateaus are about four or five microscope swaths wide. The alpha-groups, plotted in the upper part of Fig. 2, cover a region about twice this wide. However, the resolution is not such as to make a yield determination reliable. Further refinement would have improved the situation were it not for the heavy background of tracks on both sides of, and presumably throughout, the alpha-groups. The background tracks were indistinguishable from the alphas, for the most part, and for this reason further attempts to obtain the angular yields of the separated alphas with this method were abandoned.

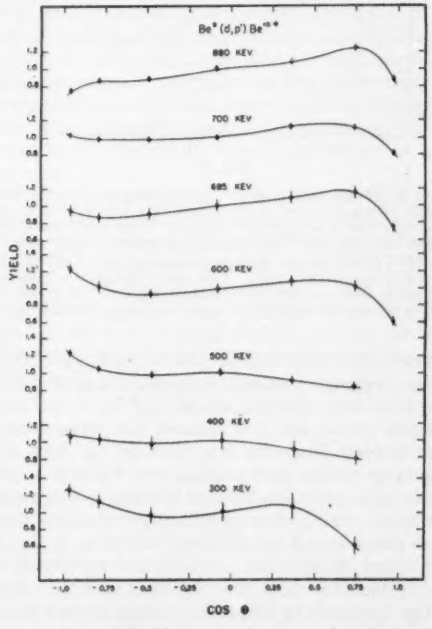

FIG. 4. Angular distributions in the center-of-mass system of the reaction $Be^9(d,p)Be^{10*}$. Yields are normalized to unity at the 90° angle of the laboratory system. The curves are sixth-power polynomials having the coefficients given in Table I.

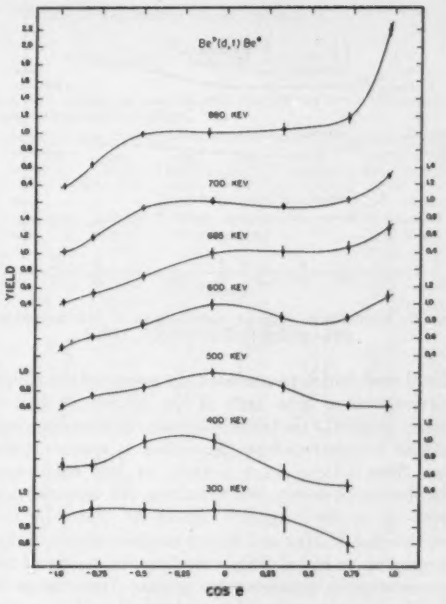

FIG. 5. Angular distributions in the center-of-mass system of the reaction $Be^9(d,t)Be^8$. Yields are normalized to unity at the 90° angle of the laboratory system. The curves are sixth-power polynomials having the coefficients given in Table I.

The background tracks were observed also on the plates exposed without a foil between the target and the deflecting field, but, in general, they were not counted and so were not recorded in Fig. 1. That these particles come from the beryllium plus deuteron reaction and not from some contaminant was established by using a beryllium target prepared in this laboratory in addition to the foils obtained from H. Bradner. The yield of the background particles relative to the yields of other particles was independent of the target used. In addition, all possible contaminants which could have given particles in this region were eliminated by searching for reaction products which the contaminants would have produced had they been present. The range of these particles excludes the possibility that they are protons or deuterons. They cannot be alphas from the beryllium plus deuteron reaction either, since many of them fall on the high energy side of the long range alpha-group. Their range and also their reduction in range on traversing matter indicates that they are tritons.

An extensive range analysis of these background tritons, summarized in Fig. 8, gave evidence of some group structure, but the results were not very reproducible. Furthermore, very little evidence of structure is to be seen in the spectrum of the particles to the left of the alphas in the upper part of Fig. 2. The absorbing

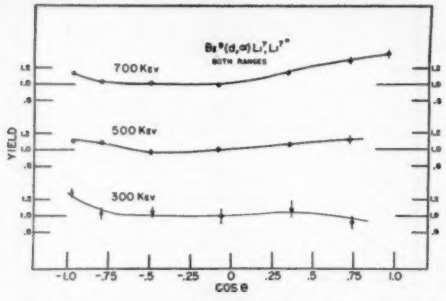

FIG. 6. Approximate angular distributions of the unresolved alpha-groups from $Be^9(d,\alpha)Li^7$, Li^{7*}.

Ni foil used in this run reduced the energy of the alphas relatively more than that of the tritons, so that a greater portion of the triton spectrum could be examined without interference from the alphas. It appears, then, that these tritons have a more or less continuous distribution in energy and arise from the three-particle break-up[4] of the compound nucleus B^{11}. The Q for this reaction is 4.68 Mev and should produce tritons having energies up to and slightly exceeding the energy of the mono-energetic ground-state group. The curves in Fig. 8 are a composite of five plates at various angles and bombarding energy, and the magnetic deflections which were analyzed span the plateau of the ground state triton group. It is interesting to note that the range (energy) of the ground-state tritons remains ostensibly constant throughout the plateau, but that the range of the background tritons decreases with increasing magnetic deflection and finally blends into the strong alpha-particle group (only a portion of which was counted). The apparent increase in intensity of the background tritons, as their energy decreases, can be attributed in large measure to the low resolution of the apparatus. From the accumulated range measurements of the ground-state triton group, we have calculated a Q value for the reaction. The weighted average of six determinations at different angles and energies gives $Q=4.61\pm0.04$ Mev, which agrees with the value of $Q=4.59$ Mev computed from the masses given by Tollestrup, Fowler, and Lauritsen.[5]

The presence of the continuous tritons made it necessary to use care in counting the ground-state tritons. As can be seen from Fig. 8, it was possible to separate them fairly well by their range, at least in the region where the background intensity is appreciable. A suitable range criterion was adopted for accepting or rejecting tracks, and it is believed that serious errors were avoided. However, as a check on the work, the long range tritons (and protons) were counted on the plates taken with the apparatus modified to give higher resolution. The proton distributions obtained from these plates agreed satisfactorily with those in Fig. 3. The triton distributions, however, are reproduced in Fig. 7, since they show some departure from the curves of Fig. 5, notably in the greater increase in yield in the forward direction.

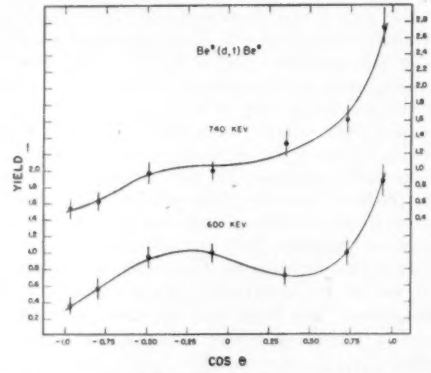

FIG. 7. Angular distributions of the tritons obtained with higher resolution but with greater statistical uncertainty.

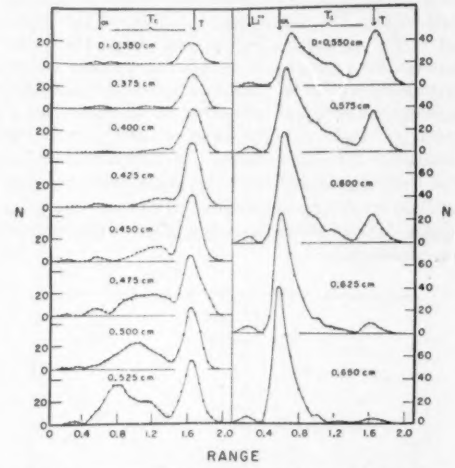

FIG. 8. Range analysis of the ground-state tritons, the continuous tritons, and part of the alphas from Be^9+d. The curves are a composite of five plates at different angles and bombarding energy. The ordinate N represents the number of tracks counted in a small range interval having the average range indicated by the abscissas (arbitrary units). Each curve represents a complete microscope swath at the given plate deflection. The arrows at the top indicate the computed range of the various groups.

[4] The alpha-particles resulting from the three-particle disintegration were observed recently in this laboratory by D. R. Inglis, Phys. Rev. 78, 104 (1950), and their magnetic spectrum has subsequently been studied by R. W. Gelinas and S. S. Hanna, Phys. Rev. 82, 298 (1951).

[5] Tollestrup, Fowler, and Lauritsen, Phys. Rev. 78, 372 (1950).

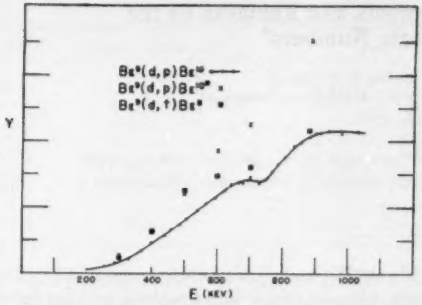

FIG. 9. Energy dependence of the 90° yield of $Be^9(d,p)Be^{10}$, measured with a proportional counter. Also shown are the relative yields of short range protons and tritons, obtained from the photographic plates used in observing the angular yields.

Some effort was made in this work to identify and count particles arising from impurities on the target. The usual proton groups from oxygen and carbon are seen in Fig. 2. The long range oxygen protons were counted on all the plates used in obtaining the angular distributions. This was done in order to obtain an estimate of the number of short range oxygen protons which might have contributed to the measured yield of the short range beryllium protons, since the former could not be distinguished from the latter in the present apparatus. The yields and angular distributions of the oxygen proton groups have not been measured completely in this energy range, and the estimate of the short range yield was based on the observations of Heydenburg and Inglis[6] at somewhat different energies. The estimated contamination is negligible at the low energies and rises to at most 5 percent at the high energies.

The yield measurements obtained with the photographic chamber do not conveniently give the variation of yield with energy for these reactions. The excitation curve for the long range protons, shown in Fig. 9, was obtained with a proportional counter. The yield increases rapidly with increasing energy up to about 900 kev and shows an anomaly at about 700 kev. Because of the very low yield of these reactions at the lower energies, the angular yields measured at 300 and 400 kev were not obtained with high statistical accuracy and are included in the results chiefly to indicate the major trends.

[6] N. P. Heydenburg and D. R. Inglis, Phys. Rev. **73**, 230 (1948).

TABLE I. Coefficients in the expansion

$$Y(\cos\theta) = Y(0)\left(1+\sum_{n=1}^{6} A_n \cos^n\theta\right)$$

for both ranges of protons and the tritons from the deuteron bombardment of beryllium.

	300 (kev)	400 (kev)	500 (kev)	600 (kev)	685 (kev)	700 (kev)	880 (kev)
				Long range protons			
A_1	−0.08	−1.18	−0.83	−0.45		−0.70	−0.80
A_2	−1.33	−0.26	0.07	0.54		−0.28	−0.49
A_3	−1.94	0.92	0.19	−1.73		0.06	1.24
A_4	2.99	1.11	1.17	−0.28		2.11	3.28
A_5	1.05	−0.89	−0.12	1.29		−0.07	−0.91
A_6	−1.70	−0.52	−0.77	0.15		−1.61	−2.50
				Short range protons			
A_1	0.38	−0.11	−0.14	0.18	0.16	0.21	0.18
A_2	−0.12	−0.61	−0.51	0.04	−0.02	0.33	−0.35
A_3	−1.75	−0.02	0.22	0.04	0.52	−0.09	0.47
A_4	−0.66	1.22	0.91	−0.05	0.27	−0.64	1.67
A_5	0.84	−0.09	−0.33	−0.62	−0.86	−0.28	−0.62
A_6	0.49	−0.80	−0.38	−0.11	−0.48	0.18	−1.65
				Tritons			
A_1	−0.07	−0.86	−0.10	−0.10	0.25	−0.21	0.03
A_2	−0.46	−0.89	−1.32	−1.53	−0.89	−0.01	0.59
A_3	−0.67	1.82	−0.08	0.45	0.09	1.03	−0.14
A_4	0.33	0.43	1.94	2.82	1.21	−0.92	−2.51
A_5	0.48	−1.17	0.19	−0.00	0.14	−0.33	1.20
A_6	−0.23	0.08	−1.04	−1.52	−0.47	0.87	2.44

The angular distributions have been analyzed into polynomials in $\cos\theta$ up to the sixth power. The coefficients are given in Table I. An inspection of these coefficients shows that the angular distributions of the beryllium plus deuteron reactions are fairly complex, even at low energies. It is possible, of course, that a less complex (smaller powers of $\cos\theta$) analysis might provide a more satisfactory description of the data. Nevertheless, the coefficients are expected still to be large and to show considerable structure in their energy dependence.

We wish to thank Dr. D. R. Inglis for many helpful discussions, and Mr. F. W. Lipps for assistance with some of the calculations.

Some New Atomic Mass Measurements and Remarks on the Mass Evidence for Magic Numbers*

HENRY E. DUCKWORTH AND RICHARD S. PRESTON†
Scott Laboratory of Physics, Wesleyan University, Middletown, Connecticut
(Received November 2, 1950)‡

New mass measurements are given for the nuclei Ti^{48}, Sr^{86}, Sr^{88}, Mo^{98}, Sn^{117}, Sn^{120}, Pt^{194}, Pt^{196}, and Pb^{208}. The evidence given for the theory of magic numbers in nuclear structure by nuclear mass measurements is discussed.

INTRODUCTION

MASS spectrographic mass measurements made in this laboratory have been extended to include Ti^{48}, Sr^{86}, Sr^{88}, Mo^{98}, Sn^{117}, Sn^{120}, Pt^{194}, Pt^{196}, and Pb^{208}. These measurements are briefly described below.

I. Ti^{48}

With a spark between two titanium electrodes, doublets were photographed at mass 16, formed by singly-charged O^{16} and triply-charged Ti^{48}. From nine doublets, the packing fraction of Ti^{48} is $f=-7.49\pm0.04$. In this measurement the mass scale was provided by the $Ti^{47}-Ti^{48}$ separation, which is assumed to be 0.99711 ±0.00043, the value recently obtained by Harvey.[1] Previous measurements of the Ti^{48} packing fraction have been -6.99 ± 0.15 (Aston, 1938),[2] -7.22 ± 0.1 (Dempster, 1938),[3] -7.64 ± 0.10 (Okuda and Ogata, 1941),[4] and -7.60 ± 0.07 (Duckworth, 1942).[5]

II. MASSES OF Sr^{86} AND Sr^{88}

With a spark between a platinum electrode and an electrode consisting of a nickel tube packed with strontium chloride, doublets were photographed at mass 44, formed by singly-charged CO_2 and doubly-charged Sr^{88}. At the same time triplets were photographed at mass 43, formed by singly-charged C_3H_7 and C_2OH_3 and doubly-charged Sr^{86}. From four photographs of the CO_2-Sr^{88} doublet, the packing fraction difference is $\delta f=8.41\pm0.04$. From six photographs, the $C_3H_7-Sr^{86}$ packing fraction difference is $\delta f=23.48$ ±0.06, while from two photographs, the value for $C_2OH_3-Sr^{86}$ of $\delta f=14.89\pm0.09$. In all cases, the $Sr^{86}-Sr^{88}$ separation, assumed to be integral, served as the mass scale. Using Bainbridge's recommended values[6] for the masses of C^{12} and H^1, the packing fractions of CO_2, C_3H_7 and C_2OH_3 are computed to be 0.88 ± 0.01, 15.92 ± 0.015, and 7.46 ± 0.015, respectively. These values, when combined with the above packing fraction differences, give the packing fraction of Sr^{88} as $f=-7.53\pm0.05$, and that of Sr^{86} as $f=-7.56\pm0.06$, from the $C_3H_7-Sr^{86}$ comparison, and $f=-7.43\pm0.09$, from the $C_2OH_3-Sr^{86}$ comparison. The packing fraction of Sr^{88} has not been measured previously; the only previous measurement of Sr^{86} was made by Mattauch[7] in 1937 who obtained, from measurement of the $Si^{29}F_3-Sr^{86}$ doublet, the preliminary value of -9.1 ± 0.40.

III. MASSES OF Sn^{117} AND Sn^{120}

With a spark between a tin electrode and a platinum electrode, the $C_3H_3-Sn^{117}$ doublet was photographed at mass 39. From six photographs, the $C_3H_3-Sn^{117}$ packing fraction difference is $\delta f=14.17\pm0.04$. This result, combined with a packing fraction for C_3H_3 of 9.22 ± 0.015, gives, for Sn^{117}, the value of $f=-4.95$ ±0.04. No previous measurement has been made of the mass of this nuclide.

The $Ni^{60}-Sn^{120}$, $Ni^{61}-Sn^{122}$, and $Ni^{62}-Sn^{124}$ doublets were photographed at masses 60, 61, and 62, using a spark between a nickel and a tin electrode. From twelve photographs, the $Sn^{120}-Ni^{60}$ packing fraction difference is $\delta f=3.61\pm0.03$. This result, combined with a previous value[8] for Ni^{60} of $f=-8.60\pm0.05$, gives, for Sn^{120}, $f=-4.99\pm0.06$. From one photograph of the $Sn^{122}-Ni^{61}$ doublet, $\delta f=3.71\pm0.10$, and from four photographs of the $Sn^{124}-Ni^{62}$ doublet, $\delta f=4.23\pm0.05$.

On many of the plates on which the $Ni^{60}-Sn^{120}$ doublets were photographed, good $Ni^{58}-Sn^{116}$ doublets were present. From nine photographs, the $Sn^{116}-Ni^{58}$ packing fraction difference is $\delta f=2.76\pm0.02$. This doublet had been studied previously in this laboratory at which time the packing fraction difference was found[9] to be $\delta f=2.66\pm0.01$. Since the reason for this discrepancy is not known, the value of 2.71 ± 0.05 will be used in recomputing the mass of Sn^{116}.

IV. MASSES OF Mo^{98}, Pt^{194}, AND Pt^{196}

With one electrode of platinum and the other of molybdenum, the $Pt^{194}-Mo^{97}$ and $Pt^{196}-Mo^{98}$ doublets

* This paper is based on work performed at Wesleyan University under contract with the AEC.
† Now in the United States Navy.
‡ Revised manuscript received January 12, 1951.
[1] J. A. Harvey, Phys. Rev. **81**, 353 (1951).
[2] F. W. Aston, Nature **141**, 1096 (1938).
[3] A. J. Dempster, Phys. Rev. **53**, 64 (1938).
[4] T. Okuda and K. Ogata, Phys. Rev. **60**, 690 (1941).
[5] H. E. Duckworth Phys,. Rev. **62**, 19 (1942).
[6] K. T. Bainbridge, *Isotopic Weights of the Fundamental Isotopes* (National Research Council, June, 1948), Preliminary Report No. 1.
[7] J. Mattauch, Naturwiss. **25**, 170 (1937).
[8] Duckworth, Preston, and Woodcock, Phys. Rev. **79**, 188 (1950).
[9] H. E. Duckworth and R. S. Preston, Phys. Rev. **79**, 402 (1950).

TABLE I. New mass values.

Nuclide	Packing fraction $\times 10^4$	Mass
Ti^{48}	-7.49 ± 0.04	47.96405 ± 0.00019
Sr^{86}	-7.52 ± 0.05	85.93533 ± 0.00043
Sr^{88}	-7.53 ± 0.06	87.93374 ± 0.00053
Mo^{98}	-6.52 ± 0.04	97.93610 ± 0.00040
Sn^{116}	-5.30 ± 0.06	115.93852 ± 0.00070
Sn^{117}	-4.95 ± 0.04	116.94208 ± 0.00047
Sn^{120}	-4.99 ± 0.06	119.94012 ± 0.00072
Pt^{194}	1.32 ± 0.07	$194.0256\ \pm0.0014$
Pt^{196}	1.40 ± 0.03	196.02744 ± 0.00060
Pb^{208}	2.03 ± 0.07	$208.0422\ \pm0.0015$

were photographed at mass numbers 97 and 98. From nine doublets, the $Pt^{194}-Mo^{97}$ packing fraction difference is $\delta f=7.78\pm0.02$, and from a similar number of $Pt^{196}-Mo^{98}$ doublets, $\delta f=7.92\pm0.03$. These doublets were measured by Dempster who found packing fraction differences of 7.7 ± 0.2 and 7.68 ± 0.2, respectively.[10] The $Mo^{97}(\gamma,n)Mo^{96}$ threshold has been measured by Hanson *et al.*[11] and found to be 7.10 ± 0.30 Mev. This result can be combined with a previously reported[8] mass value for Mo^{96} to obtain for Mo^{97} a packing fraction $f=-6.46\pm0.06$. The packing fraction of Pt^{194} can then be computed, from the above result, to be $f=+1.32\pm0.07$.

Harvey has found, from a study of the $Pt^{194}(d,p)Pt^{195}$ and $Pt^{195}(d,p)Pt^{196}$ reactions, that the $Pt^{195}-Pt^{194}$ and $Pt^{196}-Pt^{195}$ mass differences are 1.00239 ± 0.00021 and 1.00038 ± 0.00021, respectively.[1] These mass differences can be used, together with the above packing fraction for Pt^{194} and a previously reported one[12] for Pt^{195}, to deduce two independent values for the packing fraction of Pt^{196}. These are $f=+1.45\pm0.07$ and $f=+1.37\pm0.04$, respectively. Adopting a value for the packing fraction of Pt^{196} of $f=1.40\pm0.03$, one can compute, from the above $Pt^{196}-Mo^{98}$ result, that of Mo^{98} to be $f=-6.52\pm0.04$.

V. MASS OF Pb^{208}

With one palladium electrode and one lead electrode, the $Pb^{208}-Pd^{104}$ doublet was photographed at mass 104 with exposure times of 30 to 60 sec. The $Pd^{104}-Pd^{106}$ separation, assumed to be integral, was used as the mass scale. Measurements of seven doublets give $\delta f=8.15\pm0.04$. This result, combined with a previously reported[13] packing fraction for Pd^{104} of -6.12 ± 0.05, gives, for Pb^{208}, $f=2.03\pm0.07$. This doublet was studied previously by Dempster,[10] who found $\delta f=7.96\pm0.15$.

VI. SUMMARY OF RESULTS

These new mass values have been collected in Table I.

VII. DISCUSSION OF RESULTS

These mass values, plus some which have been reported earlier and others which can be computed from the mass spectrographic values by means of transmutation data,[12a] give some information concerning the effect on the atomic mass of some of the magic numbers. For this purpose, they are plotted in Fig. 1 on a packing fraction curve.

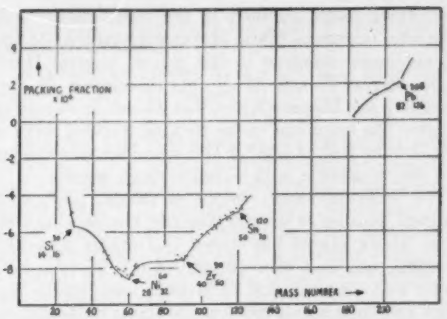

FIG. 1. A packing fraction curve representing recent atomic mass measurements.

It can be seen in Fig. 1 that there is a pronounced break in the packing fraction curve in the region of mass 90; this almost certainly marks the completion of the 50-neutron shell. It is likely that the break is located at $_{40}Zr^{90}$ and may indicate that the 40-proton configuration is making a significant contribution to the stability of this nuclide. It will be recalled that each of the recently proposed single-particle nuclear energy level schemes[13–16] predicts that 40 will be a magic number, marking the completion of the $3p$ shell. If it be true that $_{40}Zr^{90}$ is thus doubly magic, this break in the packing fraction curve corresponds to the well-known break occurring at the position of another doubly-magic nuclide, namely $_{82}Pb^{208}$.

In the 50 proton region, the packing fraction curve shows a slightly decreasing slope which may be testimony to the stabilizing influence of the 50-proton configuration. There is some evidence that the curve changes slope at $_{50}Sn^{120}$, a nuclide which is likely doubly magic according to the scheme of Maria Mayer, although not according to any of the others. Mention should also be made of $_{50}Sn^{114}$, $_{50}Sn^{116}$, and $_{50}Sn^{118}$, the first of which is doubly magic by the schemes of Mayer and Haxel *et al.*, the second of which is doubly magic by the scheme of Feenberg and is likely so according to Mayer, and the last of which is doubly magic according to the schemes of Nordheim and Haxel *et al.* The data in Fig. 1 suggest that $_{50}Sn^{116}$ possesses extra stability, that $_{50}Sn^{114}$ possibly does, but that $_{50}Sn^{118}$ does not.

The data shown in Fig. 1 may give some help in

[12a] The authors are grateful to Dr. B. B. Kinsey, Dr. J. A. Harvey, and to Dr. J. Halpern for making available to them prepublication data which were useful in computing many of the packing fractions plotted in Fig. 1.

[10] A. J. Dempster, Phys. Rev. **53**, 64 (1938).
[11] Hanson, Duffield, Knight, Diven, and Palevsky, Phys. Rev. **76**, 578 (1949).
[13] Duckworth, Woodcock, and Preston, Phys. Rev. **78**, 479 (1950).
[13] Maria Mayer, Phys. Rev. **75**, 1969 (1949); **78**, 17 (1950).
[14] E. Feenberg and K. C. Hammack, Phys. Rev. **75**, 1877 (1949).
[15] L. W. Nordheim, Phys. Rev. **75**, 1894 (1949).
[16] Haxel, Jensen, and Suess, Phys. Rev. **75**, 1766 (1949).

identifying magic numbers in the region $50<A<65$. The level scheme of Maria Mayer suggests that 28 and 32 are magic numbers in this region, whereas Haxel *et al.* suggest 28 and 34. Nordheim suggests 34, and Feenberg and Hammack hint that 32 and/or 34 may be magic. The minimum in the packing fraction curve in Fig. 1 is located at $_{28}Ni^{60}$.§ This coincides, according to the Mayer scheme, with a doubly-magic nuclide.

The heaviest stable isotope of silicon, $_{14}Si^{30}$, is of interest because of its exceptionally low packing fraction. Maria Mayer has shown that strong spin-orbit coupling can lead to a reversal of the $2s$, $3d_{5/2}$ level order with the result that 14 nucleons complete the $3d_{5/2}$ shell and constitute a particularly stable configuration. The 16-nucleon configuration, representing the completion of the $2s$ shell, should also be very stable. Thus, it may be that $_{14}Si^{30}$ owes its exceptional stability to a doubly-magic configuration. Its doubly-magic brother, $_{14}Si^{28}$, is somewhat less closely knit. The increase in stability resulting from an excess of neutrons over protons, which is so pronounced in the heavier nuclides, is presumably responsible for this difference.

It seems likely that additional mass measurements can be of considerable use in the identification of the ground states of nuclei, particularly in the case of even-even nuclei, where no information has so far been derived from spin measurements. In conclusion, one may venture to say that the mass evidence to date gives general support to the level scheme of Maria Mayer.

The authors wish to acknowledge the help of Karl S. Woodcock, Richard F. Woodcock, and Clifford Geiselbreth.

§ *Note added in proof.*—Some recent experiments suggest that Ni^{62} may mark the minimum of the packing fraction curve. These experiments are being continued.

PHYSICAL REVIEW VOLUME 82, NUMBER 4 MAY 15, 1951

Properties of Dirac Wave Functions in a Central Field*

M. E. ROSE
Oak Ridge National Laboratory, Oak Ridge, Tennessee

AND

R. R. NEWTON
Oak Ridge National Laboratory and Department of Physics, University of Tennessee, Knoxville, Tennessee

(Received August 7, 1950)†

The boundary conditions for a Dirac particle in a central scalar field are discussed for both bound and continuum states. In this development, the methods employed are considerably different from those customarily used for the corresponding nonrelativistic case.

I. INTRODUCTION

WHILE the Dirac wave functions for a particle in a central field possess properties which are, in many instances, qualitatively similar to those exhibited by the corresponding solutions to the Schroedinger problem, there are several essential differences which have apparently not been considered very completely or stated explicitly in previous investigations. An important point of difference is concerned with the boundary conditions which, in the relativistic and nonrelativistic problems, must be discussed quite independently. Intimately connected with the formulation of boundary conditions is the question of which potential functions are admissible from a physical point of view. Here, the radically different answer provided by the relativistic problem is, in part, traceable to the energy doubling (existence of positive and negative energy states) and, in part, arises from the spin properties. A third point of interest is the study of the nodal properties (oscillation theorems, etc.) in the case of bound states. Despite the fact that the Dirac equations do not form a Sturm-Liouville system, several of the theorems concerning nodal properties are applicable.

The following is devoted primarily to a discussion of the three aforementioned problems: (1) boundary conditions, (2) admissible potentials, and (3) nodal properties. In connection with the study of nodal properties, we have found it necessary to develop methods somewhat different from those generally used in the treatment of Sturm-Liouville systems. Since these methods are also applicable to such systems, they may be of interest for classes of problems other than the one discussed here (Sec. VII).

The desirability of such a study was encountered in our program for computation of L-shell internal conversion coefficients, which required extensive numerical calculation of Dirac wave functions in a central noncoulomb field.[1] Some considerations which may be

* This document is based on work performed for the AEC at the Oak Ridge National Laboratory.
† Revised manuscript received January 18, 1951.

[1] Rose, Goertzel, Spinrad, Harr, and Strong, Phys. Rev. **76**, 1883 (1949).

useful for the numerical calculation of wave functions are given below.

The wave functions for a Dirac electron in a central field are of two types (doubling caused by spin-orbital coupling).[2] Denoting the two types by indices by a and b, the four components of the wave function, for a given total angular momentum quantum number j and given magnetic quantum number m, can be written in the form

$$\begin{aligned}
(\psi_{a1}, \psi_{b1}) &= \left(\frac{|\kappa|-m+\tfrac{1}{2}}{2|\kappa|+1}\right)^{\frac{1}{2}} Y_{|\kappa|}^{m-\frac{1}{2}}(if_\kappa, g_\kappa),\\
(\psi_{a2}, \psi_{b2}) &= \left(\frac{|\kappa|+m+\tfrac{1}{2}}{2|\kappa|+1}\right)^{\frac{1}{2}} Y_{|\kappa|}^{m+\frac{1}{2}}(if_\kappa, g_\kappa),\\
(\psi_{a3}, \psi_{b3}) &= \left(\frac{|\kappa|+m-\tfrac{1}{2}}{2|\kappa|-1}\right)^{\frac{1}{2}} Y_{|\kappa|-1}^{m-\frac{1}{2}}(g_\kappa, if_\kappa),\\
(\psi_{a4}, \psi_{b4}) &= -\left(\frac{|\kappa|-m-\tfrac{1}{2}}{2|\kappa|-1}\right)^{\frac{1}{2}} Y_{|\kappa|-1}^{m+\frac{1}{2}}(g_\kappa, if_\kappa).
\end{aligned} \tag{1}$$

Here, Y_λ^μ is a (normalized) surface harmonic of degree λ, order μ, and f_κ and g_κ satisfy the differential equations

$$\begin{aligned}
d(rf)/dr &= \kappa f-(W-1-V)rg,\\
d(rg)/dr &= (W+1-V)rf-\kappa g.
\end{aligned} \tag{2}$$

For type a, $\kappa=-(j+\frac{1}{2})$, so that κ is a negative integer. For type b, $\kappa=j+\frac{1}{2}$, so κ is a positive integer. W is the total energy (including rest energy), and V the potential energy in units of mc^2; r is measured in units of $\hbar/mc$. We shall rewrite Eqs. (2) in the form

$$F'=\alpha_{11}F+\alpha_{12}G, \quad G'=\alpha_{21}F+\alpha_{22}G, \tag{2a}$$

where $F=rf$, $G=rg$, $\alpha_{11}=-\alpha_{22}=\kappa/r$, $\alpha_{12}=-(W-1-V)$, $\alpha_{21}=W+1-V$; and throughout a prime denotes differentiation with respect to r.

II. BOUNDARY CONDITIONS

The functions F and G are to be subject to the conditions that they be real and single-valued, and, in addition, for bound states

$$0<\int_a^b (F^2+G^2)dr<\infty, \quad 0\leqq a<b\leqq\infty. \tag{3a}$$

In addition, for both bound and continuum states, we require that

$$\lim_{r\to 0}(F_iG_k-F_kG_i)=0, \tag{3b}$$

where i and k each represents a triad of quantum numbers (W, κ, and m), denoting constants of the motion defining a stationary state in a central field. The radial functions are independent of m but do depend on W and κ.

Continuity and finiteness of F and G at all ordinary points of (2a) are assured if the functions satisfy Eq. (2a).

Condition (3a) is required by the probability interpretation of the wave function modulus. Condition (3b) is a consequence of the requirement that a linear superposition Ψ of stationary states satisfy the continuity equation, as the three-dimensional time-dependent wave equation demands. The continuity equation is fulfilled for Ψ if it is fulfilled for the mixed current-charge densities; that is, if

$$\operatorname{div}(\Psi_i^*\boldsymbol{\alpha}\Psi_k)+\partial(\Psi_i^*\Psi_k)/\partial t=0, \tag{4a}$$

since for $i=k$, Eq. (4a) is automatically satisfied. The contribution to the particle flux per unit solid angle from the mixed states is

$$r^2J_r^{(ik)}=Q_{ik}(\vartheta, \varphi)(F_iG_k-F_kG_i), \tag{4b}$$

where $J_r^{(ik)}$ is the radial component of $\Psi_i^*\boldsymbol{\alpha}\Psi_k$, and the angular dependent coefficients Q_{ik} are sums of terms involving products of spherical harmonics of, in general, different degree and order and are dependent on κ, m. If condition (3b) is not fulfilled, it follows that $J_r^{(ik)}\sim 1/r^2$, since, as will be shown below, $\lim(F_iG_k-F_kG_i)$ is always finite at the origin. Then $\mathbf{J}^{ik}\sim\operatorname{grad}1/r$, and $\operatorname{div}\mathbf{J}^{(ik)}\sim\delta(\mathbf{r})$, in contradiction to (4a).

We shall have use, in what follows, for the concept of left-handed and right-handed solutions (L and R solutions). By a left-handed solution of (2a), we mean one satisfying the conditions:

$$0<\int_0^b (F_L^2+G_L^2)dr<\infty, \quad b>0 \tag{5a}$$

$$\lim_{r\to 0}(F_iG_k-F_kG_i)=0, \tag{5b}$$

which are equivalent to Eq. (3) with the point at infinity excluded. By a right-handed solution, we mean one which fulfills the boundary condition

$$0<\int_a^\infty (F_R^2+G_R^2)dr<\infty, \quad 0<a<\infty, \tag{6a}$$

which is equivalent to Eq. (3) with the origin excluded. A bound state wave function, that is, one satisfying Eqs. (3a) and (3b), is both a right-handed and a left-handed solution (LR solution).

For continuum states, we still require Eqs. (5a) and (5b), and no boundary condition at infinity is necessary except for normalization purposes.

These boundary conditions are the necessary and sufficient conditions (along with Eq. (2a)) for the complete determination of the wave functions in the central field Dirac problem. In addition, Eq. (3b) restricts the choice of potential function on the basis of

[2] M. E. Rose, Phys. Rev. 51, 484 (1937). In this reference the subscripts on the functions f and g have a different meaning from that used here.

the behavior of $V(r)$ near the origin. We shall designate potentials for which Eq. (3b) is fulfilled as admissible. For such potentials, it will be seen that discrete eigenvalues are always finite. For potentials which are admissible, condition (3a) alone determines the eigenfunctions.

III. ADMISSIBLE POTENTIALS AND BEHAVIOR NEAR SINGULAR POINTS

(A) Behavior Near the Origin

Here and in the following, we shall find it helpful to use the phase function $\varphi(r)$ and the amplitude function $A(r)$, defined by[3]

$$F=A\sin\varphi, \quad G=A\cos\varphi. \tag{7}$$

From Eq. (2a), it is evident that F and G cannot vanish simultaneously at an interior point of the interval $(0-\infty)$. It follows, then, that A cannot vanish except at the end points. A cannot have any singularities except at the origin or at a point where V has a singularity. Substituting Eq. (7) into Eq. (2a), we obtain

$$A'/A=-(\kappa/r)\cos 2\varphi+\sin 2\varphi, \tag{8}$$

$$\varphi'=(\kappa/r)\sin 2\varphi-(W-V)+\cos 2\varphi. \tag{9}$$

Putting Eqs. (8) and (9) into integral form,

$$\ln A_1-\ln A_0=-\kappa\int_{r_0}^{r_1} r^{-1}\cos 2\varphi dr+\int_{r_0}^{r_1}\sin 2\varphi dr, \tag{10a}$$

$$\varphi_1-\varphi_0=\kappa\int_{r_0}^{r_1} r^{-1}\sin 2\varphi dr-W(r_1-r_0)+\int_{r_0}^{r_1} V dr+\int_{r_0}^{r_1}\cos 2\varphi dr, \tag{10b}$$

where r_1 is any interior point. In the following, we investigate the behavior of A_0 and φ_0 as their argument r_0 approaches zero.

We shall now consider two cases according to whether

$$\left|\lim_{r\to 0}(rV)\right|>1 \quad \text{or} \quad \leqslant 1.$$

This includes fields more strongly divergent than the coulomb field ($|\lim(rV)|=\infty$) and fields which are convergent or less strongly divergent than the coulomb field ($|\lim(rV)|=0$).

(1). $|\lim(rV)|>1$. If we allow r_0 to approach the origin, then in Eq. (10b) the integral $\int_0 V dr$ is a divergent term which cannot be cancelled, for *all* κ, by any other term on the right-hand side of Eq. (10b). Hence, φ becomes infinite at the origin, and F and G have an infinite number of nodes in any finite interval including the origin.

[3] H. Prüfer, Math. Annalen **95**, 499 (1926). For another application of the phase and amplitude functions in the Dirac equations, see G. Breit and G. E. Brown, Phys. Rev. **76**, 1307 (1949).

Now consider Eq. (10a). The dominant term on the right is

$$-\kappa\int_{r_0}^{r_1} r^{-1}\cos 2\varphi dr.$$

Without the $\cos 2\varphi$ factor, this would diverge as $r_0\to 0$, but the presence of the rapidly oscillating factor makes it converge.[4] Hence, $\ln A$ remains finite as $r\to 0$, and A remains finite and greater than zero.

It is now seen that $A(0)\neq 0$, and

$$\lim_{r\to 0}(F_iG_k-F_kG_i)=\lim_{r\to 0}A_iA_k\sin(\varphi_i-\varphi_k)$$

approaches a finite nonvanishing limit, since $\varphi_i-\varphi_k$ does approach a definite limit at the origin. Consequently, condition (3b) is violated. Therefore, potentials for which $|\lim(rV)|>1$ at the origin are inadmissible for all stationary as well as nonstationary states. This is in contrast to the statement made by Plesset[5] who, while noting the irregular singularity at the origin for $V(r)\sim r^{-\nu}$ (ν a positive integer>1), did not consider the flux boundary condition (3b) and, therefore, concluded that a stationary state continuum solution was admissible in this case.

(2). $|\lim(rV)|\leqslant 1$. We prove by construction that in all such cases there exists a solution of Eq. (2a) which satisfies the boundary conditions at the origin. The first and third integrals on the right-hand side of Eq. (10b) may now diverge individually as $r_0\to 0$. However, with $r_0=0$, it is now always possible to find a finite $\varphi_0=\varphi(0)$ such that the sum of these two terms and also, therefore, the right-hand side of (10b) converge and such that equation Eq. (10b) is satisfied. Thus, we set

$$\varphi=\varphi_0+\theta,$$

where θ is to vanish as r approaches zero. Then, in the neighborhood of the origin, with $\sin 2\theta\sim 2\theta$ and $\cos 2\theta\sim 1$, the required solution of Eq. (9) is

$$\theta=r^{-2\eta e^{-2r\sin 2\varphi_0}}\int_0^r r^{2\eta e^{2r\sin 2\varphi_0}}\times[V-W+\cos 2\varphi_0+(\kappa/r)\sin 2\varphi_0]dr. \tag{11}$$

In Eq. (11) $\eta=-\kappa\cos 2\varphi_0$, and we fix φ_0 (to within an additive integral multiple of π which is always arbitrary

[4] The convergence of the integral does not follow simply from the rapid oscillation of $\cos 2\varphi$, but its convergence, in this case, can be seen by changing the variable of integration,

$$\int_{r_0}^{r_1} r^{-1}\cos 2\varphi dr=\int_{\varphi_0}^{\varphi_1}(r d\varphi/dr)^{-1}\cos 2\varphi d\varphi,$$

where φ_0 is to approach infinity. Suppose $\lim rV$ is unbounded at the origin. Then, by Eq. (9) $r d\varphi/dr\sim rV$ and the integrand approaches zero so that the integral converges. The remaining possibility is $\infty>|\lim rV|=|\beta|>1$. In this case, the first term in Eq. (9) is of the same order as V. However, as is shown in paragraph (2) below, these terms can never cancel, for all κ, if $|\beta|>1$ and the integral is bounded.

[5] M. S. Plesset, Phys. Rev. **41**, 278 (1932).

by Eq. (2a)) by the conditions

$$\eta=-\kappa\cos2\varphi_0\geqslant 0, \tag{11a}$$

$$\kappa\sin2\varphi_0=-\lim_{r\to 0}(rV). \tag{11b}$$

n order that Eq. (11b) may be fulfilled for all κ, with real φ_0, the condition $|\lim(rV)|<1$ is necessary and sufficient. For definiteness, we take the principal value of φ_0 for L and LR solutions. Equation (11a) corresponds to the choice of the solution of Eq. (2a) which is regular at the origin, while (11b) is sufficient to make θ finite at $r=0$. The conditions (11a) and (11b) can always be fulfilled, for the present case, with real φ_0. For fields coulomb at $r=0$ (point charge and screened fields), $(V=-\beta/r)$, we obtain the well-known results

$$\sin2\varphi_0=\beta/\kappa,\quad \cos2\varphi_0=-\gamma/\kappa, \tag{11c}$$

with $\gamma=(\kappa^2-\beta^2)^{\frac{1}{2}}$ or $\tan\varphi_0=\beta/(\kappa-\gamma)$, while, for the case $|\lim(rV)|=0$, we find

$$\begin{aligned}&\varphi_0=\pi/2, && \kappa>0\\ &\varphi_0=0, && \kappa<0.\end{aligned} \tag{11d}$$

It is now clear that θ approaches zero at the origin. If $\eta=0$ (which occurs only for $|\lim(rV)|=1$, $|\kappa|=1$), the result is obvious. For $\eta\neq 0$, θ is indeterminate at the origin, and by l'Hôspital's rule,

$$\theta\to r[V-W+\cos2\varphi_0+(\kappa/r)\sin2\varphi_0]/2\eta, \tag{11e}$$

which clearly goes to zero [for example, see Eq. (11b)].

In Eq. (10a) we can now observe that the dominant term for $r_0\to 0$ is the first one, and by Eq. (11a) the indicial behavior of the amplitude function is

$$A\sim r^{\gamma}. \tag{12}$$

Hence, a set of functions F_L and G_L will always exist for which $(\eta\neq 0)$

$$F_L(0)=0,\quad G_L(0)=0. \tag{12a}$$

If $\eta=0$, F_L and G_L have finite nonzero limits, and $|F_L|=|G_L|$, since $\varphi_0=\pm\pi/4$. Our subsequent theorems can easily be demonstrated to hold in this limiting case but, for ease of discussion, we shall omit explicit consideration of the case $|\lim(rV)|=1$ in the following.

The indicial behavior (12) may be particularized for the two subcases considered. For $\lim(rV)=-\beta$, we find from relationships (7), (11a), (11c), (11e), and (12)

$$F=O(r^{\gamma}),\quad G\sim O(r^{\gamma}), \tag{12b}$$

where the symbol O signifies "of order of," and the ratio F_L/G_L is given in Eq. (11c). For $\lim(rV)=0$, $\eta=|\kappa|$, we find[6]

$$\begin{aligned}&F_L=O(r^{\varepsilon}), && G_L=O(r^{\kappa+1}\alpha_{21}), && \kappa>0\\ &F_L=O(r^{1-\varepsilon}\alpha_{12}), && G_L=O(r^{-\varepsilon}), && \kappa<0.\end{aligned} \tag{12c}$$

To summarize the results of this section, we conclude that if $|\lim(rV)|>1$ at the origin, there are no L solutions and, *a fortiori*, no eigensolutions in the discrete or continuous spectrum. If $|\lim(rV)|\leqslant 1$ at the origin, there is always an L solution, and for the inequality we have $A(0)=0$ [and, thus, $F(0)=G(0)=0$], and the same results must apply to eigensolutions. For an eigensolution, condition (3a) also requires that A, and therefore F and G, vanish at infinity. The explicit results concerning the behavior at the origin are given by expressions (11c), (11d), (12b), and (12c).

(B) Behavior at Infinity

In the following, we are concerned with bound state wave functions. We shall consider only potentials which are monotonic in the neighborhood of infinity. They may be bounded or unbounded. We do not consider periodic potentials, for example.

If $V(\infty)$ is infinite, we can neglect W and unity compared with V in the neighborhood of infinity, so that Eqs. (2a) become

$$F'=(\kappa/r)F+VG,\quad G'=-VF-(\kappa/r)G. \tag{13}$$

These have the asymptotic solutions

$$F=B(r)\exp(\pm i\int V dr),\quad G=\pm iF$$

(or the real parts thereof), with $|B'/B|\ll|V|$. By means of Eqs. (10a) and (10b), which are valid in all cases, it can be shown that $\lim(B(r))$ exists and does not vanish. Therefore, the solutions violate (6a). Hence, there are no bound states, but such solutions are admissible for continuum states. This differs from the result obtained with the Schroedinger equation and is a manifestation of the Klein paradox.

For bound states, then, $V(\infty)$ must be finite, and we can choose $V(\infty)=0$. Equations (2a) become, near infinity,

$$F'=(\kappa/r)F-(W-1)G,\quad G'=(W+1)F-(\kappa/r)G. \tag{14}$$

With $B(r)$ as above, these have the asymptotic solutions $F=B(r)\exp(\pm(1-W^2)^{\frac{1}{2}}r)$, $G=\pm(1+W)^{\frac{1}{2}}(1-W)^{-\frac{1}{2}}F$. If $|W|<1$, we can get a bound state by choosing the lower sign throughout; if $|W|\geqslant 1$, there are only continuum states. Hence, we have the well-known result that there is a continuous spectrum for $|W|\geqslant 1$; this differs from the Schroedinger case which, in the corresponding situation, has a continuous spectrum only for $W\geqslant 1$.

In summary, we get bound states if $V(\infty)=0$, $|W|<1$; a continuum if $V(\infty)=0$, $|W|\geqslant 1$; and only a continuum if $|V(\infty)|=\infty$, for any W, provided, of course, that the behavior, at points other than infinity, conforms to the boundary conditions imposed above.

From the results of discussion (A), we conclude that a potential $V(r)$ is admissible only if $|\lim(rV)|\leqslant 1$ at $r=0$, and (with the exception noted above) for all such admissible potentials, both F_L and G_L (and also the eigenfunctions F_{LR} and G_{LR}) vanish at $r=0$. We also note that for an admissible potential the energy is

[6] M. E. Rose, Phys. Rev. 82, 389 (1951).

always finite:

$$W\int_0^\infty (F^2+G^2)dr=\int_0^\infty \{2\kappa FG/r+G^2-F^2 +V(F^2+G^2)+G'F-F'G\}dr, \quad (15)$$

where F and G are eigensolutions. By conditions (3a) and (3b), the integral on the left and the first four terms of the right-hand side are seen to converge. The last two terms of the integrand, involving the Wronskian of F and G, behave at the origin as follows:

$$FG'-GF'\sim r^{2s}d(r\alpha_{21})/dr, \quad (\kappa>0),$$

and an integration by parts is seen to give a convergent integral at $r=0$. Convergence at ∞ follows from the asymptotic behavior already given. The case $\kappa<0$ gives the same conclusion. The convergence of the energy integrals is, of course, necessary but not sufficient, since $|W|<1$ is required. Actually, the fulfillment of Eqs. (2a) with $|W|<1$ and of Eqs. (3a) and (3b) is equivalent to this extended condition on the energy integrals.

IV. ORTHOGONALITY OF THE EIGENSOLUTIONS

The wave equations (2a) can be written in hamiltonian form by introducing the two component spinor

$$\Psi=\begin{bmatrix}F\\G\end{bmatrix}. \quad (16)$$

Then,

$$H\Psi=W\Psi, \quad (16a)$$

where

$$H=\sigma_x\frac{\kappa}{r}+i\sigma_y\frac{d}{dr}-\sigma_z+V=\begin{bmatrix}V-1 & \kappa/r+d/dr\\ \kappa/r-d/dr & V+1\end{bmatrix} \quad (16b)$$

is the self-adjoint hamiltonian operator, and the σ's are the usual Pauli matrices.

If Ψ_1 and Ψ_2 correspond to $W=W_1$ and W_2, respectively, we find

$$\Psi_2H\Psi_1-\Psi_1H\Psi_2=(d/dr)(F_2G_1-F_1G_2)=(W_1-W_2)\Psi_1\Psi_2. \quad (17a)$$

The condition for orthogonality $(W_1\neq W_2)$,

$$\int_0^\infty \Psi_1\Psi_2dr=0, \quad (17b)$$

is seen to be fulfilled if $[F_2G_1-F_1G_2]_0^\infty=0$. By the results of the previous section, the quasi-Wronskian[7] $F_2G_1-F_1G_2$ vanishes at the upper limit for all R solutions and at the lower limit for all L solutions. For eigensolutions, it vanishes at both limits and (17b) is fulfilled. If one of the Ψ functions corresponds to a continuum state and the other to the discrete spectrum, the same result applies. For both states in the continuum, Eq. (17b), of course, does not apply, and normalization in the scale of $f(W)$, where f is a function of W, is utilized in the usual manner.

V. UNIDIRECTIONAL ROTATION THEOREM

In this and the following two sections, we develop certain theorems describing the behavior of the nodes of left, right, and eigensolutions. Retaining the notation that left and right solutions are designated with the subscripts L and R, we write the wave functions without subscripts (a) whenever it is unnecessary to specify that the solution is L or R and (b) for eigensolutions. The context will distinguish between these two cases.

Consider a cartesian 2-space in which the coordinates are G and F, so that a vector from the origin to the point (G, F) makes an angle φ with the G axis. Then, the unidirectional rotation theorem states that as r changes, the aforementioned vector crosses the coordinate axis $(F=0,\ G=0)$ with a one-signed sense of rotation. There is one exceptional case of minor interest, which is discussed later (footnote 8). Leaving this case aside at present and introducing the notation $S(x)$ = sign of x, the theorem states that

$$S(\partial\varphi/\partial r)_{G=0}=S(\partial\varphi/\partial r)_{F=0} \quad (18)$$

is always positive or always negative at every internal node of F and G. In the following, references to nodes will imply internal nodes, unless explicit statement to the contrary is made.

It is useful to introduce $\rho=F/G=\tan\varphi$. Then, ρ fulfills the Riccati equation

$$\rho'=2\kappa\rho/r+\alpha_{12}-\alpha_{21}\rho^2. \quad (19)$$

Since $\partial\varphi/\partial r=(1+\rho^2)^{-1}\partial\rho/\partial r$, we have

$$S(\partial\varphi/\partial r)=S(\partial\rho/\partial r),$$

so that the theorem is equivalent to the statement that $\partial\rho/\partial r$ is one-signed at the (simple) poles and nodes of ρ. From Eq. (19),

$$S(\partial\rho/\partial r)_{\rho=\infty}=-S(\alpha_{21}),$$

and

$$S(\partial\rho/\partial r)_{\rho=0}=S(\alpha_{12}). \quad (20)$$

We now introduce the transformation

$$\mathfrak{F}=r^{-s}F, \quad \mathfrak{G}=r^sG$$

which is to be applied only in the open interval $(0-\infty)$, so that $\mathfrak{F}$ and $\mathfrak{G}$ are finite. Moreover, the internal nodes of $\mathfrak{F}$, $\mathfrak{G}$ coincide with those of F, G, respectively. Then

$$\mathfrak{F}'=a(r)\mathfrak{G}, \quad \mathfrak{G}'=b(r)\mathfrak{F}, \quad (21)$$

where $a(r)=\alpha_{12}r^{-2s}$, $b(r)=\alpha_{21}r^{2s}$. It is clear that wherever $\mathfrak{F}$ or $\mathfrak{G}$ has a node[8]

$$S(\mathfrak{F}'/\mathfrak{F})=-S(\mathfrak{G}'/\mathfrak{G})$$

at points in the immediate vicinity of the node, as can be seen immediately by an elementary graphical repre-

[7] In the nonrelativistic limit, $\frac{1}{2}(F_2G_1-F_1G_2)$ reduces to the Wronskian $G_2'G_1-G_1'G_2$. For the case $|\lim(rV)|=1$, see the remarks following Eqs. (12a).

[8] It is obvious that the rotation theorem is valid for any node which occurs in the region in which $\alpha_{12}<0$ (since we take α_{21} to be positive definite) and that such a region must exist in order that bound states exist. It is evident also that inside the turning point $(\alpha_{12}<0)$, the extrema of $\mathfrak{F}$ and $\mathfrak{G}$ are concave toward the r axis. However, outside the turning point $(\alpha_{12}>0)$, it is possible that an extreme of $\mathfrak{G}$, with opposite curvature, and a node of $\mathfrak{F}$ may occur at one point only. At such a point, $S(\partial\varphi/\partial r)>0$. This exceptional case occurs only for L-solutions which are not at the same time eigensolutions and for only a restricted energy range between the eigenvalues. We shall not make explicit mention of this exceptional case in the following, since its consideration does not affect our main conclusions.

sentation of the functions. This implies that nodes can exist only where

$$\mathfrak{F}'\mathfrak{G}'/\mathfrak{F}\mathfrak{G}=ab<0,$$

or where

$$S(\alpha_{12})=-S(\alpha_{21}). \tag{22}$$

From the continuity of α_{12} and α_{21}, this applies at the position of the node as well as in the vicinity of the node. Therefore, from Eq. (20)

$$S(\partial\rho/\partial r)_{\rho=0}=S(\partial\rho/\partial r)_{\rho=\infty}$$

which is equivalent to the theorem as stated. For negative definite V at finite r, we have $\alpha_{21}>0$.[9] This implies a clockwise sense of rotation for φ in crossing the quadrant lines. For the sake of definiteness, we shall consider this case in all further discussion.[8]

An important consequence of the result just obtained is that we can establish the relation between the number of nodes of F and G for L, R, and LR solutions. For L solutions and for eigensolutions (LR) as well, the value of φ at the origin is given by Eqs (11c) and (11d) for admissible potentials. Thus, for potentials attractive at the origin, $\varphi_L(0)$ is in the first quadrant ($\pi/2\geqslant\varphi>0$) for $\kappa>0$, and in the fourth quadrant for $\kappa<0$, ($0\geqslant\varphi>-\pi/2$). In the following, the number of internal nodes of F and G is denoted by n_F and n_G, respectively.

Corollary 1. For L solutions: With $\kappa>0$, $n_F-n_G=0$ or 1 depending upon whether $\rho_L(\infty)$ is positive or negative, respectively. If $n_F=n_G$, the nodes of F and G can be set into one to one correspondence so that each F node precedes the corresponding node of G. If $n_F=n_G+1$, the same correspondence can be set up between the first n_F-1 nodes of F and n_G nodes of G, and again the nodes of F precede the nodes of G and the last G node (node of maximum r) is followed by the last F node. With $\kappa<0$, $n_G-n_F=0$ or 1, and the nodes of G precede the nodes of F in the sense described above. In both cases (κ greater than or less than zero), the nodes of F and G separate each other.

From the asymptotic behavior at ∞ (Sec. III(B)), we have

$$\rho_R(\infty)=-[(1-W)/(1+W)]^{\frac{1}{2}}$$

for R solutions (see paragraph following Eq. (14)). Therefore, $\varphi_R(\infty)$ is in either the second or fourth quadrant. The clockwise rotation of φ, with increasing r at the nodes, then immediately leads to the following result.

Corollary 2. For R solutions, $n_F-n_G=0$ or 1, and the nodes of F precede the nodes of G as r decreases from infinity. Also, the F and G nodes separate each other. These results apply for both signs of κ.

Combining the results of Corollaries 1 and 2, we obtain the following.

Corollary 3. For an eigensolution,

$$\begin{aligned} n_F&=n_G+1, \quad \kappa>0 \\ n_F&=n_G, \quad\quad \kappa<0. \end{aligned} \tag{23}$$

For $\kappa>0$, the first and last nodes (considering F and G together) are F nodes. For $\kappa<0$, the nodes of G precede those of F as r increases. The nodes of F and G separate each other in both cases (κ greater than or less than zero).

VI. OSCILLATION THEOREMS

We consider a field such that at least two eigensolutions exist. The eigenvalues may be arranged in order of increasing numerical value W_0, W_1, ..., and the corresponding eigenfunctions are Ψ_0, Ψ_1, ..., where

$$\Psi_m=\begin{bmatrix}F_m\\ G_m\end{bmatrix}.$$

[9] This is, of course, a sufficient condition but not a necessary one.

We proceed to establish the following oscillation theorems. If the number of nodes of the eigenfunctions F_m and G_m are denoted by $n_F(m)$ and $n_G(m)$, then

$$n_G(m+1)=n_G(m)+1, \quad n_F(m+1)=n_F(m)+1. \tag{24}$$

From Corollary 3 of the preceding section, only one of the results, Eqs. (24), need be established; the other then follows immediately from Eqs. (23).[10]

In order to establish the oscillation theorem (24), we make use of the following lemma. For L solutions, φ is a monotonic decreasing function of W, while for R solution, φ is a monotonic increasing function of W. We apply the adjoint theorem (17a) to two functions Ψ_1 and Ψ_2 corresponding to energies W and $W+dW$, respectively; then, dropping the subscript 1 on the wave functions,

$$\left[F\frac{\partial G}{\partial W}-G\frac{\partial F}{\partial W}\right]_{r_1}^{r_2}=\int_{r_1}^{r_2}\Psi^2dr. \tag{25}$$

For L solutions, we apply Eq. (25) in the interval 0 to r and note that (see Sec. III(A))

$$\lim_{r\to 0}(G_L{}^2\partial\rho_L/\partial W)=0$$

for all admissible potentials. Then

$$G_L{}^2\partial\rho_L/\partial W=-\int_0^r\Psi^2dr. \tag{26a}$$

For R solutions, we apply Eq. (25) in the interval r to ∞ and again note that (see Sec. III(B))

$$\lim_{r\to\infty}(G_R{}^2\partial\rho_R/\partial W)=0$$

in all cases. Then

$$G_R{}^2\partial\rho_R/\partial W=\int_r^\infty\Psi^2dr. \tag{26b}$$

In terms of φ, Eqs. (26a) and (26b) become

$$\partial\varphi_L/\partial W=-\Psi_L{}^{-2}\int_0^r\Psi_L{}^2dr \tag{27a}$$

and

$$\partial\varphi_R/\partial W=\Psi_R{}^{-2}\int_r^\infty\Psi_R{}^2dr \tag{27b}$$

which establishes the lemma.

It follows that $\Delta\varphi(r)=\varphi_R(r)-\varphi_L(r)$ is a bounded differentiable and monotonic function of W. If we select a particular internal point r_0, the existence of an eigensolution, which requires that $\Psi_L(r_0)=\Psi_R(r_0)$, implies that

$$\Delta\varphi(r_0)=\nu\pi, \tag{28}$$

where ν is an integer. We designate by W_ν the value of W for which Eq. (28) is fulfilled. Then, as W increases, the next eigenfunction will be realized when $W=W_{\nu+1}$, at which point

$$\Delta\varphi(r_0)=(\nu+1)\pi. \tag{28a}$$

The existence of $W_{\nu+1}$ is assured by the premise that at least two eigenfunctions and the corresponding eigenvalues exist.

Taking for $\varphi_L(0)$ its principal value, it is clear that G_L will have n nodes if $(n-\frac{1}{2})\pi\leqslant-\varphi_L(r_0)<(n+\frac{1}{2})\pi$, where the equality holds if r_0 is a node of G_L. Consequently, the number of G_L nodes in the interval $0-r_0$ is[11]

$$n_G(0-r_0)=\langle-\pi^{-1}\varphi_L(r_0)-\tfrac{1}{2}\rangle, \tag{29}$$

where the symbol $\langle x\rangle$ is the smallest integer *greater* than x. Similarly, taking $\varphi_R(\infty)$ to have its principal value, the number of nodes of G_R in the interval r_0 to ∞ is

$$n_G(r_0-\infty)=\langle\pi^{-1}\varphi_R(r_0)-\tfrac{1}{2}\rangle.$$

[10] The subscript m on W and Ψ is not necessarily equal to the number of nodes of F or G. See text following Eq. (32).

[11] Obviously, we can always choose r_0 so that $G(r_0)\neq 0$. However, with the meaning assigned to $\langle x\rangle$, it is evident that Eq. (29) is valid in any case.

It follows that the total number of nodes of G is

$$n_G=\langle-\pi^{-1}\varphi_L(r_0)-\tfrac{1}{2}\rangle+\langle\pi^{-1}\varphi_R(r_0)-\tfrac{1}{2}\rangle+\epsilon, \tag{30}$$

where $\epsilon=0$, if $G(r_0)\neq 0$, and $\epsilon=-1$, if $G(r_0)=0$, so that the node at r_0 is counted only once. In the former case, we write

$$\begin{aligned}-\pi^{-1}\varphi_L(r_0)-\tfrac{1}{2}&=\nu_1+\delta,\\ \pi^{-1}\varphi_R(r_0)-\tfrac{1}{2}&=\nu-\nu_1-2+1-\delta\end{aligned} \tag{31}$$

which agrees with Eq. (28). In Eqs. (31), ν_1 is an integer ($\geqslant -1$, see Sec. V), and $0<\delta<1$. It follows then that

$$n_G=\nu_1+1+\nu-\nu_1-1=\nu.$$

If r_0 is a node, $\delta=0$ and $n_G=\langle\nu_1\rangle+\langle\nu-\nu_1-1\rangle-1=\nu$. Thus, in any case, the number of nodes of G is given by

$$n_G=\Delta\varphi(r_0)/\pi. \tag{32}$$

Consequently (see Eq. (28a)), the number of nodes of G and, by Corollary 3, of F each increases by unity as W increases from one eigenvalue to the next.

The eigenfunction G, corresponding to the eigenvalue W_ν, is constructed in the following way. For $r\leqslant r_0$, $G=G_L$; for $r>r_0$, $G=G_R$ if ν is even, and $G=-G_R$ if ν is odd.

It must not be concluded that for the nth eigenfunction G will have $n-1$ nodes. This is actually the case for Schroedinger problem, where the lowest eigenfunction is always nodeless. However, in the relativistic case, there need not be a nodeless eigenfunction for a particular hamiltonian. For example, for $\kappa=1$, an attractive square well of unit radius and depth $V_0=-10$ has a lowest eigenfunction with two internal nodes. In this case, the well has been made so deep and broad that the first two values of W, for which the wave functions F and G are continuous at the radius of the well, have been pushed below $W=-1$. The essential difference between the relativistic and nonrelativistic cases is the existence of a lower bound for the discrete energy spectrum which must be recognized in the case of the former (see also Sec. VII).

A second oscillation theorem is concerned with the direction in which the nodes of F and G move as W increases. Let r_n be a node of F. Then in the vicinity of r_n

$$\rho=(r-r_n)\alpha_{12}(r_n)$$

and

$$(\partial\rho/\partial W)_{r_n}=(\partial\varphi/\partial W)_{r_n}=-\alpha_{12}(r_n)\partial r_n/\partial W.$$

From the results of Sec. V, we conclude that

$$S(\partial\varphi(r_n)/\partial W)=S(\partial r_n/\partial W). \tag{33}$$

Similarly, let r_m be a node of G. Then in the vicinity of r_m

$$1/\rho=(r-r_m)\alpha_{21}(r_m)$$

and

$$[(\partial/\partial W)/(1/\rho)]_{r_m}=-\alpha_{21}(r_m)(\partial r_m/\partial W)$$

or

$$\partial\varphi(r_m)/\partial W=\alpha_{21}(r_m)(\partial r_m/\partial W).$$

Thus,

$$S(\partial\varphi(r_m)/\partial W)=S(\partial r_m/\partial W). \tag{33a}$$

It follows from Eqs. (26a) and (26b) that as W increases the nodes of both F and G move to the left for L solutions and to the right for R solutions.

VII. NONRELATIVISTIC LIMIT

Certain of the properties of the relativistic wave functions, as discussed in the foregoing, are known to apply to the Schroedinger wave functions. There are certain questions connected with the Schroedinger problem, in particular boundary conditions and admissible potentials, which cannot be discussed as direct reductions of the preceding analysis to the nonrelativistic limit.

In the limit $|W-1|\ll 1$, $|V|\ll 1$, but $W-1=E\sim V$; the first-order Eqs. (2a) go over to the second-order nonrelativistic wave equation with G equal to r times the radial Schroedinger function. Here, one makes the identification $\kappa(\kappa+1)=l(l+1)$; that is, $\kappa=l$ or $\kappa=-l-1$. To effect a close parallelism with the preceding discussion, we can take $\kappa=-l-1$, so that $\kappa\neq 0$. However, it is sometimes convenient to take $\kappa=0$ (see Eq. (35) and the subsequent discussion). Since $\alpha_{21}\to 2$, and is, therefore, positive definite in the closed interval $(0,\infty)$, the zero of α_{21} which occurs in the relativistic case at $W=-1$, $r=\infty$ has disappeared. For this reason, the discrete eigenvalue spectrum in the nonrelativistic case has only an upper bound ($E=0$), and, by the usual argument, there is always a nodeless eigenfunction.

Although the Schroedinger equation is a limiting form of the Dirac equation, the corresponding statement for the boundary conditions does not seem to be true. Instead, the boundary conditions for the nonrelativistic problem are:

(a) Square integrability:

$$0<\int_a^b G^2dr<\infty,\quad 0\leqslant a<b\leqslant\infty. \tag{34a}$$

This is the limiting form of condition (3a), since F, as defined above, is the so-called "small component" which vanishes in the nonrelativistic limit.

(b) Lower bound to the continuous spectrum: Without such a condition, the only stable state would have energy $E=-\infty$.

(c) Invariance under extended point transformations: At singular points of such a transformation, a function which satisfies the wave equation in one coordinate system may not satisfy it in others. An example of a singular point is the origin in the transformation from Cartesian to polar coordinates. This condition excludes[12] a singularity as strong as r^{-1} for the Schroedinger ψ, and hence,

$$\lim_{r\to 0}G=0. \tag{34b}$$

This condition also applies to the Dirac equations, but, as has been demonstrated in Sec. III, Eq. (34b) is automatically fulfilled when conditions (3a) and (3b) are met, and Eq. (34b) was unnecessary. It will be noted that while finiteness of $\psi=G/r$ is not required *a priori*, the indicial behavior of G (see below) is such that Eq. (34b) is equivalent to the statement that ψ is finite at $r=0$.

Studying the Schroedinger equation by our methods requires changing from a second-order equation to a pair of first-order equations. This process is not unique. For studying nodal properties, as in Secs. V and VI, the most convenient choice is:

$$F'=-\chi G,\quad G'=F, \tag{35}$$

[12] P. A. M. Dirac, *Principles of Quantum Mechanics* (Oxford University Press, New York, 1947), third edition, p. 155.

where $\chi=2(E-V)-l(l+1)/r^2$. A left-handed solution is one for which $G(0)=0$, so that square integrability is also assured; a right-handed solution is one which is square integrable near infinity, that is, in condition (34a), $a>0$, $b=\infty$. Corollaries 1 and 2, and the first of Eqs. (23) under Corollary 3, which is valid for $\kappa=0$, are immediate consequences of the continuity of G and G' and of $G_L(0)=G_R(\infty)=0$. The results of Sec. VI also apply, if $\kappa=0$, and are immediately applicable.

For studying admissible potentials a more convenient set of first-order equations is

$$F'=-(\chi'/2\chi)F-\chi^{\frac{1}{2}}G, \quad G'=\chi^{\frac{1}{2}}F. \tag{36}$$

Introducing A and φ as in Eqs. (7), we get

$$\begin{aligned}\ln A_1-\ln A_0&=-\int_{r_0}^{r_1}(\chi'/2\chi)\sin^2\varphi dr,\\ \varphi_1-\varphi_0&=-\int_{r_0}^{r_1}(\chi'/2\chi)\sin\varphi\cos\varphi dr-\int_{r_0}^{r_1}\chi^{\frac{1}{2}}dr.\end{aligned} \tag{37}$$

We shall consider only attractive potentials; one readily sees that there is always one and only one left-handed solution for repulsive potentials. We consider three cases based upon the behavior of $\lim(r^2V)$ as $r\to 0$.

(1) $\lim(r^2V)=-\infty$. Then $\lim(r^2\chi)=\infty$, for any l, and for sufficiently small r, $\chi>0$, $\chi'<0$. Then $\int_{r_0}^{r_1}\chi^{\frac{1}{2}}dr$ in Eqs. (37) diverges as $r_0\to 0$, and φ is infinite at the origin. Further, from the signs of χ' and χ, we see that $\ln A\to-\infty$, and A approaches zero at the origin. Hence, all solutions of (36) are L solutions. We can always find at least one R solution for the Schroedinger equation. Hence, for all E, the wave equation and boundary conditions (a) and (c) given above can be satisfied. Therefore, (b) is violated, and attractive potentials more singular than r^{-2} are inadmissible.

(2) $\lim(r^2V)=0$. Here χ has a different behavior for $l=0$ and $l>0$.

(2a) $l=0$. Then $\lim(r^2\chi)=0$. Proceeding as with the Dirac equations in Sec. III(A), we can find a finite φ_0 at the origin, with $\sin 2\varphi_0=0$. Setting $\varphi=\varphi_0+\theta$, and making the choice $\cos 2\varphi_0=-1$, we find, near the origin $\theta=-r\chi^{\frac{1}{2}}$, which approaches zero in agreement with assumption. This choice further makes A_0 approach zero and gives an L solution. The other possible choice ($\sin 2\varphi\to 0$, $\cos 2\varphi\to 1$ corresponding to the second linearly independent solution) makes A remain greater than zero at the origin, and Eq. (34b) is violated. Hence, there is only one L solution. For this solution, $A\sim\chi^{-\frac{1}{4}}$, $\cos\varphi\sim r\chi^{\frac{1}{2}}$, and $G\sim r$.

(2b) $l>0$. Then $\lim(r^2\chi)=-l(l+1)$, and φ takes on complex values sufficiently near the origin. The phase-amplitude method is not convenient for this case. However, the behavior of G near the origin now depends only upon l and not upon V. The well-known indicial behavior of G is r^ν, where

$$\nu=-l, l+1.$$

Only one solution, with $\nu=l+1$, satisfies the boundary conditions.

Hence, if $\lim(r^2V)=0$, there is one and only one L solution for all l, and such potentials are admissible. G behaves like r^{l+1} near the origin.

(3) $\lim(r^2V)=-\beta\neq 0$. The indicial behavior of G is r^ν, where

$$\nu=\tfrac{1}{2}+[\tfrac{1}{4}-2\beta+l(l+1)]^{\frac{1}{2}}.$$

With $l=0$, the real part of ν is positive for all β, and all solutions are left-handed. Therefore, boundary condition (b) is violated, and all such potentials are inadmissible.

Thus, on the basis of a consideration of bound states, the only admissible potentials which are attractive at the origin are those for which $\lim(r^2V)=0$ as $r\to 0$, whereas no restrictions need be placed on repulsive potentials. This is in contrast to the Dirac result (Sec. III), where the potentials could be classified as admissible or otherwise, without regard to the sign of V. This symmetry between attractive and repulsive potentials in the relativistic case is, of course, understandable in terms of energy doubling (quadratic energy-momentum relationship).[13]

At first glance one might conjecture that, at least in the Schroedinger case, the physical basis of admissibility of a potential is the requirement that the attraction shall not predominate over the centrifugal repulsion. The foregoing shows that this interpretation is not correct, and, in the Dirac case, such an interpretation would be definitely ambiguous.

We wish to express our appreciation to Professor F. A. Ficken of the Department of Mathematics, University of Tennessee, for a critical review of the manuscript.

[13] The second-order equations for the relativistic F and G are independent of the sign of V, in the region where V is large, in all terms including those arising from the effect of spin.

Ionization Chamber Bursts at High Altitudes*†

THOMAS COOR, JR.‡
Palmer Physical Laboratory, Princeton University, Princeton, New Jersey
(Received January 19, 1951)

A thin-walled, low pressure ionization chamber has been sent into the upper atmosphere by means of balloons to study bursts of ionization. Pulse size, barometric pressure, and temperature were telemetered to the ground by means of a FM audio subcarrier system with a 75-Mc radio link. Measurements have been made of the size and frequency of bursts of ionization greater than that produced by 0.8 polonium alpha-particles ($0.8\times5.1=4.1$ Mev) at altitudes up to that corresponding to an air mass of 17 g/cm^2 remaining overhead.

I. INTRODUCTION

THE ionization chamber has taken on a new importance for elementary particle investigations as a result of recent technical improvements in the removal of electron-capturing impurities from chamber gases, in rapid collection of electrons from such gases, and in associated fast amplifiers. In contrast with the Geiger-Müller counter, which determines only the number of particles, and the integrating ionization chamber, which yields only total ionization, the modern ionization chamber determines the ionization produced by individual particles. Such an instrument can be used in two quite different ways for the study of the cosmic radiation. (a) The chamber can be used purely as an indicator for events which produce sufficient ionization to be detected, events which we hereafter call "bursts" without any implications as to their nature or source. In this case we can measure the frequency of the bursts at several altitudes and determine the rate of change with air mass overhead of the burst producing radiation. Likewise, we can measure the *absorption* of the burst producing radiation in other substances. (b) Alternatively, we can study the size-frequency distribution of events observed in an ionization chamber at a single altitude and thus investigate the *nature* of the events which cause the bursts. The present investigation is an attempt to study nuclear processes in the upper atmosphere by means of both the above methods.

At the time when these investigations were commenced, June, 1946, burst studies in modern ionization chambers had never been carried out at altitudes above mountain-top levels. Also, the experimental picture was confused by lack of agreement between different observers,[1] largely owing to the wide variety of equipment and conditions used by the various experimenters and to the inability to distinguish between bursts due to electron showers and those due to fragments from nuclear explosions.

Euler[2] has shown that both types of events contribute to ion chamber bursts and succeeded in giving a satisfactory explanation of the observed size-frequency distribution of bursts in an ion chamber. Using the data of Stetter and Wambacher[3] for the energy distribution of star particles, he calculated the burst distribution expected from this cause. He showed that the expected distribution was in qualitative agreement with that found by Carmichael and Chou[4] if one assumed a mixture of bursts due to electron showers and nuclear disintegrations.

About 98 percent of the pulses in an ionization chamber at 3500 meters are produced by heavy particles, according to an analysis of the shapes of the pulses made by Rossi and Williams.[5] In view of this large percentage of heavy particles at this altitude and in view of the fact that this proportion should become even greater at higher altitudes, it is evident that the ionization chamber is a very useful device for studying nuclear explosion phenomena. Bridge and Rossi[6] have measured the burst rate in a cylindrical ionization chamber at altitudes up to 35,000 feet in a B-29 aircraft. They find that the rate of pulses increases rapidly with altitude and state that the increase corresponds to an exponential absorption in the atmosphere with a mean free path of 150 g/cm^2, assuming vertical radiation. Also, Tatel and Van Allen[7] have sent an identical chamber to the top of the atmosphere by means of a V-2 rocket. From their results, together with the results of Bridge and Rossi, they conclude that the bursts are nuclear explosions induced by the primary cosmic radiation with a mean free path of 200 to 225 g/cm^2, assuming isotropic incidence of the burst producing radiation. Rossi,[8] on the other hand, interprets the data as indicating a maximum and states that bursts are produced by a secondary radiation, probably neutrons.

* This paper is based on a thesis submitted to Princeton University in partial fulfilment of the requirements for the degree of Doctor of Philosophy. A preliminary account of some of the work reported here was given by T. Coor and G. A. Snow, New York Meeting of American Physical Society, January 29, 1948; Phys. Rev. **73**, 1252 (1948).

† This work was conducted under the joint auspices of the ONR and AEC.

‡ Now at Brookhaven National Laboratory, Upton, New York.

[1] H. Carmichael, Phys. Rev. **74**, 1667 (1948).

[2] H. Euler, Z. Physik **116**, 73 (1940).

[3] G. Stetter and H. Wambacher, Physik. Z. **40**, 702 (1939).

[4] H. Carmichael and C. N. Chou, Proc. Roy. Soc. (London) **A154**, 223 (1936); Nature **144**, 325 (1939).

[5] B. Rossi and R. W. Williams, Phys. Rev. **72**, 172 (1947).

[6] H. Bridge and B. Rossi, Phys. Rev. **71**, 379 (1947).

[7] H. E. Tatel and J. A. Van Allen, Phys. Rev. **73**, 87 (1948).

[8] B. Rossi, Revs. Modern Phys. **20**, 537 (1948).

Hulsizer[9] has reported results obtained from an ionization chamber sent into the upper atmosphere to look for shower-producing electrons. He observed bursts which he interprets as being due to heavy particles from stars and concludes that the frequency of the star-produced bursts does not reach a maximum below the top of the atmosphere at a geomagnetic latitude of about 54°N.

This paper reports the results of an experiment which has been carried out in order to study the variation of ion chamber bursts as a function of altitude and of burst size at 52°N geomagnetic.

II. EXPERIMENTAL APPARATUS

In our experiments, a thin copper ion chamber filled with pure argon was sent into the upper atmosphere by means of free balloons. Burst amplitude, barometric pressure, and equipment temperature were simultaneously telemetered to the ground by means of a FM radio link.[10] The balloon signals were received at a fixed ground station and the telemetered data recorded permanently by photographic means.

In this technique the balloon equipment is built into a light wooden gondola and designed to have as little weight as possible without sacrificing stability and reliability. Labile equipment, such as batteries and high voltage leads, are protected from harmful effects of the extremes of temperature and pressure encountered via dielectric sheaths and sun shields. A clock-driven standardizing system is incorporated to check periodically the entire burst measuring system with polonium alpha-particles.

The ionization chamber used in the balloon flights consists of a 30.5-cm diameter copper sphere fabricated from two spun hemispherical shells soldered together with pure tin. The wall thickness is 0.54 mm, but is not absolutely uniform, varying by about 10 percent.

The collecting electrode is a 5-cm diameter copper sphere suspended by a radial rod $\frac{1}{8}$ in. in diameter. This rod is supported by an assembly of insulating material that is force-fitted into the neck of the chamber. Figure 1 shows the construction of the chamber. The first stage of the pulse amplifier is contained within the chamber neck. It is a cathode follower providing a low output impedance for the chamber.

A special feature of the chamber is the cylindrical guard ring that surrounds the collecting electrode support and grid blocking condenser. This guard ring is connected to the output of the cathode follower through a high voltage blocking condenser and is thus fed with a pulse of approximately the same size as appears on the collecting electrode. This cancels a large fraction of the stray capacity to ground of the input circuit. With this arrangement the effective input capacity of the chamber and amplifier is only 6.5 $\mu\mu$f.

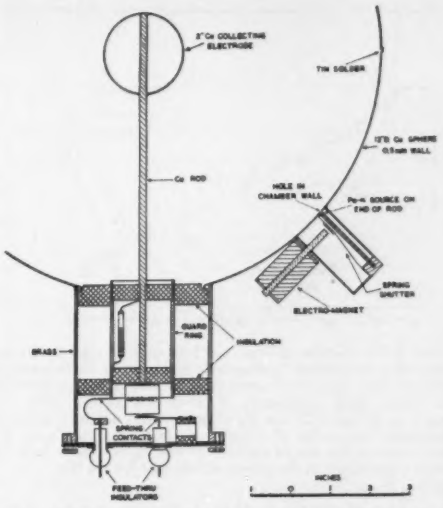

FIG. 1. The construction of the ionization chamber used in the balloon flights. The first stage of the amplifier (not shown) is located in the chamber neck just below the bronze spring contact for the central electrode. The polonium alpha-particle source for periodic calibration is shown on the side of the chamber. The chamber was filled with pure argon to a pressure of 1.3 atmos, and electron collection achieved.

The guard ring rides at the collecting potential and hence acts also in the conventional manner to protect the central electrode from leakage currents.

In order to collect electrons before they combine to form heavier negative ions, pure argon is used as the chamber gas. It is found that the amplitudes of pulses from polonium alphas originating at the wall remain essentially unchanged for chamber voltages above 550. This result applies to pure argon at 1.3 atmospheres (of 76 cm Hg, 21°C), the pressure adopted for the experiments. With 600 volts as the collecting potential, the value used in the experiments, it is found that the chamber pressure may be doubled with a consequent drop of less than 10 percent in pulse height if the gas is pure. This small drop is adopted as the criterion for gas purity and consequently for saturation. Polonium alpha-particles originating at the wall of the chamber give a pulse with a rise time of roughly 3 μsec when observed with a fast scope.

A permanent alpha-source is incorporated in the chamber for clock controlled standardization. The arrangement of the source and shutter mechanism is shown in Fig. 1. A small hole drilled into the chamber wall allows alphas from a thick source on the end of a nickel rod to enter the collection field when a thin shutter is pulled aside. The source is 2 mm from the inside wall; thus, $(37.5/39.5)^{1}\times 5.25 = 5.1$ Mev of ionization is formed in the chamber by each alpha-particle.

A moderately fast lightweight amplifier was developed for use with the chamber. It is a three-stage, resistance-coupled type employing inverse feedback to improve stability and linearity. A gain of about 500 with a rise time of about 3 μsec and a decay

[9] R. I. Hulsizer, Phys. Rev. **73**, 1252 (1948).

[10] The apparatus is described in detail in a separate article by Coor, Darago, and Snow, to be submitted to Rev. Sci. Instr.

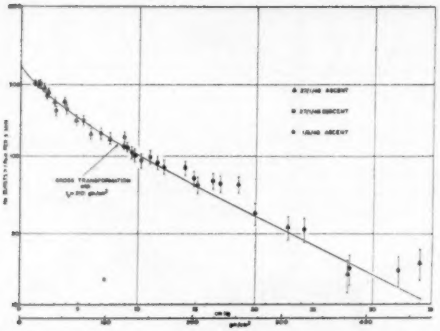

FIG. 2. The number of bursts per 5 min greater than 1 polonium alpha as a function of atmospheric thickness at 52°N magnetic latitude. Two flights were used to obtain the data represented in the figure, those of January 27, 1948 and May 1, 1948. The points at 8.9 and 1.27 cm Hg represent data obtained while the equipment floated for 45 minutes at almost constant level. The flags indicate the statistical errors. The curve drawn in is the Gross curve fitted to the points at 1.27 and 8.9 cm Hg.

time of roughly 50 μsec is obtained. The signal to noise ratio is 30:1 for a 5.1-Mev alpha-particle in the chamber.

The amplified chamber pulse is converted into a pulse whose duration is a function of the ionization produced in the chamber. This pulse is then transmitted to the ground station by means of one channel of an FM audio subcarrier—75 MC, FM radio link, system. Temperature and pressure are telemetered on another channel. The pressure sensing element is a baroswitch unit used in meterological work. It is calibrated in a bell jar before each flight. Its readings are good to about 0.5 mm Hg.

On the ground, the radio signal from the balloon is received and the telemetered information unscrambled and recorded. The recorder is of the moving mirror galvanometer type and employs photographic recording. The height of the trace on the photographic record is directly proportional to the logarithm of the size of the bursts in the chamber.

The ionization chamber, telemetering equipment, and transmitter are contained in a light wooden gondola. The ion chamber is located at the top of the gondola and is supported at five points by means of sponge rubber pads. This arrangement effectively shockmounts the chamber and the pulse amplifier, which is suspended from the chamber neck. The transmitter and its batteries are located in the lower section of the gondola. The antenna is suspended around the bottom of the gondola by four supports that project from the corners.

Before launching, the top half of the gondola is covered with aluminum foil and the lower half with several layers of cellophane. This arrangement keeps the ion-chamber from being heated by the sun's rays and prevents the batteries in the lower part of the gondola from freezing. Scotch tape is used to seal the cellophane and foil as nearly airtight as possible. The gondola is attached to the balloons by means of four Nylon ropes, fastened to the four main gondola posts. The total weight of the complete apparatus is 30 lb.

For one flight, clusters of Dewey and Almy type J-2000 balloons were used. This flight reached 1.2-cm Hg pressure. The other flight was carried out with a 20-foot General Mills polyethylene constant volume balloon. This flight reached 8.8 cm Hg, where it floated for some time.

III. EXPERIMENTAL RESULTS

The experimental results discussed in this section were obtained in two flights, January 27 and May 1, 1948. The January flight went to 1.2 cm Hg, while the May flight ascended to 8.8 cm. Data yielded by two previous flights (without periodic standardization) will not be considered, because of discrepancies and inconsistencies caused by equipment failure and drift.

A. Burst Frequency *vs* Atmospheric Depth

The dependence of burst frequency upon mass of air remaining overhead is shown in Fig. 2. The results shown are from the ascent and descent of the January 25 flight and from the ascent of the May 1 experiment. (The balloons were out of radio range during descent.) The rates given for the bursts at 1.27 cm (January 27 flight) and at 8.9 cm (May 1 flight) are each the average of nine 5-min periods, obtained while the balloons floated at an almost constant level. These two values are used to calculate the "absorption thickness," or mean free path l_0, of the burst-producing radiation in the atmosphere.

It is general practice at low altitudes to express the decrease with atmospheric depth in the intensity of a radiation as a simple exponential of the form

$$N(t)=N_0\exp(-t/l_0). \tag{1}$$

For some cosmic-ray phenomena a satisfactory fit may be obtained with this law, even at high altitudes; but it is clear that the l_0 is not the true absorption thickness for the radiation, because it is not correct to assume vertical incidence. Even at atmospheric depths of the order of three mean free paths, the error introduced in the effective mean free path by the assumption of vertical incidence is about 15 percent. The true absorption law is given by the Gross expression[11]

$$N(t)=2\pi N_0\left[\exp(-t/l_0)-(t/l_0)\int_{t/l_0}^{\infty}x^{-1}\exp(-x)dx\right], \tag{2}$$

where N_0 is the number of incident particles cm^{-2} sec^{-1} steradian^{-1}.

For bursts of ionization greater than 1 Po-α, the absorption thickness for the burst-producing radiation, assuming isotropic incidence, is found to be $l_0=210\pm7$ g/cm^2 [as defined in Eq. (2)]. This constant was evaluated graphically. A plot was made of the calculated ratio of the burst rates for 1.27 cm (17 g/cm^2) and 8.9 cm (121 g/cm^2) as a function of l_0. From this plot was determined that value of l_0 which would reproduce the experimentally observed ratio of burst frequencies. The Gross curve drawn in Fig. 2 for burst frequency as a function of altitude is determined entirely by the data at 1.27 cm and 8.9 cm. It reproduces satisfactorily the observations for all values of the air mass overhead less than 300 g/cm^2. It may be noted that at atmospheric depths in the region of 300 g/cm^2 the observed curve would correspond to an effective absorption thickness of 160 g/cm^2, if one assumed a simple exponential law and vertical incidence.

[11] B. Rossi, Revs. Modern Phys. **20**, 564 (1948), Eq. (11).

The value 210 g/cm² obtained near the top of the atmosphere in this experiment is somewhat larger than the figure obtained by observers lower in the atmosphere. Rossi,[11a] for example, finds that bursts in an ionization chamber from 35,000 ft down fit a Gross curve for a mean free path of 165 g/cm². However, this is not unexpected as the primary radiation is complex and the various components will show differing behavior as they pass down through the atmosphere.

B. Size-Frequency Distribution

It is of interest to observe the nature of the size-frequency distribution of bursts at different altitudes. The integral and differential distributions are shown in Figs. 3 and 4, respectively. The integral distribution curve gives the number of bursts per five minutes greater than a size E as a function of E at three atmospheric depths. The curves shown for 1.27 and 8.9 cm Hg

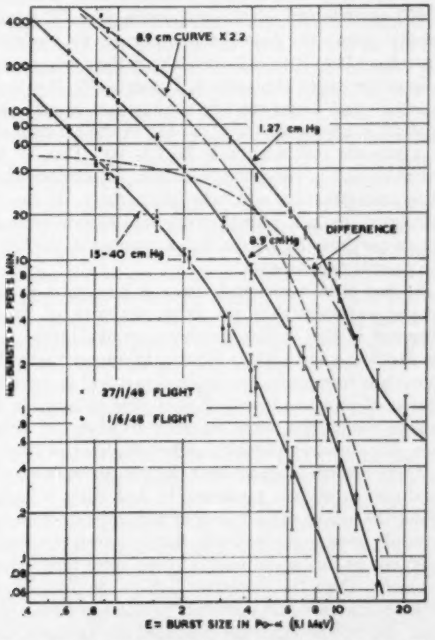

FIG. 3. The integral burst-size distribution obtained at three points in the atmosphere. The distributions at 1.27 and 8.9 cm Hg were obtained in 45 minutes while the apparatus floated at almost constant level. The data given for 15–40 cm Hg was obtained as the balloons rose through this region of the atmosphere. Best-fit curves are drawn through the points. The dashed line in the figure is calculated by multiplying all readings at 8.9 cm Hg by the constant factor 2.2. Note how different this curve is at large burst sizes from the experimental curve found for 1.27 cm Hg. The difference between the two curves is indicated by the dot-dash line. It is quantitatively in accord, as regards magnitude and shape, with what one would expect from the known flux of heavy particle primaries (see discussion in text).

[11a] Private communication.

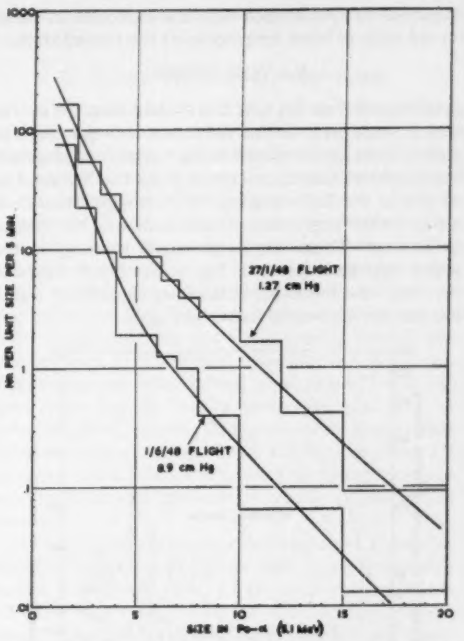

FIG. 4. The differential burst-size distributions obtained while the balloons floated at 1.27 and 8.9 cm Hg for 45 minutes. Best-fit curves are drawn in.

were obtained while the gondolas floated at an almost constant altitude. The points of the curve shown for the region 15 to 40 cm Hg were obtained in the two flights as they rapidly ascended through the lower atmosphere. The good agreement between the two experiments in this region demonstrates the reproducibility of the apparatus and validates a comparison between them when there is less air mass overhead.

The differential distribution was obtained by constructing histograms of the counts obtained at the two regions of good statistics.

It is seen that the integral distributions of pulse sizes at 8.9 cm and at 1.27 cm differ appreciably, especially in the region of larger bursts. The differential distribution, however, does not show such a marked difference. A quantitative way to describe this difference is to give the ratio of burst frequencies as a function of burst-size at the two pressures. These results are presented in graphical form in Fig. 5. The curve for the ratio of the differential distributions was obtained by taking the ratio of the "best-fit" curves for the histograms in Fig. 4. The absorption thickness corresponding to the ratio between the rates at 1.27 and 8.9 cm Hg (17 and 121 g/cm²), is given on the left-hand side of the figure. The mean free path, l_0, for the radiation responsible for bursts of each size was so

chosen as to give, in each case, the experimental value for the ratio of burst frequencies at the two altitudes

$$R=N(17)/N(121),$$

as calculated from Eq. (2). It is evident from the curves that a large part of the difference between the size distributions at the two altitudes results from the eight bursts greater than 20 polonium alpha that occurred in 45 min at the 1.27-cm level. Of these eight bursts, six are in reality larger than 30 alpha, driving the system to its limit. These very large bursts show up in the upper right-hand point in Fig. 3. For lower values of the bias, these bursts affect the *integral* curves of Fig. 3, but not the *differential* curves of Fig. 4.

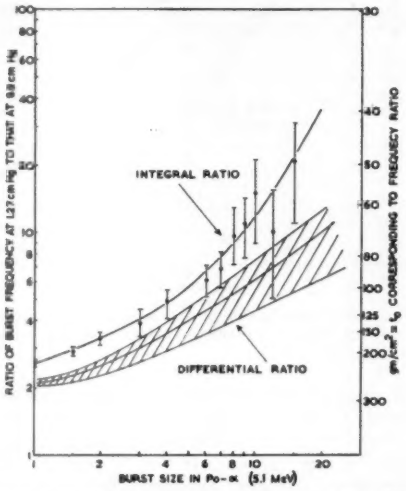
INTEGRAL RATIO
DIFFERENTIAL RATIO
BURST SIZE IN Po-α (5.1 MeV)
RATIO OF BURST FREQUENCY AT 1.27 cm Hg TO THAT AT 8.9 cm Hg
CORRESPONDING TO FREQUENCY RATIO

FIG. 5. Ratio of the burst-size distributions at 1.27 cm Hg to those at 8.9 cm Hg. The ratio of the integral distributions was plotted point by point and the best-fit curve drawn in. The curve for ratio of differential distributions was drawn by taking the ratio of the best-fit curves in Fig. 4. A scale of mean free path in g/cm² is drawn on the right. This mean free path, when inserted in the Gross formula for isotropic incidence, reproduces the ratio of rates at 1.27 and 8.9 cm Hg.

IV. DISCUSSION OF RESULTS

Experimentally, a burst represents the production of some few Mev of ionization in the active volume of a chamber within an extremely short period of time. Two explanations for this effect immediately offer themselves: that the bursts are produced by showers of electrons impinging upon the chamber, or that they are produced by one or more heavier particles. The frequency of air showers of a given density should, according to cascade theory, increase rapidly up to a certain altitude, then fall off again. Also, as was first known from the work of Stetter and Wambacher,[12] the frequency of stars, a possible source of heavy particles, increases rapidly with altitude. In addition, bursts may originate from the heavy nuclei in the primary cosmic radiation.[13] These three types of events will now be analyzed to see whether they can account for the observations. An attempt will be made to infer as much as possible about the nature of the observed events and their relation to the over-all cosmic-ray picture.

A. Negligible Frequency of Bursts Due to Electron Showers

The average path length in the spherical ionization chamber used in the experiments is $\frac{2}{3}\times 30$ cm, which is equivalent to 0.047 g/cm² of argon. An electron at minimum ionization loses energy at the rate of about 2 Mev per g/cm², so that each electron will lose, on the average, 0.094 Mev in the chamber gas. Therefore, about 55 electrons passing through the chamber in coincidence will be required to produce a burst equivalent to 1 Po-α. This number corresponds to a density of 800 particles/m². Electron showers of much greater density than this have been observed at moderate altitudes,[14] but little is known about them experimentally in the upper atmosphere. Theoretically, it is to be expected that dense cascade showers are almost nonexistent in about the top 9 cm Hg of the atmosphere, as a cascade unit for air is 3.3 cm Hg. Also, as the chamber wall is very thin, less than 0.1 cascade unit, little multiplication will take place there. It can be calculated that not more than one shower induced burst occurs per hour at 3.9 cm Hg, a number negligible in the present experiments.

As has been mentioned, there is also good experimental evidence that the large majority of bursts observed in thin-walled ion-chambers at 25,000 ft (24 cm Hg)[15] and at 11,500 ft (45 cm Hg)[5] are actually due to nuclear fragments. Consequently, it will be assumed that at *all* altitudes for which data were obtained in the balloon flights, the large majority of observed bursts were due to heavy particles, either singly or as stars.

There is some evidence that electron showers may be produced in nuclear processes,[16,17] but little is known about the nature or frequency of such events. However, it would seem quite probable that a transformation as energetic as this would release at the same time several nucleons. Then the ionization due to the protons and alpha-particles would dominate in these processes over that due to the electrons produced at the same time. Thus, such events are to be considered as normal stars for the purpose of the present experiment. Consequently, it will be legitimate to disregard the effects of electrons in the following considerations.

[12] G. Stetter and H. Wambacher, Physik. Z. **40**, 702 (1939).

[13] Freier, Lofgren, Ney, Oppenheimer, Bradt, and Peters, Phys. Rev. **74**, 213 (1948); Freier, Lofgren, Ney, and Oppenheimer, Phys. Rev. **74**, 1818 (1948).

[14] C. D. Anderson and S. H. Neddermeyer, Phys. Rev. **50**, 263 (1936).

[15] H. Bridge, Phys. Rev. **72**, 172 (1947).

[16] J. Daudin, Compt. rend. **218**, 275 (1944).

[17] F. Oppenheimer and E. P. Ney, Phys. Rev. **76**, 1418 (1949).

B. Heavy Particles from Nuclear Explosions

One or more heavy particles (alphas or protons) entering the chamber can produce a large burst. A proton near the end of its range can produce a maximum pulse equivalent to 1.1 Po-α if it traverses the diameter of the chamber. An alpha-particle can produce four times as much ionization under the same circumstances. These heavy particles are known to exist in the atmosphere, and Bagge[18] has shown that the proton intensity observed in the lower atmosphere can be accounted for in terms of nuclear explosions. Stetter and Wambacher[19] found that the rate of these nuclear explosions increases by a factor of 60 in going from sea level to 11,000 ft, which is the order of increase found for the ionization chamber bursts. We must therefore explain some of the bursts in the chamber at high altitudes as single and multiple heavy particles from stars which occur in the chamber gas and wall, and in the surrounding atmosphere.

This star picture of nuclear explosions is looked into in detail in a paper to appear later. It will be shown there that (1) the observed burst size distribution is explainable qualitatively, except at the highest altitudes, in terms of protons and alpha-particles from nuclear explosions, and (2) that the absolute number of bursts is in reasonable agreement with the rate of proton production observed in photographic emulsions.

The change in the relative frequency of bursts which occurs near the top of the atmosphere may be taken to indicate that the absorption coefficient for the radiation producing the larger bursts is greater than the coefficient governing the smaller bursts, but that the nature of the event is basically unchanged. Insofar as large bursts are due to stars, the observed change of distribution with altitude is qualitatively reasonable. It is known from photographic plate data that the frequency of large stars increases more rapidly with altitude than that of small ones.[19,20] However, it is difficult to give a quantitative estimate of this effect on the burst distribution. Since large bursts can result from the passage through the chamber of two or more particles from the same nuclear explosion, it is expected that on the average larger stars will give larger bursts. As far as statistics allow, it can be seen from Fig. 3 that there is an indication of a change in the pulse size distribution between 15–40 cm Hg and 8.9 cm Hg. However, statistical difficulties prevent any accurate estimate of the magnitude of the effect. It is difficult to explain the alteration in distribution at these depths in terms of any mechanism other than the change in the relative frequency of large and small stars produced in the wall of the chamber. The heavy particles that have recently been found in the primary radiation should not penetrate to these depths in significant number to account for the effect.

C. Heavy Nuclei from Outer Space

The heavy nuclei in the primary radiation, which were recently discovered by the Minnesota and Rochester groups,[13] have atomic numbers up to 40 and are very energetic, some penetrating more than 30 g/cm^2 of the atmosphere. The authors estimate that the majority of these particles are largely absorbed after traversing about 30 g/cm^2 (2.2 cm Hg) of atmosphere, and that the flux averaged over a hemisphere is 0.4×10^{-4} cm^{-2} sec^{-1} steradian^{-1} ($z>10$) at a depth of 14 g/cm^2 (1 cm Hg). This flux corresponds to about 50 heavy particles ($z>10$) per 5 min passing through the chamber used in the present experiments.[21] A particle at minimum ionization having $z=10$ should ionize 100 times more heavily than a proton at minimum, or about 200 Mev/(g/cm^2). In our chamber, this particle would produce an average burst of 9 Mev or about 1.8 polonium alpha; therefore, almost all heavy particles with $z>10$ should produce detectable pulses in the chamber.

The rate of 50 per 5 min calculated for 1.27 cm Hg from the Minnesota-Rochester data is an appreciable fraction (about one-third) of the total rate of bursts >9 Mev (1.8 Po-α) found at this elevation in the present experiments (about 160 per 5 min). Thus, heavy nuclei produce a significant fraction of all ionization chamber bursts in the upper 30 g/cm^2 of the atmosphere. Their effect comes more clearly into evidence when we examine (1) the abnormally high absorption coefficient of large ionization chamber bursts, (2) the large change with altitude in the burst-size distribution, and (3) the number of bursts greater than 100 Mev found at 1.27 cm Hg.

(1) The observed rapid absorption of the bursts of abnormal origin is consistent with the idea that heavy nuclei are responsible for these events. Figure 5 shows the effective mean free path of the burst-producing radiation, the normal and abnormal radiation being lumped together, as a function of the size of the burst produced by this radiation. It is seen that there is a systematic trend to higher absorption coefficients with increasing burst size. This effect is just what is to be expected on the assumption that many of the bursts are due to the traversal of the chamber by heavy nuclei. Thus, it is reasonable to consider the burst-producing radiation as a mixture of protons with a mean free path certainly no less than 60 g/cm^2, and perhaps much greater, and heavy nuclei with mean free paths of the order of 30 g/cm^2, according to Bradt and Peters.[22] As the large bursts are produced in larger and larger pro-

[18] E. Bagge, article in *Kosmische Strahlung*, edited by W. Heisenberg (Berlin, 1943), p. 119.
[19] Kaplon, Peters, and Bradt, Phys. Rev. **75**, 1329 (1949).
[20] Salant, Hornbostel, and Dollman, Phys. Rev. **74**, 694 (1948).
[21] This is in substantial agreement with the rate calculated from more recent data of H. L. Bradt and B. Peters, Phys. Rev. **76**, 156 (1949), by extrapolating their flux given for the top of the atmosphere down to 17 g/cm^2 using the Gross equation with $l_0 = 23.5$ g/cm^2.
[22] H. L. Bradt and B. Peters, Phys. Rev. **75**, 1779 (1949).

portion by heavy particles, the mean free path tends systematically to a lower and lower figure. Of course, a part of the observed effect may also be due to a possible decrease of protonic mean free path with increasing energy. Only a discrimination between proton- and heavy-nucleus-induced events, say, by the emulsion technique, would allow one to say how much of the observed shortening of the mean free path for big bursts is a proton effect and how much is due to heavy nuclei.

(2) A related effect attributable to heavy nuclei is the large change with altitude in the burst size distribution, as shown in Fig. 3. The dashed curve in the figure allows one to compare more easily the observations at 1.27 cm Hg and at 8.9 cm Hg. It is clear from the figure that it is possible to consider the burst size distribution curve at 1.27 cm Hg to be made up of two parts: (a) a component (indicated by the dashed line) which is absorbed with the same mean free path which is found for small bursts; and (b) a heavy-nucleus-induced effect, which has become negligible at a depth of 8.9 cm Hg = 120 g/cm² (dot-dash curve in figure). Obviously, this interpretation is not the only possible one (conceivably there may be a decrease of proton mean free path with energy). But the dot-dash curve corresponds to an intensity of the heavy particle component (~60 per 5 min) of just the order (~50 per 5 min) calculated from the data of Bradt and Peters. Also the shape of the dot-dash difference curve is qualitatively in agreement with this interpretation. It is difficult, therefore, to escape the conclusion that this difference curve gives a reasonable order of magnitude representation of the effect of heavy particle primaries.

(3) Eight very large bursts (>20 Po-α or 100 Mev) were observed in 45 min at 1.27 cm Hg, but none at any lower altitude. It would be a very unusual explosion in the wall or gas of the chamber which could release in the gas so much energy, for a proton can at best lose only 5 Mev in a traversal ending just short of the far wall of the chamber (densest portion of the Bragg curve). A heavy particle with a charge of $Z=33$ suffices, however, to produce a pulse of this size even at minimum ionization; and near the end of its range, a much smaller charge is enough to produce the observed effects.

We conclude from absolute intensity, from absorption coefficient, and from maximum pulse magnitude that a substantial proportion of the large bursts observed at 1.27 cm Hg are produced by heavy nuclei.

It is true, of course, that many observations have been made of heavy nuclei producing stars in a photographic plate. However, the probability for production of an event of this kind in the wall of our chamber, of thickness 0.45 g/cm², by a heavy nucleus of mean free path[23] 25 g/cm², will amount to only two chances in 100. Consequently, practically all the *bursts produced by heavy nuclei are due to the direct ionization* which they produce in the argon of the ion-chamber.

[23] H. L. Bradt and B. Peters, Phys. Rev. **75**, 1179 (1949) find a value 23.5 g/cm² for nuclei $10 \lesssim z \lesssim 18$.

D. Ionization in Bursts Compared with Total Ionization

The ionization in bursts is an important quantity in problems dealing with the energy balance in the over-all cosmic-ray picture.

Assume that the number of bursts per unit time larger than a given size E is given by $F(E)$. The total amount of ionization in units of E per unit time will then be given by

$$I = -\int_0^\infty E dF(E). \tag{3}$$

If we extended the integration literally to zero on the lower end, we would naturally include in Eq. (3) the ionization due to electrons as well as to nuclear particles. An electron at minimum ionization, however, produces a pulse equivalent only to (1/55) Po-α, and, in any case, a pulse no greater than about (1/25) Po-α. Also, a pile-up of small pulses from many independent electrons passing through the chamber has a negligible probability of accidentally producing a pulse as great as 0.5 Po-α, while no pulses smaller than 0.5 Po-α were counted in the present experiments. Finally, showers of electrons have already been excluded as a cause of any significant number of the observed bursts. Consequently, we shall obtain from Eq. (1) an amount of ionization due almost exclusively to nuclear particles if we extend the integration only down as far as 0.5 Po-α.

The procedure just described will not give the *total* ionization due to nuclear particles, of course, as many of these entities will produce pulses smaller than 0.5 Po-α. The ionization from evaporation fragments can, however, be estimated with sufficient accuracy for our purpose. We have only to compute the distribution of pulses of size less than 0.5 Po-α due to evaporation protons. Using the computed curve to extrapolate the observed curves, we find, for example, that pulses between 0.1 Po-α and 0.5 Po-α contribute less than a third of the ionization due to all nuclear bursts greater than 0.1 Po-α. Thus, the uncertainty introduced by this extrapolation will constitute only a small fraction of the total ionization. We conclude that the *integral* (3), extended down to 0.1 Po-α, *gives very nearly the whole contribution of nuclear evaporation fragments to the cosmic-ray ionization.*

The actual integrations were carried out numerically at 1.27 and 8.9 cm Hg. Figure 6 shows the observed ionization rates at these two levels joined by a smooth curve based on the observed rate of increase of bursts with altitude. The total ionization curve is taken from the work of Millikan, Neher, and Pickering[24] at 50°N magnetic latitude. Their curve refers to air in a metallic

[24] Millikan, Neher, and Pickering, Phys. Rev. **61**, 397 (1942).

chamber of volume comparable to ours, so that the two results are comparable.[25]

It is seen that an appreciable fraction of the total ionization is due to heavy particles. About 18 percent of the total at 3 cm Hg (40 g/cm²), the point of maximum, can be ascribed to nuclear fragments. It is to be emphasized that the value given for the ionization due to bursts is not for heavy particles produced in air, but essentially for heavy particles produced in an air-copper mixture. For this reason it would be interesting to repeat the experiment with an ionization chamber having a light-element wall.

V. CONCLUSIONS

(1) The majority of bursts occurring in a thin-walled ionization chamber near the top of the atmosphere is produced by heavy particles, and the contribution of electron showers is negligible. (2) The abnormally large bursts observed at the highest altitudes receive a reasonable explanation in terms of the heavy-nucleus component of the primary radiation. This explanation accounts, in order of magnitude, for the size of these events, their absolute number, and their very strong variation in number with altitude. (3) The heavy nuclei which are responsible for the anomalous distribution of pulse sizes near the top of the atmosphere produce roughly 12 percent of the observed bursts. (4) It is shown that pulses due to heavy-nucleus-induced nuclear explosions in the chamber are negligible in number compared to pulses due to direct ionization by the passage of these nuclei through the chamber. (5) The total ionization due to nuclear fragments is determined as a function of altitude and extrapolates to 3200 ev per cm³ of argon (0°C, 76 cm Hg) per sec at zero pressure. When the air mass overhead is 40 g/cm², the ionization due to nuclear fragments is 1800 ev per cm³ of argon per sec, about 18 percent of the total cosmic-ray ionization.

[25] The results of Millikan, Neher, and Pickering are obtained directly in ion-pairs/cm³-sec-atmos in air. In order to compare their values with the results of this work which yields values in Mev of ionization the factor 32 electron volts per ion pair was used.

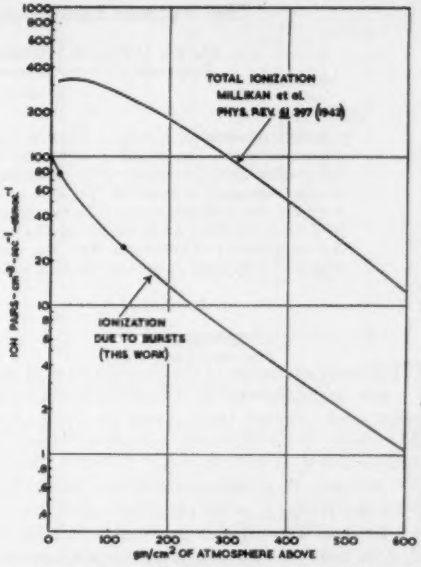

FIG. 6. Ionization of bursts of size greater than that produced by 0.1 polonium alpha compared with the total ionization (Millikan, Neher, and Pickering) produced by the cosmic radiation as a function of depth below the top of the atmosphere. Points for the burst-produced ionization were obtained at 1.27 and 8.9 cm Hg and a curve drawn through them based on the altitude dependence of bursts as measured in the present experiments.

The writer wishes to express his sincere gratitude to all who have made this investigation possible. He is especially indebted to Professor J. A. Wheeler for his generous help and advice in all phases of the work, and to Professors R. Sherr and G. T. Reynolds for many helpful discussions and suggestions. He is also indebted to Mr. G. A. Snow, with whom he worked jointly in the early part of the program.

Acknowledgment is due to the Friends of Elementary Particle Research for the gift of balloons used in some of the flights reported here.

The Nuclear Excitation of Ag^{107} and Ag^{109} by X-Rays*

ELIGIUS J. WOLICKI,† BERNARD WALDMAN, AND WALTER C. MILLER
Department of Physics, University of Notre Dame, Notre Dame, Indiana

(Received January 15, 1951)

X-rays, produced by monoergic electrons, were used to excite the separated isotopes of silver to their metastable states. The half-life of Ag^{107*} was found to be 44.0±1.0 seconds. The half-life of Ag^{109*} was found to be 40.0±1.0 seconds. These measurements are in agreement with those of Bradt, *et al.*, and the isotopic assignment of Helmholz. The electron energy was varied between 0.8 Mev and 2.3 Mev in order to obtain the excitation curves. The thresholds for x-ray excitation of both Ag^{107} and Ag^{109} were found to be below 0.8 Mev. An activation level in Ag^{107} was found at 1.285±0.018 Mev. An activation level in Ag^{109} was found at 1.210±0.018 Mev. The over-all cross section (i.e., per incident electron on thick gold target) is of the order of 10^{-34} cm^2 for both isotopes at 1.4 Mev.

I. INTRODUCTION

THE x-ray excitation of the isomeric state of silver was first observed by Collins and Feldmeier.[1] Further work[2] showed that, similar to indium,[3] one could obtain, from an x-ray excitation curve, two activation levels, at 0.85 Mev and 1.25 Mev. Wiedenbeck[4] repeated these experiments and was able to analyze the resulting x-ray excitation curve into evidence for some six activation levels, at 1.18, 1.59, 1.95, 2.32, 2.76, and 3.13 Mev. All of these experiments used ordinary silver consisting of essentially equal parts of the two isotopes 107 and 109.

The original investigation of Alvarez, Helmholz, and Nelson[5] established the metastable state in silver by a study of the decay of cadmium but did not identify the isotope. Helmholz[6] showed that in order to account for the presence of two internally converted gamma-rays, it was necessary to postulate that both isotopes of silver had metastable states of approximately 40-sec half-life. Bradt, *et al.*,[7] measured the half-lives and associated disintegration schemes of cadmium and silver, not knowing the isotopic assignment until Helmholz[8] identified the parent cadmium isotopes. The 94-kev gamma-ray of half-life 44.3 sec was assigned to Ag^{107*}, and the 89-kev gamma-ray of half-life 39.2 sec was assigned to Ag^{109*}.

With the availability of the separated isotopes of silver, it became desirable (a) to determine *directly* the half-lives and isotopic assignments, and (b) to obtain the x-ray excitation curve for each isotope.

The analysis and interpretation of x-ray excitation curves has been discussed by Miller and Waldman.[3]

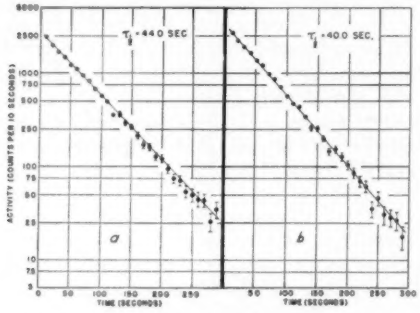

FIG. 1. (a) Decay of Ag^{107*}. (b) Decay of Ag^{109*}.

II. EXPERIMENTAL PROCEDURE

(A) Irradiation

The separated isotopes of silver were obtained as chlorides, and metallic foils were prepared by electroplating on platinum disks $\frac{7}{8}''$ in diameter. The isotopic proportions and the foil thicknesses were as follows. The Ag^{107} contained 3.2 percent of Ag^{109} and was 10.3 mg/cm^2 thick; the Ag^{109} contained 0.1 percent of Ag^{107} and was 10.8 mg/cm^2 thick. These thicknesses were greater than the range of the conversion electrons to be detected.

The x-rays were produced with the Notre Dame electrostatic generator by stopping a well-collimated beam of monoergic electrons in a thick ($\frac{1}{16}''$) gold target. As in previous experiments,[3] the current was monitored by a Brown recording potentiometer, and the voltage was measured and stabilized by a null-type generating voltmeter and associated control circuits. The voltage calibration was based on the photo-disintegration thresholds of beryllium and deuterium as measured by Mobley and Laubenstein.[9]

(B) Counting

The activities encountered in this experiment were low owing to the following facts:

* This work was supported by the joint program of the ONR and AEC.

† AEC Predoctoral Fellow; now at the University of Iowa, Iowa City, Iowa.

[1] G. B. Collins and J. R. Feldmeier, Phys. Rev. **59**, 937 (1941).
[2] J. R. Feldmeier, Ph.D. thesis, Univ. of Notre Dame (1942).
[3] W. C. Miller and B. Waldman, Phys. Rev. **75**, 425 (1949).
[4] M. L. Wiedenbeck, Phys. Rev. **67**, 92 (1945).
[5] Alvarez, Helmholz, and Nelson, Phys. Rev. **57**, 660 (1940).
[6] A. C. Helmholz, Phys. Rev. **60**, 160 (1941).
[7] Bradt, Gugelot, Huber, Medicus, Preiswerk, Scherrer, and Steffen, Helv. Phys. Acta **20**, 153 (1947).
[8] A. C. Helmholz, Phys. Rev. **70**, 982 (1946).
[9] R. C. Mobley and R. A. Laubenstein, Phys. Rev. **80**, 309 (1950).

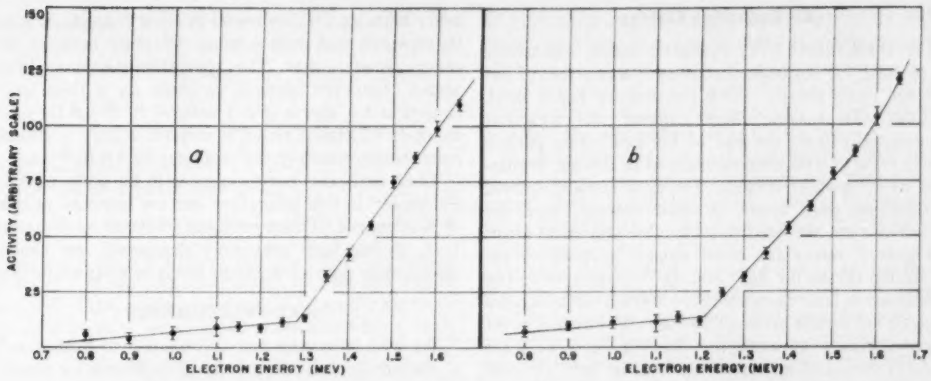

FIG. 2. (a) Thick target x-ray excitation curve of Ag^{107}. (b) Thick target x-ray excitation curve of Ag^{109}.

(1). *Small cross section.* This necessitated large electron beam currents (250 μamp average).

(2). *Short half-life.* This required a minimum delay between the end of the irradiation and the beginning of the counting. This delay was reduced to considerably less than one half-life.

(3). *Low energy conversion electrons.* Since the absorption of thin (1.5 mg/cm²) windows in Tracerlab and similar counters was found to be prohibitive, it was necessary to place the irradiated foil within the counter itself. Silver-cathode, argon-ether filled counters, after irradiation by the intense x-ray beam, had a high counting rate due to increased photosensitivity. The counting rate could be reduced by light shielding. Nevertheless, light-tight counters thus irradiated showed a spurious activity which persisted after the silver activity had decayed. Evacuated silver-cathode counters were irradiated and filled, immediately after irradiation, with a non-irradiated gas mixture. These, too, exhibited a small activity having a half-life greater than 10 times that of the metastable silver. A 0.1 mg/cm² coating of zapon lacquer on the silver reduced, but did not obliterate, this spurious activity. Finally, a Nuclear Instrument Corporation "*Q*-gas" flow counter was used. This was modified so that the sample holder was flushed with *Q*-gas before the sample was introduced into the counting volume. This reduced the waiting period for reliable counting from about 200 to about 10 sec. The total delay time between the end of the irradiation and the beginning of the counting was kept constant at 25 sec. The use of the flow counter confirmed the belief that many surfaces emit low energy "delayed" electrons for periods varying from 30 sec to several minutes. Both the "delayed" electrons and the increased photosensitivity have been observed by other workers under different circumstances.[10] Of the substances examined for these "delayed" electrons, zapon lacquer is an emitter, whereas collodion and Lucite are practically non-emitters. Consequently, the silver foils were mounted on Lucite disks, for handling purposes, and were coated with 0.2 mg/cm² collodion films.

[10] M. L. Wiedenbeck and H. R. Crane, Phys. Rev. **75**, 1268 (1949).

III. RESULTS

(A) Half-Lives

Irradiations were made at 2.6 Mev with a 200 μamp beam current, and initial activities of about 100 counts/sec resulted. Data were obtained by photographing the scaler and clock every five seconds over a period of about 300 sec. Statistical errors were reduced by adding corresponding points from separate decay curves. The decay curves for Ag^{107*} and Ag^{109*} are shown in Fig. 1. The half-life of Ag^{107*} is 44.0±1.0 sec and that of Ag^{109*} is 40.0±1.0 sec. Bradt, *et al.*,[7] measured half-lives of 44.3±0.2 sec and 39.2±0.2 sec, and Helmholz[8] assigned these to Ag^{107*} and Ag^{109*}, respectively. The direct measurements obtained in this experiment verify this assignment.

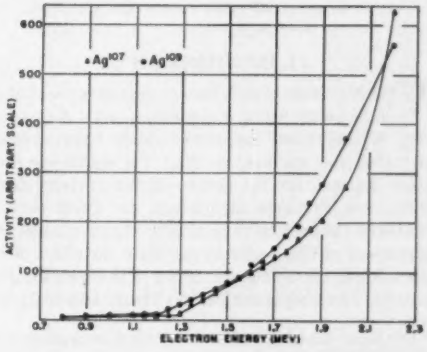

FIG. 3. Thick target x-ray excitation curves.

(B) Excitation Curves

The thick target x-ray excitation curve is obtained by plotting the normalized activity as a function of the electron beam energy. Since the activity has a short half-life, the varying target current was weighted exponentially from the end of the irradiation period. Thus, all activities were normalized to infinite irradiation with constant current. For each isotope, several irradiations were made at each voltage, and the activities were averaged to reduce the statistical error.

Figure 2 shows the lower energy portions of the excitation curves for Ag^{107} and Ag^{109}, respectively. The thresholds in both cases are below 800 kev, although the data do not permit accurate location. The breaks in the curves indicate an activation level in Ag^{107} at 1.285 $\pm$0.018 Mev and an activation level in Ag^{109} at 1.210 $\pm$0.018 Mev. Figure 3 shows both excitation curves over the entire energy range investigated and emphasizes the 75-kev difference between the corresponding levels in the two nuclei. In considering the close similarity between the two nuclei in other respects, it is to be expected that such a small difference between the energy levels exists. The approximate over-all cross section (i.e., per electron incident on a thick gold target) at 1.4 Mev is of the order of 10^{-34} cm^2 for both isotopes. In Figs. 2 and 3, to convert *activity* to *over-all cross section*, multiply the ordinates by 4×10^{-36} cm^2.

These excitation curves agree with the early work of Feldmeier[2] in this laboratory but are contrary to that of Wiedenbeck.[4] This experiment is further confirmation that, as has been previously discussed,[3] one cannot obtain more than a few energy levels by x-ray excitation.

ACKNOWLEDGMENTS

We wish to express our appreciation to Professor A. C. Helmholz of the University of California for supplying the separated silver isotopes. Assistance in taking data and operating the electrostatic generator was generously contributed by E. J. Schillinger and T. F. Ruane.

PHYSICAL REVIEW VOLUME 82, NUMBER 4 MAY 15, 1951

Effect of Finite Nuclear Size on the Elastic Scattering of Electrons*

LOUIS K. ACHESON, JR.†
Physics Department, Massachusetts Institute of Technology, Cambridge, Massachusetts
(Received August 15, 1950)

The effect of the finite size of the nucleus on the elastic scattering of electrons with energies in the neighborhood of 20 Mev has been calculated for two simple spherical nuclear models: a uniform charge distribution, and a uniform shell charge distribution, both of radius $R=1.45\times10^{-13}A^{\frac{1}{3}}$ cm. An exact phase shift analysis has been made, the phase shifts differing appreciably from those for a point nucleus only in the $j=\frac{1}{2}$ state.

Phase shifts for elements of $Z=13$, 29, 50, and 79 have been plotted as a function of energy over the interval from 15 to 35 Mev, permitting the calculation of any desired cross section within this range. Representative curves of the ratio of the scattering cross section for the finite nucleus to that for a point nucleus have been plotted.

The difference in the scattering due to the two models is large enough so that accurate experiments might distinguish between them, the actual average nuclear charge distribution probably falling somewhere between these two cases. The ability to differentiate between the two models, however, depends on the accuracy with which nuclear radii are known.

I. INTRODUCTION

WHEN a beam of high energy electrons ($\sim$20 Mev) falls on an atom, a significant part of the scattering results from electrons which have actually penetrated the nucleus, so that the scattering cross section depends on the nature of the nuclear charge distribution. Previous calculations for lower energies have taken the nucleus to be simply a point charge. It is the purpose of this paper to calculate the effect of the finite nuclear size on the scattering of these high energy electrons. Two simple nuclear models are assumed: (1) a uniform spherical charge distribution, and (2) a shell charge distribution, with the charge distributed uniformly over the surface of the nucleus.

Rose[1] has already treated this problem by means of the Born approximation, which is valid for the light elements. Here exact results are obtained by means of a phase shift analysis.

For the energies of interest here, it is necessary to use the Dirac relativistic theory of the electron. Relativistic scattering theory, for spherically symmetric scattering centers, involves the solution of a pair of simultaneous first-order differential equations, the well-known Dirac

* This paper was supported in part by the joint program of the ONR and AEC.
† Now at Hughes Aircraft Company, Culver City, California.

[1] M. E. Rose, Phys. Rev. **73**, 279 (1948).

radial equations.[2]

$$\begin{aligned}(1/\hbar)[(E-V/c)+mc]F_\kappa \\ +(dG_\kappa/dr)-[(\kappa-1)/r]G_\kappa=0, \\ -(1/\hbar)[(E-V/c)-mc]G_\kappa \\ +(dF_\kappa/dr)+[(\kappa+1)/r]F_\kappa=0,\end{aligned} \quad (1)$$

where $\kappa=\pm(j+\frac{1}{2})$, $j=l\pm\frac{1}{2}$.

From the asymptotic form of G_κ,

$$G_\kappa\sim[\sin(kr-\tfrac{1}{2}l\pi+\eta_\kappa)]/kr, \quad (2)$$

one can determine the phase shift η_κ, depending on the potential V of the scattering center, and the relativistic energy E of the incident electrons. The scattering cross section is given in terms of the phase shifts by

$$\sigma(\theta)=|f(\theta)|^2+|g(\theta)|^2,$$

$$\begin{aligned}f(\theta)=\frac{1}{2ik}\sum_{\kappa=1}^{\infty}\kappa[(e^{2i\eta_\kappa}-1)P_{\kappa-1}(\cos\theta) \\ +(e^{2i\eta_{-\kappa}}-1)P_\kappa(\cos\theta)], \quad (3) \\ g(\theta)=\frac{1}{2ik}\sum_{\kappa=1}^{\infty}[-e^{2i\eta_\kappa}P_{\kappa-1}{}^1(\cos\theta)+e^{2i\eta_{-\kappa}}P_\kappa{}^1(\cos\theta)],\end{aligned}$$

where $P_\kappa{}^1$ and P_κ are associated Legendre polynomials.

The terms in η_κ represent the contribution of the $j=l+\frac{1}{2}$ states to the scattering, while those in $\eta_{-\kappa}$ represent the $j=l-\frac{1}{2}$ states. (η_κ and $\eta_{-\kappa}$ correspond to η_l and η_{-l-1} in Mott's notation but refer to the same j value rather than the same l value.)

II. SOLUTION OF THE DIRAC RADIAL EQUATIONS

For energies of 20 Mev and above, the rest energy of the electron plays a small role, and the treatment of these equations is greatly simplified if it can be neglected completely. This is a better approximation, even, than it appears at first glance; for if kept, the rest mass appears in the results primarily in the form $E^2-m^2c^4$.

Making this simplification, the radial equations become,

$$\begin{aligned}(k-U)F_\kappa+G_\kappa'-[(\kappa-1)/r]G_\kappa=0, \\ -(k-U)G_\kappa+F_\kappa'+[(\kappa+1)/r]F_\kappa=0,\end{aligned} \quad (4)$$

where $k=E/\hbar c=p/\hbar$, $U=V/\hbar c$.

If one makes the substitution

$$F=ir^{-1}(A\psi-B\phi), \quad G=r^{-1}(A\psi+B\phi), \quad (5)$$

where A and B are constants, and then eliminates $B\phi$ from the pair of equations, one obtains the following second-order differential equation for ψ.

$$\psi''+\left[(k-U)^2+\frac{i(k-U-rU')}{r}-\frac{\kappa^2-\frac{1}{4}}{r^2}\right]\psi=0. \quad (6)$$

If ψ is eliminated rather than ϕ, the resulting equation is the complex conjugate of the above equation; thus, the problem is simplified by the fact that one can take $\phi=\psi^*$, and only one second-order equation need be solved.

The constants A and B enter the picture when the solution of the second-order equations is also required to satisfy the pair of first-order equations.

The equation for ψ is to be solved for a potential which, inside the nucleus, depends on the specific nuclear model chosen but which, outside the nucleus, equals the coulomb potential that would exist if all the charge were located at a point.

Separate solutions for these two regions are obtained with the requirement that their values and slopes coincide at the nuclear radius. This, together with the boundary condition that $\psi(0)=0$, (in order that G be finite at the origin) determines ψ uniquely, except for a constant multiplying factor which can be absorbed into A.

Thus, for $r>R$, region II, the potential is $U=-\alpha/r$, where $\alpha=Ze^2/\hbar c$,

$$\psi_{II}''+[(k+\alpha/r)^2+ik/r-(\kappa^2-\tfrac{1}{4})/r^2]\psi_{II}=0. \quad (7)$$

This equation reduces very simply to Whittaker's confluent hypergeometric equation, and the general solution[3] can be written

$$\psi_{II}=A_1\psi_{c1}+A_2\psi_{c2},$$

$$\psi_{c1}=r^{\rho+\frac{1}{2}}e^{-ikr}\,{}_1F_1(\rho+i\alpha;\,2\rho+1;\,2ikr),$$

where $\rho=(\kappa^2-\alpha^2)^{\frac{1}{2}}$,

$$\psi_{c2}=r^{-\rho+\frac{1}{2}}e^{-ikr}\,{}_1F_1(-\rho+i\alpha;\,-2\rho+1;\,2ikr). \quad (8)$$

Matching the inside and outside wave functions and derivatives at the nuclear radius,

$$\begin{aligned}\psi_I(R)=A_1\psi_{c1}(R)+A_2\psi_{c2}(R), \\ \psi_I'(R)=A_1\psi_{c1}'(R)+A_2\psi_{c2}'(R).\end{aligned}$$

Solving for the constants A_1 and A_2,

$$A_1=(\psi_I\psi_{c2}'-\psi_{c2}\psi_I'/\psi_{c1}\psi_{c2}'-\psi_{c2}\psi_{c1}'),$$

and

$$A_2=(\psi_{c1}\psi_I'-\psi_I\psi_{c1}'/\psi_{c1}\psi_{c2}'-\psi_{c2}\psi_{c1}'. \quad (9)$$

Since it is the asymptotic form of G which is of interest, it is the asymptotic form of ψ which will be considered here. Using the well-known asymptotic expressions for the confluent hypergeometric functions, one has

$$\begin{aligned}\psi_{c1}\sim\frac{\Gamma(2\rho+1)}{\Gamma(\rho+1-i\alpha)}(-2ik)^{-\rho}r^{\frac{1}{2}}e^{-ikr-i\alpha\ln 2kr}e^{-\frac{1}{2}\pi\alpha}, \\ \psi_{c2}\sim\frac{\Gamma(-2\rho+1)}{\Gamma(-\rho+1-i\alpha)}(-2ik)^{\rho}r^{\frac{1}{2}}e^{-ikr-i\alpha\ln 2kr}e^{-\frac{1}{2}\pi\alpha}.\end{aligned} \quad (10)$$

[2] Mott and Massey, *Theory of Atomic Collisions* (Clarendon Press, Oxford, 1949), 2nd edition, p. 74.

[3] Whittaker and Watson, *Modern Analysis* (University Press, Cambridge, 1927), p. 337.

The ratio of ψ_{c1} to ψ_{c2} is asymptotically a constant, which will be called κ_a.

$$\kappa_a=(-2ik)^{2\rho}\frac{\Gamma(-2\rho+1)}{\Gamma(2\rho+1)}\frac{\Gamma(\rho+1-i\alpha)}{\Gamma(-\rho+1-i\alpha)}. \tag{11}$$

Asymptotically, ψ can then be written,

$$\psi\sim A_1\psi_{c1}(1+\kappa_a A_2/A_1)\sim\psi_{c1}(1+\xi), \tag{12}$$

where the arbitrary constant in ψ_I has been chosen so that $A_1=1$, and

$$\xi=\kappa_a A_2/A_1$$
$$=-\kappa_a\frac{\psi_{c1}\,\psi_1'/\psi_1-\psi_{c1}'/\psi_{c1}}{\psi_{c2}\,\psi_1'/\psi_1-\psi_{c2}'/\psi_{c2}}\text{ evaluated at }r=R. \tag{13}$$

It is seen that only the logarithmic derivative of ψ_I appears.

The question now is how ξ is related to the phase shift η_s, which is to be determined from the asymptotic form of G_s. It becomes necessary to find the ratio A/B, which is obtained from one of the first-order equations.

Consider first the case of a point nucleus, the coulomb potential. The first radial equation gives

$$\frac{A_c}{B_c}=e^{2ikr}\frac{(-\rho+\kappa+i\alpha)F_\rho^*-rF_\rho^{*\prime}}{(\rho-\kappa+i\alpha)F_\rho+rF_\rho'}, \tag{14}$$

where $F_\rho={}_1F_1(\rho+i\alpha;\,2\rho+1;\,2ikr)$.

Since this must be a constant, it can be evaluated at the origin.

$$A_c/B_c=-(\rho-\kappa-i\alpha)/(\rho-\kappa+i\alpha). \tag{15}$$

The asymptotic form of $G_s^{(c)}$ can then be written

$$G_s^{(c)}\sim 1/kr\,\sin(kr+\alpha\,\ln 2kr-\tfrac{1}{2}l\pi+\chi_s), \tag{16}$$

where

$$e^{2i\chi_s}=\frac{\rho-\kappa+i\alpha}{\rho-\kappa-i\alpha}\frac{\Gamma(\rho+1-i\alpha)}{\Gamma(\rho+1+i\alpha)}e^{-\pi i(\rho-l)}. \tag{17}$$

The appearance of the log term in the asymptotic form arises from the fact that the potential falls off as $1/r$.

It remains to be seen how this expression is altered by the assumption of a finite nuclear size.

$$G_s\sim r^{-1}(A\psi+B\psi^*)$$
$$\sim r^{-1}[A(1+\xi)\psi_{c1}+B(1+\xi^*)\psi_{c1}^*].$$

This can be written as

$$G_s\sim 1/kr\,\sin(kr+\alpha\,\ln 2kr-\tfrac{1}{2}l\pi+\chi_s+\delta_s), \tag{18}$$

where

$$e^{2i\delta_s}=\frac{A_c}{B_c}\frac{B}{A}\frac{1+\xi^*}{1+\xi}. \tag{19}$$

The phase shift for the case of a finite nuclear size is given by

$$\eta_s=\chi_s+\delta_s. \tag{20}$$

The ratio A/B is still to be determined, and going back to the first radial equation, one obtains

$$A/B=-e^{2ikr}$$
$$\times\frac{[(rF_\rho'+A_\rho F_\rho)+(\xi/\kappa_a)r^{-2\rho}(rF_{-\rho}'+A_{-\rho}F_{-\rho})]^*}{(rF_\rho'+A_\rho F_\rho)+(\xi/\kappa_a)r^{-2\rho}(rF_{-\rho}'+A_{-\rho}F_{-\rho})}, \tag{21}$$

where $A_\rho=\rho-\kappa+i\alpha$, which can be written

$$\frac{A}{B}=\frac{A_c}{B_c}\cdot\frac{1+(A_2/A_1)^*r^{-2\rho}K^*}{1+(A_2/A_1)r^{-2\rho}K}, \tag{22}$$

where

$$K=\frac{rF_{-\rho}'+A_{-\rho}F_{-\rho}}{rF_\rho'+A_\rho F_\rho}.$$

Here it is most convenient to use the asymptotic expressions to evaluate A/B; however, one must take care to use the complete asymptotic form of the confluent hypergeometric functions when taking derivatives.

$${}_1F_1(a;\,c;\,z)\sim\frac{\Gamma(c)}{\Gamma(c-a)}(-z)^{-a}+\frac{\Gamma(c)}{\Gamma(a)}e^z z^{a-c}.$$

It can be shown that the expression for A/B reduces to

$$\frac{A}{B}=\frac{A_c}{B_c}\cdot\frac{1+\frac{1}{2}(\kappa_a+\kappa_b)^*(A_2/A_1)^*}{1+\frac{1}{2}(\kappa_a+\kappa_b)(A_2/A_1)}, \tag{23}$$

where

$$\kappa_b=(2ik)^{2\rho}\frac{\Gamma(1-2\rho)}{\Gamma(1+2\rho)}\frac{\Gamma(\rho+i\alpha)}{\Gamma(-\rho+i\alpha)}, \tag{24}$$

and the phase shift δ_s is then given by

$$e^{2i\delta_s}=\frac{1+\frac{1}{2}(\kappa_a+\kappa_b)(A_2/A_1)}{1+\frac{1}{2}(\kappa_a+\kappa_b)^*(A_2/A_1)^*}\cdot\frac{1+\kappa_a^*(A_2/A_1)^*}{1+\kappa_a(A_2/A_1)}. \tag{25}$$

Using the relation $\Gamma(1-z)\Gamma(z)=\pi/\sin\pi z$, κ_a and κ_b can be written,

$$\kappa_a=\frac{\sin\pi(\rho+i\alpha)}{\sin 2\pi\rho}\frac{\rho-i\alpha}{2\rho}\left|\frac{\Gamma(\rho+i\alpha)}{\Gamma(2\rho)}\right|^2 e^{-\pi i\rho}(2k)^{2\rho},$$
$$\kappa_b=-\frac{\sin\pi(\rho-i\alpha)}{\sin 2\pi\rho}\frac{\rho-i\alpha}{2\rho}\left|\frac{\Gamma(\rho+i\alpha)}{\Gamma(2\rho)}\right|^2 e^{\pi i\rho}(2k)^{2\rho}. \tag{26}$$

Thus, the phase shift δ_s is expressed in terms of A_2/A_1, which in turn depends on the logarithmic derivative of the inside wave function evaluated at the nuclear radius.

The next step is to see how this phase shift enters into the expression for the scattering cross section.

III. SCATTERING CROSS SECTION

Letting $\eta_\kappa=\chi_\kappa+\delta_\kappa$, the expressions for f and g can be written as

$$f=f_c+\frac{1}{2ik}\sum_{\kappa=1}^{\infty}\kappa[e^{2i\chi_\kappa}(e^{2i\delta_\kappa}-1)P_{\kappa-1}+e^{2i\chi_{-\kappa}}(e^{2i\delta_{-\kappa}}-1)P_\kappa],$$

and

$$g=g_c+\frac{1}{2ik}\sum_{\kappa=1}^{\infty}[-e^{2i\chi_\kappa}(e^{2i\delta_\kappa}-1)P_{\kappa-1}^1+e^{2i\chi_{-\kappa}}(e^{2i\delta_{-\kappa}}-1)P_\kappa^1], \quad (27)$$

where f_c and g_c are the values of f and g which give the coulomb scattering.

It can be shown that $\chi_\kappa=\chi_{-\kappa}$ and $\delta_\kappa=\delta_{-\kappa}$ in the approximation of neglecting the rest mass; therefore, one has

$$f=f_c+\frac{1}{2ik}\sum_{\kappa=1}^{\infty}\kappa e^{2i\chi_\kappa}(e^{2i\delta_\kappa}-1)(P_\kappa+P_{\kappa-1}),$$

and

$$g=g_c+\frac{1}{2ik}\sum_{\kappa=1}^{\infty}e^{2i\chi_\kappa}(e^{2i\delta_\kappa}-1)(P_\kappa^1-P_{\kappa-1}^1). \quad (28)$$

Using recurrence relations between associated Legendre functions, one has

$$P_\kappa-P_{\kappa-1}=\kappa\tan\tfrac{1}{2}\theta\cdot(P_\kappa+P_{\kappa-1}). \quad (29)$$

Thus, g can be written in term of f

$$g-g_c=\tan\tfrac{1}{2}\theta\cdot(f-f_c). \quad (30)$$

The scattering cross section is then

$$\sigma=\sigma_c+2Re[(f_c+\tan\tfrac{1}{2}\theta\cdot g_c)(f-f_c)^*]+\sec^2\tfrac{1}{2}\theta\cdot|f-f_c|^2, \quad (31)$$

where $\sigma_c=|f_c|^2+|g_c|^2$.

McKinley and Feshbach[4] have given the coulomb scattering cross section in terms of two functions, F and G (not to be confused with the radial functions F_κ and G_κ).

$$\begin{aligned}kf_c&=G-iq'F,\\ kg_c&=\tan\tfrac{1}{2}\theta\cdot G+iq'\cot\tfrac{1}{2}\theta\cdot F,\\ k^2\sigma_c&=|G|^2\sec^2\tfrac{1}{2}\theta+q'^2|F|^2\csc^2\tfrac{1}{2}\theta,\end{aligned} \quad (32)$$

where $q'=(\alpha/\beta)(1-\beta^2)^{\frac{1}{2}}$, $\beta=v/c$; $q'\simeq\alpha mc^2/E$.

G and F are given by the following expressions (taking $\alpha/\beta\simeq\alpha$):

$$\begin{aligned}&G=G_0+G_1,\quad F=F_0+F_1,\\ &G_0=\tfrac{1}{2}\alpha\cot^2\tfrac{1}{2}\theta\exp(i\alpha\ln\sin^2\tfrac{1}{2}\theta)\cdot[\Gamma(1-i\alpha)/\Gamma(1+i\alpha)],\\ &F_0=(i/\alpha)\tan^2\tfrac{1}{2}\theta G_0,\\ &G_1=E(\theta)\alpha^2+H(\theta)\alpha^3+[I(\theta)+J(\theta)]\alpha^4,\\ &F_1=A(\theta)\alpha^2+B(\theta)\alpha^3+[C(\theta)+D(\theta)]\alpha^4,\end{aligned} \quad (33)$$

where the angular functions are tabulated in the paper cited.

The terms involving q' are negligible except for large angles, where F becomes much larger than G. Thus, for angles up to 150°, the coulomb cross section can be written

$$k^2\sigma_c=|G|^2\sec^2\tfrac{1}{2}\theta \quad (34)$$

with an error of less than one percent.

Noting that

$$f_c+g_c\tan\tfrac{1}{2}\theta=k^{-1}\sec^2\tfrac{1}{2}\theta\cdot G,$$

the ratio σ/σ_c becomes

$$\frac{\sigma}{\sigma_c}=1+\frac{2}{|G|^2}\sum_{\kappa=1}^{\infty}\kappa(P_\kappa+P_{\kappa-1})Re\left[Ge^{-2i\chi_\kappa}\left(\frac{e^{2i\delta_\kappa}-1}{2i}\right)^*\right]+\frac{1}{|G|^2}\left|\sum_{\kappa=1}^{\infty}\kappa(P_\kappa+P_{\kappa-1})e^{2i\chi_\kappa}\left(\frac{e^{2i\delta_\kappa}-1}{2i}\right)\right|^2. \quad (35)$$

The phase shifts, δ_κ, will decrease very rapidly with increasing κ since, classically speaking, those electrons whose angular momenta are such that they do not penetrate the nucleus itself cannot tell the difference between a finite nucleus and a point nucleus. For most of the energies considered here, in fact, only δ_1 will be important.

Now, $P_1+P_0=\cos\theta+1=2\cos^2\tfrac{1}{2}\theta$

$$\therefore\quad \frac{\sigma}{\sigma_c}=1+\frac{4\cos^2\tfrac{1}{2}\theta}{|G|^2}Re\left[Ge^{-2i\alpha}\left(\frac{e^{2i\delta_1}-1}{2i}\right)^*\right]+\frac{4\cos^4\tfrac{1}{2}\theta}{|G|^2}\sin^2\delta_1. \quad (36)$$

This expression is valid for those energies for which δ_2 is negligible, for all Z, and for scattering angles up to 150°.

For low Z elements, such that α^2 is negligible, $G\simeq G_0$, and for energies such that δ_2 and δ_1^2 are also negligible, the cross section becomes

$$\frac{\sigma}{\sigma_c}=1+\frac{8\delta_1}{\alpha}\sin^2\tfrac{1}{2}\theta\cos(\alpha\ln\sin^2\tfrac{1}{2}\theta+2\alpha). \quad (37)$$

Having seen how the scattering cross section depends on δ_κ, it is now necessary to find out just how large these phase shifts are for the different nuclear models.

IV. EVALUATION OF δ_κ FOR SPECIFIC NUCLEAR MODELS

To determine the phase shift, one must solve Eq. (6) for the region within the nucleus and evaluate ψ_1'/ψ_1 at the nuclear radius.

The easiest case to handle mathematically is the shell charge distribution, where the potential is simply

[4] W. A. McKinley, Jr. and H. Feshbach, Phys. Rev. 74, 1759 (1948).

TABLE I. $|G|^2$.

Z	30°	60°	90°	120°	150°
13	0.467	0.0226	2.58×10^{-3}	2.91×10^{-4}	1.36×10^{-4}
29	2.54	0.1314	0.0156	1.80×10^{-3}	8.43×10^{-5}
50	8.28	0.491	0.0629	7.62×10^{-3}	3.55×10^{-4}
79	22.31	1.740	0.269	0.0370	1.788×10^{-4}

Table II. $Ge^{-2i\chi_1}$.

Z	30°	60°	90°	120°	150°
13	0.672	0.150	0.0508	0.01705	0.00368
	$-0.122i$	$-0.0096i$	$-0.00036i$	$0.00042i$	$0.00015i$
29	1.449	0.358	0.1248	0.0424	0.00915
	$-0.665i$	$-0.0588i$	$-0.0037i$	$0.0019i$	$0.00078i$
50	1.951	0.660	0.249	0.0873	0.0187
	$-2.114i$	$-0.237i$	$-0.026i$	$0.0029i$	$0.0021i$
79	0.0314	0.949	0.481	0.190	0.0423
	$-4.72i$	$-0.916i$	$-0.193i$	$-0.0314i$	$-0.0006i$

$U=-\alpha/R$. The wave equation then becomes

$$\psi_I''+\left[\left(k+\frac{\alpha}{R}\right)^2+\frac{i(k+\alpha/R)}{r}-\frac{\kappa^2-\frac{1}{4}}{r^2}\right]\psi_I=0. \quad (38)$$

This equation also reduces to Whittaker's confluent hypergeometric equation. The solution going to zero at the origin is

$$\psi_I=e^{-i(k+\alpha/R)r}r^{|\kappa|+\frac{1}{2}} \times {}_1F_1(|\kappa|+\tfrac{1}{2}-i\eta;2|\kappa|+1;2i(k+\alpha/R)r). \quad (39)$$

(The absolute signs about κ can be omitted since it is only positive κ that is now being considered.)

The phase shift depends on A_2/A_1, which is given by Eq. (9). If one writes

$$\psi_{c1}=e^{-ikr}r^{\rho+\frac{1}{2}}F_\rho,$$

$$\psi_{c2}=e^{-ikr}r^{-\rho+\frac{1}{2}}F_{-\rho}, \quad (40)$$

and

$$\psi_I=e^{-ik_\alpha r}r^{\kappa+\frac{1}{2}}F_\kappa,$$

where

$$F_\rho={}_1F_1(\rho+i\alpha;2\rho+1;2ikr),$$
$$F_\kappa={}_1F_1(\kappa;2\kappa+1;2ik_\alpha r),$$

and

$$k_\alpha=k+\alpha/R,$$

then

$$\frac{A_2}{A_1}=-R^{2\rho}\frac{RF_\rho'+(\rho-\kappa+i\alpha-RF_\kappa'/F_\kappa)F_\rho}{RF_{-\rho}'+(-\rho-\kappa+i\alpha-RF_\kappa'/F_\kappa)F_{-\rho}}, \quad (41)$$

and δ_κ is determined from Eq. (25).

For the uniform charge distribution, the potential within the nucleus is $U=-(\alpha/2R)(3-r^2/R^2)$, which leads to the equation

$$\frac{d^2\psi_I}{dx^2}-\left[\frac{\kappa^2-\frac{1}{4}}{x^2}-i\frac{k_{\alpha'}R}{x}-(k_{\alpha'}R)^2+\tfrac{3}{2}i\alpha x+\alpha k_{\alpha'}Rx^2-\tfrac{1}{4}\alpha^2x^4\right]\psi_I=0, \quad (42)$$

where $x=r/R$, $k_{\alpha'}=k+3\alpha/2R$.

This equation cannot be put into any of the standard forms, but noting that all that is required is $\psi_I'(R)/\psi_I(R)$, one can make the substitution

$$\Psi=(d\psi_I/dx)/\psi_I \quad (43)$$

which reduces the second-order equation to the Riccati first-order equation

$$d\Psi/dx+\Psi^2=J(x), \quad (44)$$

where $J(x)$ is the coefficient of ψ_I in Eq. (42).

This equation can be solved by the power series method, letting

$$\Psi=-\frac{1}{\kappa}\sum_{n=0}^{\infty}a_nx^n \quad (45)$$

and evaluating the coefficients a_n by the usual procedure.

Evaluating Ψ at $r=R$; i.e., $x=1$,

$$\Psi_{r=R}=\sum_{n=0}^{\infty}a_n. \quad (46)$$

In terms of Ψ, A_2/A_1 is

$$\frac{A_2}{A_1}=-R^{2\rho}\frac{RF_\rho'+(\rho+\frac{1}{2}-ikR-\Psi)F_\rho}{RF_{-\rho}'+(-\rho+\frac{1}{2}-ikR-\Psi)F_{-\rho}}. \quad (47)$$

Calculations have been made for four elements, of atomic number 13, 29, 50, and 79, and for a number of energies between 15 and 35 Mev. The values of $|G|^2$ $Ge^{-2i\chi_1}$, for use in Eq. (36), are listed in Tables I and II.

Using the formula $R=1.45\times10^{-13}A^{\frac{1}{3}}$ cm for the nuclear radius, and with $k=E/\hbar c=0.507\times10^{11}E_{\text{Mev}}$ cm^{-1}, kR is given by $kR=7.35\times10^{-3}E_{\text{Mev}}A^{\frac{1}{3}}$.

The phase shifts, δ_1, are plotted against energy in Figs. 1 and 2. The scattering cross sections for the above Z at 20 and 30 Mev, and for energies of 15, 25, and 35 Mev at $Z=29$ for both the shell and uniform charge distributions, are plotted in Fig. 3 (*a*, *b*, and *c*).

V. DISCUSSION OF RESULTS

The general effect produced by the finite size of the nucleus is seen to be a reduction of the scattering cross section, predominating at large angles. This is in agreement with the wave picture of the scattering; for if the

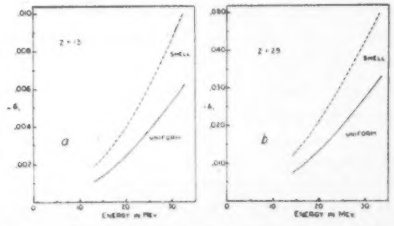

FIG. 1. Phase shift δ_1 as a function of energy for shell and uniform models for (*a*) $Z=13$, (*b*) $Z=29$.

nucleus is considered shrunk to a point, then the scattered waves from all elements of the nuclear charge will arrive at the observation point in phase, and, therefore, with maximum intensity. With a finite nucleus, the scattered waves from the different elements will not be in phase, interference will occur, and the intensity will usually be reduced. Furthermore, the forward scattering will suffer less reduction, since the path lengths of the different scattered waves will be more nearly the same and the waves more nearly in phase.

In these calculations, R has been taken as $1.45 \times 10^{-13} A^{\frac{1}{3}}$ cm, but varying the radius, with a fixed Z, produces exactly the same effect as varying the energy, because of the dependence of the phase shift on kR. Thus, the curves of phase shift as a function of energy give equally well their dependence on the radius.

The different charge distributions produce a considerable difference in the scattering, particularly for the higher energies and higher Z, thus raising the possibility that accurate scattering experiments will yield information regarding nuclear structure. However, this effect is greatest at large scattering angles, which makes it difficult to measure, since the coulomb cross section becomes very small at large angles.

It is also true that one cannot separate the two effects of type of charge distribution and size of nucleus. This comes from the fact that only one phase shift, δ_1, is necessary to describe the scattering. In general, the phase shift obtained from the uniform model at a given energy and Z is also given by the shell model using a radius about three-fourths that of the uniform model. Furthermore, the variation of the phase shift with energy for the two models does not differ enough to distinguish between them. However, radii are known accurately enough so that some indication of the nature of the nuclear charge distribution should be obtainable.

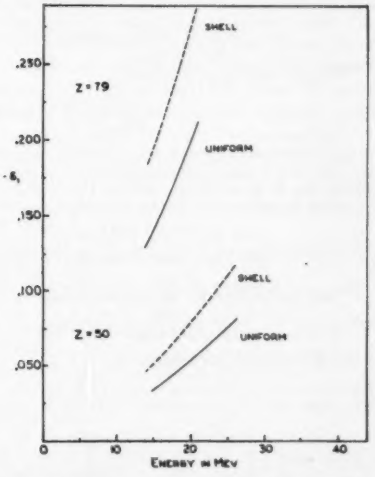

FIG. 2. Phase shift δ_1 as a function of energy for shell and uniform models for $Z=50$ and 79.

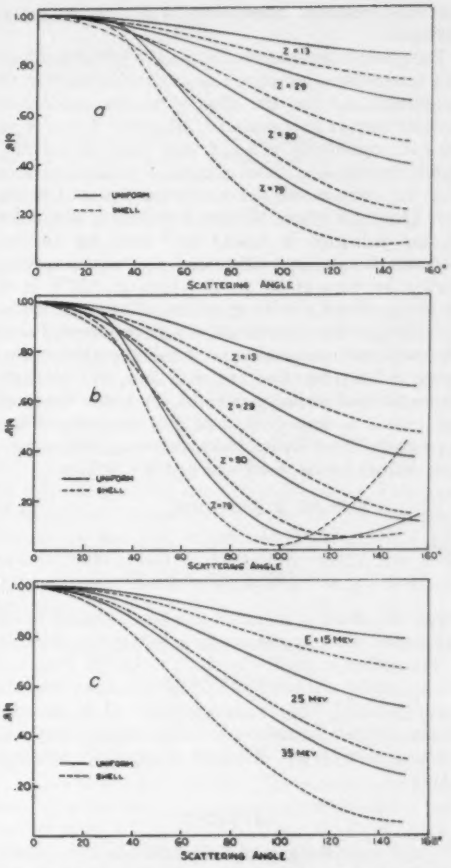

FIG. 3. (*a*) Scattering of 20-Mev electrons by shell and uniform nuclear models for various Z. (*b*) Scattering of 30-Mev electrons by shell and uniform nuclear models for various Z. (*c*) Scattering of electrons of 15, 25, and 35 Mev by shell and uniform nuclear models for $Z=29$.

The second phase shift, δ_2, varies from 0.4 percent of δ_1 for $Z=13$ and $E=15$ Mev, to 3 percent for $Z=79$ and $E=35$ Mev and thus is negligible, except perhaps for very high Z and high energy.

With the phase shifts plotted against E, one can find the scattering for any energy in the neighborhood of 20 Mev. Owing to computational difficulties, the present method is not practicable for calculating phase shifts for kR much greater than unity. Moreover, at very high energies the present treatment is inadequate in principle, for it does not suffice to consider the interaction of the electrons with the nucleus as a whole;

one must consider interactions with the individual nucleons.

The present treatment is also limited by the fact that only spherically symmetric charge distributions can be considered, and thus the effect of nuclear quadrupole moment cannot be calculated. Magnetic forces have not been considered, although they may not be completely negligible at these energies. Furthermore, it is only the cross section for elastic scattering that has been investigated here. While the total cross section for nuclear excitation is small,[5] 10^{-4} barn for 16-Mev electrons (the coulomb differential cross section varying from a few barn at 30° to 10^{-3} barn at 150°), it is necessary to say a word about the effect of radiation.

Schwinger[6] has calculated the radiative correction to the coulomb cross section for essentially elastic scattering of electrons. One can write $\sigma/\sigma_e=1-\delta(\theta, \Delta E)$, where ΔE is the energy radiated. It is only for small ΔE that δ is important, and the scattering differs appreciably from the coulomb scattering. Representative values of δ are, for $\theta=\frac{1}{2}\pi$ and $E=20$ Mev,

$$\delta=0.071 \text{ if } \Delta E=0.022,$$

and

$$\delta=0.018 \text{ if } \Delta E/E=0.20.$$

Thus, the effect of radiation can be minimized in experimental work by the use of a wide range detector.

The author is greatly indebted to Dr. H. Feshbach for suggesting this problem and for continued help and encouragement. Thanks are due to Dr. M. E. Rose for several helpful discussions, and, for computational aid, the assistance of Ann Moldauer is gratefully acknowledged.

APPENDIX

Numerical Calculations

To evaluate the confluent hypergeometric functions, it is necessary to use their series representations.

$$ {}_1F_1(a; b; z)=1+\frac{a}{b}z+\frac{a(a+1)}{b(b+1)}\frac{z^2}{2!}+\cdots$$

$$=\sum_{n=0}^{\infty}\frac{\Gamma(a+n)}{\Gamma(b+n)}\frac{\Gamma(b)}{\Gamma(a)}\frac{z^n}{n!}.$$

For the coulomb solutions, one has

$$F_\rho=\sum_{n=0}^{\infty}\alpha_\rho{}^{(n)}z^n, \quad RF_\rho{}'=\sum_{n=0}^{\infty}n\alpha_\rho{}^{(n)}z^n,$$

where

$$\alpha_\rho{}^{(n)}=\frac{\Gamma(\rho+n+i\alpha)}{\Gamma(2\rho+1+n)}\frac{\Gamma(2\rho+1)}{\Gamma(\rho+i\alpha)}\frac{1}{n!},$$

$z=2ikR$, $\alpha=Z/137$, $\rho=(\kappa^2-\alpha^2)^{\frac{1}{2}}$.

Then A_2/A_1 for the shell model can be written

$$\frac{A_2}{A_1}=-R^{2\rho}\frac{\sum_{n=0}^{\infty}(n+\rho-\kappa+i\alpha-RF_\kappa'/F_\kappa)\alpha_\rho{}^{(n)}z^n}{\sum_{n=0}^{\infty}(n-\rho-\kappa+i\alpha-RF_\kappa'/F_\kappa)\alpha_{-\rho}{}^{(n)}z^n},$$

while, for the uniform model,

$$\frac{A_2}{A_1}=-R^{2\rho}\frac{\sum_{n=0}^{\infty}(n+\rho+\frac{1}{2}-ikR-\Psi)\alpha_\rho{}^{(n)}z^n}{\sum_{n=0}^{\infty}(n-\rho+\frac{1}{2}-ikR-\Psi)\alpha_{-\rho}{}^{(n)}z^n}.$$

This method is only practical for those values of kR for which the above series converge within a reasonable number of terms, which essentially limits one to $kR<1$.

To evaluate RF_κ'/F_κ, one can make use of Kummer's second transformation, which yields

$$R\frac{F_\kappa'}{F_\kappa}=\frac{\kappa}{2\kappa+1}(2ik_aR)\frac{e^{ik_aR}\,{}_0F_1(\kappa+\frac{3}{2};\,-\frac{1}{4}(k_aR)^2)}{{}_1F_1(\kappa;\,2\kappa+1;\,2ik_aR)}.$$

To evaluate Ψ, one has

$$\Psi=\sum_{n=0}^{\infty}a_n,$$

$$a_0=\tfrac{1}{2}[1+(1+4c_0)^{\frac{1}{2}}],$$

$$a_1=c_1/2a_0,$$

$$\vdots$$

$$a_n=\Big[c_n-\sum_{l=1}^{n-1}a_la_{n-l}\Big]\Big/(2a_0+n-1), \quad n=1, 2, \cdots,$$

where c_n is given by

$$J(x)=\frac{1}{x^2}\sum_{n=0}^{6}c_nx^n \quad \text{[see Eq. (44)]},$$

$$c_n=0 \qquad \text{For } n>6.$$

The calculations have shown that $Re(A_2/A_1)=-\alpha/\rho\, Im(A_2/A_1)$ for both models.

Utilizing this result, the phase shift δ_κ can be written as

$$\delta_\kappa=-\arctan\frac{e^{\pi\alpha}\frac{\kappa^2}{2\rho^2}\left|\frac{\Gamma(\rho+i\alpha)}{\Gamma(2\rho)}\right|^2(2k)^{2\rho}Im\frac{A_2}{A_1}}{2-(e^{\pi\alpha}\cot 2\pi\rho-e^{-\pi\alpha}\csc 2\pi\rho)\times\frac{\kappa^2}{2\rho^2}\left|\frac{\Gamma(\rho+i\alpha)}{\Gamma(2\rho)}\right|^2(2k)^{2\rho}Im\frac{A_2}{A_1}}.$$

The complex gamma-function is not tabulated, and the best way to evaluate it is to use the asymptotic formula in conjunction with repeated use of the recurrence relation $\Gamma(z+1)=z\Gamma(z)$.

The resulting expressions for magnitude and phase are

$$|\Gamma(\rho+i\alpha)|^2\simeq\frac{2\pi e^{-2x-2\alpha\phi}r^{2(x-\frac{1}{2})}(1+x/6r^2+\cdots)}{\kappa^2(\kappa^2+2\rho+1)(\kappa^2+4\rho+4)(\kappa^2+6\rho+9)},$$

$$\arg\Gamma(\rho+1+i\alpha)=\Phi-\sum_{n=1}^{3}\arctan(\alpha/\rho+n),$$

$$\Phi=(x-\tfrac{1}{2})\arctan(\alpha/x)+\alpha(\ln r-1)-\alpha/12r^2,$$

where $x=\rho+4$, $r^2=x^2+\alpha^2$, $\phi=\arctan(\alpha/x)$.

[5] Skaggs, Laughlin, Hanson, and Orlin, Phys. Rev. **73**, 420 (1948).

[6] J. Schwinger, Phys. Rev. **75**, 898(L) (1949).

Elastically Scattered Protons from Carbon*

GERSON GOLDHABER† AND R. M. WILLIAMSON‡
University of Wisconsin, Madison, Wisconsin
(Received January 12, 1951)

The excited states of N^{13} were investigated by use of the $C^{12}(p,p)$ reaction. Only the two resonances, at 465-kev and 1.7-Mev proton energies, previously known from the $C^{12}(p,\gamma)N^{13}$ reaction were found. The energy region covered was from 0.3- to 4.0-Mev proton bombarding energy. The elastically scattered protons were observed by the use of a 90° magnetic analyzer at an angle of 164° to the incident beam. The intensities at the resonances show that the 465-kev level has $J=\frac{1}{2}$ and that the 1.7-Mev level has probably $J=3/2$ or $5/2$.

I. INTRODUCTION

THE recent determination of the two lowest resonances in gamma-ray yield for the $C^{12}(p,\gamma)$ reaction (at proton energies of[1] 465 kev and[2] 1.7 Mev) led to an apparently poor correspondence of levels in N^{13} and its mirror nucleus C^{13}. The two N^{13} levels under consideration here are at ~2.4 and 3.5 Mev, and the two corresponding levels[3] in C^{13} are at ~3.1 and 3.7 Mev. However, since our data were taken, theoretical work has been brought to our attention which makes these shifts plausible.[4,5] The present work was undertaken to check further the two known levels in N^{13} and to search for new levels. The data give the yield of protons scattered elastically from carbon at an angle of 164°; proton energies range from 0.3 to 4.0 Mev, corresponding to excitation energies of 2.2 to 5.7 Mev in the compound nucleus N^{13}.

II. APPARATUS

A magnetically separated proton beam from the Wisconsin electrostatic generator passes through the 90° electrostatic analyzer (Fig. 1) for energy measurement and definition. After passing through the exit slit of the electrostatic analyzer, the beam passes through two further slits of the 90° magnetic analyzer, described by Shoemaker, *et al.*,[6] which reduce the beam to a 2×2 mm square striking the target. This "illuminated" target spot is the "object" of the 90° magnetic analyzer which was here used to separate the elastically scattered protons from the various target elements. This analyzer was here, as in previous experiments,[6] set up to analyze the protons scattered at 164° to the incident beam, with an angular spread of ±5°.

In the present investigation, the flip coil and fluxmeter that had previously been used was replaced by a more accurate and less tedious magnetic flux balance, similar to that described by Buechner, *et al.*[7] It was, thus, possible to reproduce magnetic field measurements to an accuracy of better than 0.1 percent.

A scintillation counter, consisting of a 1P21 photomultiplier tube with a zinc sulfide screen dusted on, was used for counting the scattered protons. This was placed at the "image" position of the 90° magnetic analyzer and was used for the entire yield curve. In the absolute cross section determination (Sec. IV), a proportional counter with a 0.00005-inch nickel window was used.

III. THE YIELD CURVE

(A) Procedure

The targets used for the yield curve were thin soot deposits on 1000A nickel backings.[8] The targets were prepared by holding the nickel foils on nickel frames in the smoke of burning camphor. The targets were then mounted in position for bombardment while still in the nickel frames. An approximate target thickness determination was made by measuring the energy loss of protons scattered by the nickel backing on two tra-

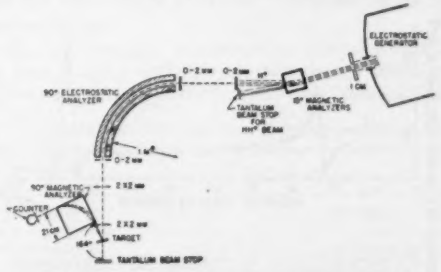

FIG. 1. Proton beam collimating slits and analyzers.

* Work supported by the AEC and the Wisconsin Alumni Research Foundation.
† Now at Department of Physics, Columbia University, New York.
‡ Now at Department of Physics, Duke University, Durham, North Carolina.
[1] W. A. Fowler and C. C. Lauritsen, Phys. Rev. **76**, 314 (1949).
[2] D. M. Van Patter, Phys. Rev. **76**, 1264 (1949).
[3] All energy levels quoted are taken from the recent compilation by Hornyak, Lauritsen, Morrison, and Fowler, Revs. Modern Phys. **22**, 291 (1950).
[4] J. B Ehrman, Phys. Rev. **81**, 412 (1951).
[5] R. G. Thomas, Phys. Rev. **80**, 136(A), 138(A) (1950); and private communication.
[6] Shoemaker, Faulkner, Bouricius, Kaufmann, and Mooring (to be published).
[7] Buechner, Strait, Sperduto, and Malm, Phys. Rev. **76**, 1543 (1949).
[8] Nickel foils are obtained on copper backings from the Chromium Corporation of America, 100 East 42nd St., New York 17, N. Y. For handling, see article by S. Bashkin and G. Goldhaber, Rev. Sci. Instr. **22**, 112 (1951).

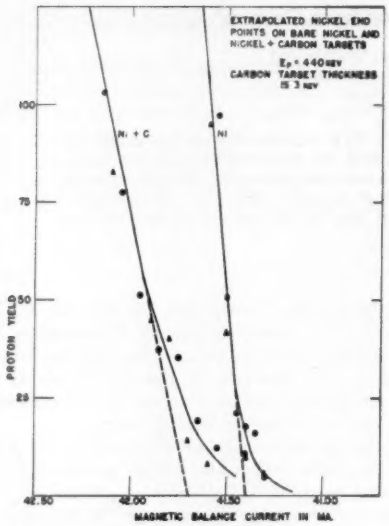

FIG. 2. High energy edges of proton groups scattered from nickel. Different symbols refer to different runs.

versals through the carbon layer. The sharp rise of the yield of elastically scattered protons from nickel at the high energy side of the peak (nickel end point) was measured as a function of magnetic field settings. The shift between the extrapolations of two such nickel end-point curves (Fig. 2), one for a bare nickel target and one for a carbon on nickel target, corresponds to the energy loss for two traversals of the carbon. It is estimated from the comparison with weighed targets (Sec. IV) that this method is probably good within ± 30 percent. Some of the nickel end-point curves for carbon on nickel targets varied in slope, and we believe that this is attributable to carbon target inhomogeneity and straggling. It is possible that the shift half-way up the curve would give a better average target thickness estimation than does the extrapolated shift. Further investigations with evaporated targets would be necessary to establish this as a quantitative method. The targets used ranged in thickness from 1 kev to 3 kev at 500-kev bombarding energy.

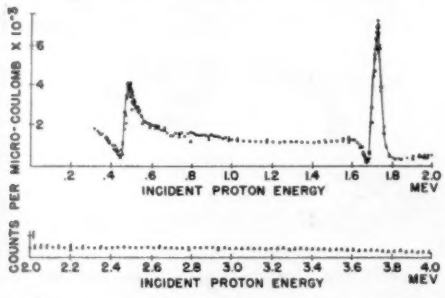

FIG. 3. Yield curve of elastically scattered protons from carbon at 164°, uncorrected for scintillation counter efficiency. 765 counts/μcoulomb corresponds to 10^{-25} cm^2/steradian. Rutherford scattering amounts to 3900 counts/μcoulomb at 0.3 Mev and just passes through the minimum of the 1.7-Mev resonance. Different symbols refer to different targets used.

At each point of the yield curve (Fig. 3), partial $H\rho$ curves were taken over the top of the elastically scattered proton yield from carbon. (Figure 4 shows a typical complete $H\rho$ curve.) The points of the $H\rho$ curve were taken by the use of a current integrator[9] which stopped the scaler after a predetermined charge was collected. The peak value of each partial $H\rho$ curve was used as the value shown in the yield curve for that bombarding energy. The detector window was always wider than the energy spread of particles from the thin target. Thus, the yield was always proportional to the number of target atoms.

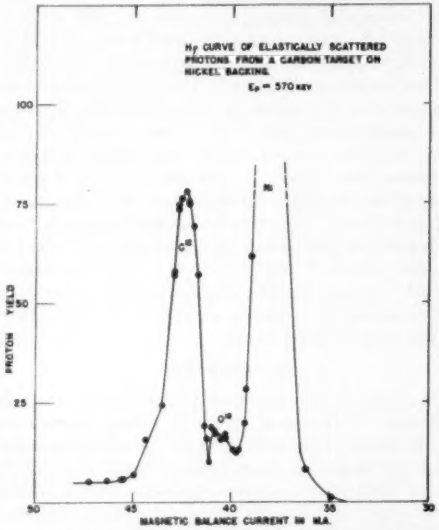

FIG. 4. Proton groups scattered from carbon, nickel, and oxygen.

For the general survey of the region from 0.3 to 4 Mev, points were taken 30 kev apart with a resolution of 0.2 percent. In the region of the two resonances found, points were taken with a much closer spacing. Below 1-Mev bombarding energy the diatomic beam (HH^+) was used, while above that energy the proton beam (H^+) was used. Below 400 kev the elastically scattered protons from nickel and carbon could no longer be clearly separated. The data below that energy was taken by reversing the target. This placed the carbon layer behind the nickel foil and, thus, again gave a clear separation on the $H\rho$ plot. The effective

[9] G. M. B. Bouricius and F. C. Shoemaker, Rev. Sci. Instr. 22, 183 (1951).

bombarding energy for these points was determined by remeasuring the points at the minimum of the 456-kev resonance with the target reversed, and then realigning the two energy scales at this minimum yield point. This gave a 15-kev energy loss due to the passage through the 1000A (nominal thickness) nickel foil at 440-kev proton energy.

(B) Results

In the region covered by the yield curve (0.3- to 4-Mev bombarding energy), only two resonances were found. These are the[1] 456-kev and the[2] 1.7-Mev resonances, both previously observed for the $C^{12}(p,\gamma)N^{13}$ reaction (see Table I). The 1.7-Mev resonance has associated with it, aside from the pronounced minimum and maximum at 1.68 and 1.73 Mev, respectively, an additional small maximum at 1.61 Mev and a minimum at 1.83 Mev. These are believed to be real. There is a rather high "nonresonance yield" of 1.45×10^{-25} cm²/steradian (considerably above Rutherford scattering) in between the two resonances which drops off sharply to 0.63×10^{-25} cm²/steradian as the 1.7-Mev resonance is crossed. This nonresonance yield then continues out to 3 Mev at essentially the same cross-section value. A further decrease in yield to 0.34×10^{-25} cm²/steradian is then observed around 3.5 Mev. Cross checks between the proportional counter, used for the absolute cross section determination (Sec. IV), and the scintillation counter, used for the yield curve at 1.3 and 2.7 Mev, seem to indicate that the scintillation counter efficiency decreases at the higher bombarding energies by about 10 to 20 percent. A similar cross check at the low bombarding energies (around the 456-kev resonance) was not possible, as the proportional counter window did not allow a reliable counting of protons of less than 500-kev energy. Visual observation of pulse-height distribution suggests, however, some loss of counting efficiency below 500 kev causing the yield curve to be low in this region.

No evidence was found for any other resonances of width and intensity comparable to the two resonances observed. However, recent work at this laboratory[10] on elastically scattered protons from O^{16} showed a very narrow level (width about 3 kev) in F^{17}. It is conceivable that similar levels in N^{13} could have been missed in the present survey. Some small wiggles in the yield curve between 0.5 and 1.0 Mev could arise from the natural C^{13} abundance in the carbon target, as the analyzer could not resolve elastically scattered protons from C^{12} and C^{13}.

IV. ABSOLUTE CROSS SECTION

Two types of weighed targets were used in ascertaining an absolute value for the differential cross section. Three soot targets, having weights of 40, 130, and 330 μg/cm², were deposited on nickel foils. Two Formvar foils, weighing 110 and 300 μg/cm², were also used. A microchemical analysis[11] of the Formvar "E" used gave 56.7 percent carbon and 8.1 percent hydrogen, the remainder being oxygen plus small impurities. The weighing techniques were estimated to be accurate to ±3 μg. The target areas, about 1 cm², were known to ±10 percent. The uniformity of both types of targets and the stability under bombardment are estimated to be good to ±20 percent.

The magnetic analyzer, equipped with a proportional counter, was used as described in Sec. II. Fluctuations in yield of ±10 percent arose as the proton beam shifted in the slits which define the target spot and are probably attributable to target inhomogeneity. Net yields from the five targets at 1.3 Mev give cross sections of 1.60, 1.71, 1.39, 1.46, 1.37×10^{-25} cm²/steradian. The unweighted average is $1.5\pm0.14\times10^{-25}$ cm²/steradian. Considering the previously discussed possible systematic errors, the total estimated error is ±25 percent. 765 counts/μcoulomb (Fig. 3), thus, corresponds to 10^{-25} cm²/steradian.

TABLE I. Data on the two observed resonances.

Resonance (Mev)	E_{min} (Mev)	E_{max} (Mev)	ΔE[a] (kev)	σ_{min} (10^{-25} cm²/steradian)	σ_{max}
0.456	0.441	0.485	44	0.62[b]	5.3[b]
1.7	1.68	1.73	50	0.12	9.3

[a] $\Delta E = E_{max} - E_{min}$.
[b] These values may be too small because of a possible loss of scintillation counter efficiency.

V. DISCUSSION

The over-all yield curve shows only the two resonances previously reported[1,2] from the $C^{12}(p,\gamma)$ reaction. No other resonances were found in the region of observation, although this region overlapped that in the mirror nucleus C^{13} in which an uncertain level at 5.7 Mev has been reported.[3] Quantitative comparison of the values E_r and Γ with those derived from the proton capture data awaits a detailed theoretical fit of the scattering data.

If $(\sigma_{max})^{\frac{1}{2}}-(\sigma_{min})^{\frac{1}{2}}$ at a resonance is large compared to $(\sigma_{min})^{\frac{1}{2}}$ and if $\sin^2\theta$ is small compared to unity, the following formula is valid for spin $\frac{1}{2}$ particles scattered

TABLE II. Calculated resonance scattering amplitudes.

	$(\sigma_{max})^{\frac{1}{2}}-(\sigma_{min})^{\frac{1}{2}}$	
Resonance	465 kev	1.7 Mev
Experimental	0.48×10^{-12} cm	0.85×10^{-12} cm
Calculated $^2S_{\frac{1}{2}}$	0.70	0.37
$^2P_{\frac{1}{2}}$	0.67	0.36
$^2P_{\frac{3}{2}}$	1.3	0.71
$^2D_{\frac{3}{2}}$	1.2	0.67
$^2D_{\frac{5}{2}}$	1.8	1.0

[10] Laubenstein, Laubenstein, Mobley, and Koester, Phys. Rev. 81, 654 (A) (1951).

[11] We are indebted to Dr. A. L. Wilds of the Wisconsin Organic Chemistry Department for this analysis.

by a spin zero nucleus.[12,13]

$$(\sigma_{max})^{\frac{1}{2}}-(\sigma_{min})^{\frac{1}{2}}=(J+\tfrac{1}{2})\lambda P_L(\cos\theta).$$

Table II shows that the 465-kev level is best assigned $J=\frac{1}{2}$. Some loss in scintillation counter efficiency would account for the smaller experimental intensity. Since only the assumption of $L=0$ gives a level "width without barrier" of reasonable value,[14] the level is probably $^2S_{\frac{1}{2}}$. Further, the gamma-radiation intensity from the corresponding level in C^{13} to its ground state, presumed to be $^2P_{\frac{1}{2}}$, appears to be electric dipole radiation.[5] The data for the 1.7-Mev level[15] show an intensity midway between $J=3/2$ and $J=5/2$. However, the small concomitant maximum at 1.61 Mev and minimum at 1.83 Mev may be the result of a second level in this neighborhood, and the single level intensity analysis may not be valid.§

It is apparent that a more reliable absolute cross section would be of value in the assignment of level configurations. The cross-section measurement could be improved by extending the present data below 300 kev into a region of pure Rutherford scattering. Another possibility is the use of a methane gas target and a proportional counter for both absolute cross section and angular distribution measurements. Angular distributions, taken at the two resonances, would help further in assignment of angular momenta.[16]

We wish to thank Professor H. T. Richards for suggesting this problem to us and for many helpful discussions. We are also indebted to R. A. Laubenstein, H. L. Jackson, and M. J. W. Laubenstein for aid in taking data.

[12] C. L. Critchfield and D. C. Dodder, Phys. Rev. **76**, 602 (1949).

[13] This extension of the formulas in reference 12 is due to R. A. Laubenstein.

[14] Fowler, Lauritsen, and Lauritsen, Revs. Modern Phys. **20**, 236 (1948).

[15] From comparison of the calculated level shift between the levels in N^{13} (3.5 Mev) and C^{13} (3.7 Mev) with the experimental value, R. G. Thomas concludes that a p wave should be assigned here (private communication).

§ *Note added in proof.*—Preliminary results of an analysis by H. L. Jackson and A. I. Galonsky (to be published) show that a $P_{\frac{1}{2}}$ (1.68-Mev) level and a $D_{\frac{3}{2}}$ (1.73-Mev) level of comparable widths account for the shape near resonance. For the corresponding level of the mirror nucleus C^{13}, J. Rotblat (Proc. of the Harwell Nuclear Physics Conference, 1950) reports finding a doublet in place of the 3.7-Mev level, from the $C^{12}(d,p)C^{13}$ reaction. He gives the values 3.77 and 3.90 Mev for the two components. See also a forthcoming paper by R. G. Thomas on this subject.

[16] W. D. Whitehead, Phys. Rev. **79**, 1022 (1950), has measured the angular distribution of elastically scattered protons from carbon for bombarding energies between 2 and 2.75 Mev. The data indicate the scattering of both s and p waves.

PHYSICAL REVIEW VOLUME 82, NUMBER 4 MAY 15, 1951

Radiations of UY

ARTHUR H. JAFFEY, JEROME LERNER, AND SYLVIA WARSHAW
Argonne National Laboratory, Chicago, Illinois

(Received January 10, 1951)

The radiations of UY have been examined by absorption curve techniques. Among the radiations are: (1) 0.2-Mev beta, (2) L x-rays, (3) 35-kev gamma-ray, (4) soft electronic component, probably conversion electrons about 50 kev, (5) soft quantum component, probably M x-rays, and (6) two harder gamma-rays, 65 to 75 kev and about 100 kev. On abundance and coincidence considerations, a tentative decay scheme is suggested which includes a 0.2-Mev beta followed by 35- and 65-kev gamma-rays in cascade with a 100-kev cross-over transition. The half-life was found to be $25.6_4\pm0.1$ hours.

I. INTRODUCTION

IN the course of a cross-section measurement[1] on the reaction $Th^{230}(n,\gamma)Th^{231}$ by direct determination of the Th^{231} (or UY) disintegration rate, it was found necessary to have some information on the UY decay scheme. Such information was necessary in order to evaluate the fraction of the counts measured which were due to disintegration betas. Some preliminary work has been done on the decay scheme, by the use of absorption methods. The poor resolution of these methods enabled the determination of only the gross features of a decay scheme, which were, we believe, sufficient for the purposes of evaluating disintegration rates (with the aid of suitable corrections). Our results indicate that further work is necessary to determine the correct scheme.

As indicated above, UY can be made through the absorption of neutrons by ionium, or it can be isolated from uranium samples, since it is the daughter of U^{235} decay ($U^{235}\xrightarrow{\alpha}Th^{231}$). Prior to World War II, the usual source of UY had been natural uranium. By separating the thorium fraction from a large amount of uranium, it is possible to get a reasonable amount of UY.

Unfortunately, UY so separated always has large amounts of $UX_1(Th^{234})$ and UX_2 present, even when short periods (one to two days) of growth are used in order to increase the relative concentration of the short-lived (25.6 hr) UY over that of the 24.1-day UX_1. Most measurements made on UY separated from natural uranium were made by difference. The UX_2 radiation was measured after the decay of the UY, and after correcting for the UX_1 decay, these measurements were subtracted from the measurement on the original UX_2+UY radiations.

Because of the difficulties in such measurements,

[1] A. H. Jaffey and E. K. Hyde, Argonne National Laboratory Report ANL-4249, Febuary, 1949, unpublished.

most of the work[2–6] prior to the war gave incomplete results. A soft component was found, although the observed aluminum half-thicknesses varied considerably [3.2 mg/cm² (Erchova); 6.2 (Antonoff); 6.2 (Kirsch); 7.6 (Nishina)]; Erchova also found a harder component with a 35-mg/cm² half-thickness, while Antonoff found a very soft component (0.75 mg/cm² half-thickness) which he ascribed to alpha-radiation.

With the availability of sources of concentrated U^{235} from the Oak Ridge plants, it has become possible to isolate UY samples with much smaller amounts of UX contamination. Such samples have been studied[6–8] at this laboratory and by Knight and Macklin at Oak Ridge. Earlier measurements reported from this laboratory[7] on a UY preparation separated from uranium containing 65 percent U^{235}, showed the presence of a number of radiations, including a soft beta of 5.6-mg/cm² aluminum half-thickness, *L* x-rays with half-thicknesses ranging from 40 to 120 mg/cm² aluminum, and a very soft radiation with about 1.4-mg/cm² half-thickness. The abundance of the very soft radiation was almost twice that of the beta-particle component. In addition to the *L* x-rays, a harder quantum was found, for which the data were too poor to determine the energy, although it was suspected that it might be a *K* x-ray. The quantum radiations were proved to be such by measurement through sufficient beryllium absorber to cut out all beta-particles.

Knight and Macklin[8] found the soft beta-particle, determining a value of 7.0 mg/cm² for the aluminum half-thickness. In addition, they found two more components, with half-thicknesses of 820 mg/cm² and 104 mg/cm², which they ascribed to a 34-kev gamma-ray and to a 16-kev *L* x-ray. They suggested a decay scheme involving a beta-decay (7-mg/cm² component) followed by a 34-kev gamma, which was highly converted, thus giving rise to *L* x-rays. They ascribed the very soft component found in this laboratory to a mixture of conversion electrons and *M* x-rays.

More recent investigation in this laboratory has shown that this decay scheme is probably incomplete. The work described in this paper summarizes both the earlier experiments and the more recent measurements. Since both our results and those of Knight and Macklin suggest a single beta-particle followed by a number of other radiations (very soft conversion electrons, x-rays, gammas), it is hoped that the determination of the true disintegration rate from the counting rate is not affected seriously by the details of the disintegration scheme.

[2] G. N. Antonoff, Phil. Mag. **22**, 419 (1911).
[3] G. Kirsch, Sitzberichte Akad. Wiss. Wien, Math.-naturw. Klasse. Abt. IIa **129**, 309–34 (1920).
[4] Z. V. Erchova, J. phys. radium **8**, 501 (1937).
[5] Nishina, Yasaki, Kimura, and Ikawa, Nature **142**, 874 (1938).
[6] G. B. Knight and R. L. Macklin, Phys. Rev. **75**, 34 (1949).
[7] A. H. Jaffey and E. K. Hyde, Metallurgical Laboratory Report CN-3001, pp. 21-4, May, 1945, unpublished.
[8] Jaffey, Lerner, and Warshaw, Argonne National Laboratory Report ANL-4112, January 15, 1948, unpublished.

TABLE I. Radiations of UY.

Probable type of radiation	Aluminum half-thickness	Energy	Relative cpm at zero absorber	Approx. relative abundance
Mixture *M* x-rays and conversion e's	~1 mg/cm²	2.5 to 5 kev ~50 kev	2	~2
Beta-rays	6.1 mg/cm²	0.20 Mev	1.0	1.0
L x-ray	47 mg/cm² 108	12.3 kev 16.3 kev	0.03	1
Gamma-ray	800 mg/cm²	35 kev	0.003	1
Gamma-ray		65 to 75 kev	small	
Gamma-ray		100 kev or greater	small	

II. CHEMICAL SEPARATION PROCEDURE

The enriched uranium sample used contained about 95 percent U^{235} by weight, which meant that the U^{235}/U^{238} activity ratio was approximately 100. Since, at equilibrium, the UY/UX_2 activity ratio would be the same, a thorium sample directly separated from the uranium could have been used. However, to insure that the UX_2 activity would not interfere seriously even after the sample had decayed somewhat, the thorium fraction was completely separated, the uranium was purified, and the daughters allowed to grow in for one or two days. The thorium daughters were then separated from the uranium, the resulting UY/UX_2 activity ratio being increased by a factor of 12 to 15 over the equilibrium value.

In the first purification of the uranium, the thorium fraction was removed by precipitation with a LaF_3 carrier, after which the uranium was separated from fluoride ion by precipitation as the hydroxide, and further purified by a hexone (methyl isobutyl ketone) extraction from 10 *M* ammonium nitrate. Following the growth period, the thorium daughters were separated by precipitation with LaF_3 carrier. To complete the separation from uranium, two more purification cycles were used, involving precipitations with zirconium iodate and LaF_3 carriers. On solution of the LaF_3, the activity was separated from the lanthanum salt by extracting the thorium activity with TTA (thenoyl tri-fluor-acetone) in benzene solution. The nitric acid extract from the TTA contained essentially carrier-free UY, and the samples were prepared from this solution.

III. MEASUREMENTS

The results are summarized in Table I. Our best value for the aluminum half-thickness of the soft beta-component is about 6.1 mg/cm². According to the data summarized by Libby[9] this corresponds to an energy of 0.20 Mev. Our results also indicate that the harder radiations are due to *L* x-rays and several gamma-rays.

[9] W. F. Libby, Anal. Chem. **19**, 2 (1947).

An aluminum absorption curve gave two components with half-thicknesses 47 mg/cm² and 108 mg/cm², which correspond to 12.3 kev and 16.3 kev, respectively. These energies are in the region of the Pa L x-rays, which could be excited if a gamma following the beta-decay were internally converted. Although the L x-rays of Pa range from 13 to 20 kev, an aluminum absorption curve of the mixture of components can be (somewhat arbitrarily) "resolved" into two components, as shown in the case of Np^{239} decay by Jaffey and Magnusson.[10] Thus, the identification of these two components with L x-rays arising in UY decay seems reasonable. In addition to the L x-rays, the aluminum absorption curve showed a component with a half-thickness of about 800 mg/cm² (34 kev). All these components were proven to be quantum radiations by measuring them in a magnetic field strong enough to bend away all electrons, and also by measuring them through a beryllium absorber sufficiently thick to absorb all emitted electrons (1900 mg/cm², 234 mg/cm²).

Lead absorption curves showed components with half-thicknesses 4.5 mg/cm² and 40 mg/cm², which were shown to be quantum radiations by bending away electrons with a magnetic field. Since the first value lies in the midst of the lead L-absorption edges, the 4.5-mg/cm² component could correspond to 9.6, 13.4, or 16.5 kev. Evidently, this is the L x-ray observed in the aluminum curve. The harder component corresponds to an energy of 38 kev, which checks fairly well with the results of the aluminum absorption curve. Silver and copper absorption curves similarly showed L x-rays and a gamma of either 34 or 38 kev, respectively.

In addition to these components, harder quantum radiations of lower intensity were apparent in the absorption curves taken with aluminum, lead, silver, and copper. Agreement on energy values was quite poor, but it seemed fairly certain that there was a gamma with an energy lying between 65 and 75 kev and one with an energy at or above 100 kev which could possibly be ascribed to a K x-ray.

A soft component was observed in a low absorption counter[11] with a half-thickness (aluminum) of 0.9 to 1.0 mg/cm², and an abundance about twice that of the 6.1-mg/cm² component. The same radiation was also observed in absorption curves taken with ordinary mica window G-M tubes with fairly thin windows. When a beryllium absorber or a magnetic field was used to remove electrons, the half-thickness increased to about 1.25 mg/cm². It is possible, then, that the 0.9-mg/cm² component represents a mixture of soft conversion electrons and M x-rays.

For x-rays, a 1.25-mg/cm² half-thickness may be due to a 1.3-kev or a 3.4-kev x-ray (multivalued because of K-absorption edge of aluminum). The M x-rays from the Pa^{231} daughter of UY range from 2.4 to 4.9 kev, which is consistent with these results, considering the experimental error in the half-thickness measurements. If the soft conversion electrons were 0.5 to 0.7 mg/cm² in half-thickness, their energy would lie[9] between 45 and 55 kev. If these electrons were due to conversion in the L-shell, the converted gamma would have an energy of approximately 65 to 75 kev (20 kev taken as average Pa binding energy in the L shell), which apparently checks with the observation of a low intensity gamma-ray of about this energy. If the soft electrons had been due to conversion of the 35-kev gamma, as suggested by Knight and Macklin,[6] their energy would have been about 15 kev which corresponds[9] to an aluminum half-thickness of about 0.15 mg/cm². No such component was observed in the low absorption counter (minimum absorption 0.3 mg/cm²).

It is further unlikely that the large number of conversion electrons observed were due to conversion of the 35-kev gamma, since, after correcting for counting efficiencies, the abundances of the L x-rays and the gamma seemed to be equal (Table I). The ratio (at zero absorber) of the L x-ray counts to the counts due to the 35-kev gamma-ray was found to be approximately 10. Taking the average energy of the L x-ray to be 16 kev, the half-thickness in argon of this radiation would be 42 mg/cm², while the corresponding half-thickness for a 35-kev gamma is 380 mg/cm². For low energy quanta, most of the counts in a G-M tube are those arising from absorption of the quanta in the gas of the tube, so that at low efficiencies, the counting efficiency for a given type of such radiation is inversely proportional to the half-thickness for absorption in the gas. Neglecting the small effect due to the alcohol, the absorption of a 16-kev x-ray in an ordinary argon-alcohol G-M tube relative to the absorption of a 35-kev gamma would be $380/42=9.0$. The agreement between this value and the ratio of observed counts suggests that the number of L x-rays and 35-kev gammas are approximately equal, with a relatively small percentage (if any) of conversion of the gamma.

It also seems likely that the number of beta-particles is about equal to the number of L x-rays emitted (Table I). Using an argon-alcohol G-M tube, the ratio of the 6.1-mg/cm² (beta) component counts (at zero absorber) to the x-ray counts was found to be about 30. If it is assumed that the number of L x-rays is approximately equal to the number of betas, the efficiency for counting the L x-rays of Pa is found to be about 3 percent. This value is not unreasonable, since Jaffey and Magnusson[10] found a value of 2½ percent[11a] for the L x-rays of Pu from the decay of Np^{239}.

[10] A. H. Jaffey and L. B. Magnusson, "Radiations of Np^{239} and the half-life of Pu^{239}," *The Transuranium Elements* (McGraw-Hill Book Company, Inc., New York, 1949), Paper No. 14.2, National Nuclear Energy Series, Vol. 14B, Division IV.

[11] Elliott, Sullivan, Sleight, Gladrow, Raynor, and Freedman, "Low Absorber Counters," *Radiochemistry: The Fission Products* (McGraw-Hill Book Company, Inc., New York, to be published in 1951), Paper No. 2.8, National Nuclear Energy Series, Vol. 9B, Division IV.

[11a] Since the L x-rays of Pa are lower in energy than those of Pu, the absorption coefficient in argon of the former would be greater, and hence the counting efficiency higher.

As mentioned above, the very soft component may be a mixture of soft conversion electrons and *M* x-rays. The absorption coefficients of the *M* x-rays in argon are quite large, so that their counting efficiency is high. It is fairly reasonable to assume, then, that somewhat less than half of the soft component counts is due to *M* x-rays and the remainder due to conversion electrons.

Some coincidence-measurements were made, but proved relatively little, because of the very low counting efficiencies for the soft gammas involved. In these measurements, two G-M tubes were used with a permanently fixed absorber over one and coincidences measured as a function of the aluminum absorber thickness in front of the other tube. In one measurement, 475 mg/cm² Be was used as the permanently placed absorber; in another, 1000 mg/cm² Al was used. The former cut out electrons, but allowed the *L* x-rays and gammas through; the latter cut out *L* x-rays as well as electrons. The results showed that the 6.1-mg/cm² component and the *L* x-rays were in coincidence with radiation that could penetrate 475-mg/cm² Be or 1000 mg/cm² Al; i.e., the beta-particle and *L* x-rays were in coincidence with quantum radiation, some of which were gamma-rays.

The half-life of UY was measured by means of a thin-walled glass G-M tube; this type of tube has been found to have more reproducible characteristics than the mica window tubes available. The tube was frequently checked with a standard and most of the counts were within the expected statistical deviation of 0.3 percent. Because this glass tube had a minimum absorption of about 30 mg/cm², it attenuated the UY beta-radiation by almost 5 half-thicknesses (a factor of about 30). As a result, the hard radiation of UX_2 was found to give a long-lived tail in the decay curve. Although the UX_2 concentration was quite a small fraction of the total activity, the severe attenuation of the UY betas made the UX_2 radiation (which was only partially attenuated) a sizeable part of the total counts measured.

A better decay curve was determined by using 1230 mg/cm² of Be to cut out all betas. Under these conditions only the quanta emitted in the UY decay were measured, although a nondecaying residuum of several counts was found, after the UY decayed out. This was ascribed to incomplete separation of U^{235} and U^{234}, both of which emit quantum radiation.[12–15] The resolution losses were determined by using the paired-source technique,[16] and were found to be 0.42 percent per

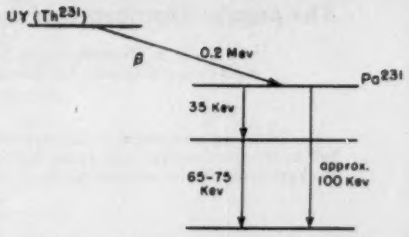

FIG. 1. Tentative decay scheme for UY disintegration. The results are consistent with the assumptions that the 35-kev gamma is relatively unconverted, while the 65- to 75-kev gamma is highly converted. Associated with the conversion are *L* and *M* x-rays and conversion electrons.

1000 cpm. Two separate preparations of UY were made from the U^{235} sample. Sample I (initial counting rate about 700 cpm) was counted down to background (about six half-lives). Sample II (initial counting rate about 3600 cpm) was also counted down to background (about eight half-lives). The half-lives were calculated using a least-squares method, Sample I giving a value 25.56±0.06 hours and Sample II giving 25.73±0.06 hours. (The deviations represent the standard deviation calculated from the dispersion of the data.) The results probably justify a half-life value of 25.6$_4$±0.1 hours.

SUMMARY

The results described indicate that the following components are probably present with approximately equal intensity (within perhaps 25 percent): 0.20-Mev beta, *L* x-rays, *M* x-rays, 50-kev conversion electrons, 35-kev gamma. In addition there seems to be evidence for the existence of a highly converted gamma in the range 65 to 75 kev and of a low intensity gamma with an energy of 100 kev or greater. Despite the scanty evidence, it may be possible to combine these data into a consistent decay scheme.* A tentative scheme is suggested in Fig. 1. The order of the two softer gamma-rays is, of course, uncertain.

At zero absorber (Table I), using an argon-alcohol mica window G-M tube (9 cm argon, 1 cm alcohol) the very soft component (presumably *M* x-rays and conversion electrons) had almost twice as many counts as the beta-ray component; the counting rate of the *L* x-rays was about 1/30 that of the beta-rays; the 35-kev counting rate was about 1/10 that of the *L* x-rays; while the counting rates of the other gammas were somewhat lower yet.

The half-life of UY was measured as 25.6$_4$±0.1 hours.

[12] R. L. Macklin and G. B. Knight, MDDC-976, December, 1946 (unpublished).
[13] R. L. Macklin, Carbon and Carbide Report No. A-3640, April, 1946 (unpublished).
[14] R. L. Macklin, Carbon and Carbide Report No. K-97, December, 1947 (unpublished).
[15] B. Scott, Metallurgical Laboratory Report CC-3715, Nov., 1946 (unpublished).
[16] T. P. Kohman, "A general method for determining coincidence corrections of counting instruments," Paper No. 22.50, *The Transuranium Elements;* Metallurgical Laboratory Report CP-3275, June, 1945 (unpublished).

* *Note added in proof.*—Further work in this laboratory with a beta-spectrometer and a NaI scintillation gamma-spectrometer indicates that the decay scheme is much more complex than was found by absorption techniques. The single beta-ray described in this paper has been resolved into three components, the hardest beta having an energy of 302 kev, and a total of nine gamma-rays have been found. A disintegration scheme has been devised from which it appears that the total disintegration energy is 324 kev. It is planned to publish these results in the near future.

The Angular Distribution of the Products of the $T(d,n)He^4$ Reaction*

J. E. Brolley, Jr., J. L. Fowler,† and E. J. Stovall, Jr.
University of California, Los Alamos Scientific Laboratory, Los Alamos, New Mexico

(Received January 18, 1951)

The differential cross section of the reaction $T(d,n)He^4$ for 10.5-Mev deuterons has been measured from 180° to 33° center-of-mass angle of the alpha-particle. Both neutrons and alpha-particles were counted. The angular distribution is similar to that of the mirror reaction, $He^3(d,p)He^4$.

I. INTRODUCTION

A VERY useful source of monoenergetic neutrons of high energy is furnished by the $T(d,n)He^4$ reaction.[1] The differential cross section of the mirror reaction, $He^3(d,p)He^4$, has been measured[2] at 10.2 Mev. The present investigation gives the cross section of the $T(d,n)He^4$ reaction using 10.5-Mev deuterons. It is of theoretical interest to compare the absolute differential cross sections of these two reactions. The $T(d,n)He^4$ reaction was studied from 33° to 94° in the center-of-mass system by counting alpha-particles; from 94° to 180° in the center-of-mass system by counting neutrons.

II. EXPERIMENT AND RESULTS

The deuterons were accelerated by the 42-in. cyclotron and brought to a focus outside of the water tank shield 15 feet from the cyclotron exit port.[3] The energy of the deuterons was measured several times during the course of this experiment by taking aluminum absorption curves and was found to be 10.94 Mev with a maximum spread of 0.10 Mev. Allowing for absolute errors in this determination, as well as for drift of energy between the measurements, one takes the energy to be 10.9 ± 0.3 Mev. This agreed with the energy measurement found by magnetic deflection,[3] which at the beginning of the experiments on tritium gave an energy of 11.0 ± 0.2 Mev.

The part of the experiment designed to count alpha-particles was carried out with apparatus similar to that described previously.[4] The deuteron beam entered a gas cell mounted in the center of the 58-cm diameter reaction chamber. The beam was delimited to a diameter of 0.47 cm, with an angular divergence of $\pm0.5°$ by a circular gold aperture; thence it impinged upon a thin aluminum window at the front of the target cell. The alpha-particles produced in the target cell emerged through an aluminum side window (3.4 mg/cm^2), 6.3 cm long and 1.5 cm wide. The alpha-particles were detected by a proportional counter which could be rotated to any angle in the horizontal plane. The reaction volume was defined by a 0.318-cm vertical slit mounted on the proportional counter support and located 10.8 cm from a 0.318-cm diameter hole immediately in front of the proportional counter. After passing through the gas, the deuteron beam was stopped by a gold disk soldered to the back of the gas cell. The gas cell was insulated from ground so that it could be used as a faraday cage for monitoring the beam current. In order to prevent secondary electrons from the front aluminum window from introducing an error in the current measurement a brass sleeve extending 4.5 cm beyond the window was fastened to the gas cell at the entrance end, and permanent bar magnets were fastened on either side of the gas cell.

The calibration of the apparatus, including the current measurement, was checked by measuring the differential cross section of *d-d* scattering at 45° and comparing with the value reported previously.[4] This measurement gave the differential cross section within one percent of the previous value.

The tritium gas was handled by absorbing it in uranium contained in a small stainless steel vessel. When it was desired to fill the gas cell, the tritium was evolved from the uranium by heating, and the valve to the stainless steel vessel was closed. To empty the gas cell this valve was opened and the tritium was reabsorbed rapidly. The pressure of tritium in the target cell was measured by using a Bourdon-type gauge as a null indicator. A small weight pan was attached to the sensitive element of the gauge; and, with the pressure of tritium in the system, weights were added to the pan until the indicator of the gauge reached a position it would have had if there had been a vacuum in the system. After calibration of the gauge one could determine the pressure of tritium gas to about one percent. The hydrogen impurity of the tritium sample was checked by counting scattered deuterons from the hydrogen and recoil protons at an angle of 25°. This number was compared with the recoil protons from deuterons impinging upon a sample of high purity hydrogen. The gas analysis determined in this way, which was reproducible to 1.5 percent, agreed with the analysis of the gas furnished with the samples used to the accuracy of the latter measurement which was ±3 percent.

To detect the alpha-particles with the proportional counter at various angles to the deuteron beam, the

* Work done under the auspices of the AEC.

† Now at Oak Ridge National Laboratory, Oak Ridge, Tennessee.

[1] Hanson, Taschek, and Williams, Revs. Modern Phys. **21**, 635 (1949).

[2] J. C. Allred, Phys. Rev. **77**, 753 (1950).

[3] Curtis, Fowler, and Rosen, Rev. Sci. Instr. **20**, 388 (1949).

[4] Allred, Erickson, Fowler, and Stovall, Phys. Rev. **76**, 1430 (1949).

pressure in the counter was adjusted so that the track of the alpha-particle calculated from range-energy curves ended inside the back edge of the counter. The amplified pulses from the counter were analyzed by means of a ten-channel discriminator. Figure 1 gives a sample alpha-peak obtained together with the background. The abscissa is the amplified pulse height and the ordinate is the number of pulses per 5-volt interval. For determining backgrounds aluminum foils were placed in front of the counter to stop the alpha-particle before it entered the counter. This was accomplished by a selsyn-controlled foil shutter mounted in front of the proportional counter with which a hundred combinations of absorber could be selected. Background determined in this way was found to be the same as background obtained by replacing the tritium in the target cell with hydrogen. The triangles in Fig. 1 show the background obtained with the aluminum absorber. The alpha-peak was well resolved for the laboratory angles at which data are recorded here.

In Fig. 2 the points indicated by the circles give the results of the alpha-particle measurement when converted to the center-of-mass system. The open circles give the results when the entrance window of the tritium cell was 3.4-mg/cm² aluminum foil. In this case the deuteron energy where the detected alpha-particles are produced is reduced from 10.9±0.3 to 10.7±0.3 Mev. The solid circles give the results when a 6.8-mg/cm² aluminum foil is used as an entrance window. In this case the deuteron energy was 10.5±0.3 Mev. To examine the effect of scattering of the alpha-particles by the 3.4-mg/cm² side window of the gas cell, runs were made in which a second 3.4-mg/cm² foil was fastened adjacent to the side window. The increasing of this window thickness by a factor of two had no appreciable effect on the measurement of the differential cross section within 2 percent.

The random error of the data taken by counting alpha-particles, that is, the measurements over the center-of-mass angular region from 33° to 94°, amounts to about 1.5 percent as deduced from the reproducibility of the data. Other sources of error occuring in the absolute current measurements, geometrical factors, tritium pressure, and gas analysis increase the absolute error of this section of the curve to about 3.5 percent.

To extend the measurements from 94° to 180° center-of-mass angle of the alpha-particle, neutrons were counted in the laboratory system from 0° to 74.5°. In this part of the experiment the scattering chamber was removed and the target cell was replaced by a simple thin-walled gas cell fastened at the end of the tube through which the deuteron beam passes. A fourfold coincidence proton recoil telescope was employed to measure the neutrons at various angles. The description of the equipment and the alignment procedure, together with the procedure used in taking data, are given in a paper[5] on *n-p* scattering at 27 Mev.

[5] Brolley, Coon, and Fowler, Phys. Rev. 82, 190 (1951).

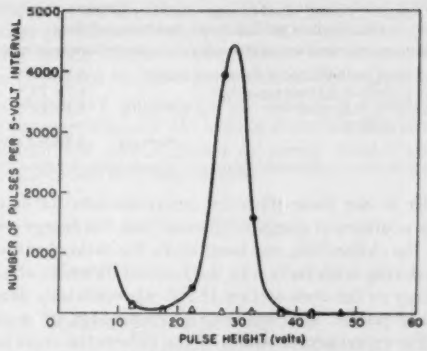

FIG. 1. Distribution of pulses from the proportional counter due to alpha-particles produced by the $T(d,n)He^4$ reaction at 25° to the direction of the deuteron beam plus background. Points designated by triangles give background.

For counting the absolute number of neutrons in this experiment it was necessary to find the efficiency of the counter telescope. This was done in three ways. First, a run was made using the 14-Mev *d-t* neutrons from the Los Alamos Cockcroft-Walton accelerator, from which the neutron flux is approximately known. The second method used the cyclotron *d-t* neutron flux associated with the angular region in which the detection of alpha-particles makes possible the determination of the differential cross section as described above. In

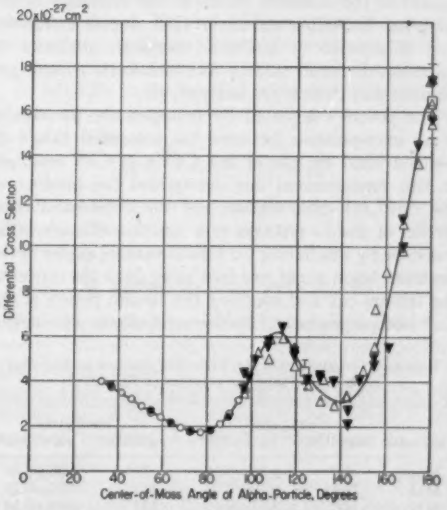

FIG. 2. The differential cross section of the $T(d,n)He^4$ reaction in the center-of-mass system. Circles represent data obtained by counting alpha-particles with a proportional counter. Squares give results of neutron counting with a proton recoil telescope counter. Triangles give the results of counting neutrons by means of the $Cu^{63}(n,2n)Cu^{62}$ reaction. Solid symbols give the results for a deuteron bombarding energy of 10.5 Mev.

TABLE I. Proton recoil counter efficiency at 20.75 Mev in quadruple coincidences/sec/unit neutron flux.

With Cockcroft-Walton *d-t* neutron source	4.1×10^{-6}
With cyclotron *d-t* neutron source	4.7×10^{-6}
Calculated from geometry and *n-p* scattering cross section	4.4×10^{-6}
Average	$4.4\pm0.2\times10^{-6}$

order to use these efficiency determinations for detecting neutrons at energies different from the energy used for the calibration, one must know the ratio of the *n-p* scattering cross section in the forward direction at any energy to the cross section at the experimentally determined points. This quantity was estimated by a plot of the experimental values of the differential cross section at zero degrees taken from the literature.[5-7] For neutrons below 14 Mev, the differential cross section in the center-of-mass system was obtained by dividing the total cross section[7] by 4π. The third method of finding the counter efficiency was a calculation from the geometry of the apparatus, the known weight of the polyethylene radiator, and the absolute *n-p* scattering cross section. Table I gives the results of these different efficiency estimates when they are extrapolated to a neutron energy of 20.75 Mev.

In Fig. 2 the points designated by squares give the results of the neutron measurements at two angles as determined with the counter telescope. The estimated standard error of this absolute neutron cross section amounts to about 11 percent and is the root mean square of the standard errors in the efficiency determination (including the uncertainty due to extrapolating efficiencies to different energies), statistics of counting, deuteron current measurements, tritium gas pressure and tritium gas analysis, etc.

The points designated by triangles are the results of an extrapolation between the measured values of neutron yield by use of the $Cu^{63}(n,2n)Cu^{62}$ reaction. In this measurement one determined the product of the $Cu(n,2n)$ cross section and the differential cross section of the *d-t* reaction as a function of angle. This was done by irradiating Cu foils at various angles to the deuteron beam about one foot away from the center of the tritium cell and counting the 10-min period of the Cu^{62} isotope produced.[8] Background effects were evaluated by making runs with the tritium replaced by hydrogen. As in the case of reference 8, the Geiger counters were calibrated by use of the beta-particles from Cu^{66} produced by thermal neutrons on Cu^{65}. The $Cu(n,2n)$ cross section itself varies with angle because the energy of the neutrons varies with angle. However, the value of this cross section is determined at the angles at which the independent neutron measurement is made by use of the counter telescope or by detecting alpha-particles. Thus, a curve of the $Cu(n,2n)$ cross section as a function of energy can be drawn in this energy region. Since the $(n,2n)$ cross section does not change rapidly in this region, one can use a smooth curve through the points to estimate the value at intermediate energies. The points represented by diamonds, then, give the experimental values of the *d-t* differential cross section determined by this method and converted to the center-of-mass system.

TABLE II. Comparison of the $T(d,n)He^4$ reaction at 10.5 Mev with the $He^3(d,p)He^4$ reaction at 10.2 Mev.

Type point	$T(d,n)He^4$ Angle (CM)	σ(cm²)$\times10^{27}$	$He^3(d,p)He^4$ Angle (CM)	σ(cm²)$\times10^{27}$
Min	77°	1.76±0.06	77°	1.96±0.09
Max	112°	6.20±0.93	115°	4.95±0.23
Min	141°	3.07±0.46	135°	2.90±0.14

In order to obtain reasonable counting rates, as well as to make the backgrounds small relative to the real counts, considerably higher pressure of tritium gas was used for the neutron detection experiments than was necessary for counting the alpha-particles produced by the $T(d,n)He^4$ reaction. To hold this increased pressure a 13.7-mg/cm² aluminum entrance window was necessary in front of the target cell; and this, together with the increased stopping power of the tritium gas, reduced the average bombarding deuteron energy from 11.0±0.3 to 9.8±0.3 Mev. This condition prevailed for the case of the points marked by squares and open triangles.

The points marked by closed triangles are the results of Cu activation runs taken when the tritium gas cell had a one-mil front window, so that the average energy of the deuterons in the cell was 10.4 Mev. In these runs the relative values of the cross section were determined and the curve through the points was normalized to the alpha-data in the region of 97° in the center-of-mass system. First-order corrections (<6 percent) have been applied to that part of the curve in Fig. 2 found by counting neutrons by Cu activation to account for the angular resolution of the detectors. Also, for this part of the curve the data have been corrected for inelastic scattering of the neutrons by the walls of the target cell (<7 percent). It is apparent that these data lie within the spread of the activation data taken at 9.8 Mev and that within the accuracy of these measurements the *d-t* cross section does not change appreciably in this energy region when the energy of the deuteron is changed by 6 percent.

III. CONCLUSIONS

The composite curve through the solid points in Fig. 2 gives the differential *d-t* cross section for a bombarding energy of 10.5±0.3 Mev. Since the curve in Fig. 2 has only to be extrapolated through a relatively small angle to zero degrees, it can be integrated over all solid angles to give the total cross section of the $T(d,n)He^4$

[5] Hadley, Kelly, Leith, Segrè, Weigand, and York, Phys. Rev. 75, 351 (1949).
[7] R. K. Adair, Revs. Modern Phys. 22, 249 (1950).
[8] J. L. Fowler and J. M. Slye, Jr., Phys. Rev. 77, 787 (1950).

reaction at 10.5 Mev. This gives a value for the total cross section at this energy of 48±6 millibarns. Table II gives a comparison of the maximum and minimum of the absolute value together with the position of the maximum and minimum of the differential cross-section curve for the $T(d,n)He^4$ reaction and the mirror reaction, $He^3(d,p)He^4$.[2,9] It is apparent that these reactions are closely similar at this bombarding energy, where the effects of coulomb forces are small compared with purely nuclear forces. Since the intermediate nuclei formed by these two reactions differ from each other in that a neutron is substituted for a proton, this comparison suggests the approximate identity of the neutron and proton insofar as purely nuclear forces are concerned at these energies.

[9] J. C. Allred, LA-981 (unpublished).

PHYSICAL REVIEW VOLUME 82, NUMBER 4 MAY 15, 1951

The Gamma-Ray Yield of Phosphorus Bombarded with Protons*

G. R. Grove† and John N. Cooper
Department of Physics, Ohio State University, Columbus, Ohio

(Received January 15, 1951)

Protons from a van de graaff generator have been used to bombard P^{31}, and the reaction $P^{31}(p,\gamma)S^{32}$ has been studied. The gamma-ray yield has been measured, as a function of proton energy, in the region between 400 and 1700 kev. Maxima in the gamma-ray yield occur at proton energies of 440, 550, 650, 817, 890, 1067, 1100, 1129, 1162, 1265, 1421, 1458, 1495, 1538, 1583, and 1610 kev. Absorption measurements of the gamma-rays from the strongest resonance, that at 1265 kev, indicate a quantum energy of 12 Mev, which is consistent with the assumption that the compound nucleus decays to the ground state by a single transition.

I. INTRODUCTION

THE gamma-rays induced by proton bombardment of phosphorus were first observed by Curran and Strothers,[1] who reported maxima of a thick target excitation curve at proton energies of 460, 580, 700, and 950 kev. They measured the energy of the gamma-rays and concluded that the radiation must be associated chiefly with the reaction

$$H^1+P^{31}\rightarrow S^{32*}\rightarrow S^{32}+h\nu,$$

which has a Q-value of approximately 10.7 Mev. In studying this same reaction, Hole, Holtsmark, and Tangen[2] found three sharp resonances situated at 347, 433, and 530 kev. More recently, Tangen[3] has re-examined these resonances, which he reported at proton energies of 355, 440, and 540 kev. Thick targets were used in these investigations of the proton-capture process in phosphorus, and proton energies above one Mev were not available.

Some work with thin phosphorus targets and proton energies above one Mev was done by Herb[4] and his collaborators, who elected to discontinue this study in favor of other problems. The present authors have made careful runs over the levels studied at Wisconsin and have discovered several new levels. Both thick and thin targets have been bombarded with protons of energies between 400 and 1700 kev, and the gamma-resonances have been studied. Preliminary results of measurements on phosphorus were reported earlier.[5]

In addition to the reaction under consideration, the bombardment of phosphorus with protons may lead to the reaction

$$H^1+P^{31}\rightarrow S^{32*}\rightarrow Si^{28}+He^4,$$

which has a Q-value of approximately 1.8 Mev. The alpha-particles from this reaction have not been observed as yet.

II. EXPERIMENTAL PROCEDURE

The electrostatic generator at the Ohio State University was used as the source of bombarding protons. The voltage stability of the generator depends on corona drain to grounded needle points above the high voltage cap. With large drains the cap voltage is held constant to about $\frac{1}{4}$ percent with respect to rapid fluctuations.

An analyzing magnet located at the grounded end of the accelerating tube separates ions of the desired e/m and energy value from the several types of particles which come down the tube. A variable slit located in the path of the bombarding beam allows protons of

* Assisted by the joint program of the ONR and AEC through a contract with The Ohio State University Research Foundation.
† AEC Predoctoral Fellow; now at the National Bureau of Standards.
[1] S. C. Curran and J. E. Strothers, Proc. Roy. Soc. (London) A172, 72 (1939).
[2] Hole, Holtsmark, and Tangen, Naturwiss. 28, 668 (1940).
[3] R. Tangen, Kgl. Norske Videnskab. Selskabs Skrifter (1946), NR I.
[4] R. G. Herb, private communication. The authors are deeply grateful to Professor Herb for suggestions and, especially, for making available the complete results of the preliminary work at Wisconsin.
[5] Grove, Cooper, and Harris, Phys. Rev. 80, 107 and 131 (1950).

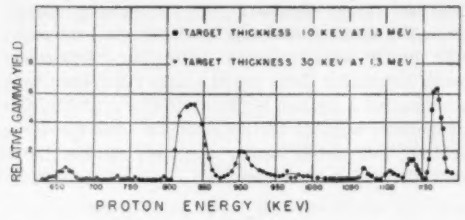

FIG. 1. Relative gamma-ray yield from P^{31} bombarded with protons of energies between 600 and 1200 kev.

only a few kilovolts energy spread to pass through and strike the target. Under favorable conditions, 1.5 μamp pass through this slit. The current in the coils of the magnet is determined by measuring the voltage drop across a one-ohm standard resistance with a Leeds and Northrup Type *K* potentiometer. It is found that the magnet current is a very reliable means of measuring the generator voltage because of its sensitivity and reproducibility. The magnet current was calibrated in terms of the accelerating potential from the accurately known resonances in lithium and fluorine at 440 and 873.5 kev as determined by Herb, Snowdon, and Sala.[6] The magnet current was always increased during the course of a run, after which it was increased to a fixed large value and then decreased zero. Usually, steps of 1.25 mamp were taken, which corresponds to about a 2 kev step at 1 amp. Resonance maxima were reproducible to about 3 kev on independent runs.

With a single Geiger tube placed 9.5 mm from the target an effective relative solid angle of 0.128 was obtained. With this counting geometry, the efficiency of the Geiger tube was determined for the 17 and 6.2 Mev quanta of lithium and fluorine, respectively, from the known cross sections of these resonances.[7] The charge collected on the target was recorded by a thyratron current integrator and mechanical recorder and the concomitant number of gamma-rays counted

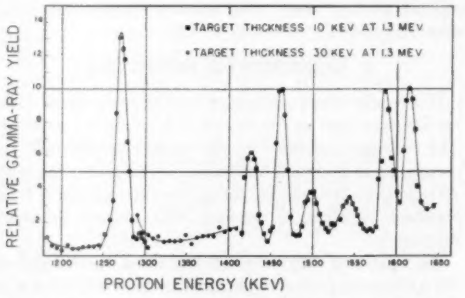

FIG. 2. Relative gamma-ray yield from P^{31} bombarded with protons of energy between 1200 and 1650 kev.

[6] Herb, Snowdon, and Sala, Phys. Rev. **75**, 246 (1949).
[7] T. W. Bonner and J. E. Evans, Phys. Rev. **73**, 666 (1948).

was recorded by a scale-of-4096 scaler and a mechanical recorder.

Phosphorus targets were prepared by vacuum evaporation of zinc phosphide and calcium phosphide on five mil tantalum disks. Zinc phosphide targets of 75, 40, 30, and 10 kev thicknesses at 1.3 Mev, as well as thick targets, were bombarded. These targets were very durable and showed no appreciable deterioration during the time they were used. Several thin calcium phosphide targets were also prepared and bombarded; these targets were somewhat less stable.

III. EXPERIMENTAL RESULTS

The excitation curves resulting from the proton bombardment of zinc phosphide are shown in Figs. 1 and 2. The yield from a target of about 30-kev thickness at 1.3 Mev is shown in the energy region below 1.0 Mev and in the low yield regions around 1.2 and 1.35 Mev. A target of 10-kev thickness at 1.3 Mev (87 $\mu g/cm^2$) was used for the energy region above 1.0 Mev to get better resolution of the resonance levels. Proton excitation energies of 650, 817, 890, 1067, 1100, 1129, 1162, 1265, 1421, 1458, 1495, 1538, 1583, and 1610 kev have been assigned to the observed resonance levels. These resonance energies are believed to be not more than 15 kev in error with respect to the absolute voltage scale. In addition to the resonances shown, the levels at 440- and 540-kev bombarding energy were observed. At most points on these resonances, over 1000 Geiger counts were taken.

The data plotted have been corrected only for the background not associated with the ion beam. At off-resonance points the Geiger counting rate was of the same order of magnitude as this background counting rate, so that the difference of the two rates gives rise to large percentage variations. The statistical fluctuations of these off-resonance regions are to be distinguished from the less intense levels which were always indicated in data from other thin targets as well as from thick targets. The excitation curve obtained from the bombardment of thin calcium phosphide targets showed the presence of all the levels observed from zinc phosphide.

A check of the gamma-ray yield from targets of tantalum, zinc, and calcium oxide was made. Tantalum gave a very small yield which increased slowly with proton energy. The yield from the zinc and calcium oxide targets was much greater than that from the tantalum, but there was no indication that any of the reported resonances could be attributed to zinc or to calcium.

IV. DISCUSSION OF THE RESULTS

In comparing the data of Fig. 1 with that of Curran and Strothers, it should be noted that they reported the *maxima* of a thick target excitation curve at 700 and 950 kev, while Fig. 1 shows thin target resonances

at 650, 917, and 890 kev. The level they reported at 950 kev is probably due to the combined contributions of the 817- and 890-kev levels of Fig. 1. Indeed, if the curve is drawn through the 850-kev point in the figure of Curran and Strothers,[1] a definite suggestion of two levels is apparent.

Absorption measurements of the radiation from the 1.265-Mev resonance made with lead, copper, and aluminum absorbers were consistent with a gamma-ray of approximately 12-Mev energy. Since the proton capture process in phosphorus is 10.7-Mev exothermic, a gamma-ray of about 12-Mev energy would be expected if the excited sulfur nucleus decays to the ground state by a single transition.

The efficiency of the Geiger tube was estimated for quanta of 12-Mev energy from the previously determined efficiencies for the lithium and fluorine radiations. From the Geiger counter efficiency, the effective solid angle subtended by the counter, the number of gamma-rays counted per incident proton, and the average number of phosphorus nuclei per unit area of the target, the cross section of the 1.265-Mev resonance was calculated to be 6.4×10^{-25} cm^2. The natural half-width of this level was estimated to be 6.5 kev; this corresponds to a mean life of the excited state of the compound nucleus of approximately 10^{-19} sec.

A comparison of the proton-capture resonance energies for target nuclei which lack one proton of having an even number of alpha-particles shows that there is a similarity between P^{31} and F^{19}. On the other hand, Na^{23} and Al^{27} have progressively denser level spacings. Conceivably, there may be a correlation with the nuclear spin, which is $\frac{1}{2}$ for phosphorus and fluorine, $\frac{3}{2}$ for sodium, and 5/2 for aluminum.

The authors are grateful to Professor R. G. Herb for his generous help, to Professor J. C. Harris for stimulating discussions and for his participation in actual measurements during part of the investigation, and to Roger Buehler and Warren E. Taylor for their assistance in taking data and in keeping the generator in operation. The generous support of the Ohio State University Development Fund is gratefully acknowledged.

PHYSICAL REVIEW VOLUME 82, NUMBER 4 MAY 15, 1951

Microwave Resonance Absorption in Paramagnetic Salts*

YU TING AND DUDLEY WILLIAMS
Mendenhall Laboratory of Physics, Ohio State University, Columbus, Ohio
(Received January 8, 1951)

Thirteen paramagnetic salts of the iron group in powdered or crystalline form have been investigated for their resonance absorption at microwave frequencies. Effective g-factors are obtained from the frequencies and magnetic field strengths at which absorption peaks occur. The effects on line shape from dipole-dipole and exchange interactions, and from the crystalline electric field, have been studied.

I. INTRODUCTION

THIS work is intended as a general survey of paramagnetic absorption, at room temperature, in various salts of the iron group, with particular attention to the study of line shapes.

It is well known that the magnetic moments of the iron group are due to electrons of the inner incomplete shell $3d$. The shapes of $3d$ orbits permit their energies to be perturbed seriously by the electric fields of neighboring atoms or ions. Immersed in a crystal lattice, these ions will then have their orbital degeneracy reduced in accordance with the particular symmetry[1] of the crystalline Stark field. The removal of orbital degeneracy implies that orbital magnetism is quenched, so that the effective magnetic moments of the ions result from spin only. When a dc magnetic field is applied, the lowest Stark level (or, possibly, several closely spaced levels) is split further into Zeeman components. The spacing between these components in a field of several thousand gauss falls in the microwave region. As magnetic dipole transitions of considerable intensity can occur[2] between levels of $\Delta m=\pm1$, m being the magnetic quantum number, the field H_0 for resonance absorption at a given frequency ν is

$$h\nu=|\Delta m g\beta H_0|=|g\beta H_0|, \tag{1}$$

where β is the Bohr magneton, and g is a measure of the effective gyromagnetic ratio.

Actually, the levels have been widened considerably by various interactions between ions. Such interactions, therefore, broaden the absorption line. Besides, they are chiefly responsible for the restoring of thermal equilibrium in the spin system, which in turn makes possible a net absorption when the microwave field is applied. While the phenomenon of spin relaxation is not completely understood, particularly in its relation to

* Some of the equipment used in this study was made available in connection with related work being conducted under a contract between the Geophysical Directorate of the Air Force Cambridge Research Laboratories and The Ohio State University Research Foundation.

[1] H. A. Bethe, Ann. Physik 3, 133 (1929).

[2] C. Kittel and J. M. Luttinger, Phys. Rev. 73, 1621 (1948).

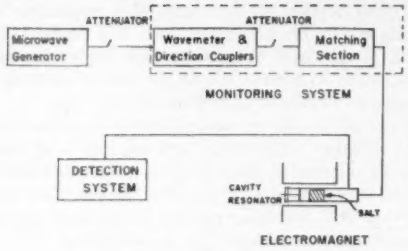

FIG. 1. Block diagram of apparatus.

the dc magnetic field and temperature, it is accepted[3,4] that the spin-lattice relaxation is not important in this process of transverse absorption (i.e., absorption occurring when the rf magnetic field is perpendicular to the dc field). The spin-lattice relaxation time τ_{LS}, however, contributes additively, with the spin-spin relaxation time τ_S, to line width through the relation

$$\Delta\nu_{\frac{1}{2}}=1/\tau_S+1/\tau_{LS}. \quad (2)$$

The observation of spin absorption was first reported by Zavoisky[5] in 1946. Subsequently, similar work was carried out by several other investigators.[4,6–8] The Rutgers group[7] first succeeded in finding the detailed line structure for crystals of the chrome alum.[8]

II. EXPERIMENTAL ARRANGEMENTS

The general arrangement of apparatus is shown in Fig. 1. The microwave source is followed by attenuators, wave meter, forward and backward direction couplers, and matching screw, for monitoring and matching purposes. The frequency used is 9516 Mc/sec, corresponding to 0.3174 cm^{-1}. Following the matching section is a transmission cavity containing the sample. The cavity was cut out of a long section of rectangular wave guide with an input iris at the center of the guide cross section and an output iris in the broad face of the wave guide. As the cavity was operated on the TE_{01n} mode ($n=8$), it was mounted with the broad face normal to the dc magnetic field to insure transverse absorption.

The detection system in Fig. 1 consists of a crystal detector, amplifier, a crystal rectifier, and a shielded wall-type galvanometer. As the detector voltage output was less than 0.02 v (open circuit value) in all absorption measurements, square-law detection can safely be assumed.[9] The evaluation of the detector voltage (which is proportional to the cavity power output) from galvanometer readings was made possible by a calibration of the latter against the detector voltage after each absorption measurement.

At least two successive runs were made in determining an absorption curve. Each run began at high field (6800 gauss), where magnetic absorption was zero, and continued through the resonance region to zero field. The field current, which was used as a measure of field strength, was calibrated against a fluxmeter, which in turn was calibrated with the proton resonance experi-

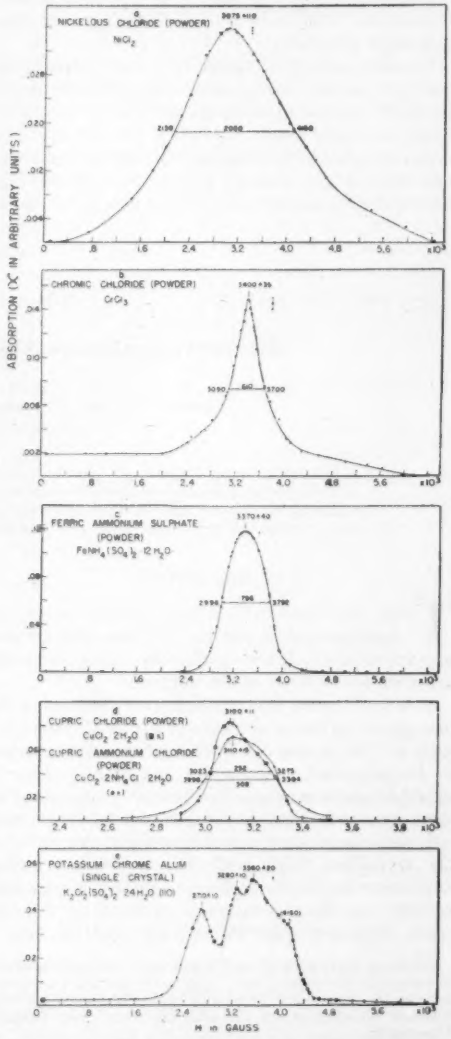

FIG. 2. Typical magnetic resonance curves for paramagnetic salts.

[3] I. G. Shaposhnikov, J. Exp. Theoret. Phys. (U.S.S.R.) **19**, 225 (1949).
[4] Bagguley, Bleaney, Griffiths, Penrose, and Plumpton, Proc. Phys. Soc. (London) **61**, 551 (1948).
[5] E. Zavoisky, J. Phys. (U.S.S.R.) **10**, 170, 197 (1946).
[6] Cummerow, Halliday, and Moore, Phys. Rev. **72**, 1233 (1947).
[7] Whitmer, Weidner, Hsiang, and Weiss, Phys. Rev. **74**, 1478 (1948).
[8] Ting, Weidler, and Williams, Phys. Rev. **74**, 1889 (1948); **75**, 980 (1949); and **80**, 226 (1950).
[9] H. C. Torrey and C. A. Whitmer, *Crystal Rectifiers* (McGraw-Hill Book Company, Inc. New York, 1948), p. 334, Fig. 11.1.

ment. The probable error in field readings is ±20 gauss in fields of 3000 gauss. In determining the resonance field H_0, an additional small error in reading galvanometer deflections, and errors in locating the peak of broad absorption lines must be included. These additional errors are indicated on each absorption curve (Fig. 2).

The salt samples were sometimes found to absorb or give off water vapor. This gain or loss of water by the sample changed the dielectric loss; this affected the cavity Q and hence the power output of the cavity. To avoid such drifts in cavity power output, the powdered samples were sealed in polystyrene boxes, while single crystals were coated with polystyrene. The coating around single crystals was in some cases (ferric alum and chrome alum) also necessary for their preservation.

III. EXPERIMENTAL RESULTS

The ratio of cavity output, with and without magnetic absorption, i.e., P_a/P_{em}, was evaluated from the galvanometer reading at each dc field setting. It can be shown[6] that the ratio of magnetic energy absorption per cycle to mean stored energy in the cavity, and hence the imaginary component of susceptibility, χ'', is proportional to $[(P_a/P_{em})^{\frac{1}{2}}-1]$. This quantity $[(P_a/P_{em})^{\frac{1}{2}}-1]$ was then plotted against the dc magnetic field. The absorption lines so determined can be collected into five groups according to their shapes, and also, incidentally, according to ions. Group (a): the lines of nickelous halides (powders) are weak and broad. Group (b): the lines of chromic salts (powders) are peaked at center but prolonged on tails; the weak lines of group (b) are those of $CrCl_3$ and $CrBr_3$. Group (c): the lines of ferric salts are strong and fairly flat at center. The shape of the ferric sulfate line is intermediate between groups (b) and (c). Group (d): the lines of cupric salts (powders) are strong, sharp, and asymmetrical. Group (e): the lines of potassium chrome alum, in powdered and crystalline form, are partially resolved into several components. Typical curves of each group from (a) to (e) are shown in Fig. 2a–e. In Fig. 2d, the peak portion of $CuCl_2\cdot 2NH_4Cl\cdot 2H_2O$ line is considerably wider than that of the $CuCl_2\cdot 2H_2O$ line.

TABLE I. Effective g-factors and half-widths.

Salt	g	Δg	Half-width $\Delta\nu_{\frac{1}{2}}$ Observed	Calculated
$CuSO_4\cdot 5H_2O$	2.22	0.02	290 gauss	475 gauss
$CuCl_2\cdot 2H_2O$	2.19	0.02	250	750
$CuCl_2\cdot 2NH_4Cl\cdot 2H_2O$	2.19	0.03	310	350
$FeNH_4(SO_4)_2\cdot 12H_2O$				
Powder	2.02	0.04	800	590
100 Orien.	2.02	0.03	850	436
110 Orien.	2.06	0.05	740	580
111 Orien.	2.04	0.05	850	636
$Fe_2(SO_4)_3\cdot 3H_2O$*	2.01	0.03	750	
$NiCl_2$	2.21	0.09	2020	3000
$NiBr_2$*	2.27	0.11	2150	2700
$CrCl_3$*	2.00	0.03	610	2350
$CrBr_3$	1.99	0.06	1160	2540
CrF_2	2.00	0.03	660	
$Cr_2(SO_3)_3$	2.00	0.06	730	
$Cr_2(SO_4)_3$	1.98	0.03	660	
$K_2Cr_2(SO_4)_4\cdot 24H_2O$				
Powder*	1.98	0.02		
110 Orien.	1.98	0.01		

TABLE II. Resonance fields of potassium chrome alum crystal at 110 orientation.

	Calculated for $d=0.140$ cm^{-1}	Observed
H_1	2470 gauss	
H_2	2700	2710 gauss
H_3	3300	3280
H_4	3530	3560
H_5	3960	
H_6	4180	(4160)

From the observed absorption lines, effective g-factors were computed by means of Eq. (1). These g-factors, their uncertainties, Δg, and the half-widths, $\Delta\nu_{\frac{1}{2}}$, are given in Table I. The half-width is defined as the width in gauss between two half-power points of the absorption curve. Except for those salts for which orientations relative to the dc magnetic field are listed, all salts in Table I are powders. The stars indicate salts with appreciable zero (magnetic) field absorption. The last column, giving the calculated half-width, is explained below.

In Table I, the g-factors of cupric and nickelous ions are greater than 2. This is understandable when one considers the perturbation[10] of ground-level wave functions by crystalline fields and the fact that both ions have negative spin-orbital constants.

The effective g-factor (Table I) of potassium chrome alum crystal at 110 orientation, and the separation d between its lowest Stark levels, were determined by Weiss' theory[7,11]

$$g=1.98, \quad d=0.140 \text{ cm}^{-1}. \tag{3}$$

With these values of g and d, resonance fields were recalculated and compared in Table II with the observed values (Fig. 2e).

The observed half-width of $CrCl_3$ given in Table I and Fig. 2b is almost 12 times that reported in reference 4 (50 gauss). Calculations given below show that the root-mean-square-width $\Delta\nu_{rms}$ of the line is comparable with the calculated dipole-dipole value. As exchange interaction does not affect $\Delta\nu_{rms}$, this approximate agreement partially justifies the present result.[12]

It must be pointed out that while Table I indicates the observation of 17 absorption lines, many other

[10] D. Polder, Physica **9**, 709 (1942). R. Schlapp and W. G. Penney, Phys. Rev. **42**, 666 (1932).

[11] In reference 7, p. 1484, the three resonance equations under $\theta=90°$ should be interchanged with the three under $\theta=35°\,16'$. The d-value obtained in the present work is slightly higher than Rutgers' value, $d=0.130$ cm^{-1}.

[12] B. M. Kozyrev and S. G. Salikov, J. Exp. Theoret. Phys. (U.S.S.R.) **19**, 185 (1949), found the line width at 1/100 of our frequency (and hence at 1/100 of the magnetic field we used) to be nearly 2×90 gauss. From the relations of magnetic anisotropy and $1/\tau_{LS}$ to the dc magnetic field, one would expect the half-width at the present frequency to be larger than 180 gauss.

TABLE III. Root-mean-square-widths, $\Delta\nu_{rms}$.

Salt	Calculated	Observed
$NiCl_2$	1260 gauss	1070 gauss
$NiBr_2$	1140	1120
$CrCl_3$	1000	870
$CrBr_3$	1080	850
$CuCl_2 \cdot 2NH_4Cl \cdot 2H_2O$	150	190

salts have been studied (at room temperature and 3 cm wavelength) without observing a line, particularly those of Ni^{++} and CO^{++} ions. The absence of observable lines may be due to short spin-lattice relaxation time [Eq. (2)] or to large dielectric losses in the salt sample.

IV. LINE WIDTH

In Van Vleck's theory[13] of line width of spin absorption, the root-mean-square-width is given by

$$\Delta\nu_{rms}=[\tfrac{3}{8}g^2\beta^2S(S+1)\Sigma_j r_{ij}^{-6}]^{\frac{1}{2}} \text{ gauss} \quad (4)$$

for powders, and by

$$\Delta\nu_{rms}=[\tfrac{3}{8}g^2\beta^2[a+b(\lambda_1^4+\lambda_2^4+\lambda_3^4)]S(S+1)]^{\frac{1}{2}} \text{ gauss} \quad (5)$$

for cubic crystals. Here S is the spin of an ion; λ, a, and b are functions[13] of various direction cosines and of the distance r_{ij} between neighboring ions. The equations have been altered slightly from the original form by assuming the constancy of the g-value. If there were no exchange interaction, and the absorption line could be approximated by a gaussian curve, then the width between half-half-power points would be

$$\Delta\nu_{\frac{1}{2}}=2.35\Delta\nu_{rms}. \quad (6)$$

This will be called the dipole width. Since exchange interaction contributes positively to $\langle(\Delta\nu)^4\rangle_{Av}$ but nothing to $\langle(\Delta\nu)^2\rangle_{Av}$, it tends to prolong the tail and narrow the peak. When the magnetic ions in a salt are diluted by foreign ions, such as NH_4^+, exchange interaction is reduced, which explains why one observes a wider peak for $CuCl_2 \cdot 2NH_4Cl \cdot 2H_2O$ than for $CuCl_2 \cdot 2H_2O$ (Fig. 2d). In cases for which data on crystal structures[14] were available, the dipole widths were computed from Eqs. (4–6) and are listed in Table I (last column) for comparison with the observed half-widths. It is seen that, except for ferric ammonium alum, the widths of the observed lines are smaller than the calculated values. The largest difference occurs in $CrCl_3$ line (1700 gauss). The opposite effect in ferric ammonium alum is not surprising, since this salt has a cubic field splitting of 0.13 cm^{-1}, and, hence, the observed line is a superposition of several peaks. For this reason, this salt will not be included in the comparison of root-mean-square-widths.

While the assumption of a spin-only system for the magnetic ions is justifiable from the closeness of g to 2 (Table I), the other assumption[13] in Van Vleck's theory, that the crystalline electric field has a negligible effect on the line-widths, needs to be examined for individual cases. This can be done by a comparison of mean-square-widths in which exchange interaction has no effect. The last column in Table III was obtained from the relation

$$\Delta\nu_{rms}=\left[\int Y(\Delta H)^2dH \Big/ \int Y dH\right]^{\frac{1}{2}} \text{ gauss}, \quad (7)$$

Y being the ordinate of the observed absorption curve, and ΔH the deviation from resonance field H_0. It is seen that, except for the cupric salt, there is an approximate agreement. This approximate agreement indicates that the crystalline field has a negligible effect on line width in $NiCl_2$, $NiBr_2$, $CrCl_3$, and $CrBr_3$.

The writers wish to express their appreciation to Dr. R. C. Weidler for his assistance in certain phases of the experimental work, to Professor Preston Harris and Mr. Donald Tuomi for advice on crystal growth and structures, and to Professor George Mueller for his suggestion on cavity design.

[13] J. H. Van Vleck, Phys. Rev. 74, 1168 (1948).

[14] R. W. G. Wyckoff, *Crystal Structures* (Interscience Publishers, New York, 1948), chapters IV, V. R. W. G. Wyckoff, *The Structures of Crystals* (The Chemical Catalog Company, New York, 1931), pp. 310–319.

Photo-Production of N^{17}

W. E. Stephens, J. Halpern, and R. Sher
Physics Department, University of Pennsylvania, Philadelphia, Pennsylvania*
(Received December 22, 1950)

The delayed neutron activity associated with N^{17} has been produced by the x-ray irradiation of oxygen, the reaction being identified as $O^{18}(\gamma,p)N^{17}$. The threshold for this transmutation has been observed as 16.35±0.2 Mev, and the integrated cross section calculated to be 0.15±0.1 Mev-barn. The N^{17} produced was identified by measuring the neutron activity half-life as 4.15±0.1 sec.

I. INTRODUCTION

THE first light element delayed neutron activity was observed following the bombardment of fluorine with high energy deuterons.[1] The neutron activity was found to result from the beta-decay[2] of N^{17} with a half-life[1] of 4.14±0.04 sec and a beta-ray maximum energy[3] of 3.7±0.2 Mev. This leads to an excited state of O^{17} about 5 Mev above the ground state. This broad excited state of O^{17} breaks up into O^{16} and a neutron of approximately 0.9 Mev energy.[3,4] Many spallation reactions have been observed[5] to produce N^{17}, and it has been produced by[6] $C^{14}(\alpha,p)N^{17}$ and[7] $O^{17}(n,p)N^{17}$. Another possible reaction leading to N^{17} is $O^{18}(\gamma,p)N^{17}$. Despite the natural low abundance of O^{18}, the unique neutron activity makes it possible to detect this (γ,p) reaction with betatron x-rays. This paper reports measurements of the yield curve of this reaction determined by flow methods. Preliminary results were reported earlier.[8]

II. EXPERIMENT

In the initial experiments a 250-cc beaker of ordinary water was placed one foot from the target of a 25-Mev betatron. An enriched[9] BF_3 proportional counter, six inches behind the water, was used to detect the neutrons slowed down by the water plus several inches of paraffin. The water was irradiated at the rate of 15 roentgen units per second with the bremsstrahlung x-rays from the betatron run at 25 Mev for 15 sec. When the betatron was turned off, the counter was turned on and the neutron counts recorded by photographing the scalar with a movie camera. The initial neutron activity of about 30 counts/sec decayed with a half-life of approximately 4 sec. Water enriched in[9] O^{18} showed an increased delayed neutron activity consistent with its enrichment. These tests indicated that the transmutation involved is $O^{18}(\gamma,p)N^{17}$. It was checked that no appreciable amount of this activity was induced by the background neutrons through $O^{17}(n,p)N^{17}$ by activation in and out of the x-ray beam. No activity above background was observed when the water was out of the beam, although the number of neutrons should be about the same. By varying the betatron energy, the yield was observed to appear at about 18 Mev and keep rising up to 25 Mev.

In order to increase the sensitivity of detection, a flow method of irradiation was set up. Water was flowed through a Lucite container of approximately conical shape placed in the x-ray beam about 16 cm from the betatron target. The irradiated water was carried through a ¼-in. tube, about 864 cm long, to the neutron detector outside the betatron room. By varying the water pressure from 3 to 30 lb/in.^{2}, the flow rate could be varied from 0.35 to 1.5 liters/min, which corresponded to flow times of from 25 to 6 sec. The flow rate was measured by a flow meter and kept constant by a water pressure reducing valve. The flow tube was coupled to an equally long copper tube coiled around an enriched BF_3 proportional counter[9] immersed in water. This region was enclosed in cadmium and shielded by additional water. This detector had an efficiency of approximately 0.02 for radium-beryllium neutrons. This arrangement was considerably more sensitive than the initial setup, and counts could be continued for times long compared to the half-life under constant conditions of flow and irradiation. The yield curve measured under these conditions is shown in Fig. 1. In this curve the abscissa gives the maximum betatron energy, which was changed by varying the betatron magnet current when expanding at the peak of the magnetic field. The ordinate gives the observed neutron counts for 10 ionization chamber monitor integrator counts. The integrator was calibrated against a Victoreen r-meter, and it was found that 10 counts were equivalent to 140 r-units at three feet. The flow rate was kept at 1.44 liters/min, and several runs were made.

In order to investigate the threshold more carefully, extended observations (up to half an hour) were made in the threshold region, using a "variable" expander on the betatron so that the maximum energy of the x-rays

* This research was supported by the joint program of the ONR and AEC.
[1] Knable, Lawrence, Leith, Mayer, and Thornton, Phys. Rev. 74, 1217 (1948).
[2] L. W. Alvarez, Phys. Rev. 74, 1217 (1948).
[3] L. W. Alvarez, Phys. Rev. 75, 1127 (1949).
[4] E. Hayward, Phys. Rev. 75, 917 (1949).
[5] W. W. Chupp and E. M. McMillan, Phys. Rev. 74, 1217 (1948).
[6] Sun, Jennings, Shoupp, and Allen, Phys. Rev. 75, 1302 (1949).
[7] Charpie, Sun, Jennings, and Nechaj, Phys. Rev. 76, 1255 (1949).
[8] Sher, Halpern, and Stephens, Phys. Rev. 79, 241 (1950).
[9] Allocated by the Isotopes Division of the AEC.

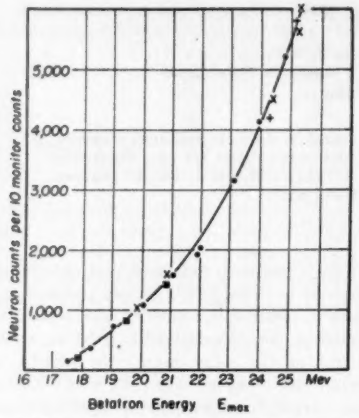

FIG. 1. Neutron counts as a function of betatron energy.

could be changed in small steps and held more constant during a run. A typical curve is shown in Fig. 2. In this curve is shown the delayed neutron activity associated with the production of N^{17} by $O^{18}(\gamma,p)N^{17}$ and, also, the O^{15} positron activity produced by $O^{16}(\gamma,n)O^{15}$. This O^{15} activity was observed in the same run with the N^{17} counts by inserting a thin-wall Geiger counter in the water outlet pipe. The O^{15} activity took longer to build up to equilibrium, since its half-life is 2 min, but the equilibrium activity was quite strong.

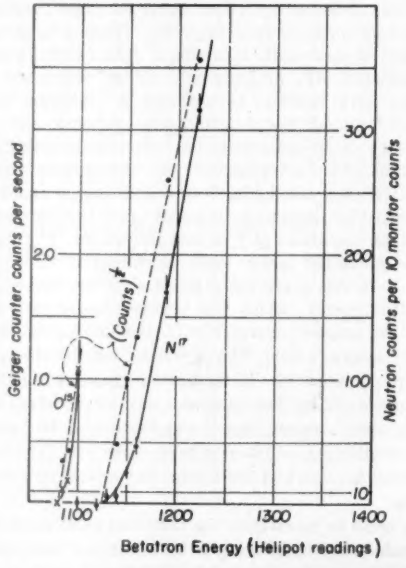

FIG. 2. Neutron counts on right, and O^{15} activity on left as a function of the betatron energy.

The variable expander was calibrated against the assumed known values of the photo-neutron thresholds of deuterium (2.23 Mev), copper (10.9 Mev), and carbon (18.7 Mev). The threshold is at least as low as 16.6 Mev, with an uncertainty of ±0.2 Mev due to the calibration. When the square roots of the counts are plotted (this gives a straight line near (γ,n) thresholds),[10] a straight line extrapolates to 16.35 Mev. Since it might be expected that the (γ,p) yield curve tails off differently than the (γ,n), owing to the coulomb penetration factor, there is still a slight uncertainty in what should be called the threshold. The N^{17} extrapolated threshold relative to that of O^{18} has a smaller calibration uncertainty and is 1.048.

In order to check the half-life and determine the cross section, several corrections have to be applied to the data. The number of neutron counts of the detector during 10 monitor counts (equivalent to 140 roentgen units at three feet) can be expressed as

$$y=\epsilon\exp(-t_f/t_m)[1-\exp(-t_d/t_m)]\pi\alpha^2RN\cdot YS,$$

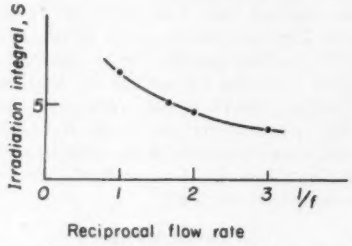

FIG. 3. Irradiation integral S as a function of reciprocal flow rate.

where

$$Y=\int_0^{E_{max}} n(E,E_{max})\sigma(E)dE,$$

and

$$S=\int_{x_{max}}^{x_{min}}\exp\left[\frac{\pi\alpha^2(x_{min}^3-x^3)}{3ft_m}\right]dx,$$

where

ϵ is the detector efficiency;
t_f is the flow time $=A_f l_f/f$;
A_f is the area of the flow tube;
l_f is the length of the flow tube;
f is the flow rate;
t_m is the mean life of the N^{17} activity;
t_d is the time spent by the water near the detector $=A_d l_d/f$;
α is the approximate angle of the cone of the irradiation box and is the same as the angle of divergence of the x-ray beam;
R is the number of roentgen units/cm² at 1 cm for 10 monitor counts;
N is the number of O^{18} nuclei per cc;
$n(E,E_{max})$ is the number of photons per cm² of energy E per roentgen unit per Mev interval when the betatron energy is E_{max};

[10] McIlhinney, Hanson, Becker, Duffield, and Diven, Phys. Rev. 75, 542 (1949).

$\sigma(E)$ is the $O^{18}(\gamma,p)N^{17}$ cross section; and
x is the distance from the betatron target, x_{max} and x_{min} being the maximum and minimum distances the water occupies.

The first exponential gives the decay during the flow time. The brackets give the fraction of decays occurring while the irradiated water is near the detector. Y gives the bremsstrahlung photon energy distribution times the cross section, and S is an approximate expression of the irradiation process which estimates the fraction of saturation irradiation that is produced. This irradiation integral, S, was evaluated graphically and its value as a function of $1/f$ is given in Fig. 3. The other constants used are, $x_{min}=16$ cm, $x_{max}=40$ cm, $N=0.68\cdot10^{20}$ nuclei/cc, $t_m=6$ sec, $\epsilon=0.02$, $\alpha=0.1$, $t_d=9.18/f$. Holding the flow and irradiation conditions constant and varying E_{max} gives the yield curve of Fig. 1. Since under these conditions

$$y=c\int_0^{E_{max}} n(E, E_{max})\sigma(E)dE,$$

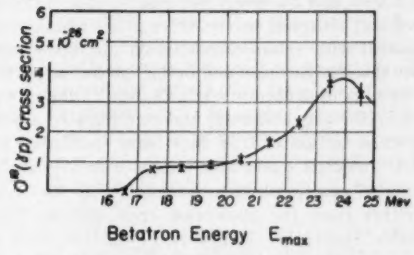

FIG. 4. Calculated cross-section curve for $O^{18}(\gamma,p)$ as a function of betatron energy.

it is possible to find $c\sigma(E)$, knowing n and y. The n values were taken from a set of curves calculated by Katz,[11] who kindly supplied us with copies. The cross-section curve calculated in this fashion is shown in Fig. 4. Keeping E_{max} constant and varying f should allow t_m to be determined. Since the expected value of t_m is known, we can insert $t_m=6$ sec in the correction terms and evaluate t_m, for this experiment, from the flow time exponential. Under these conditions,

$$\Omega\equiv y/[1-\exp(-t_d/t_m)]Y=c\exp(-t_f/t_m)$$

so that plotting Ω against t_f should give a regular decay curve. This has been done for several different flow tubes, and the resulting curves are shown in Fig. 5. A long Tygon tube, $A=0.1808$ cm^2, $l=888$ cm; a short Tygon tube, $A=0.1808$ cm^2, $l=435$ cm; and a long copper tube, $A=0.1808$ cm^2, $l=864$ cm were each used. These runs were all corrected to $E_{max}=22.8$ Mev and 10 monitor counts. These curves give half-lives of about 4 sec. A more reliable method for determining the half-life is one in which the correction for irradiation

[11] Katz, Johns, Douglas, and Haslam, Phys. Rev. **80**, 131 (1950).

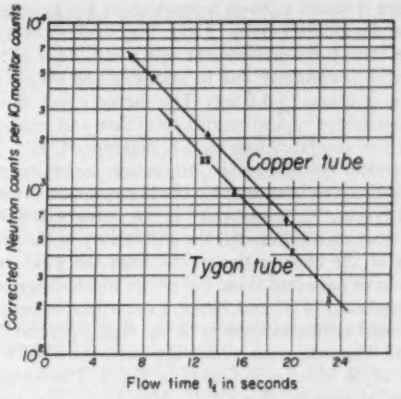

FIG. 5. Corrected neutron counts as a function of flow time.

drops out, since this is the least reliable and most approximate correction. At the same flow rate, the counts for the long and short Tygon tube differ only in the flow time. Hence,

$$\frac{y_{short}}{y_{long}}=\exp\frac{(t_{f\,long}-t_{f\,short})}{t_m}$$

$$=\exp\frac{(l_{long}-l_{short})A_f}{ft_m}=\exp\frac{4.72}{ft_m}.$$

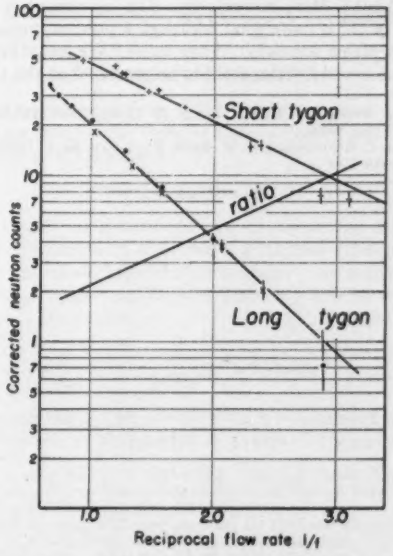

FIG. 6. Corrected neutron counts as a function of reciprocal flow for different length flow tubes. Also shown is the ratio of these two smoothed curves.

Figure 6 shows y_s/y_l as a function of $1/f$ as obtained from smoothed curves of the long and short tygon tube. This curve is consistent with a half-life of 4.15 sec, but the uncertainty due to statistics and other variations is about ± 0.1 sec. The factor c can now be evaluated for typical conditions of flow and irradiation and the absolute cross section determined. It will be uncertain, because of the irradiation correction term, the difficulty of determining the absorption in the water and holder, the uncertainty in the actual efficiency of the neutron counter, and the uncertainty in the derivation of the cross-section curve from the yield curve. We have neglected those N^{17} nuclei which decay to the ground state of O^{17} and, hence, give no delayed neutrons. Alvarez[8] estimates these to be less than 5 percent of the total. The peak cross section appears to be 0.037×10^{-24} cm^2 at 24 Mev, as indicated in Fig. 4. The integrated cross section is about 0.15 Mev-barn. The relative uncertainties in the cross section curve due to statistics in the yield curve data are indicated in Fig. 4. The absolute uncertainty is estimated at ± 50 percent. The integrated cross section has an additional uncertainty because of the assumed shape of the high energy part of the cross-section curve of ± 0.1 Mev-barn.

III. DISCUSSION

The threshold values of $O^{16}(\gamma,n)O^{15}$, 15.6 ± 0.2 Mev and of $O^{18}(\gamma,p)N^{17}$, 16.35 ± 0.2 Mev can be compared with the values calculated from the nuclear masses. Using Rosenfeld's masses[12] and the N^{17} beta-ray and neutron energy, we calculate values of 15.58 ± 0.08 and 16.01 ± 0.3 Mev, respectively. The agreement in the case of O^{16} is quite good, although a previous measurement gave a somewhat higher value.[13] We would expect the observed O^{15} threshold to be greater than the value calculated from the masses by the effective barrier height. The N^{17} coulomb barrier for protons is about 3 Mev. The height of the barrier for 0.1 penetration can be estimated[14] to be 0.8 Mev, while for 0.01 penetration it drops to 0.4 Mev. The observed difference, 0.34 ± 0.36 Mev, then seems reasonable for the extrapolated threshold.

Since O^{18} is such a light nucleus, its photo-disintegration can probably not be discussed reasonably in terms of the statistical theories. The (γ,n) threshold is calculated to be 8.0 Mev, so it can be assumed that the photo-neutron emission is the predominant reaction and that the photo-proton cross section is only a fraction of the photon absorption. The resonance energy and the integrated cross section are comparable with those measured on other light nuclei.[15,16] It is reassuring to note that a (γ,p) reaction observed with this somewhat different technique (i.e., delayed neutrons) exhibits a cross-section curve similar to those measured by radioactivity and proton scintillations.

The value of the energy at the peak cross section, 24 ± 2 Mev, and the integrated cross section, 0.15 ± 0.1 Mev-barn, observed in the $O^{18}(\gamma,p)N^{17}$ reaction, are consistent with values calculated on the dipole interaction theories. Levinger and Bethe[17] predict an average energy of photon absorption of 29 Mev (Yukawa well, $r_0=1.5\cdot 10^{-13}$ cm, and $x=\frac{1}{2}$) and an integrated absorption cross section of 0.38 Mev-barn. Goldhaber and Teller[18] calculate a resonance energy of 25 Mev and an integrated absorption cross section of 0.26 Mev-barn. In either case, the absorption cross section, which includes $(\gamma,n)(\gamma,2n)$, $(\gamma n,p)$ etc., would be expected to be several times the (γ,p) cross section.

[12] L. Rosenfeld, *Nuclear Forces II* (Interscience Publishers, New York, 1949).
[13] G. C. Baldwin and H. W. Koch, Phys. Rev. **67**, 1 (1945) give 16.3 ± 0.4 Mev.
[14] We are indebted to Professor V. Weisskopf for sending us his latest barrier penetration tables.
[15] A. K. Mann and J. Halpern, Phys. Rev. **80**, 470 (1950).
[16] H. Waffler and S. Younis, Helv. Phys. Acta **22**, 614 (1949).
[17] J. S. Levinger and H. A. Bethe, Phys. Rev. **78**, 115 (1950).
[18] M. Goldhaber and E. Teller, Phys. Rev. **74**, 1046 (1948).

The Noncentral Electric Interaction in Alpha-Radioactivity*

MELVIN A. PRESTON
McLennan Laboratory, University of Toronto, Toronto, Canada
(Received July 24, 1950)†

Apart from the penetrability of the coulomb potential barrier, which determines the order of magnitude of the intensity of α-decay, there are three secondary effects which alter the decay constant: angular momentum, "formation" prohibition as discussed by Perlman, Ghiorso, and Seaborg, and noncentral electric interaction with the product nucleus. The general theory of this last effect is discussed and its magnitude estimated. It is suggested that it may be of considerable importance in determining the intensity of highly forbidden ground state transitions described by Perlman, Ghiorso, and Seaborg. Further numerical work would be desirable.

I. INTRODUCTION

THE standard formula for the decay constant in α-activity is of the form

$$\lambda=(v_i/2r_0)G\exp(-2\omega_0). \qquad (A.1)$$

Here v_i is the velocity of the α-particle inside the nucleus of radius r_0, so that the first factor is the frequency of collisions of the α-particle with the nuclear barrier. The last factor, $\exp(-2\omega_0)$, describes the "leak" through the coulomb potential barrier around the nucleus and determines the order of magnitude of λ. (ω_0 will be defined later.) The remaining factor G depends in general on v_i, r_0, and v, the velocity at infinity. The form of G is determined by the model used to describe the forces holding the α-particle in the nucleus. For a rectangular well potential, G can be obtained explicitly.

This basic formula (A.1) applies only to the case in which the α-particle is emitted with zero angular momentum from an even–even nucleus in which the "formation" time of the α-particle is negligible. This point has been demonstrated by the analysis of Perlman, Ghiorso, and Seaborg.[1] In nuclei other than even–even, the α-particle must be formed from the nucleons; and in order to obtain full energy, it must include the unpaired nucleon(s) in the highest energy state. This effect makes the α-decay of such nuclei forbidden to some extent with respect to a hypothetical even–even decay of the same energy and same charge number. Also, in the decay of any one nuclear species, the ground-state transition requires that the α-particle carry away the maximum energy, which must be obtained from the unpaired nucleon(s). Hence, apart from barrier penetration, the low energy lines of a complex α-spectrum might be expected to be more probable than the ground-state transition. In other words, for their respective energies, the ground-state transition is forbidden relative to the other transitions possible. This effect requires a modification of the factor G; the exact theory is clearly complicated.

The formula for λ is also changed if the α-particle has non-zero angular momentum.[2,3]

There is a third mechanism[4] which can alter the value of λ given by the standard formula; namely, the noncentral interaction of the α-particle outside the nucleus with the unsymmetrically distributed protons in the product nucleus. By means of this coupling, the α-particle can take energy from or give energy up to the nucleus and thus alter its own ability to penetrate the barrier. The study of this effect arose from an attempt to understand, theoretically, certain observations[5] of the α-ray spectra of Po and Ra. The connection of the theory with this particular problem has already been given in a paper[6] hereafter referred to as P. In the present paper we propose to discuss this noncentral electric interaction effect in general. In P it was suggested that this mechanism might be important if a ground-state transition could be forbidden; a physical basis for this assumption is provided by the formation prohibition.

II. PERTURBATION SOLUTIONS

The general equations of the theory are given in P. We may summarize them as follows. The total wave function of the system is

$$\Psi=\sum_m \phi_m(\mathbf{r})u_m(\xi), \qquad (1.1)$$

where $u_m(\xi)$ are the complete set of normalized orthogonal eigenfunctions of the residual nucleus, ξ referring to all the coordinates which determine a nuclear configuration. The α-particle has position $\mathbf{r}$ and its wave functions are written

$$\phi_n(\mathbf{r})=r^{-1}f_n(r)\sum_{M=-l_n}^{l_n} c_M P_{l_n}{}^M(\cos\theta)e^{iM\varphi}. \qquad (1.2)$$

The potential $\sum(2e^2/|\mathbf{r}-\mathbf{r}_i|)-2Ze^2/r$ is treated as a perturbation. It is expanded in powers of $1/r$ and it is

* Most of the work here described was carried on at The University, Birmingham, England.
† Revised manuscript received January 22, 1951.
[1] Perlman, Ghiorso, and Seaborg, Phys. Rev. **77**, 26 (1950).
[2] G. Gamow and C. L. Critchfield, *Theory of Atomic Nucleus and Nuclear Energy Sources* (Clarendon Press, Oxford, 1949).
[3] M. A. Preston, Phys. Rev. **71**, 865 (1947).
[4] Originally suggested some years ago by Professor Gamow.
[5] W. Y. Chang, Phys. Rev. **69**, 60, and **70**, 632 (1946).
[6] M. A. Preston, Phys. Rev. **75**, 90 (1949). This work suggested that Chang's results were spurious. See W. G. Wadey, Phys. Rev. **74**, 1846 (1948).

deduced that the radial functions f_n satisfy

$$(d^2f_n/dr^2)+\{(2m/\hbar^2)(E_n-V)-l_n(l_n+1)/r^2\}f_n = \sum_{m=0}^{N-1} f_m \sum_{k=|l_m-l_n|}^{l_m+l_n} A_k{}^{nm} r^{-(k+1)}, \quad (1.3)$$

$$k\neq 0,\ n=0,\ 1,\ \cdots,\ N-1.$$

Here

$$V=2Ze^2/r, \quad r>r_0. \quad (1.4)$$

$A_k{}^{nm}$ is a mean transition matrix element averaged over the possible orientations of the angular momentum kh and is of order of magnitude

$$(4\sqrt{2}/2k+1)(me^2/\hbar^2)\int u_n{}^* \textstyle\sum_i r_i{}^k P_k(\cos\theta_i) u_m d\xi,$$

where $(r_i,\ \theta_i,\ \varphi_i)$ are the coordinates of the ith proton in the nucleus and the summation is over all such protons. These A's represent roughly the coupling which changes the angular momentum and energy of the α-particle. The origin is at the center of mass of the residual nucleons, m is the reduced mass, and E_n is the (strictly complex) energy of the nth α-particle group.

To simplify the problem, we shall study the case in which the residual nucleus has one or more excited levels all of the same spin. We assume that the transitions between these levels are unimportant compared with those between any one of them and the ground level; i.e., $A_k{}^{nm}\ll A_k{}^{n0}$ when $m\neq 0$. The case of only one excited level is, of course, included. Also, one of the terms of the summation over k in Eq. (1.3) is much greater than the rest. If the ground state has spin zero, there is only one term; otherwise the term with the least value of k is the important one. Let this value of $k=p-1$.

We now proceed to set up a perturbation calculation by the substitution

$$f_n(r)=w_n(r)\chi_n(k_nr), \quad (1.5)$$

where $\chi_n(x)$ is the confluent hypergeometric function defined by

$$(d^2\chi_n/dx^2)+\{1-(\kappa_n/x)-l_n(l_n+1)/x^2\}\chi_n=0, \quad (1.6)$$

and as $x\to\infty$,

$$\chi_n\to\exp i\{x+\tfrac{1}{4}\pi+\tfrac{1}{2}\kappa_n\ln(\kappa_n/4ex)\}. \quad (1.7)$$

$$\kappa_n=4Ze^2/hv_n, \quad k_n=mv_n/\hbar, \quad E_n=\tfrac{1}{2}mv_n{}^2. \quad (1.8)$$

Thus, χ_n is the wave function of the α-particle in the standard theory which does not take account of the interaction with the individual protons of the nucleus. χ_n is studied in P, Sec. IV. With this substitution and the simplifications indicated in the previous paragraph, Eqs. (1.3) become

$$\chi_0w_0''+2k_0\chi_0'w_0'=\sum_{m\neq 0}\chi_mw_mA_{p-1}{}^{0m}r^{-p}, \quad (1.9a)$$

$$\chi_nw_n''+2k_n\chi_n'w_n'=\chi_0w_0A_{p-1}{}^{n0}r^{-p}, \quad n\neq 0. \quad (1.9b)$$

t he argument of the function, that is, with respect to k_nr for χ_n and with respect to r for w_n.

To solve these equations one might be inclined to use a perturbation technique. At infinity, both χ_0 and χ_n have magnitude unity; the high energy α-particles are always observed to be considerably more intense than those of even slightly lower energy. Since the subscript 0 refers to the ground state, $E_0>E_n$; and hence at infinity $w_n\ll w_0$, and we might therefore assume the usual perturbation conditions; *viz.*, $w_0=a_0$, a constant, and w_n small. Then Eq. (1.9a) is discarded and we obtain

$$w_n(r)=v_{n0}(k_0r)+a_n\exp i\delta, \quad (1.10a)$$

$$w_n(\infty)=a_n\exp i\delta, \quad (1.10b)$$

$$w_0(r)=a_0. \quad (1.10c)$$

Here v_{n0} is given by P (3.17) and P (4.12), *viz.*,

$$v_{n0}(x)=\tfrac{1}{2}a_0\gamma_{0n}\rho_{n0}(\cot\alpha_0\cot\beta_0)^{\frac{1}{2}}\exp(\omega_0-\Omega_0)k_0{}^{p-2} \times A_{p-1}{}^{n0}\{I_{n0}{}^-(p-1)-I_{n0}{}^+(p-1)\}x^{-p}. \quad (1.11)$$

$\gamma_{nj}=k_n/k_j$ and the other functions in Eqs. (1.10) are defined in P, Sec. IV.

This is a straightforward perturbation calculation, which is suggested by the fact that $a_n\ll a_0$. However, in general, this solution is not valid. The value of the ratio a_n/a_0 predicted by a simple theory, based only on the barrier penetrability, is the ratio of the Gamow factors, *viz.*, $\exp(\omega(r_0)-\Omega(r_0))$, where r_0 is the nuclear radius and ω and Ω refer, respectively, to states 0 and n, being defined explicitly in P(4.2) and P(4.10). If a_n/a_0 has this value, then χ_n will equal χ_0a_0 at $r=r_0$, because of the corresponding exponential increase of χ_n/χ_0. Hence, χ_nw_n will be of at least the same order as χ_0w_0 in the region near the nucleus, unless a_n/a_0 is much less than the Gamow ratio. Hence the neglect of the right-hand side of Eq. (1.9a) is not usually justified.

Consequently, this simple perturbation calculation has had to be modified. The method used in P consists essentially of treating as a small perturbation not the functions f_n, but rather the departure of both the f_n's and f_0 from the functions $a_n\exp(i\delta_n)\chi_n$ and $a_0\chi_0$ which would be their forms if there were no interaction of the type we are studying. That is, we have there written

$$f_0=w_0\chi_0=(a_0+\textstyle\sum_n v_{0n})\chi_0, \quad (1.12a)$$

$$f_n=w_n\chi_n=(a_n\exp i\delta_n+v_{n0})\chi_0, \quad (1.12b)$$

and have assumed $|v_{0n}|\ll a_n\chi_n/\chi_0$ and $|v_{n0}|\ll a_0\chi_0/\chi_n$. The right-hand sides of these inequalities are, respectively, the unperturbed values of a_0 and a_n. Substitution in Eq. (1.9) then yields equations for v_{0n} and v_{n0} which are solved in P, with the result that v_{n0} is given as above by Eq. (1.11) and

$$v_{0n}(k_nr)=\tfrac{1}{2}a_n\rho_{0n}(\cot\alpha_0\cot\beta_0)^{\frac{1}{2}}\exp(\Omega_0-\omega_0)k_0{}^{p-2} \times A_{p-1}{}^{n0*}\{I_{0n}{}^-(p-1)-I_{0n}{}^+(p-1)\}x^{-p}. \quad (1.13)$$

The solutions (1.12) have much wider applications than Eqs. (1.10), but there are conditions in which Eqs. (1.12) also do not hold. These are if $|v_{0n}|$ or $|v_{n0}|$

becomes comparable with $a_n\chi_n/\chi_0$ or $a_0\chi_0/\chi_n$, respectively. If we look at the forms of v_{0n} and v_{n0}, we see that the orders of magnitude of all the terms but the integrals I^- are roughly independent of E_0-E_n, but as $E_0-E_n \to 0$, the I^- terms may become large, and the solution (1.12) becomes invalid. In this case, of course, Eq. (1.10) also fails. The quantities $(I^- - I^+)x^{-p}$ are largest for points near the nucleus. Hence, we can expect our perturbation calculations to fail first at points near the nucleus as E_0-E_n is decreased.

III. SOLUTION FOR SMALL ENERGY DIFFERENCE

It is possible, however, to give an alternative method of solution which may be useful when the perturbation solution begins to fail. This depends on the fact that, since E_0-E_n is small, χ_0 and χ_n are not very different. In Eq. (1.6) for χ_n, the term κ_n/x arises from the coulomb potential and is numerically the ratio of this potential to the total energy of the particle (about 5 near the nucleus and for representative α-energies). It is much more important than the centrifugal term. For small changes in energy the percent variation of κ_n/x is the same as that of the energy. In other words, changes in energy of 500 kev or less will not have a large effect on the coefficient of χ in the differential equation. Thus, if we renormalize χ_n so that it has the same value as χ_0 at $r=r_0$, it will be a good approximation to replace both χ_0 and χ_n by the same function χ, provided r is not extended too far from r_0. Details as to the meaning of "too far" consistent with any prescribed degree of accuracy are given elsewhere.[7] For example, if $E_0-E_n=250$ kev, the method gives 10 percent accuracy for $r \lesssim 1.6r_0$, and for smaller energy differences or less accuracy the range can be extended. Since, as E_0-E_n is decreased the breakdown of perturbation theory occurs near the nucleus, these ranges appear to be sufficient. (Actually, we shall see that for 250 kev the perturbation method is valid.)

For simplicity, we consider the case where there is significant interaction between the ground state "0" and one excited state "n". Then we use $\chi(kr)$ to represent both $\chi_0(k_0r)$ and $\chi_n(k_nr)\chi_0(k_0r_0)/\chi_n(k_nr_0)$. We define χ exactly by

$$\chi''+(1-\kappa/kr)\chi=0, \quad \chi(kr_0)=\chi_0(k_0r_0). \tag{2.1}$$

Here κ, k, and v are certain mean values.

We now replace $\chi_0(k_0r)$ and $\chi_n(k_nr)$ in Eq. (1.9) by $\chi(kr)$, and after some substitutions find that we can write

$$f_0(r)=w_0\chi_0=\tfrac{1}{2}a_0A[\Gamma_1C_+(r)+\Gamma_2D_+(r)+\Delta_1C_-(r) +\Delta_2D_-(r)]\chi_0(k_0r)/\chi_0(k_0r_0), \tag{2.2a}$$

$$f_n=\tfrac{1}{2}a_0Ae^{i\delta}[\Delta_1C_-+\Delta_2D_--\Gamma_1C_+-\Gamma_2D_+]\chi_n/ \chi_n(k_nr_0). \tag{2.2b}$$

Here, $A_{p-1}{}^{n0}=Ae^{i\delta}$, Γ_1, Γ_2, Δ_1, Δ_2 are constants and χC_+, χD_+, χC_-, χD_- are the independent solutions, corresponding to the two signs of A, of the equation

$$d^2F/dx^2+[1-(\kappa/x)\pm A/x^p]F=0. \tag{2.3}$$

It is only in the region near the nucleus that the solution (2.2) is valid. If the lowest value of r for which the perturbation solution (1.12) is sufficiently accurate is less than the highest value for which Eq. (2.2) is reliable, we can then join the two solutions at some intermediate value r_1. Whether or not this can be done in any particular case can be determined numerically.

It is necessary to fix the four constants Γ_1, Γ_2, Δ_1, Δ_2 in Eq. (2.2) and a_0 and $a_n \exp i\delta$ in Eq. (1.12). These are fixed by boundary conditions. At the nuclear radius we have, apart from the constant of proportionality between f_0 and f_n, a matrix of four complex constants α, β, γ, δ determining the values of df_0/dr and df_n/dr:

$$\text{at } r=r_0 \begin{cases} f_0'=\alpha f_0+\beta f_n & \text{(2.4a)} \\ f_n'=\gamma f_0+\delta f_n. & \text{(2.4b)} \end{cases}$$

Clearly, Γ_1, Γ_2, Δ_1, Δ_2 can be found in terms of α, β, γ, δ. Then at some value of $r=r_1$, the solutions (2.7) and (1.15) are joined by the four conditions

$$(f_0, f_n, df_0/dr, df_n/dr)_{(2.2)} = (f_0, f_n, df_0/dr, df_n/dr)_{(1.12)} \tag{2.5}$$

at $r=r_1$. This implies that the perturbation solutions also involve four undetermined constants, which are thus given in terms of α, β, γ, δ. However, we have only two constants available in Eq. (1.12), viz., a_0 and $a_n \exp i\delta$; knowledge of the other two is equivalent to assuming the presence of only outgoing waves at infinity. Thus, instead of α, β, γ, δ, knowledge of which depends on details of intranuclear phenomena, we use the absence of incoming waves at infinity. The constants which remain are Γ_1, Γ_2, Δ_1, Δ_2, $C=(f_n/f_0)_\infty = a_n \exp i\delta/a_0$ and $\mu=(f_n/f_0)r_0$. Equations (2.5) determine the Γ's and Δ's as functions of C and then Eqs. (2.2) allow us to find the relationship between C and μ. Thus we can express the relative intensity of the two states at infinity in terms of the relative intensity at r_0. We can also find λ, the decay constant, from

$$(f_0f_0^{*\prime}-f_0^*f_0'+f_nf_n^{*\prime}-f_n^*f_n')r_0 = (2im\lambda/\hbar)\int_0^{r_0}(f_0f_0^*+f_nf_n^*)dr. \tag{2.6}$$

The integral on the right can be estimated only roughly.

Apart from obtaining explicit forms for the functions $C_\pm$, $D_\pm$ in the solutions of Eq. (2.3), this completes the general solution of the problem. In a given numerical case, it is desirable to discuss the solutions for a range of values of A, since this nuclear parameter cannot be well known *a priori*.

It is to be noted that, although Eqs. (2.5) involve r_1, the value of r at which the two solutions are joined, the final result should not be at all sensitive to this parameter, if it really lies in an interval of r where both solutions are reasonably accurate. In a numerical case, it

[7] M. A. Preston, Thesis, University of Birmingham (1949).

would be wise to repeat the calculations with a slightly different value of r_1, thus obtaining a final check on the over-all accuracy of the various approximations.

IV. EXPLICIT FORMS FOR $C_\pm$, $D_\pm$

We have still to solve explicitly

$$(d^2F/dx^2)+[1-(\kappa/x)\pm A/x^p]F=0. \tag{2.3}$$

If we are dealing with a dipole transition, $p=2$, and the solutions of Eq. (2.3) are confluent hypergometric functions. We base the solution of Eq. (2.3) on the known expressions [P(4.1) and (4.6)] for the solutions of

$$d^2\chi/dx^2+(1-\kappa/x-l(l+1)/x^2)\chi=0. \tag{3.1}$$

Since these solutions are known for the first few integral values of l, we can express the solutions F of Eq. (2.3) in terms of the solutions χ and the difference between A and the nearest value of $l(l+1)$.

Now by P, Eq. (5.1),

$$A_1^{n0}=4\sqrt{2}me^2R/3\hbar^2\sim 2.53$$
$$\times 10^{13}\left(\int u_n^*\Sigma r_i\cos\theta_i u_0 d\xi \text{ cm}\right). \tag{3.2}$$

It is difficult to estimate the matrix element R, but as it refers to a dipole transition it will be at most a few times 10^{-13} cm and may be as small as 10^{-14} cm. Hence, for the dimensionless quantity A, we have the approximate limits

$$1\gtrsim A\gtrsim 10^{-2}. \tag{3.3}$$

Thus, if $\lambda=l(l+1)\pm A$, Eq. (3.3) shows that λ has its smallest value when $l=0$. Therefore, we shall study the equation

$$(d^2F/dx^2)+[1-(\kappa/x)+\lambda/x^2]F=0 \tag{3.4}$$

and shall make use of the functions χ which satisfy

$$(d^2\chi/dx^2)+(1-\kappa/x)\chi=0. \tag{3.5}$$

For higher multipoles, similar considerations show that near the nucleus $A_p x^{-p}$ is small compared with $(1-\kappa/x)$; and therefore we express solutions of

$$(d^2F/dx^2)+[1-(\kappa/x)+\lambda/x^p]F=0 \tag{3.6}$$

in terms of the solutions χ of Eq. (3.5).

Our procedure is to put

$$F(x)=\chi(x)\sigma(x) \tag{3.7}$$

and express σ as a power series in the parameter λ, *viz.*:

$$\sigma=\sum_0^\infty c_n(x)\lambda^n. \tag{3.8}$$

We want two independent solutions of Eq. (3.6). One is obtained by making F almost the same as the solution

$$\chi=(\cot\alpha)^{\frac{1}{2}}e^{\omega}; \qquad [\text{P (4.1)}]$$

that is, we take $F=\chi$, $F'=\chi'$ at the nuclear boundary. The other independent solution of Eq. (3.6) is obtained in the same way, using for χ the other solution of Eq. (3.5), *viz.*, $(\cot\alpha)^{\frac{1}{2}}e^{-\omega}$.

For the second solution we write

$$\sigma=\sum_0^\infty \gamma_n\lambda^n. \tag{3.9}$$

Then,

$$\begin{aligned} C_+&=\textstyle\sum c_nA^n, \quad D_+=\sum \gamma_nA^n, \\ C_-&=\textstyle\sum c_n(-A)^n, \quad D_-=\sum \gamma_n(-A)^n. \end{aligned} \tag{3.10}$$

Recursion formulas for c_n and γ_n have been obtained.[7] These involve numerical integration, but usually c_n and γ_n are required for only a few low values of n.

V. NUMERICAL RESULTS FOR A DIPOLE CASE

Numerical calculations have been made for a typical case. For E_0 we have taken 5.303 Mev, simply because some of the quantities had already been obtained for this energy, which is that of the main line of polonium. For the small energy difference, we have taken $E_n-E_0=250$ kev, so that the calculations of Sec. II on the validity of replacing χ_0 and χ_n by the same function apply. We have assumed a dipole transition; i.e., $p=2$. However, the methods of this section are applicable to higher multipoles.

For $E=5.30$ Mev, and $r_0=8.27\times 10^{-13}$ cm, it is necessary in calculating $C_\pm$, $D_\pm$ to take the power series (3.10) only to the terms in A^2.

We now proceed to solve (2.5) and use (2.2) to obtain the relationship between $C=(f_n/f_0)_\infty$ and $\mu=(f_n/f_0)_{r_0}$. It is found that terms in A^2 can be neglected; to this order the result is

$$\mu=\frac{\Pi C+Ae^{i\phi}\{-[(\gamma_1'-c_1')/\gamma_0']-(\Pi\psi I^+\gamma_0/\gamma_0')+\frac{1}{2}\Pi\tau(I_{n0}^--I^+)\}}{1+ACe^{-i\phi}\{-[\Pi(\gamma_1'-c_1')/\gamma_0']-(\phi I^+\gamma_0/\gamma_0')+\frac{1}{2}\rho(I_{n0}^--I^+)\}}. \tag{4.1}$$

The following abbreviations have been used.

$$\Pi=(\cot\beta_0\tan\alpha_0)^{\frac{1}{2}}\exp(\Omega_0-\omega_0). \tag{4.2}$$

Π^2 is the ratio of the barrier penetrabilities at the two energies.

$$\rho=(\cot\alpha_1\cot\beta_1)^{\frac{1}{2}}\exp(\Omega_1-\omega_1)(kr_1)^{-2}. \tag{4.3}$$

$$\tau=\gamma_{0n}(\cot\alpha_1\cot\beta_1)^{\frac{1}{2}}\exp(\omega_1-\Omega_1)(kr_1)^{-2}. \tag{4.4}$$

$$\phi=\kappa\sin 2\tilde{a}_1\,\rho\tan\alpha_1. \tag{4.5}$$

$$\psi=\kappa\sin 2\tilde{a}_1\,\tau\tan\beta_1. \tag{4.6}$$

$$I^+=I_{0n}^+(r_1)=I_{n0}^+(r_1); \quad I_{0n}^-=I_{0n}^-(r_1). \tag{4.7}$$

In these equations the subscript 0 refers to values at $r=r_0$, the nuclear radius; subscript 1 refers to $r=r_1$, the point where the solution of Sec. III is joined to the perturbation solution; $\tilde{a}=\arccos(kr/\kappa)^{\frac{1}{2}}$; α and β are

the corresponding quantities for E_0 and E_n, defined exactly in P Eqs. (4.1), (4.11). $' \equiv d/d\tilde{a}$.

Let us compare this result with those of the perturbation methods. If the perturbation solution (1.12) is carried right down to $r=r_0$, instead of using the alternative method near the nucleus, it can be seen that

$$\mu=\frac{\Pi C+Ae^{i\theta}\tfrac{1}{2}\Pi\tau_0(I_{n0}^{-}-I^{+})_{r0}}{1+ACe^{-i\theta}\tfrac{1}{2}\rho_0(I_{0n}^{-}-I^{+})_{r0}}, \tag{4.8}$$

where τ_0 and ρ_0 are τ and ρ with r_1 replaced by r_0. Also the more restricted perturbation solution (1.10), if extended to $r=r_0$, gives

$$\mu=\Pi C+Ae^{i\theta}\tfrac{1}{2}\Pi\tau_0(I_{n0}^{-}-I^{+})_{r0}. \tag{4.9}$$

In our numerical case, Eq. (4.1) gives

$$\mu=\frac{\Pi C+Ae^{i\theta}(7.9_6+6.1_8i)\times10^{-2}}{1+CAe^{-i\theta}(1.6_4-0.08_4i)\times10^{-1}} \tag{4.1a}$$

and Eq. (4.8) gives

$$\mu=\frac{\Pi C+Ae^{i\theta}(8.3_6+6.4_9i)\times10^{-2}}{1+CAe^{-i\theta}(1.5_1-0.08_0i)\times10^{-1}} \tag{4.8a}$$

and Eq. (4.9), of course, gives

$$\mu=\Pi C+Ae^{i\theta}(8.3_6+6.4_9i)\times10^{-2}, \quad (\Pi=4.84). \tag{4.9a}$$

In these expressions we have taken $r_1=14.72\times10^{-13}$ cm. If we had taken $r_1=16.81\times10^{-13}$ cm, the coefficient in the numerator of Eq. (4.1a) would have been $(7.8_8+6.1_8i)\times10^{-2}$ and in the denominator it would have been $(1.6_7-0.08_4i)\times10^{-1}$. Thus, the result is not sensitive to the value of r_1. The calculations for I^{+} and I^{-} are given elsewhere.[7]

The observed relative intensity of the α-particles of the lower energy E_n to that of particles of energy E_0 is $|C|^2$. When $A=0$, that is, when the effect of the electrostatic interaction is not taken into account, we have $|C|^2=\mu^2/\Pi^2$, which simply expresses the result of the standard theory, Π^2 being the ratio of the penetrabilities of the coulomb potential barrier at the two energies.

The results of the perturbation calculation as given in Eq. (4.8a) are clearly very close to those of the second method (4.1a). This is not surprising, however, for in this case the criteria stated in Sec. I for the validity of Eq. (1.12) imply $0.11A\ll1$, which is certainly satisfied. Thus, even with the energy difference of 250 kev, the improved perturbation method is valid.

The original perturbation method, corresponding to Eq. (4.9a) is valid if $|v_{n0}+a_n\exp i\delta|\chi_n\ll a_0\chi_0$ for all r. This holds only if C is very small and then, of course, there is no real difference between Eqs. (4.8a) and (4.9a).

Let us now consider the magnitude of the interaction effect we have been studying. Rewrite Eq. (4.1) in the form

$$C=\frac{(\mu/\Pi)-Ae^{i\theta}\{-[(\gamma_1'-c_1')/\gamma_0'\Pi]-(\psi I^{+}\gamma_0/\gamma_0')+\tfrac{1}{2}\tau(I_{n0}^{-}-I^{+})\}}{1-\mu Ae^{-i\theta}\{-[(\gamma_1'-c_1')/\gamma_0']-(\phi I^{+}\gamma_0/\gamma_0'\Pi)+\tfrac{1}{2}\rho(I_{0n}^{-}-I^{+})/\Pi\}}. \tag{4.10}$$

Firstly, we take the case $|\mu|=1$. This expresses that, in the absence of the potential barrier, decay with either energy E_0 or E_n is equally probable. Since the energies are close together, this seems a reasonable assumption in the absence of any special restrictive conditions. Then, if $\mu=\exp i\Theta$, we obtain, to order A,

$$|C|^2=\Pi^{-2}-\Pi^{-1}A3.11\times10^{-2}\cos(\theta-\Theta-\tan^{-1}1.32).$$

For the energies chosen, $\Pi^{-2}=4.269\times10^{-2}$; and this is the relative intensity at infinity on the standard theory. Thus, the second term measures the interaction effect; and, numerically,

$$|C|^2=4.269\times10^{-2}\{1-0.15A\cos(\theta-\Theta-\tan^{-1}1.32)\}.$$

Thus, the effect produces at most a 10 percent change in the relative intensities at infinity, and with the more reasonable values $0.2>A>0.01$, the effect is less than 3 percent.

The above is for $|\mu|=1$. Next consider $\mu=0$. This means that there is no direct α-emission with energy E_n but that all the rays with this energy are due to the interaction. Then

$$|C|^2=4.4\times10^{-4}A^2.$$

Thus, the maximum relative intensity (of the lower energy particles to the greater) due to the interaction alone is about 4×10^{-4}; and more probable values corresponding to smaller values of A are 10^{-5} down to 10^{-6}.

We can also put $|\mu|=\infty$, i.e., no direct emission of the higher energy particles. Then the intensity of the higher energy particles is less than that of the lower energy ones and the ratio is

$$|1/C|^2=2.3\times10^{-3}A^2.$$

Thus, this effect is 100 times as great as the reverse; i.e., it is about 100 times more probable that the α-particle will absorb the energy of a nucleus left in an excited state than that it will excite a nucleus left in its ground state. Both these processes of course give weaker lines than the corresponding direct decay with $|\mu|=1$.

The case $|\mu|=\infty$ is the extreme limit of the forbidden ground-state transition suggested by Perlman, Ghiorso, and Seaborg. Their model for non-even-even nuclei would suggest values of $|\mu|$ between one and infinity. It is seen that in such cases the effect here studied might be of some importance. The numerical values above are for $E_0=5.30$ Mev, $E_0-E_n=250$ kev. From the calculations in P with $E_0-E_n=1.2$ Mev, we find that for $|\mu|=\infty$, $|1/C|^2\sim10^{-3}A^2$. It would be

interesting to repeat the calculations for energy difference in the region where perturbation methods really fail and a larger value of $|1/C|^2$ might occur. The value $E_0-E_n\sim 50$ kev should provide such a case and would be interesting in view of the two lines of Bi^{212}(ThC), which differ by 40 kev.[8] The greatest difficulty in such a calculation would be the numerical evaluation of I_{n0}^- and I_{0n}^-.

In addition to Bi^{212}, there are a number of other cases[1] where this effect might be of some importance. These are shown in Table I. It is difficult to separate the contributions of the various phenomena which affect the intensities. Usually, neither the angular momentum of the α-particle nor the degree of prohibition (value of μ) can be estimated with any certainty. (The penetrability of the coulomb barrier is, of course, the factor which fixes the order of magnitude of the intensities.) In any given experimental case, we would like the difference between the observed partial decay constant and that predicted by standard theory [Eq. (A.1)] to be apportioned among the three effects: angular momentum, "formation" prohibition, and noncentral electric interaction. At present, this does not seem possible, but there appears to be evidence that all three play some role.

TABLE I. Relatively forbidden transitions in which the electric interaction may be important. For Ra^{226}, the figures refer to lines I and II.

Nucleus	E_0-E_n, kev	$\lvert C\rvert^{-2}$
U^{235}	160	0.11
Th^{229}	100	0.5
Ra^{226}	80	0.40
Bi^{212}	40	0.39
Bi^{214}	60	0.82

I am much indebted to Professor R. E. Peierls for stimulating discussion and to my wife for help with the rather heavy numerical calculations.

[8] G. T. Seaborg and I. Perlman, Revs. Modern Phys. **20**, 585 (1948).

PHYSICAL REVIEW VOLUME 82, NUMBER 4 MAY 15, 1951

Conductivity of Cold-Worked Metals*

ROLF LANDAUER
Lewis Laboratory, NACA, Cleveland, Ohio
(Received November 10, 1950)

In the vicinity of an edge type dislocation, the density of electrons, and therefore the width of the filled portion of the conduction band is not uniform. To keep the electrons in equilibrium, an electrostatic potential is required. The scattering caused by this potential is used to calculate the increased resistance of isotropically cold-worked copper.

I. INTRODUCTION

COLD working produces an increase in the resistance of metals. This increase has been attributed to the formation of dislocations by Koehler.[1,2] Koehler's calculations have been refined by Mackenzie and Sondheimer,[3] who give a very elegant treatment of the problem. In particular, they calculated the change in resistance produced by cold-working, at high temperatures, whereas Koehler calculated the resistance arising from dislocations at absolute zero. These two quantities need not be equal.[4-6] Both treatments attribute a screened coulomb potential to each ion of the crystal. The perturbation that scatters the conduction electrons arises from the fact that these ions, and consequently their screened coulomb fields, are displaced from their normal lattice positions.

In the earlier treatments it is assumed, therefore, that the screening electrons which are associated with a particular ion stay with that ion as the latter is displaced from its position. No large scale redistribution of electronic charge is permitted.

Actually, however, the electrons can redistribute themselves. An edge dislocation contains an extra plane of ions, above or below the slip plane. Consider the case in which the extra plane is above the slip plane. If each ion were to keep its screening electrons, the Fermi energy above the slip plane would be larger than below, and, as a result, some electrons would go from the upper to the lower region. This in turn gives an unbalance of charge and an electric field. Equilibrium will be attained when the Fermi levels in the different regions have come together.[7] If the number of electrons which are displaced to establish the field is small, the effect of this change of electron density on the Fermi energy can be neglected. The purpose of this paper is to calculate the incremental resistance per dislocation due to this electrostatic field. It will turn out to be

[1] J. S. Koehler, Phys. Rev. **75**, 106 (1949).
[2] J. S. Koehler, Am. J. Phys. **10**, 275 (1942).
[3] J. K. Mackenzie and E. H. Sondheimer, Phys. Rev. **77**, 264 (1950).
[4] E. H. Sondheimer and A. H. Wilson, Proc. Roy. Soc. (London) **A190**, 435 (1947).
[5] M. Kohler, Z. Physik **126**, 495 (1949).
[6] J. W. Rutter and J. Reekie, Phys. Rev. **78**, 70 (1950).
[7] J. Bardeen and W. Shockley, Phys. Rev. **80**, 72 (1950).

considerably larger than the resistance Mackenzie and Sondheimer found.

II. THEORY

The stresses surrounding an edge dislocation have been given by Koehler.[8] According to these, the relative change in ionic density about a dislocation is given by

$$\frac{\Delta n}{n}=\frac{a}{2\pi}\frac{(1-\nu-2\nu^2)}{(1-\nu^2)}\frac{\sin\theta}{r}. \tag{1}$$

Here, a is the lattice spacing of the simple cubic lattice on which this picture is based, and ν is Poisson's ratio. The usual polar coordinate system is used in which the z-axis is taken to be the axis of the dislocation and the angle θ is measured with respect to the slip plane. Now let us assume, for the moment, that the electronic density changes likewise. The width of the filled portion of the conduction band is[9]

$$E=(h^2/2m^*)(3n/8\pi)^{\frac{1}{3}}, \tag{2}$$

where m^* is the effective mass, and n is the density of electrons. The change in the width due to the stresses will then be

$$\Delta E=\tfrac{2}{3}E\Delta n/n, \tag{3}$$

or

$$\Delta E=\frac{a}{3\pi}\frac{(1-\nu-2\nu^2)}{(1-\nu)^2}\frac{\sin\theta}{r}. \tag{4}$$

This neglects a possible change in the effective mass.

In equilibrium, the top of the filled portion of the conduction band must be at the same level everywhere. Therefore, since the width varies, the bottom of the conduction band must deviate from its normal level by an amount opposite to that given in Eq. (3). The electrons will, therefore, act as if moving in an electrostatic potential V, which satisfies the relation

$$eV=\Delta E, \tag{5}$$

where e is the absolute magnitude of the electronic charge. Hence,

$$V=\frac{a}{3\pi e}\frac{(1-\nu-2\nu^2)}{(1-\nu^2)}\frac{\sin\theta}{r}. \tag{6}$$

This is just the potential of a line dipole, located along the dislocation axis. Actually, not all of the potential in Eq. (6) is really an electrostatic potential. Part of it arises from the fact that the bottom of the band is itself sensitive to lattice spacing. It is, however, the deviation of the bottom of the band that must be used as an effective potential.[10]

The calculation of the incremental resistance can proceed from this perturbing potential, exactly as Mackenzie and Sondheimer did. This computation gives, for the change of resistivity,

$$\frac{\Delta\rho}{\rho}=\frac{16}{27}E^2a^3\left[\frac{1-\nu-2\nu^2}{1-\nu^2}\right]^2\frac{\tau m^*k_0}{h^3n}N. \tag{7}$$

Here N is the number of dislocations per cm^2, k_0 is the wave vector at the top of the Fermi distribution, and τ is the mean free time between electron collisions. This last quantity can be found from the experimental value of conductivity by using the condition

$$\sigma=ne^2\tau/m^*. \tag{8}$$

We shall use the values for copper, obtained from specific heat measurements,[9] $E=4.78$ ev, $m^*/m=1.47$. Furthermore, taking $k_0=1.37\times10^8$/cm, $n=0.85\times10^{23}$/cm^3, $\nu=0.34$, and $a=2.55\times10^{-8}$ cm, we obtain

$$\Delta\rho/\rho=2.5\times10^{-14}N. \tag{9}$$

The experimental value[1] of $\Delta\rho/\rho$ for heavily cold-worked copper is 2 percent. This gives $N=8\times10^{11}$. Koehler[8] estimated on the basis of energy storage measurements that $N=6\times10^{11}$.

It must be kept in mind that actually dislocations occur in the form of half-dislocations in a face centered cubic crystal.[11] Furthermore, some of the stored energy may come from screw dislocations, or the screw components of dislocation rings. The resistance of screw dislocation is presumably much smaller than our result, since no volume compression is associated with them.

The author is indebted to Dr. Sondheimer for his introduction to this problem.

[8] J. S. Koehler, Phys. Rev. **60**, 398 (1941).

[9] F. Seitz, *Modern Theory of Solids* (McGraw-Hill Book Company, Inc., New York, 1940), chapter IV.

[10] J. C. Slater, Phys. Rev. **76**, 1592 (1949). We should use the effective mass wave equation derived by Bardeen and Shockley in reference 7, which covers the case of elastic deformations as well as electrostatic disturbances. This equation is:

$$[(h^2/2m^*)\nabla^2+\delta U_0]A(r)=EA(r),$$

where δU_0 represents the height of the energy level above the bottom of the band. $A(r)$ is a function which modulates $\psi_0(r)$, which in turn is the wave function corresponding to the band edge. The variation of m^* in the $h^2/2m^*\nabla^2$ term compensates exactly for the variation of m^* in (2) which was neglected. Hence, the treatment given in this paper, gives the correct answer.

[11] R. D. Heidenreich and W. Shockley, *The Strength of Solids* (Physical Society, London, 1948), p. 1.

Silver Bromide Crystal Counters*†

K. Alan Yamakawa‡
Palmer Physical Laboratory, Princeton University, Princeton, New Jersey
(Received January 15, 1951)

Single crystals of silver bromide and mixed crystals of sodium and silver chloride have been used to count ionizing radiation. The energy per ion pair in silver bromide for electrons was found to be approximately 5.8 ev. The mobility and the mean free path for the trapping of electrons in the conduction band of silver bromide crystals at 77°K were found to be 210 cm²/volt-sec and 5×10^{-4} cm²/volt, respectively. A study of the polarization of the counters for beta- and gamma-radiation was also made.

I. INTRODUCTION

IN 1945, van Heerden[1] found that a single crystal of silver chloride can be used as a counter. Carefully annealed single crystals of silver chloride were placed between electrodes and cooled to liquid nitrogen temperature, where silver chloride is an insulator. With an electric field of several thousand volts per cm across the crystal, the ionization of a single particle or quantum was found to be observable. The magnitude of the pulse was found to be proportional to the energy of the incident particle under proper conditions. Since then there has been considerable interest in the investigation of various substances as counters of this type, and several other substances have been found to be satisfactory crystal counters; i.e., diamond,[2–4] single crystals of zinc sulfide,[5] and a mixed crystal of the bromide and iodide of thallium.[6]

It is the purpose of this paper to add silver bromide and a few other substances to the list of suitable crystal counters and to give an account of some of the properties of silver bromide crystal counters, such as the energy loss per ion pair, the mobility of electrons, and the polarization of silver bromide counters.

II. EXPERIMENTAL PROCEDURE

(A) The Growth of the Crystals

Single crystals of silver bromide were prepared from chemically pure silver bromide powder by Bridgman's method.[7] The lower two-thirds of the crystals grown in this way were clear and yellow in color. The upper portion was darker and opaque. In order to see whether or not these were single crystals, the clear portion was etched in a solution of hypo and viewed under strong white light. The crystals were found to be single when viewed in this way. They darkened appreciably when exposed to white light; however, they regained their color when annealed at a temperature somewhat below the melting point. McFee[8] has investigated the growth of sodium chloride crystals by this method and has found that foreign atoms are concentrated in the upper portion of the crystals when grown in this way. In an effort to grow crystals which would be as free from impurities as possible, the lower portions of those grown from the powder were remelted and the process of growth repeated. These recrystallized samples were much lighter in color and had less tendency to darken on exposure to white light. The crystals used in these experiments are third and fourth crystallizations. They were pale yellow in color and had very little tendency to darken even when exposed to bright white light for several hours. The darkening mentioned previously is probably associated with the presence of impurities. All of the crystals, including those grown directly from the powder, were observed to count beta- and gamma-rays when properly annealed and cooled to liquid nitrogen temperature.

(B) The Annealing of the Crystals

A silver bromide crystal that had been protected as much as possible from white light was cooled to liquid nitrogen temperature before annealing. When exposed to gamma-radiation from radium no pulses were observed. It was then heated in an annealing furnace to 380°C and cooled to room temperature in about 16 hours. When cooled to liquid nitrogen temperature and then exposed to gamma-rays it was observed to count. Similar behavior has been observed by van Heerden in silver chloride and by Hofstadter in a mixed crystal of thallium bromide and thallium iodide. Another crystal cut from the same sample was heated to about 300°C and cooled to room temperature in about 8 hours. This crystal, when cooled, responded to beta- and gamma-radiation; however, the pulse heights were about a third of those observed in the previous case. In order to establish a satisfactory annealing procedure the state of strain of a crystal of silver bromide was observed, as the temperature of the crystal was raised, by observing its strain pattern through crossed Nicol prisms. A sodium arc lamp was used as a light source in order to

* Part of Ph.D. thesis, Princeton University, 1949.
† This work was supported in part by the joint program of the ONR and AEC. The author is indebted to the AEC for making available the radioactive isotopes used in these experiments.
‡ Now at Ballistic Research Laboratory, Aberdeen, Maryland.
[1] P. J. van Heerden, *The Crystal Counter*, Utrecht Dissertation, 1945.
[2] Wooldridge, Ahearn, and Burton, Phys. Rev. **71**, 913 (1947).
[3] L. F. Curtiss and B. W. Brown, Phys. Rev. **72**, 643 (1947).
[4] Friedman, Birks, and Gauvin, Phys. Rev. **73**, 186 (1948).
[5] A. J. Ahearn, Phys. Rev. **73**, 1113 (1948).
[6] R. Hofstadter, Phys. Rev. **72**, 1120 (1947).
[7] P. W. Bridgman, Proc. Am. Acad. Arts Sci. **60**, 305 (1925).
[8] R. H. McFee, J. Chem. Phys. **15**, 856 (1947).

produce as little darkening as possible. Two plane parallel surfaces were cut on the sides of a crystal 0.8 cm thick, and the strain pattern was obtained on a photographic plate through the side of the crystal. It was found that strains begin to disappear at about 300°C and disappear rapidly above 350°C. Even at these high temperatures a longer exposure brought out some structure. The crystal was then cooled to room temperature in about 15 hours and a strain pattern obtained. This pattern showed very little change in cooling to room temperature in this manner. It was also found that there was no appreciable change in the strain pattern of the crystal on cooling the crystal to liquid nitrogen temperature in a period as short as a half hour. Also, repeated cooling from room temperature to liquid nitrogen temperature without annealing did not appreciably affect either the strain patterns or the counting properties of the crystal. The crystals were handled in a way similar to that described by Haynes.[9] A typical annealing schedule adopted for these crystals is shown in Fig. 1. Crystals annealed in this way were found to be quite uniform in their response to radiation.

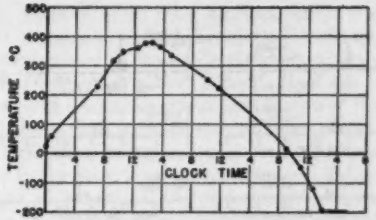

FIG. 1. Typical annealing and cooling schedule used for silver bromide crystal counters.

III. RESULTS AND DISCUSSION[10]

(A) The Energy Loss per Ion Pair

The energy loss per ion pair can be defined as the ratio of the energy of the incident particle to the number of secondary electrons produced by the particle in the absorbing medium. In the case of a gas this quantity is known to have a value of about 30 ev. Van Heerden has found that the analogous quantity in single crystals of silver chloride is 7.6 ev for beta-particles, a value which is considerably lower than that in a gas.

The energy loss per ion pair for beta-particles stopped by single crystals of silver bromide was determined in the following manner. Beta-particles from P^{32} which have a maximum energy of 1.71 Mev were used as the source of radiation. The maximum pulse heights obtained from this source at four different values of electric field ranging from 1000 to 4000 volts/cm were estimated from photographs of the pulses. Figure 2 shows typical pulses obtained. These pulses were assumed to be due to 1.71-Mev beta-particles. The pulse heights were calibrated by comparison with pulses from a precision pulser. The number of electrons freed by the beta-particles was obtained from this data by comparison with the theoretical saturation curve of Hecht:[11]

$$N=N_0\frac{\omega}{d}\left[1-\exp\left(\frac{d-\frac{1}{2}\epsilon}{\omega}\right)\right]. \qquad (1)$$

This relation assumes that electrons are trapped in trapping centers which are distributed uniformly throughout the crystal. N_0 is the number of electrons released by the beta-particles. N is the effective number of electrons contributing to the pulse height; that is, $N=CV/e$, where C is the crystal capacitance, V the pulse height in volts, and e the electronic charge. ω is the mean free path for the trapping of electrons, d is the crystal thickness, and ϵ is the penetration of the beta-particles into the crystal.

By fitting a curve of this type to the data obtained, one obtains values for N_0 and ω. The energy per ion pair is then $(1.7\times10^6/N_0)$ ev. The energy loss per ion pair at saturation fields for single crystals of silver bromide was found in this way to be 5.8 ev, a value lower than that found for silver chloride. The accuracy of this measurement is estimated to be within 10 percent. It is interesting to compare the energy loss per ion pair for silver chloride with the energy required to raise an electron from the filled band to the conduction band; i.e., the energy corresponding to the edge of the continuous optical absorption region. In the silver halides the position of this absorption edge is approximated by the position of the excitation levels, which are quite close to the absorption edge. From the

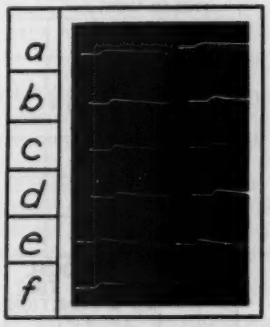

FIG. 2. Traces of typical pulses obtained from silver bromide crystal counters for energetic beta-particles from P^{32}. Traces *a*, *b*, *c*, *d* were obtained at electric field strengths of 1870, 2730, 3640, and 4550 volts/cm, respectively. Traces *e* are due to a precision pulser with a rise time faster than that of the amplifier system. Traces *f* are due to gamma-rays from radium at a field strength of 3640 volts/cm.

[9] J. R. Haynes, Rev. Sci. Instr. **19**, 51 (1948).

[10] The apparatus used for this study was designed and built by R. Hofstadter. It is described in Nucleonics **4**, No. 4 (1949).

[11] K. Hecht, Z. Physik **77**, 235 (1932).

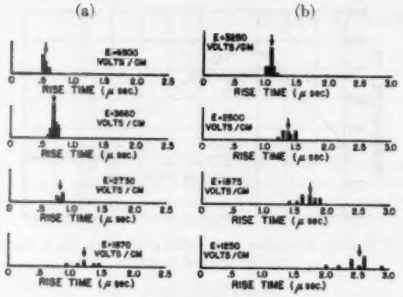

FIG. 3. The rise times of silver bromide crystal counter pulses due to energetic beta-particles from P^{32} observed at various field strengths. (a) crystal thickness 0.55 cm. (b) crystal thickness 0.8 cm. Each unit square represents one observation.

observations of Fesefeldt and Gyulai,[12] the continuous absorption edge for silver chloride occurs at about 5 ev and for silver bromide at about 4 ev. This is consistent with a lower value for the energy loss per ion pair in silver bromide as compared with that in silver chloride. It can also be said that approximately two-thirds of the energy of the incident beta-particle is effective in producing secondary electrons in both silver chloride and silver bromide, whereas in a gas such as hydrogen, about half of the energy of the incident particle is effective in freeing electrons.

The fact that saturation characteristics are obtained from the pulse size as the field is raised does not necessarily mean that most of the secondary electrons traverse the thickness of the crystal as the field is raised to saturation values. It would be possible that strains, etc., form one or more barriers in the crystal through

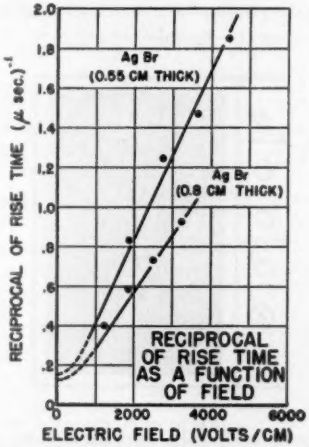
Ag Br
(0.55 CM THICK)
Ag Br
(0.8 CM THICK)
RECIPROCAL OF RISE TIME AS A FUNCTION OF FIELD
RECIPROCAL OF RISE TIME (μ sec.)⁻¹
ELECTRIC FIELD (VOLTS/CM)

FIG. 4. Average rise times observed at various field strengths in two silver bromide crystal counters of different thicknesses.

which electrons will not pass even at high fields. The pulse size in this case would also show saturation characteristics as the field is raised. However, the fact that the energy required to raise an electron from the filled band to the conduction band is relatively large, being about two thirds the energy loss per ion pair, indicates strongly that such barriers do not exist and that most of the secondary electrons do traverse the thickness of the crystal at field strengths that produce saturation in the pulse heights.

A value of 5×10^{-4} cm²/volt was found for the trapping mean free path for the secondary electrons from the curve fitting procedure. The uncertainty in this determination is somewhat greater than that for the energy per ion pair. This value is of the same order of magnitude as that found for silver chloride by Lehfeldt,[13] i.e., 4×10^{-4} cm²/volt.

(B) The Mobility of the Electrons

If the value of the electric field applied across the crystal is sufficiently high so that the mean free path for the trapping of secondary electrons is of the same order or larger than the thickness of the crystal, so that most of the secondary electrons travel the full thickness of the crystal, the rise time of the pulses is the time required for these electrons to traverse this distance. Thus, under these conditions the mobility of the electrons in the conduction band (the velocity of drift in unit field) can be obtained from a study of the rise times of the pulses. It can be seen from Fig. 2 that the slope of the pulse rise is reasonably constant indicating that most of the electrons do traverse the thickness of the crystal with a constant drift velocity. The mobility of electrons in silver bromide crystals at 77°K was determined in this way for two crystals, one 0.55 cm thick and the other 0.8 cm thick. The rise times of the pulses corresponding to various electric field strengths were measured for a number of pulses at each value of field. Figure 3 gives the results obtained in the form of histograms. It can be seen that the rise times measured in this way do not show a unique value at each value of field but rather a distribution about a mean value. This dispersion in the values of the rise times is seen to be greater at the lower field values. The dispersion in the values for the rise times is larger than the estimated error in measurement, being approximately two and five times the estimated error in measurement at the high and low values of field, respectively. It is unlikely that this dispersion is due to slight differences in the distances traveled by the electrons because one would then expect a correlation between the rise times and the corresponding pulse heights, slightly smaller pulses showing a faster rise time. No such correlation was found. Fluctuation in noise can, in general, give such a distribution;[14] however, it is felt that the dispersion is greater than can be accounted for by noise because the

[12] H. Fesefeldt and Z. Gyulai, Nachr. Ges. Wiss. Göttingen (1929), p. 226.

[13] W. Lehfeldt, Nach. Ges. Wiss. Göttingen (1935), p. 171.

[14] Suggested by R. H. Dicke.

peak noise level was only about 5 percent of the pulse height. It is possible that strains and other imperfections in the crystals cause local regions in which the mobilities are altered; that is, these imperfections may not be sufficient to cause appreciable trapping of electrons but may be sufficient to affect the mobility appreciably. In the absence of more complete knowledge, the mean value of the rise times at each field strength was estimated and used as the basis for the determination of the mobility. Figure 4 gives the results as a plot of the reciprocals of the average rise times as a function of the electric field strength. The mobilities obtained for the two crystals are 208 and 213 cm²/sec-volt for the 0.55-cm and 0.8-cm crystal, respectively. Correction has been made for the finite penetration of the beta-particles. The internal agreement is satisfactory. A Fröhlich-Mott formula, modified by Bardeen,[15] for the mobility of electrons in the conduction band of ionic crystals given in Eq. (2) gives a value of 308 cm²/sec-volt in silver bromide at 77°K. The agreement with the theoretical value is reasonable. A further study of mobilities at different temperatures and for other substances is contemplated.

$$v=2\left(\frac{3}{\pi mk\theta}\right)^{\frac{1}{2}} ea_0(e^{\theta/T}-1)\frac{KK_0}{K-K_0}, \qquad (2)$$

where $\theta=(hc/k\lambda)(K/K_0)^{\frac{1}{2}}$. λ is the absorption eigen-wavelength = 124 microns (Barnes),[16] T is the absolute temperature, and a_0 is the radius of first Bohr orbit. The effective mass of the electron, m, in the conduction band is taken to be the mass of the free electron.

(C) Polarization Effect

The polarization effect in crystal counters, which can be observed as a gradual decrease in pulse height as the number of counted events increases, is of interest because it limits the usefulness of these counters in many applications.

A preliminary study of the polarization effect in silver bromide counters due to beta-particles from P^{32}, which produce ionization in a thin layer of the crystals, and to gamma-rays from radium, which produce essentially volume ionization in these crystals, was made by observing the counting rate as a function of the number of events counted. A discriminator was used to exclude pulses smaller than a given height. In both cases, the counting rate decreased slowly as the number of counted events increased. The decrease in counting rate was more rapid for gamma-rays than for beta-particles. However, after prolonged exposure to the radiation, the counting rate became erratic and rose considerably above the initial counting rate in both cases. At low discriminator levels, a little above noise level, spurious counts appeared after a much smaller number of counts than at higher discriminator levels; however, in all cases spurious counts were observed eventually. It is believed that these spurious counts arise from an increase in the conductivity of the crystal. Observation of the conductivity of the crystal by means of a sensitive galvanometer showed that the conductivity does increase with exposure of the crystal to radiation and does so in an erratic manner, similar to the behavior of the counting rate. Subsequent warming of the crystal to room temperature and recooling to liquid nitrogen temperature restored the insulating properties of the crystal considerably.

In order to investigate the polarization effect more fully, a ten-channel discriminator was used to obtain pulse height distributions as a function of the number of counted events. Figure 5 gives the results obtained for beta- and gamma-rays. The polarization effect was evaluated from these data in the following manner. The pulse height is proportional to the total distance

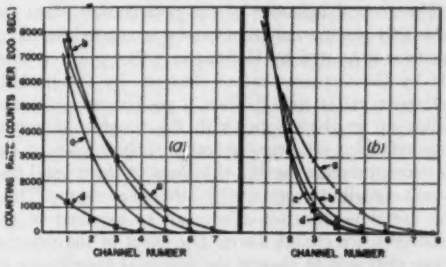

FIG. 5. Pulse-height distribution curves for beta-particles from P^{32} and gamma-rays from radium obtained by means of a ten-channel discriminator. The channel number is proportional to pulse height. Pulses larger than 10 volts were counted, and the channel width was 10 volts. (*a*) Beta-particles from P^{32}. Effective crystal area—0.4 sq cm; Crystal thickness—0.6 cm; Field strength —3300 volts/cm. Curve a after 40,000 counts, curve b after 0.2×10^6 counts, curve c after 0.5×10^6 counts, and curve d after 0.7×10^6 counts. (*b*) Gamma-rays from radium. Effective crystal area—1 sq cm; Crystal thickness—0.7 cm; Field strength—2860 volts/cm. Curve a after 20,000 counts, curve b after 0.25×10^6 counts, curve c after 0.5×10^6 counts, and curve d after 0.75×10^6 counts.

traveled by the secondary electrons. From these data we cannot follow the effect of polarization on a pulse due to a given energy radiation; however, we can obtain the over-all effect of polarization on all the pulses by observing the change in the pulse height distribution with the number of particles counted. The total distance, D, traveled by the secondary electrons released in unit time by the radiation is proportional to[17]

$$\Sigma_{\text{channel number}}(\text{counting rate})(\text{channel number}).$$

The behavior of D with the number of counted events gives the over-all effect of polarization on the pulse heights. Figure 6 gives the results for beta- and gamma-rays. It can be seen that the polarization occurs much

[15] J. Bardeen, by private communication to R. Hofstadter.
[16] R. B. Barnes, Z. Physik **75**, 732 (1932).
[17] The channel number is proportional to the pulse height, and thus to the total distance traveled by the electrons for a given pulse.

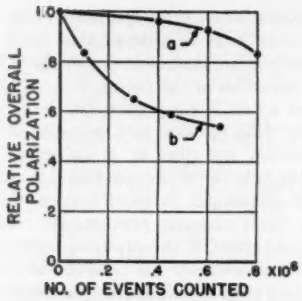

FIG. 6. Over-all polarization effect caused by (a) beta-particles from P^{32} (surface ionization), and (b) gamma-rays from radium (volume ionization). Data reduced for crystal area of 1 sq cm.

more quickly for gamma-rays (volume ionization), than for beta-particles (surface ionization).

The general behavior of the polarization effect for beta- and gamma-radiation can be accounted for along the lines suggested by Hofstadter.[18] The positive holes left by the displacement of electrons by the field do not move in the field.[18] Thus, a positive space charge builds up in the crystal with the number of events counted. Also, at near saturation fields, most of the electrons traverse the full thickness of the crystal and do not contribute very much to the space charge. Thus, the initial polarization effect can be ascribed to the positive space charge alone. The effect of the positive space charge is to change the potential distribution in the crystal, resulting in regions in the crystal where the electric field, and thus the mean free path for the trapping of electrons, ω, is small. Of course, there will be regions where the electric field is higher than the original value; however, this does not affect the pulse size appreciably at near saturation fields.

In the case of beta-particles for which the ionization takes place in a thin layer of the crystal, the positive space charge is localized in this thin layer. The net result is to increase the field strength in the region of positive space charge above the original value and to reduce it in the remaining region of the crystal. Thus, the decrease in the pulse height can be attributed to a decrease in the mean free path in the region of the crystal outside the region of positive space charge. Assuming a uniform distribution of positive holes in a layer of crystal thickness, t, it can be shown that the mean free path is

$$\omega=[E_0-(2net/kd)]vT, \tag{3}$$

where E_0 is the original field strength, n is the number of secondary electrons, d is the thickness of the crystal, and T is the average time for which an electron is free. It can be seen that the reduction in the mean free path depends on the relative thickness of the region of space charge as compared to the thickness of the crystal.

[18] R. Hofstadter, Nucleonics 4, No. 4 (1949).

For example, polarization effects are thus expected to occur more slowly for alpha-particles, which do not penetrate very deeply into the crystal, than for beta-particles of comparable energies. The pulse heights decrease slowly in the region of saturation fields and more rapidly as the field, and thus the mean free path, reaches a value corresponding to the "knee" of the pulse-height saturation curve given by Eq. (1). This general behavior is shown by the experimental polarization curve for beta-particles.

For gamma-rays the positive space charge is distributed throughout the crystal. Assuming a uniform distribution of space charge, it can be shown that the mean free path for the trapping of electrons is

$$\omega=[E_0-(2\pi ne/kd)(d-2x)]vT, \tag{4}$$

where E_0 is the original electric field strength, x is the position in crystal (positive in direction of motion of secondary electrons), and d is the crystal thickness. It can be seen that the effect of the positive space charge is to increase the mean free path above the original value in one-half of the crystal and to decrease it in the remaining half. Thus, the pulse heights caused by the motion of electrons in one-half of the crystal (region of large mean free path) are not appreciably affected, while those caused by motion of electrons in the remaining half of the crystal are decreased in height with the number of counted events. This general behavior is shown in the experimental polarization curve in that polarization occurs relatively rapidly at the beginning and then more gradually.

(D) Other Crystals

In addition to silver bromide crystals, single mixed crystals of silver chloride and sodium chloride were observed to count beta-particles and gamma-rays. A single crystal of the mixture, containing approximately 15 percent sodium chloride by weight after annealing and cooling to liquid nitrogen temperature, gave pulses approximately one-third the height of silver chloride pulses. Another crystal, containing approximately 50 percent by weight of sodium chloride, gave pulses about $\frac{1}{8}$ that of the pulses from silver bromide. The fact that mixed crystals of sodium chloride and silver chloride count while sodium chloride crystals do not indicates the following: first, sodium atoms in the lattice of silver chloride crystals do not cause appreciable trapping of electrons; second, the fact that sodium chloride is not a counter cannot be attributed to trapping centers due to impurities in the sodium chloride crystals because a substantial amount of such impurities are present in the mixed crystals.

The author is indebted to Professor R. Hofstadter for his continuous interest and aid in all phases of these experiments. He wishes to thank C. Graves, E. Dexter, L. Hamner, and C. Lambert for their technical aid and H. Schrader for his help with drawings and photographs.

The Emission of Short-Range Charged Particles in the Slow Neutron Fission of Uranium

K. W. Allen and J. T. Dewan
Atomic Energy Project, National Research Council of Canada, Chalk River, Ontario, Canada

(Received January 15, 1951)

A coincidence counting method has been employed to investigate short-range charged particles produced in the slow neutron fission of U^{235} and U^{233}. In the case of U^{235}, charged particles with ranges up to 8 mm of air were observed with a frequency of one in 76±8 fissions. The maximum initial specific ionization of these particles was ten times that of α-particles from uranium, which suggests that some of the particles have masses considerably greater than that of the α-particle. The mass distribution could not be determined from the experimental data. Additional experiments proved that the observed particles were not nuclear recoils produced by fission fragments in their passage through the source and counter gas or fission fragments scattered by the backing material of the source. In the fission of U^{233}, particles were observed with ranges up to 7.4 mm of air with an abundance of one in 72±6 fissions.

I. INTRODUCTION

WHEN fission of uranium occurs, the compound nucleus occasionally disintegrates into three or more charged particles instead of into the usual two fragments. Several cases of quadripartition have been seen in photographic plates,[1] and it has been reported that, in one out of every 250,000 fission events, division into three particles of comparable mass takes place.[2,3] In about 0.2 percent of fission events, an energetic α-particle with a range up to 50 cm of air is emitted in addition to the two main fragments; this mode of fission has been discussed in detail by many authors.[4] Still more often, in roughly one percent of all fission events, a charged particle with a range less than one cm of air is emitted along with the two main fragments. The present paper deals exclusively with these short-range particles.

The occasional emission of short-range charged particles in the fission of U^{235} was first detected by Cassels *et al.*,[5] using a pair of proportional counters in coincidence. They reported that, assuming isotropic emission, approximately 4 percent of fission events gave rise to a short-range charged particle that was tentatively identified as an α-particle of about 1-Mev energy. Green and Livesey,[6] searching for these particles in uranium loaded photographic emulsions, observed that there were more short spurs branching from the fission track near the origin of the event than were to be expected from calculations on the number of nuclear recoils which should be produced by the fast moving fission fragments. They concluded that, in one percent of fission events, a short-range ternary particle was emitted, preferentially at 90° to the main fission track, with a range up to 8 mm of air. Having determined the angular distribution, they corrected the abundance of Cassels *et al.* to 1 in 90 fission events, thus bringing the two experiments into good agreement. On the other hand, Tsien and his collaborators[7,8] observed particles with the same abundance but with ranges up to 3 cm of air. The mean angle of emission of the particles was found to be 70° with respect to the lighter of the two main fragments.

Investigation of the short-range particles by means of photographic plates containing uniformly dispersed uranium, aside from being laborious, has two disadvantages. Firstly, ignorance of the exact origin of a fission event makes it difficult to distinguish short ternary tracks from nuclear recoils, and secondly, the short ranges of the particles in the emulsion do not allow an accurate estimation of their masses. For these reasons coincidence counting methods were used in the present investigation. Even so, special experiments were necessary to demonstrate that the observed particles were not nuclei recoiling from the fission fragments. A preliminary account of this work has already been given.[9]

II. APPARATUS AND METHOD

The distribution in range of the charged particles was studied by means of the apparatus shown in Fig. 1. A thin source of uranium S, less than 0.1 mg/cm² in thickness, was placed in a chamber containing a pair of proportional counters F and P, the whole chamber being filled with methane to a suitable pressure. A collimated beam of slow neutrons from the Chalk River heavy water pile produced fissions in the source, and coincidences were sought between fission fragments detected in F and charged particles in P. The fission counter, generally operated at a gas multiplication of about 10, detected roughly 10 percent of all fissions occurring in the source and was prevented from recording particles of less than one cm range by a thin Nylon film stretched across its entrance. Wire grids across the entrances to

[1] Tsien, Ho, Chastel, and Vigneron, Phys. Rev. **71**, 382 (1947).
[2] Tsien, Ho, Vigneron, and Chastel, Nature **159**, 773 (1947).
[3] L. Rosen and A. M. Hudson, Phys. Rev. **76**, 181(A) (1949).
[4] K. W. Allen and J. T. Dewan, Phys. Rev. **80**, 181 (1950). This paper contains complete references to earlier work on the subject.
[5] Cassels, Dainty, Feather, and Green, Proc. Roy. Soc. (London) **A191**, 428 (1947).
[6] L. L. Green and D. L. Livesey, Trans. Roy. Soc. (London) **A241**, 323 (1948).
[7] Tsien, Ho, Chastel, and Vigneron, J. phys. radium **8**, 165, 200 (1947).
[8] Tsien San-Tsiang, J. phys. radium **9**, 6 (1948).
[9] J. T. Dewan and K. W. Allen, Phys. Rev. **76**, 181(A) (1949).

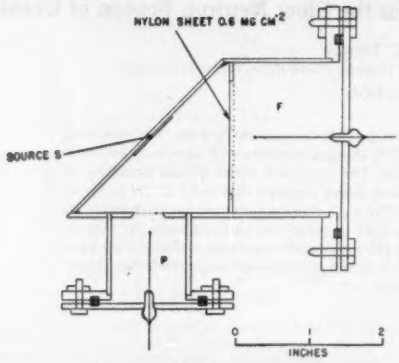

FIG. 1. Apparatus for range measurements.

both counters insured that ions produced in the source region by a particle entering one counter would not be dragged into the other counter, thereby causing a spurious coincidence.

The proportional counter P was operated at a gas multiplication of about 20 and was calibrated in energy by means of α-particles from a thin source of U^{233} placed at S. The initial ionization of these α-particles was about 0.1 Mev/mm. Using this calibration, the initial ionization produced by fission fragments traversing P at a very low pressure (2.2 cm of methane) was found to be 5.5 Mev/mm, which is in good agreement with the value of Sherr and Peterson[10] although rather lower than that reported by some authors. Hence, the counter response was reasonably linear over the desired working region of 0.1 to 5.5 Mev/mm. The solid angle of detection for P, as determined by counting a source of α-particles of known strength, was 1/250 of 4π-steradians.

The method of the experiments was to study the dependence of the true coincidence rate between F and P on the pressure in the apparatus and on the energy spent in counter P, relative to that spent by natural α-particles from the source at the same gas pressure. It will be evident that the counter P, when set to detect particles of low specific ionization and range less than 1 cm of air, counted natural α-particles and fission fragments from the source S. This gave rise to a large random coincidence rate, and long counting periods at relatively low intensity were necessary to obtain significant results. It soon became apparent, however, that most of the short-range particles had specific ionizations considerably greater than α-particles but smaller than those of fission fragments. Figure 2 is a typical bias curve of pulses from P. Natural α-particles produced pulses up to 2 v in height; short-range fission particles gave pulses up to 23 v, while all pulses above 23 volts came from normal fission fragments traversing P. It was seen from the flatness of this bias curve that a very considerable improvement in the ratio of true to random coincidences could be obtained by recording only coincidences between pulses from F and those pulses from P lying between 2 and 30 v. This region included all of the short-range particle pulses but excluded normal fission fragments which could only contribute to the random coincidence rate (since F did not detect short-range particles). An anticoincidence circuit was therefore arranged in such a manner that the large pulses from P (greater than 30 v) momentarily deadened the output of the coincidence mixer and prevented the recording of undesired random coincidences. In this way, the ratio of true to chance coincidences was increased by about a factor of ten without the loss of any true coincidences, since the slight increase in dead time due to the anticoincidence arrangement had a negligible effect at the relatively low counting rates employed. Figure 3 is a block diagram showing the arrangement of the electronic circuits. The anticoincidence discriminator level was normally set at 30 v.

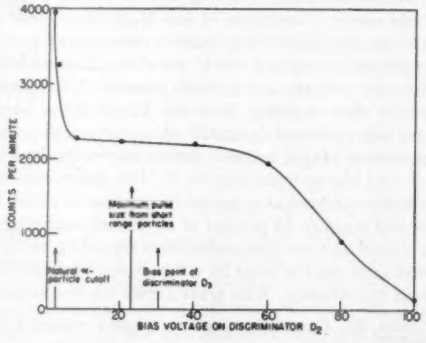

FIG. 2. Bias curve of pulses from the proportional counter P.

[10] R. Sherr and R. Peterson, Rev. Sci. Instr. 18, 567 (1947).

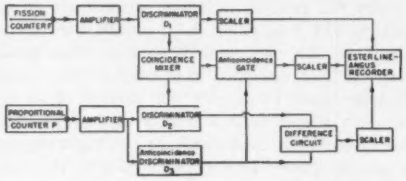

FIG. 3. Block diagram of the electronic arrangement.

The apparatus was made completely automatic and self-recording. A single Esterline-Angus chart recorded, after suitable scaling, the number of coincidences, the number of fissions counted in F, and the *difference* in the number of pulses passed by discriminators D_2 and D_3. By means of a step switch, the bias level of discriminator D_2 could be preset to a number of desired values between 2 and 20 volts. At any setting, the information was recorded for a given number of fissions,

generally about 5×10^6; then, the step switch automatically set the bias at the next preset level and the process was repeated. A shift in base line of the Esterline-Angus chart accompanied each change in bias setting. In this manner, complete bias curves could be run and recycled without attention to the apparatus.

III. RESULTS FOR U^{235}

To investigate the range distribution of the particles, the pressure in the counter system was varied from 2.2 cm (the lowest convenient working pressure) to about 16 cm Hg in a number of steps. At each pressure the bias of discriminator D_2 was varied from 2 to 20 v, as described above, and a curve of coincidence rate, after correcting for casual coincidences, was plotted against bias. Figure 4 shows a typical curve obtained at a pressure of 3.7 cm of methane, and it is apparent that practically all of the particles ionize more heavily than do the 5 Mev α-particles from the uranium source. Each of the curves so obtained was extrapolated back

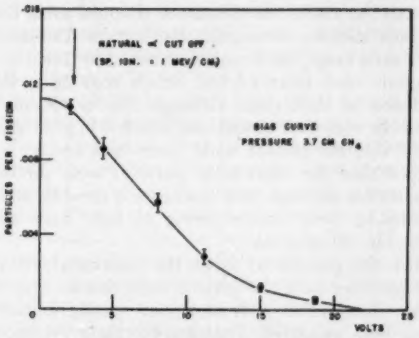

FIG. 4. Typical bias curve of coincident pulses.

to zero bias in order to obtain the total abundance of short-range particles entering P at that pressure. Plotting these extrapolated abundances against pressure resulted in the range distribution curve of Fig. 5. The equivalent ranges shown are those which particles must have in order to reach the proportional counter at the corresponding pressures. It is evident that the maximum range of the particles is 8 mm of air, but it is difficult to deduce much about the actual range distribution of the observed particles because of lack of information concerning their specific ionizations. The coincident rates which were obtained in our system have been corrected on the basis of Green and Livesey's[8] angular distribution to give the abundances plotted as ordinates on Fig. 5. Extrapolation to zero pressure results in a total abundance of 1 in 76±8 fissions for all short-range particles.

Figure 6 (similar to Fig. 4) shows the bias curve of coincident pulses taken at a pressure of 2.2 cm of methane, which was the lowest pressure at which

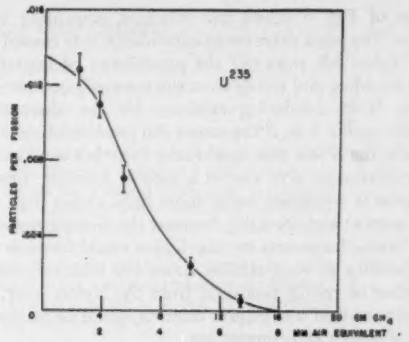

FIG. 5. Range distribution of short-range particles from U^{235}.

the counter operated satisfactorily. At this pressure the equivalent length of counter P was only 0.6 mm of air, so that this curve is effectively the distribution of *initial* specific ionization of the particles. The maximum specific ionization is 1.02 Mev/mm, which is 10 times greater than that produced by the uranium α-particles from the source, and 4.5 times greater than the maximum possible specific ionization of an α-particle of any range. Thus, at least some of the particles must have masses appreciably greater than that of the α-particle.

There are three plausible mechanisms which would give rise to short-range particles which are not true ternary fission fragments. Firstly, the observed particles may be recoil atoms projected into the counter P by the fission fragments as they pass through the uranium source or gas surrounding the source; secondly, they may be spurious coincidences caused by imperfect shielding of the source region by the two wire grids; and thirdly, they may be fission fragments back scattered into P by the platinum backing of the source S. The first two hypotheses were tested by placing a thin Nylon film, just sufficiently thick to stop particles of 8 mm range, directly over the source S. The dotted

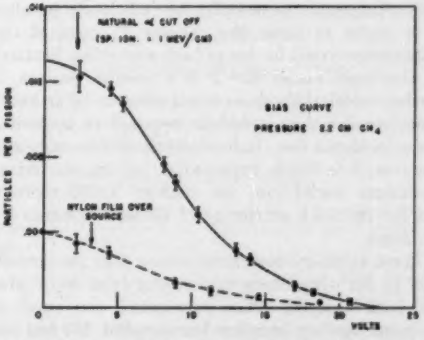

FIG. 6. Initial specific ionization of the coincident pulses.

curve of Fig. 6 shows the resultant coincident bias curve. The large decrease in coincidence rate caused by the Nylon foil rules out the possibilities of imperfect grid shielding and recoils from the counter gas. Furthermore, it is convincing evidence for the absence of source recoils. For, if the source did produce observable recoils, the Nylon film would stop them but would itself be expected to give rise to a greater number; firstly, because it contained many more light atoms than did the source; and secondly, because the slowing down of the fission fragments by the Nylon would increase the probability of such recoils. From the relatively small number of recoils produced from the Nylon layer, we concluded that a negligible number would be produced in the source and counter gas.

Calculations based on the Rutherford scattering formula indicated that less than 0.2 percent of the observed coincidences should be caused by fission fragments back scattered into P by the platinum

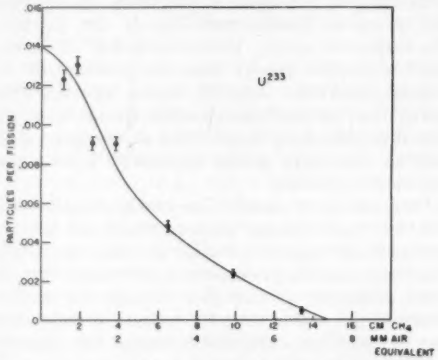

FIG. 7. Range distribution of short-range particles from U^{233}.

backing of the source. However, experimental verification was obtained by replacing the uranium source on platinum by one on aluminum backing. This caused no change in the coincidence rate per fission nor in the shape of bias curve obtained. As it is impossible for fission fragments to be deflected sufficiently by aluminum nuclei to enter the counter P, none of these coincidences could be due to back scattering. Scattering of aluminum nuclei into P is a possible process, but further calculations showed this effect to be at least 50 times smaller than would be required to account for the coincidence rate. Independently of this calculation, however, it is highly improbable that the scattering of aluminum nuclei into the counter would reproduce exactly the back scattering of fission fragments from platinum.

These auxiliary experiments show that the contribution to the coincidence rate arising from recoil atoms and back scattered fission fragments is very small, and no correction has therefore been applied. We feel confident in concluding that the true coincidences observed were due to short-range particles produced directly in the fission process.

IV. RESULTS FOR U^{233}

The emission of short-range particles from U^{233} was investigated in the same manner as for U^{235} and similar results were obtained. Figure 7 shows the resulting range distribution curve.

The maximum range was 7.4 mm, and the abundance one in 72 ± 5 fissions, on the assumption that the angular distribution is the same as that for U^{235}. The maximum initial specific ionization of the particles was slightly lower than that found in the fission of U^{235}, although still considerably greater than that of α-particles.

V. NATURE OF THE PARTICLES

The experiments described above show that in approximately 1.3 percent of fission events in U^{235} short-range charged particles considerably more massive than α-particles are emitted. The range distribution of the particles measured in the present experiments is in excellent agreement with that obtained by Green and Livesey, as also is the abundance obtained using these authors' data on the angular distribution. The greater maximum range, *viz.* 3 cm air, obtained by Tsien *et al.* suggests that some nuclear recoils may have been included in their data, although this is difficult to reconcile with their abundance, which is in good agreement with the present work. Green and Livesey concluded that the short-range particles were probably α-particles, although they pointed out the difficulty of estimating their masses owing to their very short ranges in the emulsion.

It is not possible to obtain the mass distribution of the particles from the present data because only the range distribution and maximum specific ionization have been measured. Photographic plate evidence is against the existence of particles with mass numbers greater than about 12, while the present measurements suggest that most of the particles are heavier than α-particles. Owing to the rather meager data on range-energy relations for particles heavier than α-particles, it is not possible to estimate masses accurately. If it is assumed that the maximum initial specific ionization corresponds to the maximum range, then an estimated mass of 13 ± 4 is obtained,[11] although there seems to be little justification for this assumption. It is clear, however, that a different process is involved in the emission of short-range particles than that concerned with the emission of long range α-particles.

It is a pleasure to acknowledge the interest shown by Dr. B. W. Sargent and Dr. B. Pontecorvo concerning these experiments. The cooperation of the pile operating staff, under the direction of Mr. D. D. Stewart and Mr. G. M. James, is greatly appreciated; thanks are also due Dr. J. G. MacHutchin for the preparation of the sources of fissile material.

[11] This mass was misquoted as 12 ± 1 in a recent publication. [E. W. Titterton and T. A. Brinkley, Phil. Mag. 41, 500 (1950).]

Electron-Neutrino Angular Correlation*

E. Greuling and M. L. Meeks†
Department of Physics, Duke University, Durham, North Carolina
(Received December 18, 1950)

Angular correlation functions are calculated for allowed and first forbidden beta-decay transitions including the effect of the nuclear coulomb field. The process of beta-decay is viewed as a kind of scattering in which an incident negative energy neutrino is transformed by the Fermi interaction in to scattered electron in a positive energy state. The outgoing electronic wave function is calculated, and the angular correlation functions are determined from the angular dependent electron probability current through sections of a sphere at large distances from the nucleus. For allowed transitions, the angular correlation is found to be independent of atomic number and identical with the results of previous calculations which assumed $Z=0$. The $Z=0$ approximation is shown to be unreliable for first forbidden transitions in which correlation terms proportional to the first and second powers of the potential energy of an electron at the surface of the nucleus appear. This effect is important even for moderately heavy nuclei.

I. INTRODUCTION

THE relation between the directions of emission of the electron and neutrino emitted by a β-active nucleus depends on the type of light particle-nucleon interaction assumed in the Fermi theory.[1] This was first pointed out by Bloch and Møller.[2] More recently, the electron-neutrino angular correlation was investigated theoretically for the five different types of β-decay coupling[3] by Hamilton.[4] His results, for allowed and first forbidden transitions, were based on the $Z=0$ approximate treatment of the Fermi theory. Rose[5] considered the effect of finite nuclear charge on the allowed transition β-neutrino angular correlation functions. We not only confirm his concludion that the effect is small, but also, as is shown in Sec. III (A), treat the problem more exactly and conclude that, aside from the appearance of the usual Z dependent Fermi function, *the allowed correlation functions are identical with those obtained by Hamilton.*

In all previous work on β-neutrino angular correlation that has come to our attention, the effect of the nuclear coulomb field on the outgoing electron has been either neglected or, as in reference 5, been treated approximately. The shapes of forbidden transition energy spectra may depend strongly on the nuclear charge. In Sec. III (B), the Z dependent angular correlation functions for first forbidden transitions are computed and are shown to differ from the $Z=0$ results of Hamilton in just those cases where the energy spectrum also exhibits a strong Z dependence.

II. ANGULAR DEPENDENT DECAY PROBABILITY

It is helpful to visualize the β-radioactive processes as a kind of scattering of a light Dirac particle by a heavy nucleon. The usual negatron decay process[6] can be described as the scattering of a light particle from its vacuum neutrino state of negative energy by a nucleon into its positive energy, negative charge, electron state. Charge is conserved in the process by the transformation of the target nucleon from its neutron into its proton state. The electron and neutrino are considered as two possible states of a light Dirac particle, differing as to charge and rest mass.

The interaction hamiltonian between nucleon and light particle is presumed to be some linear combination of the five Lorentz invarient operators designated as scalar (S), polar vector (V), axial vector (A), tensor (T), or pseudoscalar, (P).

$$H_X=G(\mathbf{O}_H\cdot\mathbf{O}_L)_X(\tau_H\tau_L+\tau_H^*\tau_L^*)\delta(\mathbf{x}_H-\mathbf{x}_L), \quad (1)$$

where

$$X=S,\ V,\ T,\ A,\ \text{or}\ P.$$

The strength of the interaction is determined by the Fermi constant G; H and L refer to nucleon and light particle operators, respectively; τ_H transforms a neutron into a proton; τ_L transforms a neutrino into an electron; τ_H^* and τ_L^* are the inverse operators making positron decay possible. The different coupling operators, $(\mathbf{O}_H\cdot\mathbf{O}_L)_X$, are constructed by the contraction of the usual contravariant light particle Dirac operators with their covariant heavy particle analogs.[7]

(A) Asymptotic Wave Function

We specify the initial system, β-radioactive nucleus plus incident vacuum neutrino of spin s, and momentum $-\mathbf{q}$, by the wave function,[8]

$$\psi_I=\psi_I(\mathbf{x}_H,\mathbf{x}_L)\exp(-iE_It),$$

* Part of a thesis by M. L. Meeks submitted to the Graduate School, Duke University, May, 1950, in partial fulfillment of the requirements for the Ph.D. degree.
† Now at Clemson College, Clemson, South Carolina.
[1] E. Fermi, Z. Physik **88**, 161 (1934).
[2] F. Bloch and C. Møller, Nature **136**, 912 (1935).
[3] E. J. Konopinski, Revs. Modern Phys. **15**, 209 (1943).
[4] D. R. Hamilton, Phys. Rev. **71**, 456 (1947).
[5] M. E. Rose, Phys. Rev. **75**, 1444 (1949).
[6] To apply our results to positron decay, it is only necessary to change the sign of Z for the product nucleus where it appears in Eqs. (22) and (37) of Sec. III (B).
[7] The five operators, $(\mathbf{O}_H\cdot\mathbf{O}_L)_X$, as given explicitly in terms of β, σ, α, and γ_5 by J. Tiomno and John A. Wheeler, Revs. Modern Phys. **21**, 144 (1949), were found most convenient. See also reference 3.
[8] All quantities are made dimensionless by using the usual relativistic electron units of energy (mc^2), time ($\hbar/mc^2$), and length ($\hbar/mc$).

where (2)

$$\psi_I = U(\mathbf{x}_H) B_s(\mathbf{q}) \exp(-i\mathbf{q}\cdot\mathbf{x}_L),$$

and $E_I = E_U - K$; E_U = energy of initial nucleus. The neutrino rest mass is assumed to be zero; thus, the anti-neutrino emitted in the β-decay has an energy $K = q \geqslant 0$. The spinor amplitude B_s is normalized to unit incident neutrino current density. We designate the initial and final nuclear isobars by U and V, respectively. The interaction (1) transforms one neutron of U into a proton of V. These nuclear states are orthogonal.

Possible final states of the system involve the continuum positive kinetic energy ($W \geqslant 1$) electron wave functions in the coulomb potential field of the product nucleus. These Dirac functions are conveniently tabulated by Rose.[9] We use his notation with one exception. The radial functions f and g are given a more appropriate subscript $\kappa = \pm(j+\frac{1}{2})$, where j is the total angular momentum. The angular dependent functions are spherical harmonics, their order depending only on the pair of quantum numbers, κ and $m = [-j, -(j-1), \cdots, +j]$.

For our purpose, it is convenient to factor the electron wave functions into radial and angular dependent parts.

$$\psi_f = R_\kappa(W, r) A_f(\theta, \varphi). \tag{3}$$

The subscript f stands for the discrete pair of eigenvalues κ and m. In our notation, R is the diagonal matrix:

$$R_\kappa = \begin{pmatrix} f_\kappa & 0 & 0 & 0 \\ 0 & f_\kappa & 0 & 0 \\ 0 & 0 & g_\kappa & 0 \\ 0 & 0 & 0 & g_\kappa \end{pmatrix}, \tag{4}$$

and the angular dependent spinors are:

$$A_f(\theta, \varphi) = \begin{matrix} i\left(\frac{\kappa+m-\frac{1}{2}}{2\kappa-1}\right)^{\frac{1}{2}} (Y_{-\kappa}^{m-\frac{1}{2}}, Y_{\kappa-1}^{m-\frac{1}{2}}) \\ i\left(\frac{\kappa-m-\frac{1}{2}}{2\kappa-1}\right)^{\frac{1}{2}} (Y_{-\kappa}^{m+\frac{1}{2}}, -Y_{\kappa-1}^{m+\frac{1}{2}}) \\ \left(\frac{\kappa-m+\frac{1}{2}}{2\kappa+1}\right)^{\frac{1}{2}} (Y_{-\kappa-1}^{m-\frac{1}{2}}, Y_{\kappa}^{m-\frac{1}{2}}) \\ \left(\frac{\kappa+m+\frac{1}{2}}{2\kappa+1}\right)^{\frac{1}{2}} (-Y_{-\kappa-1}^{m+\frac{1}{2}}, Y_{\kappa}^{m+\frac{1}{2}}) \end{matrix} \tag{5}$$

$$\kappa \leqslant -1, \quad \kappa \geqslant +1.$$

After a transition, the system may be in a superposition of the basic eigenstates F represented by the time dependent wave function,

$$\psi_F = \psi_F(\mathbf{x}_H, \mathbf{x}_L) \exp(-iE_F t), \tag{6}$$

where

$$\psi_F = V(\mathbf{x}_H)\psi_f(W, \mathbf{x}_L),$$

and

$$E_F = E_V + W; \quad E_V = \text{energy of final nucleus.}$$

The subscript F differs from f in that it includes the continuum eigenvalues W for the electron. The functions $\psi_f(W, \mathbf{x}_L)$ are normalized to one electron per unit energy range

$$\left(\text{i.e.} \int d\mathbf{x}_L \psi_f^*(W, \mathbf{x}_L)\psi_{f'}(W', \mathbf{x}_L) = \delta(W - W')\delta_{\kappa\kappa'}\delta_{mm'}\right).$$

If the system is initially in the state I, we obtain, upon applying the usual first-order time dependent perturbation theory, subsequent states of the system as a superposition of the wave functions (2) and (6).

$$\chi(\mathbf{x}_H, \mathbf{x}_L, t) = \left\{\psi_I + \sum_f \int dW (f|H|s) \times \left\{\frac{\exp[-i(W_0 - W - K)t] - 1}{W_0 - W - K}\right\}\psi_F\right\} \exp(-iE_I t), \tag{7}$$

where the nuclear energy difference is $W_0 = E_U - E_V$, and the matrix element of the perturbation, Eq. (1), reduces to the time independent expression:

$$(f|H|s) = G\left[\int d\mathbf{x}_H (V^* \mathbf{O}_H \tau_H U)\psi_f^*(\mathbf{x}_H) \times \exp(-i\mathbf{q}\cdot\mathbf{x}_H)\right]\cdot \mathbf{O}_L B_s. \tag{8}$$

We obtain from Eqs. (7) and (3), since V and U are orthogonal, the time dependent superposition of electron states resulting from the "scattering" of a neutrino by a nucleon. We call this scattered wave function resulting in the product nucleus V,

$$\psi_{sc} \exp(-iE_I t) = \int d\mathbf{x}_H V^* \chi(\mathbf{x}_H, \mathbf{x}_L, t),$$

where $\psi_{sc} = \sum_f \int dW (f|H|s)$ (9)

$$\times \left\{\frac{\exp[-i(W_0 - W - K)t] - 1}{W_0 - W - K}\right\} R_\kappa A_f.$$

These "scattered" electron waves contain both incoming and outgoing particles. However, we can show, by a relativistic generalization of the method developed by Bethe,[10,11] that only the outgoing part contributes to the transition probability. The radial functions (4) for large r can be expressed as:[9]

$$R_\kappa = (2r)^{-1}[N \exp(i[pr + \delta_\kappa]) + \text{c.c.}], \tag{10}$$

[9] M. E. Rose, Phys. Rev. **51**, 484 (1937).

[10] H. A. Bethe, Ann. d. Physik 4, 443 (1930).

[11] N. F. Mott and H. S. W. Massey, *The Theory of Atomic Collisions* (Oxford University Press, New York, 1933), chapter XIV, section 3.

where

$$N=\begin{pmatrix} a & 0 & 0 & 0 \\ 0 & a & 0 & 0 \\ 0 & 0 & b & 0 \\ 0 & 0 & 0 & b \end{pmatrix}, \quad a=i[(W-1)/\pi p]^{\frac{1}{2}}, \quad b=[(W+1)/\pi p]^{\frac{1}{2}},$$

and $p=(W^2-1)^{\frac{1}{2}}$ is the magnitude of the electron momentum far from the nucleus. Substituting expression (10) into (9), we evaluate the energy integral, by a method similar to Bethe's, thereby obtaining conservation of energy and the following asymptotic, time-dependent, scattered electron wave function:

$$\psi_{s\epsilon}\underset{W=W_0-K}{\overset{r\gg 1}{=}}\begin{cases}(\pi/r)\sum_f(f|H|s)NA_f\exp(i[pr+\delta_\kappa-\pi/2]), \\ \qquad\qquad r<(p/W)t \\ 0, \qquad\qquad r>(p/W)t=r_0.\end{cases} \quad (11)$$

The phase δ_κ is conveniently separated into two terms, one depending on κ, the other produced by the coulomb field and independent of κ. $\delta_\kappa=\epsilon_\kappa+\delta_c$,

$$\text{where} \quad \epsilon_\kappa=\eta_\kappa-(\pi/2)\gamma_\kappa-\arg\Gamma[\gamma_\kappa+i(\alpha ZW)/p], \quad (12)$$

$$\gamma_\kappa=[\kappa^2-(\alpha Z)^2]^{\frac{1}{2}},$$

and

$$\exp(2i\eta_\kappa)=-(\kappa-i\alpha Z/p)/(\gamma_\kappa+i\alpha ZW/p).$$

Here the asymptotic phase shift δ_c produced by the coulomb field depends on the atomic number Z and the fine structure constant α.

$$\delta_c=[\alpha ZW\ln(2pr)]/p. \quad (13)$$

In evaluating the integral (9), the coulomb factor $\exp(i\delta_c)$ need not be considered as a rapidly varying function of W for two reasons. First, the effect of orbital electron screening of the nuclear coulomb field would, if taken into account, cause the asymptotic value of δ_c to approach a constant. Secondly, even if the nucleus had been treated as stripped of orbital electrons and $\exp(i\delta_c)$, therefore, not removed from the integrand of (9), we would have obtained a different value for r_0 which would take into account the influence of the coulomb field on the electron velocity.[10]

(B) Electron Probability Current

To complete the proof that the wave function (11) contains only outgoing electrons and to obtain the final expression for the probability per unit time of observing an electron moving at an angle θ relative to the anti-neutrino momentum, it is convenient to make use of the Gordon decomposition[12] of the probability current density. At distances far from the nucleus, the electron current density per incident neutrino is:

$$\mathbf{J}=\tfrac{1}{2}[\psi_{s\epsilon}^*(i\nabla\beta\psi_{s\epsilon})-(i\beta\psi_{s\epsilon})(\nabla\psi_{s\epsilon}^*)] +\mathbf{curl}(\psi_{s\epsilon}^*\mathbf{M}\psi_{s\epsilon})+(\partial/\partial t)(\psi_{s\epsilon}^*\mathbf{P}\psi_{s\epsilon}). \quad (14)$$

The vector operators $\mathbf{M}$ and $\mathbf{P}$ are defined in reference 12. Clearly, the so-called "magnetic and electric polarization" current densities, involving $\mathbf{M}$ and $\mathbf{P}$, do not contribute to the radial probability current of electrons. By inserting (11) into (14) we can obtain, as follows, the probability per unit time for the emission of an electron outward from the nucleus along a radius vector $\mathbf{r}$ inclined at an angle θ to $\theta+d\theta$ relative to the anti-neutrino momentum direction which is selected as the polar axis x_3.

$$d\gamma=\int_0^{2\pi}d\varphi(\mathbf{J}\cdot\mathbf{r})r\sin\theta d\theta =\int_0^{2\pi}d\varphi\psi_{s\epsilon}^*(-p\beta)\psi_{s\epsilon}r^2\sin\theta d\theta. \quad (15)$$

An alternative expression for the radial electron current can be obtained by using the following relation,[13] valid for free electrons having energy $W\geqslant 1$: $\psi^*(\beta W)\psi=-(\psi^*\psi)$. Thus, it follows that (15) has the alternative form:

$$d\gamma=(p/W)\int_0^{2\pi}d\varphi(\psi_{s\epsilon}^*\psi_{s\epsilon})r^2\sin\theta d\theta. \quad (16)$$

This latter expression clearly indicates that the radial current of electrons is positive definite.

On insertion of (11) into (15) or (16), we obtain alternative explicit expressions for the angular dependent probability current of electrons.

$$d\gamma=2\pi^2\sum_{ff'}(f'|H|s)(s|H|f) \times\exp(i[\epsilon_{\kappa'}-\epsilon_\kappa])(f|f')\sin\theta d\theta. \quad (17)$$

Here the angular dependent factors are defined alternatively as

$$2\pi(f|f')=\int_0^{2\pi}d\varphi(A_f^*[1-\beta/W]A_{f'}) =\int_0^{2\pi}d\varphi(A_f^*[1-\beta W]A_{f'}). \quad (18)$$

Thus, it follows that the angular dependence of the decay probability arises from the spinor products $(A_f^*A_{f'})$ alone, because $(A_f^*[\beta/W]A_{f'})$ must vanish to satisfy the requirement that

$$(A_f^*[\beta/W]A_{f'})=(A_f^*[\beta W]A_{f'})$$

for $W\geqslant 1$. The integral over the azimuthal angle of the electron, of course, vanishes except for those sets of quantum numbers f, f' in which $m=m'$. Therefore, (18) simply reduces to:

$$(f|f')\equiv(\kappa,m|\kappa',m)=(A_{\kappa m}^*A_{\kappa' m}), \quad (19)$$

and the summation in (17) is restricted to κ, κ', and m.

It must be kept in mind that $d\gamma$ gives the probability current for an electron produced when a neutrino of a

[12] E. L. Hill and R. Landshoff, Revs. Modern Phys. **10**, 116 (1938).

[13] H. A. Bethe, Z. Naturforsch. **3a**, 470 (1948). This relation follows simply from the Dirac equation with $r\gg 1$. Our choice of sign for the operators α and β is opposite from Bethe's.

particular momentum and spin is absorbed. The matrix elements $(f|H|s)$, given by (8), depend explicitly on the neutrino momentum and spin. To find the angular and energy dependent rate of β-decay, we sum $d\gamma$, given by (17), over all possible states of the incident neutrino. This introduces the usual statistical factor $q^2dq/(2\pi)^3$ for a neutrino of a definite spin and momentum in the direction of the solid angle $d\Omega$. The summation over neutrino spin is independent of the angle between electron and neutrino. However, in integrating over neutrino directions $d\Omega$, we hold the electron-neutrino angle fixed and instead integrate over all directional orientations of the transforming nucleus. In this manner, we obtain the probability per unit time of observing an electron in the energy range W to $W+dW$, having an electron anti-neutrino angle between θ and $\theta+d\theta$.

$$P(\theta, W, W_0, Z)d\theta dW = q^2 \sum_{jj'} [f|f'](f|f') \sin\theta d\theta dW, \quad (20)$$

where $q=W_0-W$. The bracketed factors are a simplified notation for the angular independent part of the β-spectrum.

$$[f|f'] \equiv [\kappa, m|\kappa', m] = \sum_s \langle (f'|H|s)(s|H|f)\rangle_{Av} \exp(i[\epsilon_{\kappa'} - \epsilon_\kappa]). \quad (21)$$

The brackets $\langle\ \rangle_{Av}$ indicate the nuclear orientation average, and s stands for the two spin values of the neutrino of momentum components $q_1=q_2=0$, $q_3=q$.

Terms in Eq. (20) which make important contributions to the angular dependent decay probability include the interference between outgoing electrons for which $\kappa \neq \kappa'$. If Eq. (20) is integrated over all angles of β-emission, only the $f=f'$ terms do not vanish, and one obtains the usual angular independent β-energy spectrum.

III. ANGULAR DEPENDENT CORRECTION FACTORS

In order to calculate the angular correlation functions for allowed and first forbidden transitions, we shall make use of the expression for the angular dependent decay probability in a slightly modified form. The expression (20) gives the angular correlation and energy spectrum as well. For allowed transitions, the energy spectrum is the same for all five types of coupling. To present the angular correlations in convenient form, we introduce the factors C_{nX} from which the factor giving rise to the allowed energy spectrum has been removed. The subscript n is zero for allowed transitions and one for first forbidden transitions, and the subscript X equals S, V, A, T, or P designating the interaction (1) considered. Rewriting (20) in the nth-forbidden approximation as

$$P_{nX}d\theta dW = C_{nX}(\tfrac{1}{2}\sin\theta d\theta)[(G^2/2\pi^3)F_0 pWq^2 dW], \quad (22)$$

we define the correction factors as

$$C_{nX} = [(G^2/4\pi^3)F_0 pW]^{-1} \sum_{jj'} [f|f']_{nX}(f|f'), \quad (23)$$

where F_0 is the usual Fermi function.

Now to calculate the matrix element $(f|H|s)$ given by (8), we expand the electron wave function appearing therein[14] in the following manner:

$$\psi_f = \psi_{f0} + r^{-1} \sum_{i=1}^{3} x_i \chi_{fj} + \cdots. \quad (24)$$

Here the first-order spherical harmonics have been expressed in the cartesian coordinates x_1, x_2, x_3, and the terms x_j/r factored out. ψ_{f0} is that part of ψ_f containing only zero-order spherical harmonics. For values of $\kappa=\pm1$, the electron wave function contains only zero- and first-order spherical harmonics; for $\kappa=\pm2$, it contains first- and second-order spherical harmonics. However, second-order spherical harmonics contribute only to second and higher orders of forbidden transitions. The selection of the axis of quantization (x_3) to correspond to the momentum direction of the anti-neutrino enables us to expand the factor $\exp(-i\mathbf{q}\cdot\mathbf{x})$, also appearing in the matrix element (8), as $1-iqx_3+\cdots$.

(A) Allowed Transitions

The matrix element for allowed transitions is, using the conventional approximation,

$$(f|H|s)_{0A} = G\left(\int \mathbf{O}_H\right)\cdot(\psi_{f0}^* \mathbf{O}_L B_s), \quad (25)$$

in which the light particle wave functions are removed from the integral and evaluated at the nuclear radius ρ. For simplicity, the integral over nucleon coordinates is abbreviated $\int \mathbf{O}_H$ as is usual.

To indicate the method employed in determining the allowed correlation factors C_{0X}, we shall consider a representative example, axial vector coupling. In this case $\mathbf{O}_H\cdot\mathbf{O}_L$ may be set equal to $\boldsymbol{\sigma}_H\cdot\boldsymbol{\sigma}_L$, since $\int\gamma_5=0$ for allowed transitions with this coupling. The factors $[f|f']_{0A}$ may then be calculated as follows: Make use of the Casimir trick for evaluating the neutrino spin sum and obtain

$$\sum_s (f'|H|s)(s|H|f) = G^2 \sum_{j,k} \left(\int \sigma_j\right)^* \left(\int \sigma_k\right) [\tfrac{1}{2}\psi_{f0}^* \sigma_j (1-\alpha_3)\sigma_k \psi_{f'0}]. \quad (26)$$

Average the product of nuclear matrix elements over all possible orientations of the nucleus,[15] multiply by the phase factor, and obtain

$$[f|f'] = \tfrac{1}{3}G^2 \left|\int \boldsymbol{\sigma}\right|^2 \times [\tfrac{1}{2}\psi_{f0}^*(3-\alpha_3)\psi_{f'0}] \exp(i[\epsilon_{f'} - \epsilon_f]). \quad (27)$$

The quantum numbers designated by f and f' can have the values $\kappa=\pm1$ and $m=\pm\frac{1}{2}$ for allowed transi-

[14] Clearly, the subscript H can now be dropped, nucleon coordinates being understood in Eq. (8).

[15] The products of nuclear matrix elements are averaged over nuclear orientations by the method discussed on p. 337 of Max Born, *Optik* (Verlag. Julius Springer, Berlin, 1933).

tions. Thus, since $m=m'$, the sum over f and f' involves eight terms. In four of these terms, $\kappa=\kappa'$; hence, $f=f'$. The factors $(f|f')$ in these four cases are

$$(f|f)=(2\pi)^{-1} \text{ for } (f|=(\pm 1, \pm\tfrac{1}{2}|. \tag{28}$$

In the four remaining terms, $\kappa=-\kappa'$, and the factors $(f|f')$ are

$$\begin{aligned}(\pm 1, \tfrac{1}{2}|\mp 1, \tfrac{1}{2})&=(2\pi)^{-1}\cos\theta,\\ (\pm 1, -\tfrac{1}{2}|\mp 1, -\tfrac{1}{2})&=-(2\pi)^{-1}\cos\theta.\end{aligned} \tag{29}$$

The exponential factors in Eq. (27) reduce to $\exp(i[\eta_{\kappa'}-\eta_\kappa])$, since for $|\kappa|=|\kappa'|$, $\gamma_\kappa=\gamma_{\kappa'}$. This can be seen by reference to Eq. (12).

Now summing over f and f', we obtain, on inserting (27), (28), and (29) into Eq. (23),

$$C_{0A}=\tfrac{1}{3}(F_0pW)^{-1}\left|\int\sigma\right|^2\left[\frac{3\pi}{2}(f_1^2+g_{-1}^2)\right.$$

$$\left.-\frac{\pi}{2}(if_1g_{-1}\exp(i[\eta_1-\eta_{-1}])+\text{c.c.})\cos\theta\right]. \tag{30}$$

The combinations of radial functions and phase factors, enclosed in parentheses in this expression, are common to all five types of coupling. The choice of a particular type of coupling affects only the sign of the term containing $\cos\theta$ and a numerical factor.

The correlation functions C_{0X} are given below for the five types of coupling.

$$\left.\begin{aligned}C_{0S}&=\left|\int\beta\right|^2\tfrac{1}{2}(1+\gamma_1)[1-(p/W)\cos\theta]\\ C_{0V}&=\left|\int 1\right|^2\tfrac{1}{2}(1+\gamma_1)[1+(p/W)\cos\theta]\\ C_{0A}&=\left|\int\sigma\right|^2\tfrac{1}{2}(1+\gamma_1)[1-\tfrac{1}{3}(p/W)\cos\theta]\\ C_{0T}&=\left|\int\beta\sigma\right|^2\tfrac{1}{2}(1+\gamma_1)[1+\tfrac{1}{3}(p/W)\cos\theta]\\ C_{0P}&=\left|\int\beta\gamma_5\right|^2\tfrac{1}{2}(1+\gamma_1)[1-(p/W)\cos\theta].\end{aligned}\right\} \tag{31}$$

The common factor $\frac{1}{2}(1+\gamma_1)$ is independent of W and for the light elements is nearly unity. The angular correlations are clearly different in the first four coupling cases. The scalar and pseudoscalar couplings give the same angular correlation, but, on the other hand, their parity selection rules are different and their nuclear matrix elements are of different orders of magnitude. Hence, it is possible to distinguish between the five types of coupling. In all cases shown above, the angular dependent term is proportional to $p/W=v/c$ which indicates that the angular correlation is essentially a relativistic effect.

A comparison of the angular correlation factors (enclosed in brackets) with those calculated by Hamilton[4] for $Z=0$ shows that the nuclear coulomb field produces no effect. The correlation factors given above are the same as Hamilton's.

The allowed correlation functions C_{0X} do not agree exactly with those calculated by Rose.[5] This is because in his calculation the phase factor, $\exp(i[\eta_{\kappa'}-\eta_\kappa])$, was treated approximately.

(B) First Forbidden Transitions

The method of computing the factors C_{1X} for first forbidden transitions parallels the calculation of C_{0X}, although it is much more tedious because the matrix elements $(f|H|s)$ contain many more terms. Consider the matrix element for first forbidden transitions, using axial vector coupling again as an example,

$$(f|H|s)_{1A}=G\left[\sum_{jk}\left(\int\sigma_j x_k\right)P_k^*\sigma_j B_s\right.$$

$$\left.-\left(\int\gamma_5\right)\psi_{f0}\gamma_5 B_s\right], \tag{32}$$

where

$$P_k=\rho^{-1}\chi_{fk}+iq_k\psi_{f0}.$$

Notice here that the anti-neutrino moves along the x_3 axis; thus, $q_k=q\delta_{3k}$.

We express the nuclear matrix elements in Eq. (32) in terms of irreducible tensor components[16] as follows:

$$\int\sigma_j x_k=\tfrac{1}{3}Q_{jk}+\tfrac{1}{2}A_{jk}+\tfrac{1}{3}S_{jk}. \tag{33}$$

Under space rotations S, A, and Q transform, respectively, like the spherical harmonics of order 0, 1, and 2, and, consequently, give rise to different selection rules. Explicitly, the tensor components are[17]

$$\begin{aligned}Q_{jk}&=\int[\sigma_j x_k+\sigma_k x_j-\tfrac{2}{3}(\boldsymbol{\sigma}\cdot\mathbf{r})\delta_{jk}],\\ A_{jk}&=\int[\sigma_j x_k-\sigma_k x_j],\\ S_{jk}&=\int(\boldsymbol{\sigma}\cdot\mathbf{r})\delta_{jk}.\end{aligned} \tag{34}$$

Similar tensors, $\hat{A}$, etc., can be formed from the combinations $P_k^*\sigma_j$. We express the first term in (32) as a contraction of the tensors A, Q, and S, formed from the nuclear matrix elements, with the tensors $\hat{A}$, etc.,

[16] E. J. Konopinski and G. E. Uhlenbeck, Phys. Rev. **60**, 308 (1941).
[17] E. Greuling, Phys. Rev. **61**, 568 (1942).

formed from the electron-neutrino factors. These tensors cannot mix upon contraction, because Q is symmetric with trace zero, A is antisymmetric, and S is a scalar times a unit tensor. The second term in (32) does not contain the coordinates x_n in the nuclear matrix element and is, thus, no more complicated than the allowed matrix elements.

When the product $(f'|H|s)(s|H|f)$ is formed, cross products of the type occurring between the first and second terms of (32) will not be considered. In the case of axial vector coupling, they would have the form $(\int\boldsymbol{\sigma}\cdot\mathbf{r})^*(\int\boldsymbol{\gamma}_5)f(W,\theta)$+complex conjugate. This particular cross term may be expected to vanish, because $\boldsymbol{\gamma}_5$ and $\boldsymbol{\sigma}$ do not transform in the same way under a time reversal.[18]

The procedure used to obtain the factors $[f|f']$ is involved because of the large number of terms, but the steps are straightforward. As in allowed transitions, we average over all orientations of the nucleus[19] and make use of the Casimir trick in performing the neutrino spin sum.

In order to show the types of terms which appear, we shall sketch the calculation of one term in $[f|f']$. Choosing as a sample term of $(f'|H|s)(s|H|f)$, the product $A\,\hat{A}$, the nuclear orientation average yields

$$\sum_{jk}\sum_{j'k'}\langle A_{jk}{}^*A_{j'k'}\rangle_{\text{Av}}\hat{A}_{jk}{}^*B_sB_s{}^*\hat{A}_{j'k'}$$
$$=\tfrac{2}{3}\left|\int\boldsymbol{\sigma}\times\mathbf{r}\right|^2\sum_{jk}\hat{A}_{jk}{}^*B_sB_s{}^*\hat{A}_{jk}. \quad (35)$$

Here we have written the equivalent form $2|\int\boldsymbol{\sigma}\times\mathbf{r}|^2$ for $\sum|A_{jk}|^2$. Performing the spin sum, we obtain for this term of $[f|f']$, neglecting a numerical coefficient and the phase factor,

$$\left|\int\boldsymbol{\sigma}\times\mathbf{r}\right|^2[2\mathbf{P}^{s\prime}\cdot\mathbf{P}+\sum_{i\neq j}P_i{}^{s\prime}\sigma_i\sigma_jP_j+(\mathbf{P}^{s\prime}\cdot\boldsymbol{\alpha})P_3$$
$$+P_3{}^{s\prime}(\boldsymbol{\alpha}\cdot\mathbf{P})-P_1{}^{s\prime}\sigma_1\alpha_3\sigma_2P_2-P_2{}^{s\prime}\sigma_2\alpha_3\sigma_1P_1], \quad (36)$$

where the prime indicates that the electron wave function has the quantum numbers f', otherwise f.

For first forbidden transitions, f (and f') can have the following values: $\kappa=\pm2$, $m=\pm\frac{1}{2}$, $\pm\frac{3}{2}$ (for $j=\frac{3}{2}$), and $\kappa=\pm1$, $m=\pm\frac{1}{2}$ (for $j=\frac{1}{2}$). There are 40 possibilities for the combination f, f' with $m=m'$. It is convenient to divide these possibilities into eight groups, making use of the fact that the angular dependent factors $(f|f')$ consist of eight different types. The groups are chosen so that all the members of a particular group have the same angular dependence. In three of the groups $f=f'$; thus, the exponential phase factors of $[f|f']$ are unity. In the remaining groups, three have $\kappa=-\kappa'$ so that the exponential has the form $\exp(i[\eta_{\kappa'}-\eta_\kappa])$; and two groups have $|\kappa|\neq|\kappa'|$ so that the complete factor $\exp(i[\epsilon_{\kappa'}-\epsilon_\kappa])$ is required.

To evaluate C_{1X} from Eq. (23), the summation over f and f' is done by summing first over the terms in each group and then summing over the eight groups themselves. The results of this involved process are as follows:

$$C_{1S}=\tfrac{1}{3}\left|\int\mathbf{r}\right|^2B_S{}^{(1)},$$

$$C_{1V}=\tfrac{1}{3}\left|\int\mathbf{r}\right|^2A_V{}^{(1)}+\left|\int\boldsymbol{\alpha}\right|^2\tfrac{1}{2}(1+\gamma_1)$$
$$\times[1-\tfrac{1}{3}(p/W)\cos\theta],$$

$$C_{1A}=(1/60)\sum_{i,j}|Q_{ij}|^2A_A{}^{(2)}$$
$$+\tfrac{1}{6}\left|\int\boldsymbol{\sigma}\times\mathbf{r}\right|^2A_A{}^{(1)}+\tfrac{1}{6}\left|\int\boldsymbol{\sigma}\cdot\mathbf{r}\right|^2A_A{}^{(0)} \quad (37)$$
$$+\left|\int\boldsymbol{\gamma}_5\right|^2\tfrac{1}{2}(1+\gamma_1)[1+(p/W)\cos\theta],$$

$$C_{1T}=(1/60)\sum_{i,j}|Q_{ij}|^2B_T{}^{(2)}$$
$$+\tfrac{1}{6}\left|\int\boldsymbol{\sigma}\times\mathbf{r}\right|^2B_T{}^{(1)}+\tfrac{1}{9}\left|\int\boldsymbol{\sigma}\cdot\mathbf{r}\right|^2B_T{}^{(0)}$$
$$+\left|\int\boldsymbol{\alpha}\right|^2\tfrac{1}{2}(1+\gamma_1)[1+\tfrac{1}{3}(p/W)\cos\theta].$$

Pseudoscalar coupling gives the same angular correlation as scalar coupling. The coefficient C_{1P} can be obtained by replacing $|\int\mathbf{r}|^2$ in C_{1S} by $|\int\boldsymbol{\gamma}_5\mathbf{r}|^2$. The correlation factors[20] A_X and B_X, which are given in the approximation $\alpha Z\ll1$, are adequate for elements as heavy as RaE, for example, for which the error intro-

[18] C. L. Critchfield, Phys. Rev. **63**, 423 (1943), has pointed out that no such interference terms should appear because of the time reversal parity property of nuclear states. Matrix elements of $\boldsymbol{\gamma}_5$ and $(\boldsymbol{\sigma}\cdot\mathbf{r})$ are nonvanishing if the isobaric states have opposite space parity and have, respectively, the same and opposite "time parity."

[19] The nuclear orientation average for the products of irreducible tensors can be obtained from Born's *Optik* (reference 15, p. 348). Using Born's method, we obtain

$$\langle A_{ij}{}^*A_{i'j'}\rangle_{\text{Av}}=\tfrac{1}{5}\delta_{ii'}\delta_{jj'}\,\Sigma_{m,n}|A_{mn}|^2,$$
$$\langle Q_{ij}{}^*Q_{i'j'}\rangle_{\text{Av}}=\tfrac{1}{5}\delta_{ii'}\delta_{jj'}\,\Sigma_{m,n}|Q_{mn}|^2.$$

The fractional factor in these equations is just the reciprocal of the number of independent components in the tensor.

[20] The operator β does not appreciably affect the magnitude of the nuclear matrix elements and has been omitted from them; however, this operator is important in the electron-neutrino portion of $(f|H|s)$ because of its commutation properties. The notation $A_X(n)$ and $B_X(n)$ is chosen so that B indicates that the coupling contains β and A indicates that it does not; $(n)=(0)$, (1), (2) indicates that the corresponding quantity multiplies the square of a 0th, 1st, or 2nd rank tensor nuclear matrix element, respectively.

duced by this approximation amounts to 15 percent or so.

$$\left.\begin{matrix}A_V^{(1)}\\ B_S^{(1)}\end{matrix}\right\}=\tfrac{2}{3}V^2[1\mp\tfrac{1}{3}(p/W)\cos\theta]$$
$$+V[(p/W)(p+q\cos\theta)\pm(q+p\cos\theta)]$$
$$+[1\pm(p/W)\cos\theta]D,$$
$$\left.\begin{matrix}A_A^{(2)}\\ B_T^{(2)}\end{matrix}\right\}=[5\mp(p/W)\cos\theta]D\pm pq(p/W)\sin^2\theta,$$
$$\left.\begin{matrix}A_A^{(1)}\\ B_T^{(1)}\end{matrix}\right\}=\tfrac{2}{3}V^2[1\mp\tfrac{1}{3}(p/W)\cos\theta] \qquad (38)$$
$$+2V[(p/W)(p+q\cos\theta)\mp(q+p\cos\theta)]$$
$$+[1\mp(p/W)\cos\theta]D\mp pq(p/W)\sin^2\theta,$$
$$\left.\begin{matrix}A_A^{(0)}\\ B_T^{(0)}\end{matrix}\right\}=(9/4)V^2[1\pm(p/W)\cos\theta]$$
$$+3V[(p/W)(p+q\cos\theta)\pm(q+p\cos\theta)]$$
$$+[1\pm(p/W)\cos\theta]D\pm 2pq(p/W)\sin^2\theta.$$

Here $D=p^2+q^2+2pq\cos\theta$, and the factor $V=\alpha Z/\rho$ is the magnitude of the potential energy of an electron at the surface of the nucleus.

For elements at light as Be^8, $V=1.8$ Mev, and for A^{36}, $V=10$ Mev. Thus, for all but the lightest elements the angular correlation term proportional to V^2 will be the dominant one in the correlation factors A_X and B_X. The terms proportional to V^2 resemble the allowed correlation functions. The terms proportional to V are of two types, depending on the sign in front of $(q+p\cos\theta)$. For the plus sign, emission of the anti-neutrino and the electron in the same hemisphere is favored; this is generally referred to as a forward correlation. For the minus sign, a comparatively much weaker correlation results which favors emission of the anti-neutrino and electron in opposite hemispheres; a so-called backward correlation. The terms independent of V represent the $Z=0$ limit. They are identical with the first forbidden correlation functions calculated by Hamilton.[4]

Of the correlation functions shown in Eqs. (38), only the second rank tensor factors $A^{(2)}$ and $B^{(2)}$ show no coulomb effect. Both $A^{(2)}$ and $B^{(2)}$ give a forward correlation. The factor $B^{(2)}$ favors a forward anti-neutrino somewhat more strongly than $A^{(2)}$, but it would be difficult to distinguish between them experimentally.

In Eqs. (38) the correlation factors $A^{(1)}$, $B^{(1)}$, $A^{(0)}$, and $B^{(0)}$ show a strong Z effect. The V^2 term is larger than the other terms in these correlation factors for elements with atomic number $Z>Z_c\sim 1.6W_0^{\frac{1}{2}}$, where W_0 is the maximum electron energy.[3] If $Z\gg Z_c$, then only the V^2 term is of consequence.

IV. CONCLUSIONS

Some general conclusions can be drawn concerning the angular correlation functions, if we consider together the allowed transitions and the V^2 terms in the first forbidden transitions. First, scalar nuclear matrix elements are multiplied by correlation factors proportional to $1\pm(p/W)\cos\theta$. Second, vector nuclear matrix elements multiply factors of the form $1\pm\frac{1}{3}(p/W)\cos\theta$. Furthermore, for $Z\gg Z_c$ the electron energy independent V^2 terms are dominant, and, therefore, some first forbidden β-emitters may have allowed-looking energy spectra. If $Z\gg Z_c$, then, clearly, from C_{0X} and C_{1X} it is possible for any one of the five types of coupling to give allowed-looking spectra and either a forward or a backward angular correlation. To interpret angular correlation data in this case ($Z\gg Z_c$), either the spin change must be known or the half-life must be so short that the transition can unambiguously be classified as allowed, as, for example, is the case with He^6.

Experimental evidence (i.e., unique first forbidden spectra and allowed transitions with spin change one) favors tensor or axial vector coupling. These two couplings give the Gamow-Teller selection rules. To distinguish between them, angular correlation data for a spin change ($0\leftrightarrow 1$) or ($0\leftrightarrow 0$) would be particularly valuable. These transitions should be either allowed or first forbidden, depending on the parity change. In the case of ($0\leftrightarrow 1$) transitions, axial vector coupling gives a backward angular correlation in both C_{0A} and C_{1A}, and tensor coupling gives a forward correlation in C_{0T} and C_{1T}. In the case of ($0\leftrightarrow 0$) transitions, axial vector coupling gives a forward correlation in C_{1A}, and tensor coupling gives a backward correlation in C_{1T}. Thus, it should be possible to distinguish between tensor and axial vector coupling by the general forwardness or backwardness of the correlation, provided the spin change is definitely ($0\leftrightarrow 1$) or definitely ($0\leftrightarrow 0$).

The authors take pleasure in thanking Professor L. W. Nordheim for several interesting discussions and helpful suggestions. We also would like to thank Professor V. F. Weisskopf for suggesting the use of the Gordon decomposition of the electron probability current.

Magnetic Effects and the Hartree-Fock Equation*

J. C. SLATER
Research Laboratory of Electronics, Massachusetts Institute of Technology, Cambridge, Massachusetts
(Received January 19, 1951)

The Hartree-Fock equations state that each electron in an atom or molecular system should move in a different potential. In some cases, particularly magnetic cases, this leads to important consequences, since electrons with opposite spins move in different potentials. In particular, in an antiferromagnetic substance, electrons of + and − spin have different potentials; and for an electron of + spin, for instance, the potential energy is lower in those atoms whose spins are pointed in the + direction than in those with the opposite spin. This results in a periodic perturbation of potential, with periodicity twice the atomic periodicity, and leads to a splitting of each energy band in half, with a gap in the middle. In a case where the energy band was half full, resulting in a conductor: when we disregard this effect, the resulting half-band will be just filled when we consider it; this may explain the insulating nature of some antiferromagnetics. A similar argument applied to a diatomic molecule like H_2 can result in two alternative types of solutions of the Hartree-Fock equations: one leading to atomic orbitals, the other to molecular orbitals. The solution with atomic orbitals shows an analogy to the antiferromagnetic problem; that with ordinary molecular orbitals shows an analogy to the band theory of a non-magnetic conductor.

THE Hartree-Fock equations, as has been recently pointed out by the writer,[1] can be interpreted as ordinary Schrödinger equations for the one-electron wave functions or orbitals $u_i(x)$ out of which we can set up a determinantal wave function for an atom or molecular system. Each electron moves in a potential which is made up of the electrostatic fields of the nuclei and of all electrons, including itself, but with a correction because of the fact that the electron really does not act on itself. This correction takes the form of subtracting from the total charge density of all electrons an exchange charge density, representing a density whose total magnitude is one negative electronic charge concentrated, in general, about the electron in question. This exchange charge density, for the electron whose wave function is $u_i(x)$, takes the form

$$-e\sum_{k=1}^{n}\frac{u_i^*(x_1)u_k^*(x_2)u_k(x_1)u_i(x_2)}{u_i^*(x_1)u_i(x_1)}. \qquad (1)$$

This charge density is located at point x_2, and an integration must be carried out over this variable to find the corresponding potential at the point x_1, where we are finding $u_i(x)$. In the reference just quoted, it was pointed out that often the exchange charge density does not depend in a very striking manner on the index i; that is, almost the same potential can be used for the various wave functions. In such a case it was pointed out that it may be an advantageous simplification to replace (1) by a weighted mean over the various wave functions, securing, in this way, a single potential to use for all wave functions of the problem.

It is the purpose of the present note, on the other hand, to point out certain cases in which there is a very real advantage in using the different potentials for different wave functions indicated by (1). These cases seem to come up particularly when we are dealing with magnetic problems. The wave functions u_i concerned in (1) are assumed to be functions of spin as well as coordinates; they are products of an ordinary coordinate wave function and the Pauli functions α or β of the spin coordinate. Thus, automatically, the product $u_i^*(x_1)u_k(x_1)$ is zero, unless functions i and k correspond to the same spin, so that the sum (1) really includes only terms coming from wave functions u_k whose spin quantum number is the same as that of u_i. Thus, it comes about that when there are not equal numbers of wave functions with + and − spins in a problem, the potential in which these two types of electrons move will be different. The difference is easily interpreted in a qualitative way from the results of the reference already quoted. There it was shown that the effect of the exchange potential is to depress the potential energy of the electron by an amount which depends on the local charge density of electrons: the greater this charge density, the lower the potential energy. Thus, if, for instance, there are more electrons of + than of − spin, the Hartree-Fock potential for an electron of + spin will be lower than that for an electron of − spin.

These differences in the potentials for electrons of the two spins will, of course, result in differences in the one-electron energies resulting from the solution of Schrödinger's equation and hence in energy terms in computing the diagonal energy of the state. These effects are familiar when we handle the exchange effect by perturbation methods. In finding the total energy, we must multiply (1) by $u_i^*(x_1)u_i(x_1)$ and integrate the resulting expression, multiplied by a potential energy function involving the coulomb expression $1/r_{12}$, over the coordinates of electrons 1 and 2. When we do this, we recognize the familiar exchange integrals coming from the perturbation treatment of multiplet theory, and the dependence on spin is the equivalent of the statement that exchange integrals occur only between pairs of electrons with the same spin. Thus, to the

* This work was supported in part by the Signal Corps, the Air Materiel Command, and ONR.
[1] J. C. Slater, Phys. Rev. **81**, 385 (1951).

extent that first-order perturbation theory is adequate, it makes no qualitative difference whether we use the Hartree-Fock exchange charge (1) in computing the exchange potential or merely use the Hartree equations without exchange. This freedom of choice is merely a statement of the theorem that the diagonal energy of a wave function is a correct energy up to second orders of small quantities; first-order modifications of the wave function, such as would come about if we used the Hartree instead of the Hartree-Fock equations, make only second-order errors in the energy. In many cases, of which the application to atomic multiplets is one, the situation is as just described, and the greatly added complication of using the Hartree-Fock rather than the Hartree method is not really justified by its results.

There are some cases, however, of which antiferromagnetism and covalent binding are two examples, in which a qualitative, and not merely a small quantitative, difference is found, depending on whether we use the Hartree-Fock method, with its different potentials for electrons of opposite spin, or not. The reason for this rather profound effect is that the magnetic modification of the potential in the Hartree-Fock case results in modification of the energy levels or energy bands of a type which would have to be described by second-order or higher order perturbation theory, and which would be missed entirely if we proceeded only by first-order perturbation theory, as in the usual theory of multiplet structure. The most striking example is in antiferromagnetism. We shall elaborate on this case in a moment; but, for the moment, let us consider a one-dimensional array of like atoms, each with the same number of electrons, but with the spins of the outer electrons pointing in the + direction in one atom, − in the next, and alternating in this way. Then the Hartree-Fock potential will have different values in alternate atoms, so that the period of the periodic potential will be two atoms for the Hartree-Fock potential, though it is only one atom for the ordinary Hartree potential. If we ask how the energy bands as calculated from the Hartree potential would be modified in going to the Hartree-Fock potential, we take advantage of our knowledge of the effect on energy bands of a perturbative potential with a period twice the lattice spacing: we know that the bands develop gaps in the middle, each band splitting into two, the half-bands holding half as many electrons per atom as the whole bands. If, then, we were dealing with the case where there were half enough electrons per atom to fill the complete band, the Hartree treatment would indicate a half-filled energy band, leading to a conductor, while the Hartree-Fock treatment would show the half-band to be filled, with an energy gap above, so that it would predict that the material would be an insulator. It is attractive to suppose that the fact that such antiferromagnetics as NiO and MnO are insulators rather than conductors may arise from such an explanation as this, though they are far from being as simple as the one-dimensional case just described.[2]

It is easy to verify that the effect of going from the Hartree to the Hartree-Fock method in the example above arises from a higher order perturbation effect, if it is treated by perturbation methods. For we recall that when the effect of a periodic perturbing potential on energy bands is investigated, we find that this potential introduces interactions like those between an incident wave and a Bragg reflected wave. These interactions are a maximum when the incident and reflected wave have identical unperturbed energies (this corresponds to the position of the energy gap). This problem must be treated like a perturbation of a degenerate system; not even a second-order perturbation treatment is adequate. First-order perturbation methods, then, are completely inadequate to investigate such energy gaps, which neverthless can have a great practical significance.

Let us look a little closer at this one-dimensional antiferromagnetic problem to analyze its nature more closely. For an electron of + spin, the Hartree-Fock potential energy will be lower in those atoms which are known to have a net + spin than in those of net − spin. Each energy band will be split, as we have just mentioned, into two half-bands; but more than that, the wave function in the lower half-band will be concentrated largely in those atoms with + spin, while the wave function in the upper half-band will be concentrated in those atoms with − spin. The physical reason for the energy gap between the two half-bands is just the difference in average potential energy arising from this different charge distribution. If now we have only the lower half-band filled, the electrons will go largely into those atoms which were assumed from the beginning to have + spin, thus verifying the self-consistent nature of the assumption about potentials. Similarly, the potential energy function for an electron of − spin will be lower in the atoms with − spin. The energy bands for such an electron will be identical with those for an electron of + spin; but the wave functions in the lower half-band, which are occupied with electrons, will correspond to having the charge concentrated largely in the atoms with − spin.

In the model which we have been discussing, the effect of the alternation of the Hartree-Fock potential from atoms with one spin to those with the other is to set up wave functions which are concentrated on atoms of one spin or the other. Thus, if the lower half-band is filled and the upper one is empty, the effect is the segregation of electrons of opposite spin, one from the other, so that they will not have random fluctuations of charge and will not lead to probabilities of ionic states. On the contrary, if we used the Hartree potential with a band half-filled with electrons, it is known that we have such fluctuations. The alternation of the Hartree-

[2] The difficulty of understanding the insulating nature of NiO has been pointed out by Mott, Proc. Phys. Soc. (London) **62**, 416 (1949) as a difficulty with the energy band theory.

Fock potential then has somewhat the same effect on the charge density that we get from the well-known Heitler-London method, as applied to the hydrogen molecule. To the extent that there is such a similarity, we agree with the remark of Mott[2] that in an insulator like NiO, we must use something more like a Heitler-London than an energy band picture. We may, in fact, examine the H_2 molecule from the point of view we have been describing for an antiferromagnetic and thus throw light on the relation of the Heitler-London method to the Hartree-Fock method. We shall see that they have similarities but are by no means identical.

Suppose we have two hydrogen atoms at a considerable distance from each other, and that we try to find a self-consistent solution by the Hartree-Fock method for the ground state, with one electron with each spin. We may first make the usual assumptions leading to symmetric or antisymmetric molecular orbitals. We assume that the wave function corresponding to the electron of each spin is either symmetric or antisymmetric in the midpoint of the nuclei, so that its charge density is symmetric. Then the exchange charge (1) will be symmetric, so that the Hartree-Fock potential for an electron of either spin is symmetric in the nuclei, and by the well-known solution of the two-potential problem the wave functions will be either symmetric or antisymmetric. Thus we have a self-consistent solution. On the other hand, suppose we start by assuming that the wave function corresponding to one spin will be concentrated on one nucleus and that of the other spin on the second nucleus, as in the antiferromagnetic problem. If the atoms are far enough apart so that the wave functions do not appreciably overlap, examination of the expression (1) then shows that the potential for an electron of + spin will be that of the two nuclei plus that of the electron of − spin; that is, this potential will be that of the free nucleus of the atom with + spin plus a neutral atom for that with − spin. Near the atom with + spin, the other neutral atom will exert no field, so that the Schrödinger equation will be just like that of a hydrogen atom, leading to an ordinary hydrogen wave function concentrated about that atom. Similarly, the Schrödinger equation for an electron of − spin will be that of a hydrogen atom at the other nucleus.

We see, in other words, that the solution of the Hartree-Fock equations is not unique in such a case, as has been surmised, for instance, by Seitz.[3] One can, in fact, assume that the solution of the Hartree-Fock equation for H_2 can be approximated as a linear combination of the atomic functions a and b located on the two atoms; that is, one can assume that the function corresponding to the + spin is $c_{11}a+c_{12}b$, and that corresponding to the − spin is $c_{21}a+c_{22}b$. One then forms the energy integral, expressing it in terms of the c's, and varies the c's to make the energy stationary, subject to the condition that the wave functions remain normalized (which can be handled by the method of undetermined multipliers).[3a] When we do this, we find that the equations have two types of solutions. In all cases the symmetric or antisymmetric orbitals, corresponding to $c_{12}=\pm c_{11}$, $c_{22}=\pm c_{21}$, form a solution, but there are other solutions as well, which, at infinite separation, go to the limiting case $c_{11}=1$, $c_{12}=0$, $c_{21}=0$, $c_{22}=1$, or corresponding cases with the nuclei interchanged, but which depart more and more from these limits as the internuclear distance is decreased. This demonstrates in a simple case the existence of the two types of solution.

These atomic solutions that we have found are analogous to those which we described earlier for the antiferromagnetic case. They are not, however, identical with the Heitler-London description of the ground state of the molecule. If we recall the argument leading to the wave function by this method, we start with a function like that which we have been describing, corresponding, say, to having an electron of + spin on atom a, an electron of − spin on atom b; but we consider also the other state, degenerate with the first, with an electron of − spin on atom a, and one of + spin on atom b. The degenerate perturbation problem between these two states leads to two solutions: one the sum of these wave functions, the other the difference. One of these corresponds to the ground state, the other to the component of the triplet which has no spin along the axis with respect to which we are measuring spin. As we know from the Heitler-London method, these two states, the ground state and the triplet, lie far apart; and the two degenerate states which lead to them, and which lie roughly half-way between them, have energies approximately given by the Heitler-London coulomb energy, without the Heitler-London exchange energy. We know, however, that the exchange term is responsible for the major part of the binding in the ground state. Thus, the atomic type of wave function which we found in the preceding paragraph is not like the Heitler-London function for the ground state. We could not have expected that it would be. The perturbation problem of spin degeneracy is an essential part of the Heitler-London method, and the Hartree-Fock scheme, in which we definitely assign a spin to each wave function, cannot incorporate such an effect in a single wave function. If we wish to get the equivalent of the Heitler-London theory of valence for a complicated molecule, we must carry through the same treatment of spin degeneracy as in the conventional Heitler-London method, even though we start with wave functions derived from the Hartree-Fock method.

It is interesting to see in this way that the Hartree-Fock method can form the first step of a Heitler-London calculation. This is not, however, of any particular value in the solution of molecular problems. The great

[3] F. Seitz, *The Modern Theory of Solids* (McGraw-Hill Book Company, Inc., New York, 1940), p. 251.

[3a] The attention of the writer has been called by Prof. H. M. James to the fact that a similar (but not identical) calculation has been made by C. A. Coulson and I. Fischer, Phil. Mag. **40**, 386 (1949).

technical difficulty in the application of the Heitler-London method for complicated molecules is the non-orthogonality of the wave functions. It is true that the wave functions derived by the Hartree-Fock method can be proved to be orthogonal to each other, and this might seem to remove the difficulty. It does not, however; for the orthogonality of two Hartree-Fock functions corresponding to electrons of opposite spin arises from the spin part of the wave function, not from the orbital part. In the H_2 problem, for instance, the two atomic orbitals around atoms a and b are non-orthogonal, even if they are derived strictly by application of the Hartree-Fock method. Two Hartree-Fock atomic orbitals corresponding to electrons of the same spin, however, are necessarily orthogonal, and it is possible that this would make the Heitler-London method simple enough to make its use worthwhile.

It is interesting to consider the diagonal energy of the H_2 molecule according to the two types of Hartree-Fock approximations. At great distances, the atomic type of approximation will have a diagonal energy reducing properly to the sum of the energies of two neutral atoms; thus, it will lie below that of the molecular-orbital solution, which has an energy which is the average of the energy of two neutral atoms and the energy of a polar state consisting of a positive and a negative ion. As the distance decreases, however, this situation is reversed. The molecular-orbital solution approximates very closely the Heitler-London solution for the ground state at the actual internuclear distance in the molecule. On the other hand, as we have seen, the Hartree-Fock atomic approximation has an energy more like the coulomb Heitler-London energy, which does not lie nearly so low. Thus, we conclude that if we wish to use a single Hartree-Fock function, without further perturbation calculations, the atomic function is good at large values of internuclear distance, the molecular function at small values, and neither is very good in between.

We may now return to our antiferromagnetic case and ask whether it is as far from the truth as the atomic Hartree-Fock solution for H_2. The answer will come by considering the spin degeneracy problem in the antiferromagnetic case. Here it is not immediately obvious what other arrangements of spin we are to consider, analogous to the simple interchange of spins between the two atoms in the Heitler-London model of H_2. If we interchange all spins in a one-dimensional chain of alternating spins, we should find the nondiagonal matrix component of energy between the two states equal to zero to a very high order of approximation, on account of the very large number of electrons which would interchange spins in going from one function to the other. The only sort of function which would have an appreciable nondiagonal matrix component of energy from the state of alternating spins we start with would be one in which only a few spins are changed; for instance, we could modify the regular alternation $+-+-+-$ by interchange of two adjacent spins, obtaining $+--++-$, for instance.[4] To set up such a function, we might start with the regular Hartree-Fock problem of the alternating spins and treat the effect of the modified potential resulting from the interchanged spins as a local modification of the regular periodic potential. If we set up approximate solutions of this modified potential by superposing solutions of the periodic potential problem, we should presumably find that we had to use wave functions from the upper half-band in making up such a solution, and would certainly find that the diagonal energy of the modified state was different from that of the unmodified state. In fact, if the antiferromagnetic arrangement of alternating spins had a lower energy than the ferromagnetic arrangement where all spins are the same, this modified state would have a higher diagonal energy than the unmodified one.

In the antiferromagnetic problem, then, an interchange of spins changes the diagonal energy of a state, in contrast to the case of the H_2 molecule. As a result, the nondiagonal matrix component of energy will have a much less perturbing effect than in the molecule. Such a situation was found in reference 4, where the effect of spin degeneracy was found to be much less important in a crystal lattice than in a molecule. Hence, we may conclude that we commit a much smaller error in the antiferromagnetic case than in the molecule if we merely use the diagonal energy of a state with alternating spins as representing the real energy of the system.

There are many questions concerning antiferromagnetics, ferromagnetics, and related problems, which the present note does not answer. The most important one, which we have not even tried to answer, is that of which state has lower energy in a given crystal: the antiferromagnetic state, corresponding to alternating spins, and the half-band structure we have been describing; the random state, in which every atom on the average has as many $+$ as $-$ spins, so that we have the ordinary molecular orbital or energy band functions, with the possibility of charge fluctuations on the atoms; or the ferromagnetic state, which we have hardly mentioned, in which all atoms have spins of the same sign, so that the effect of the exchange terms in the Hartree-Fock equation is mainly to depress the potential energy, and energy levels, of those electrons with the same spin as the spin of the atoms, and to raise the energy of those with opposite spins. Rather than waiting until all these questions can be solved, however, it seems worthwhile to point out, in the present note, the close relation of the Hartree-Fock equations to these problems, and, in particular, to the problem of antiferromagnetism. That problem is one which ought to be amenable to the methods of energy bands, even though the attempts to treat it have, so far, been by modified Heitler-London methods.

[4] This problem has been treated by the Heitler-London method by J. C. Slater, Phys. Rev. 35, 509 (1930); H. Bethe, Z. Physik 71, 205 (1931); and other writers.

A Precise Mechanical Measurement of the Gyromagnetic Ratio of Iron

G. G. Scott
Research Laboratories Division, General Motors Corporation, Detroit, Michigan
(Received December 4, 1950)

In this experiment the gyromagnetic ratio of a sample of very pure iron was determined. The sample was wound with a magnetizing coil and supported as a torsional pendulum in an evacuated space almost completely free of residual magnetic fields. Changes in pendulum amplitude were brought about by repeated and synchronized reversals of the magnetizing current. These changes were measured along with corresponding changes in magnetic moment of the sample. The average value obtained for the gyromagnetic ratio was 1.0278 ± 0.0014 times the mass-to-charge ratio of the electron.

I. INTRODUCTION

IN 1908, it was predicted, by Richardson,[1] that the magnetization of an object should produce an angular momentum about its magnetic axis. He showed that the ratio of this angular momentum to the corresponding magnetic moment should be $2m/e$ for orbital electron motion.

This gyromagnetic ratio has been determined mechanically by several investigators,[2] and, in the case of iron, is known to be very nearly ½ the amount predicted by Richardson. This is now satisfactorily explained by considering the major part of the magnetic moment of the ultimate magnetic particle to be caused by a spinning electron.

Barnett[3] gives, in his most recent publications, a value of 1.031 m/e for the gyromagnetic ratio of iron. Most other investigators have obtained values lower than this but still definitely greater than m/e.

Recently, it has become possible to obtain a measure of the gyromagnetic ratio by means of microwave resonance absorption techniques. By this method, most investigations have resulted in values considerably less than m/e. Kittel[4] has attempted to explain this discrepancy between the values obtained by microwave techniques and those obtained mechanically.

Because of this discrepancy, and because of the wide variation of results obtained by the various investigators who have determined the gyromagnetic ratio mechanically, it was felt that a precise determination by a very direct mechanical method would be of interest.

Since apparatus was available at the General Motors Research Laboratories, which was ideally suited for making mechanical measurements of this type, it was decided to utilize it for obtaining a precise determination of the gyromagnetic ratio of iron.

A cylinder of high purity iron was obtained. This cylinder was wound with a uniform magnetizing coil and supported as a torsional pendulum rotating about its magnetic axis with a long period and a very low damping coefficient.

II. EXPERIMENTAL FACTORS INVOLVED

If the angular momentum of an undamped torsional pendulum is changed by an amount Δz as the pendulum is crossing the center of its swing, the change in amplitude will be $\Delta\theta=\Delta zP/(2\pi I)$, where P is the period of the pendulum and I its moment of inertia. $\Delta\theta$, which is the change in amplitude in radians, was observed in these experiments by measuring the change in double amplitude d on a scale at a distance X from the rotating element mirror. Therefore, $\Delta\theta=d/(4X)$, and $\Delta z=\pi Id/(2PX)$. This equation assumes that the angular momentum impulse is applied exactly as the pendulum is crossing the center of its swing, or at a zero phase angle. If a slight error, either positive or negative, in phase angle is made, the measured value of d will be too small. In this case, the value d in the above equation would be replaced by d/k, where k is the cosine of the phase angle error.

In these experiments the current in the element is reversed periodically, and the resulting changes in angular momentum and magnetic moment are measured. Also, a large number of readings are taken throughout a small range in values of the magnetizing current. For this condition a linear relationship exists between the element current i_e and the magnetic moment, so that $M=ai_e+b$. The change in magnetic moment when the current is reversed is $\Delta M=2(ai_e+b)$.

These values of Δz and ΔM are the measured values of the total changes in angular momentum and magnetic moment. It is necessary to subtract from these the changes in angular momentum and magnetic moment developed by the change in flow of electrons in the magnetizing winding in order to obtain the values for the iron alone.

If the summation of the areas of all the turns in the element winding is ΣA_e, and if the current is changed through this winding by an amount Δi_e, then the change in magnetic moment of the winding is $\Delta i_e\Sigma A_e$, and the corresponding change in angular momentum is $(2m/e)\Delta i_e\Sigma A_e$.

[1] O. W. Richardson, Phys. Rev. **66**, 248 (1908).
[2] A. P. Chattock and L. F. Bates, Trans. Roy. Soc. (London) **22**, 257 (1923); W. Sucksmith and L. F. Bates, Proc. Roy. Soc. (London) **104**, 499 (1923); L. F. Bates, Nature **134**, 50 (1934); F. Coeterier, Helv. Phys. Acta **8**, 522 (1935); A. J. P. Meyer, Compt. rend. **228**, 1934 (1949).
[3] S. J. Barnett, Proc. Amer. Acad. Arts Sci. **73**, 401 (1940); S. J. Barnett, Phys. Rev. **66**, 224 (1944).
[4] C. Kittel, Phys. Rev. **76**, 743 (1949).

Therefore, for the iron alone,

$$\Delta z = \pi Id/(2PXk) - (2m/e)\Delta i_e \Sigma A_e,$$

and

$$\Delta M = 2(ai_e + b) - \Delta i_e \Sigma A_e.$$

The ratio between these two quantities is the gyromagnetic ratio of the iron.

Since the element current is always reversed, $\Delta i_e = 2i_e$. Making this substitution, and taking the ratio $\Delta z/\Delta M$,

$$G = \frac{\pi Id/(2PXk) - 4(m/e)i_e \Sigma A_e}{2(ai_e + b) - 2i_e \Sigma A_e}.$$

This is the equation which is used for determining the gyromagnetic ratio from the experimental data.

III. INSTRUMENTATION AND EXPERIMENTAL PROCEDURE

The instrumentation herein described was set up at a test station located in a region free from all artificial magnetic and mechanical disturbances.

Readings on the gyromagnetic element were taken in an evacuated instrument mounted on a pier having its foundation ten feet below the ground level. Surrounding magnetic fields were almost completely eliminated. A light beam about 52 ft in length was used for determining the changes in angular momentum. The various necessary pieces of equipment will be described separately.

(A) Field Neutralizing System

Neutralization of the earth's magnetic field was accomplished by a system of three mutually perpendicular Helmholtz coils having a common center and with axes in the NS, EW, and vertical directions.

The forms for both the NS and vertical components were accurately machined on massive aluminum structures. The NS coils were 8 ft in diameter; the vertical coils were 9 ft in diameter.

The EW system was made of rolled aluminum channel and was 4 ft in diameter. All systems had a winding cross section one inch square.

The NS coil was oriented so that its magnetic axis was horizontal and in the mean direction of the earth's horizontal component. The EW coil was set very nearly at right angles to this direction. The currents in both the NS and EW coils were controlled by a system of variometers so as to follow the naturally occurring changes in the horizontal component of the earth's field. No variometer was used on the vertical system. The proper current was determined for these coils so as to neutralize the mean value of the earth's vertical component.

(B) The NS Variometer

The variometer used to determine the proper value for the main NS Helmholtz coil current was located in a small auxiliary building 135 ft north of the primary system. This variometer included a 4 ft diameter Helmholtz coil with its axis aligned, as nearly as possible, with the direction of the earth's total field. At the center of this Helmholtz coil was located an airtight case containing a suspended feeler coil having its magnetic axis horizontal and in an east-west direction. The current in this coil was reversed by means of a manually operated switch located at the variometer control station, which was in the main building. Also located inside of this airtight case was a photoelectric multiplying system for electrically transferring information concerning the feeler coil position back to the central control point.

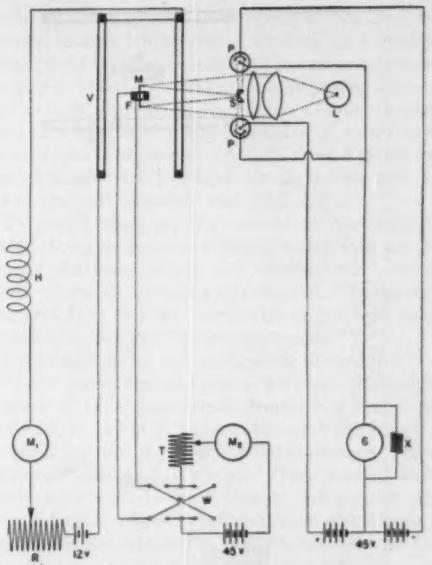

FIG. 1. North south variometer system. P, Type SR 53 vacuum photocells; S, light splitting prism; L, lamp; M, mirror carried by feeler coil; F, feeler coil; V, four-foot diameter Helmholtz coils; H, main NS Helmholtz coil; M_1, M_2, indicating ammeters; G, galvanometer to indicate feeler coil motion; X, damping resistance; R, field control rheostats; W, reversing switch.

If any horizontal north-south field were present at the center of this variometer system, a reversal of the feeler coil current would be accompanied by a corresponding motion of the feeler coil.

An operator continually checked the field value by reversing the feeler coil current and adjusting the Helmholtz current to obtain zero motion.

This variometer Helmholtz coil had its horizontal NS component matched to the main NS Helmholtz system and was then electrically connected in series with it. A diagram of the NS variometer system is shown in Fig. 1.

(C) The EW Variometer System

The variometer used to determine the proper current for the main EW Helmholtz coil was located 15 ft directly north of the primary system. It consisted of a magnetized rod of alnico, hung in a suitable container by a very fine filament. This magnetized rod carried a mirror and was oil damped.

On the outside of the case was a coil having its magnetic axis east and west. This coil was matched to the main EW Helmholtz coil and connected in series with it; a control rheostat was located at the variometer control point. By means of a high quality projector, a beam of light was directed onto the mirror which, in turn, focused a cross hair on a scale located at the variometer control center, which was 54 ft away. A zero point for the mean position of the horizontal component of the earth's field was located on this scale. When the field varied from this position, it was returned by the variometer operator, who moved a field rheostat to keep the cross hair always on zero, thus compensating

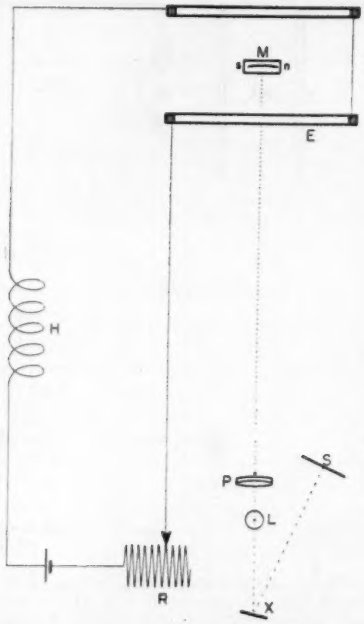

FIG. 2. East-west variometer system. ns, magnetized alnico rod; M, mirror; E, EW coil system; H, main EW Helmholtz coil; P, projecting lens; L, Western Union concentrated arc lamp; X, plane mirror; S, scale; R, field control rheostats.

for the field changes. A diagram of the EW variometer system is shown in Fig. 2.

(D) Precision of Field Neutralization

Throughout a set of gyromagnetic readings, which would usually last about 6 hours, the above variometer systems could be operated so as to prevent variations in the residual horizontal magnetic field of more than 1 gamma (1 gamma $= 10^{-5}$ oersteds). The homogeneity of the large Helmholtz coil fields was such that a field difference between center and ends of the gyromagnetic element of about $\frac{1}{2}$ gamma could be expected.

(E) The Gyromagnetic Element

The material used to measure the gyromagnetic ratio of iron consisted of an accurately ground and annealed cylinder 1.5 cm in diameter and 22 cm long.

TABLE I. Analysis of iron of gyromagnetic element. All elements present to 0.001 percent or greater shown.

Iron	99.94%
Oxygen	0.04%
Carbon	0.005%
Nitrogen	0.004%
Sulfur	0.003%
Nickel	0.0015%
Cobalt	0.001%
Phosphorous	0.001%
Silicon	0.001%
All others	0.0035%

An analysis of the sample is given in Table I. All elements present to greater than 0.001 percent are shown. The cylinder was wound carefully with a magnetizing winding consisting of 14 layers of No. 41 formex covered wire. At the lower end, a small ratchet-operated reversing switch was located so that the current through the element could be reversed with respect to that flowing in the suspension system. When the element was in position, this reversing switch could be operated by a bellows system located in the bottom of the instrument. It was found in previous work on electron inertia[5] that systematic errors could be introduced by the suspension system if a reversing switch was not used on the element. At the upper end a tube carrying the suspension and mirror systems was located. The mirror consisted of four optically flat faces so that readings on the element could be taken at four 90° azimuth positions.

Adjusting screws were provided at the necessary locations so that the element could be brought into both static and dynamic balance about its axis of rotation. This was necessary to prevent transverse disturbances from producing rotational motion. When properly adjusted, the element had an extremely small horizontal magnetic moment, in addition to having mechanical symmetry. A diagram of the element is shown in Fig. 3.

(F) Optical System

The general optical arrangement was the same as that used in a conventional galvanometer projection system. However, in this case, a much longer optical arm was used, requiring very precise optical components throughout. It was also necessary to enclose the optical path in a tunnel to prevent the disturbing effects of air currents. The distance from the element mirror to the scale was about 52 ft. The width of the cross-hair image on the scale was about $\frac{1}{4}$ mm. The scale was observed with a low power magnifying glass, and it was possible to estimate readings to 0.1 mm.

(G) Instrumentation for the Measurement of Magnetic Moment

The change in magnetic moment accompanying a given change in the gyromagnetic element current was measured concurrently with the measurements of the changes in angular momentum. This was done by means of an astatic magnetometer and standard coil system. The magnetometer was located at a point halfway between the element and the standard coil, and the circuits were so arranged that the two currents could be reversed simultaneously. The current in the standard coil was adjusted so that its field annulled the field produced by the standard coil at the magnetometer position. The magnetometer was fitted with a photo electric multiplying device similar to that used on the NS variometer. It was thus a null device of high sensitivity.

It was found that a magnetometer system such as this had certain errors which made it impossible to obtain sufficiently precise values for the changes in magnetic moment. The most important of these were,

[5] C. F. Kettering and G. G. Scott, Phys. Rev. **66**, 257 (1944).

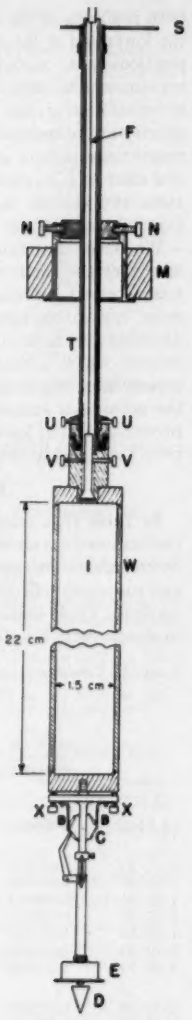

FIG. 3. Gyromagnetic element. S, return current spiral; F, supporting filament; N, mirror adjusting screws; M, four-sided, optically flat element mirror; T, tube; U, tube adjusting screws; V, suspension centering screws; I, iron sample; W, winding; X, reversing switch centering screws; B, brushes; C, commutator; E, disk which is raised by bellows arrangement to operate reversing switch; D, damping cone.

uncertainty as to the distribution of magnetic intensity throughout the iron of the gyromagnetic element, and difficulty in determining the exact midpoint position for the magnetometer.

These difficulties were overcome by using a form of torsion balance working in the very uniform fields generated by the large Helmholtz coil system. This torsional system was used to calibrate the magnetometer. The gyromagnetic element, with its axis in a horizontal EW position, was suspended on a critically damped torsional system rotating about a vertical axis. The element could be quickly replaced in this system by an air core standard accurately made for this purpose. This standard coil consisted of 28 layers of No. 34 double formex insulated wire wound on a $\frac{3}{16}$ inch diameter brass rod 22 cm long. In winding this coil, a micrometer, reading to 0.0001 inch, was used to determine the inside and outside diameter of each layer, and two counters were used to eliminate any possibility of obtaining the wrong count of the number of turns. Over 1000 micrometer readings were averaged for the entire coil. The ΣA_S value, as computed, was 28131 cm².

In taking readings, the current in the large NS Helmholtz system was so adjusted in each instance that exactly the same torque was obtained for both the standard and the gyromagnetic element. The magnetic moments then had the same ratio as the field values required to produce this common torque.

Data obtained by this method are plotted in Fig. 4. This plot shows the relationship between the magnetic moment of the gyromagnetic element and the current flowing in it. In Fig. 5, a plot of the same two variables, obtained by the approximate magnetometer system previously described is shown. These magnetometer values were found to be in error by 1.9 percent. This error is largely caused by differences in distribution of magnetic intensity between element and standard coil.

(H) Measurement of Moment of Inertia

The moment of inertia of the element was measured by a comparison of its period, on the same suspension, with the periods of two brass cylinders accurately made for the purpose. The moment of inertia of one of the cylinders was about equal to that of the element. The other was about 4 times as great. The mass of each

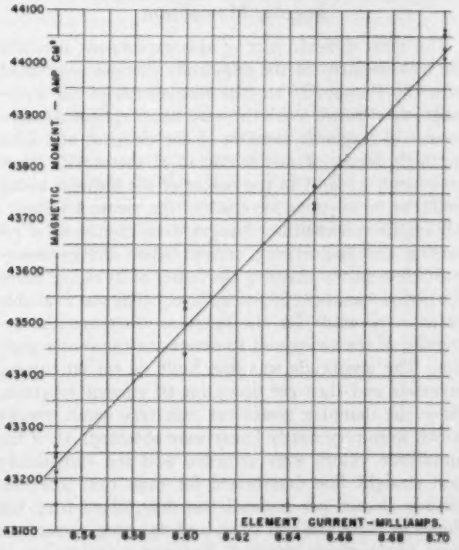

FIG. 4. Plot of element current *vs* magnetic moment—torque method. M = magnetic moment, amp cm²; $M = 5.2832 \times 10^3\, i_e - 1944.2$; i_e = element current, amp.

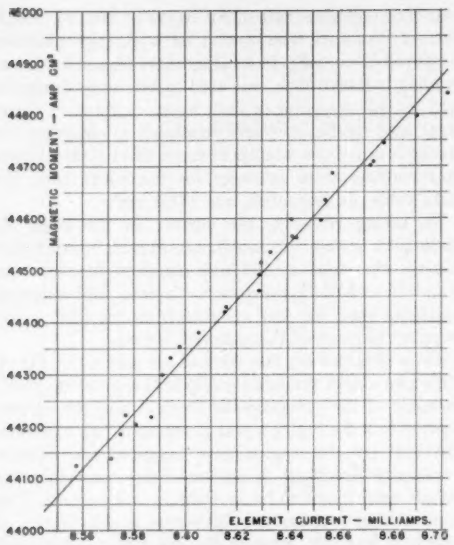

FIG. 5. Plot of element current *vs* magnetic moment magnetometer method. These values were taken concurrently with the readings to determine changes in angular momentum.

cylinder was made very nearly equal to that of the element. This was done to eliminate any possible difference in restoring force due to a difference in tension in the suspension ribbon.

(I) Measurement of the Changes in Angular Momentum

The most difficult part of this experiment involves the measurement of the amplitude changes associated with the changes in angular momentum of the gyromagnetic element. With the very small horizontal component of magnetic moment of the element, and with the high degree of neutralization of the earth's magnetic field, no shift in the center of the element swing could be noted upon reversal of the element current. All angular momentum changes were produced by reversing the magnetizing current when the gyromagnetic element was crossing the center of its swing. Since the period was about 26 sec, sufficient time was available between reversals for the operator to record the extremity of the swing and to determine the center position. The amplitude was first built up for 60 current reversals and then cut down for 60 current reversals. Since the damping coefficient was very small, results which were very nearly linear were obtained. All of the amplitude values were recorded and the statistically best straight line determined for each run. The amplitude change per reversal was determined from the slopes of these straight lines, and damping corrections were made where required. For one complete set of data, the amplitude was built up and cut down for each of two 180° azimuth positions of the element and for both positions of the small reversing switch located at the lower end of the element. These two 180° azimuth positions were varied throughout the course of the experiments to reduce further the possibility of any systematic error that might be caused by an inhomogeneity in the residual magnetic field. The value of the magnetizing current was determined immediately before and after each increase or decrease run. The average of these two current values was used to determine the magnetic moment for the run.

Whenever the azimuth position was changed, or whenever the small reversing switch was operated, it was necessary to remove lateral vibrations of the element caused by these changes. To do this, a small damping pot containing a heavy oil was located on the bellows which actuated the switch mechanism. The arrangement was such that raising the bellows brought the oil up and around a small cone located below the reversing switch; lowering the bellows left the element free. This quickly eliminated lateral vibrations.

IV. RESULTS

In Table II, a condensation of all data obtained for the various days on which readings were taken is given. Systematic errors caused by small residual fields and by any suspension effects have been eliminated from these readings. These values were used to compute the gyromagnetic ratio for the day. Table III gives the gyro-

TABLE II. Condensed data for the determination of the gyromagnetic ratio of iron.

Date	Double amplitude change per reversal-cm d[a]	Element current amperes i_e[b]	Element magnetic moment amp cm² $M_e = ai_e + b$	Period seconds P
		First set-up		
12–14–49	0.046684	0.0058472	29039	26.340
		Second set-up		
1–12–50	0.071195	0.0087514	44291	26.270
1–13–50	0.071135	0.0087006	44023	26.265
1–16–50	0.070902	0.0086935	43985	26.245
1–17–50	0.070644	0.0086931	43983	26.245
1–18–50	0.071057	0.0086996	44017	26.250
1–19–50	0.070606	0.0086878	43955	26.255
1–20–50	0.070910	0.0086835	43932	26.260
		Third set-up		
2–22–50	0.070190	0.0086245	43622	26.315
2–24–50	0.070696	0.0086706	43864	26.310
2–27–50	0.070594	0.0086681	43851	26.310
3–1–50	0.070373	0.0086219	43607	26.315
3–2–50	0.070174	0.0086068	43527	26.305
3–3–50	0.070098	0.0086286	43642	26.300
3–6–50	0.070476	0.0086436	43722	26.320

Factors common to all sets of data

Moment of inertia	$I = 195.52$ gram cm²
Scale distance	$X = 1589.5$ cm
Mass-charge ratio of electron	$m/e = 5.6844 \times 10^{-9}$ grams per coulomb
Area summation of element winding	$\Sigma A_e = 73715$ cm²
Phase angle correction factor	$k = 0.99941$

[a] Each value of d obtained from 240 separate amplitude readings.
[b] Each value of i_e obtained from 16 separate potentiometer readings.
[c] Values of M_e obtained from plot shown in Fig. 7. k determined from a separate oscilliograph study in which the cosines of approximately 350 phase angle errors were averaged.

TABLE III. Value of gyromagnetic ratio of iron computed from Table II.

Date	Gyromagnetic ratio in terms of m/e of the electrons
12-14-49	1.0235
1-12-50	1.0264
1-13-50	1.0322
1-16-50	1.0304
1-17-50	1.0266
1-18-50	1.0318
1-19-50	1.0263
1-20-50	1.0312
2-22-50	1.0257
2-24-50	1.0276
2-27-50	1.0264
3-1-50	1.0288
3-2-50	1.0281
3-3-50	1.0244
3-6-50	1.0274
Average	1.0278±0.0014 m/e

magnetic ratio for the 15 days on which readings were taken.

(A) Estimation of the Probable Accidental Error

The quantities contributing in a major manner to accidental error are listed in Table IV, along with the values of the probable errors assigned.

Repeated readings of a quantity were taken, and the probable error was computed from the variations of the individual values from the mean. The error in $d/(ai_s+b)$ was obtained by using the variations from the mean in the final results shown in Table III. In the case of ΣA_s, two standard coils, each made with equal precision, were compared, to obtain an idea of the error in this quantity.

V. EARLIER DETERMINATIONS OF GYROMAGNETIC RATIO AT THIS LABORATORY

There have been two earlier determinations of the gyromagnetic ratio of this same sample of iron made at the General Motors magnetic laboratory. These determinations were made before the 8 and 9 ft diameter Helmholtz systems were installed. The neutralizing system at this time consisted of three Helmholtz coils, about 4 ft in diameter, which were not nearly as accurately made.

TABLE IV. Probable accidental errors.

Moment of inertia	I	±0.041%
Double amplitude change per reversal per unit of magnetic moment	$d/(ai_s+b)$	±0.044%
Period	P	±0.005%
Scale distance	X	±0.016%
Area summation of standard coil	ΣA_s	±0.032%
0.138% of 1.0278=0.0014	Total	±0.138%

In these earlier measurements the magnetic moments were determined by the magnetometer system alone. However, the distance between the magnetometer and the element was twice as great, a factor which would considerably decrease errors due to differences in the distribution of magnetic intensity between element and standard coils. Also, in these earlier measurements, smaller element currents were used, and the sensitivity of the optical system was greater.

Between January 15 and February 16, 1948, readings were taken on 11 different days, using an element current of 1.61 mamp. The average value for the gyromagnetic ratio for this set of data was 1.031 m/e. Also, between November 16 and November 24, 1948, readings were taken on 7 different days, using an element current of 2.00 mamp. This set of data produced a gyromagnetic ratio of 1.028 m/e.

VI. CONCLUSIONS

The final value obtained for the gyromagnetic ratio of iron is 1.0278±0.0014 times the reciprocal of the specific electronic charge. This value is in good agreement with the value given by Barnett for this ratio for iron.

The author wishes to express his appreciation to Dr. E. J. Martin and other members of the General Motors Research Staff who cooperated in this experiment. Also to Dr. S. R. Williams of Amherst College who has recently been a research consultant at this laboratory. Thanks are also due Dr. G. M. Rassweiler for help in preparation of the manuscript. Special thanks are due Dr. C. F. Kettering whose many valuable suggestions and continued interest made this work possible.

Letters to the Editor

PUBLICATION of brief reports of important discoveries in physics may be secured by addressing them to this department. The closing date for this department is five weeks prior to the date of issue. No proof will be sent to the authors. The Board of Editors does not hold itself responsible for the opinions expressed by the correspondents. Communications should not exceed 600 words in length.

Radioactivity of Nickel

H. W. WILSON
Department of Natural Philosophy, The University, Glasgow, Scotland
(Received April 5, 1951)

IN a recent letter[1] a search for low energy gamma-rays of radioactive nickel by the proportional counter technique, which resulted in the discovery of an x-ray line ascribed to the K x-radiation of cobalt arising from K-capture in Ni^{59}, was described. In view of the results of Thomas and Kurbatov,[2] who reported photon groups of energies 7.5±1, 15±2, 38±3, and 80±5 kev with intensities in the ratios 6:1:1:1 in long-lived nickel, a further search for gamma-rays using a stronger source was carried out. The source was irradiated in a higher slow neutron flux at Harwell, England, the ratio of the intensities of the present and former sources being 21:1. The counter and gas filling were the same as previously described, and the same thorough chemical purification of the source was carried out.[1,3] The results are shown in Fig. 1.

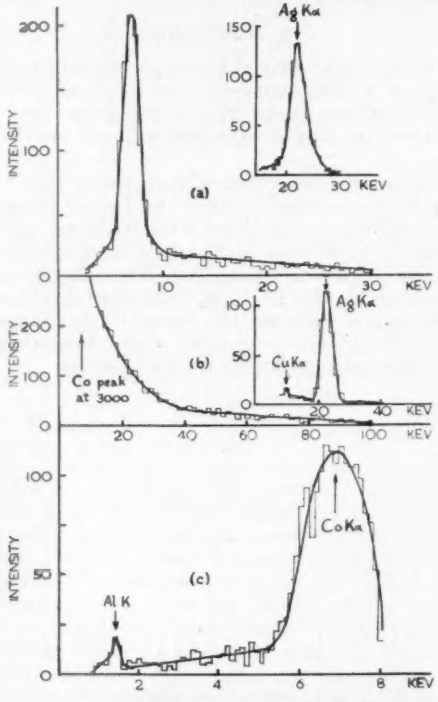

FIG. 1. Histograms of radiations of long-life nickel.

Graph (a), covers the region 0–30 kev; graph (b), 0–100 kev; graph (c), under 8 kev. The K x-radiation of silver was used for calibration (see inset figures in graphs (a) and (b)). The only radiation detected, apart from that due to K-capture in nickel (cobalt K x-rays) was taken to be the K x-rays of aluminium due to excitation of the aluminium cathode in the counter by cobalt x-rays (see graph (c)). Allowing for the efficiency of the counter, the 15- and 38-kev x-rays could have been detected if their intensities were more than one-twentieth and one-tenth of the intensity of the cobalt x-radiation, respectively. The 80-kev radiation would have been detected only if its intensity was of the same order as that of the cobalt x-rays.

The results seem to confirm that Ni^{59} decays by a simple K-capture process, and imply that the gamma-rays detected by Thomas and Kurbatov arise from the decay of some element other than nickel.

The half-lives of Ni^{59} and Ni^{63} have been recalculated using more recent slow neutron cross-section values of Ni^{59} and Ni^{63},[4] i.e., 4.17 and 14.8 barns, respectively. The new values, which are based on the activities produced by a known slow neutron flux density in a given time, are as follows,

Ni^{59}: 7.5×10^5 yr,
Ni^{63}: 61 yr.

These values are in reasonable agreement with the value of 2.3×10^5 yr given by Friedlander for Ni^{59} [5] and 85 yr given by Brosi and Griess for Ni^{63}.[6]

It is a pleasure to thank Dr. S. C. Curran for his continued interest in this work. Also, I should like to thank Mr. J. S. Story, of A.E.R.E., Harwell, for helpful comments on this work.

[1] H. W. Wilson, Phys. Rev. **79**, 1032 (1950).
[2] D. G. Thomas and J. D. Kurbatov, Phys. Rev. **77**, 151 (1950).
[3] H. W. Wilson and S. C. Curran, Phil. Mag. **40**, 631 (1949).
[4] H. Pomerance, Atomic Energy Commission Declassified Document No. 2502 (1949) (unpublished).
[5] G. Friedlander, BNL-AS-2, 49 (unpublished).
[6] A. R. Brosi and J. C. Griess, ORNL-499 (unpublished).

Restriction of Possible Interactions in Quantum Electrodynamics*

A. PETERMANN AND E. C. G. STUECKELBERG
Lausanne and Geneva, Switzerland
(Received March 27, 1951)

IT can be shown that the integral method of collision theory[1] permits the development of a unitary and causal S-matrix in terms of one or more scalar and hermitian local interaction densities of the type

$$h(x)=\Omega(\partial^{u\dagger},\ \partial^{u},\ \cdots A^{\alpha},\ \cdots)_{AB\ldots\alpha\ldots}(u^{\dagger A}u^{B}\cdots A^{\alpha}\cdots)^{*}(x). \quad (1)$$

Such a density may involve an arbitrary product of quantized fields $u^{\dagger}$, u, $\cdots A^{\alpha}$ and an arbitrary coupling operator Ω containing derivation operators $\partial^{u\dagger}$ operating upon the different factors. (The symbol * implies that the creation operators operate after the annihilation operators.) To make our problem specific, let u be the field of charged particles and A^{α} the electromagnetic potential.

To a given term in the development of S, there corresponds a Feynman graph.[2] The derivation operators at a given point x operate upon the free field factors $u^{A}(x)$ and upon the causal functions $\Delta^{(c)AB}(x-y)$, $D^{(c)\alpha\beta}(x-y)$, $\cdots$ corresponding to the external lines and internal lines ending at x. The anti-hermitian parts in each approximation involve a certain number of arbitrary constants. Their contribution to a conservative process can be shown to be equivalent to the introduction of new local interaction densities of the type (1). Therefore, an arbitrary choice of interaction densities (1) will in general introduce an infinite number of such interactions and will thus introduce, for instance, infinite series of derivatives which correspond to nonlocal interactions contradicting causality.

This contradiction can be avoided in the following way. In the

Dyson[3] terminology, to a given order term there corresponds a complicated graph. This can be reduced to a simpler graph by formally substituting into the latter "effective" causal functions and "effective" coupling operators for the true functions and operators. Only if the degree of linearity in momentum space of these effective quantities is (aside from a logarithmic term) of no higher order than the degree of the true quantities will this complicated graph not introduce additional interaction densities. The arbitrary constants reduce, therefore, to a renormalization of the (arbitrary) constants (coupling parameters) of a finite number of interaction densities.

A sufficient condition for this reduction is the following inequality between the degrees of linearity c, $-s$, $-i$, in momentum space of $\Omega(p, \cdots)\to p^c$, $\Delta^{(c)AB}(p)\to p^{-s}$, $D^{(c)\alpha\beta}(p)\to p^{-i}$, and the multilinearities m of the charged field u and $u^\dagger$, and k of A^α in (1):

$$0\leqslant c\leqslant m(s-4)+\tfrac{1}{2}k(i-4)+4. \qquad (2)$$

This condition (2) is also necessary because we can show that if the highest powers of the contributions from two or more different graphs compensate each other, the total contribution is zero identically. This particular property of the graphs has the consequence that the contributions arising from the terms $\sim\mu^{-2}$ in $D^{(c)\alpha\beta}$ for photons of non-zero rest mass μ compensate each other.[4] Therefore, we can put $i=2$ (instead of $i=0$).

If we apply this condition to charged particles of spin 0, $\frac{1}{2}$, 1, we see at once that the method used cannot be applied to the interaction of vector mesons ($s=0$) with the photon field.[5] For Dirac electrons ($s=1$), only the coupling of zero order is possible (charge-potential interaction). The interaction between magnetic moment and field (Pauli term) cannot be introduced. For scalar mesons ($s=2$), the coupling of order one allows the charge-potential interaction. Furthermore, the quadrilinear couplings $u^\dagger u A^\alpha A_\alpha$ (necessary for gauge invariance) and $u^\dagger u^\dagger u u$ (found by Rohrlich[6]) have to be introduced. In every case, the bilinear mass renormalization interactions are necessary and the non-gauge-invariant quadrilinear term $(A^\alpha A_\alpha)^2$ is also[7] compatible with (2). However, no other interactions can be introduced.

* Assisted by the Swiss Atomic Energy Commission.

[1] E. C. G. Stueckelberg and D. Rivier, Helv. Phys. Acta **23**, 216 (1950); **23**, Supp. 3, 236 (1950).
[2] R. P. Feynman, Phys. Rev. **76**, 749, 769 (1949).
[3] F. J. Dyson, Phys. Rev. **75**, 486, 1736 (1949).
[4] E. C. G. Stueckelberg and T. A. Green, Helv. Phys. Acta **24**, No. 2 (1951).
[5] T. Kinoshita and Y. Nambu, Prog. Theor. Phys. **5**, 473, 749 (1950).
[6] F. Rohrlich, Phys. Rev. **80**, 666 (1950).
[7] P. T. Matthews, Phil. Mag. **41**, 185 (1950).

Maximum Rate of Wave Function Amplitude Change

ROLF LANDAUER
Lewis Laboratory, NACA, Cleveland, Ohio
(Received March 28, 1951)

THE WKB approximation supplies us with an estimate of how fast the amplitude of wave functions can change. Near a turning point, where $E=V$, the WKB approximation changes amplitude with distance at a far greater rate than the actual wave function does. Far away from turning points, it is, however, possible for the actual wave function to change its amplitude at a greater rate than the WKB approximation does. An example is an electron suffering a Bragg reflection in a one-dimensional crystal. The wave function for such an electron has an envelope which decreases exponentially into the crystal. The WKB approximation would predict an amplitude which is the same in each cell of the crystal. The purpose of this note is to give an upper bound to the rate at which the wave function envelope can change its amplitude.

The author has recently given an expansion[1] for the wave function in terms of successive reflections. An upper bound for the wave function can be obtained by summing the absolute values of all the wavelets which contribute to the wave function and ignoring their phase differences. Let the correct wave function, $\psi(x)$, have a vanishing derivative at $x=a$. Then our summation gives us a factor $\sigma(x)$ such that

$$|\psi(x)|\leq\sigma(x)\,|\psi(a)|.$$

The factor $\sigma(x)$ has the value unity at $x=a$. As we move away from $x=a$, we will go through two types of regions: those in which $E-V$ is increasing as we move away from $x=a$, and those in which it is decreasing. In the regions in which $E-V$ increases, $\sigma(x)$ remains constant. In the regions in which $E-V$ decreases $\sigma(x)$ varies as $1/(E-V)^{\frac{1}{2}}$. In going from one type of region to the other, $\sigma(x)$ is continuous. These statements, which completely determine $\sigma(x)$, apply only to regions throughout which $E-V$ remains positive.

If, instead of taking a point at which the derivative vanishes, we are given the value of the wave function and its derivative, a maximum can also be found. A more complicated expression results in this case.

In the particular case of the periodic potential, consisting of a series of simple troughs where $(E-V)^{\frac{1}{2}}$ has the maximum value p_a and the minimum value p_b, the wave function increases at most by a factor p_a/p_b, in going from cell to cell.

[1] R. Landauer, Phys. Rev. **82**, 80 (1951).

Influence of the Atomic Shell on Nuclear Angular Correlation

HANS FRAUENFELDER
Swiss Federal Institute of Technology, Zurich, Switzerland
(Received April 5, 1951)

THE influence of the atomic shell on the angular correlation of successive nuclear radiation has been discussed by several authors.[1-4]

In general, one would expect a reduction of the angular correlation when the energy of interaction between the nucleus and the electron shell (hfs splitting) is greater than that between the nucleus and the radiation field. In most cases, then, a reduction of correlation by the magnetic field of the shell would be expected in those transitions in which the lifetime of the intermediate nuclear state is of the order of 10^{-11} sec or larger.

There exist, however, a number of isotopes (Table I) which have rather large half-lives of the intermediate level (10^{-10} or longer) and which nevertheless exhibit a strong angular correlation.

In each case of Table I, the magnetic moment of the atom in its ground state is zero. The same is true for the normally occurring doubly ionized ions (e.g., Cd^{++}). Thus, there is no magnetic interaction between shell and nucleus, and therefore no perturbation of the angular correlation occurs.

A strong perturbation can be expected, however, if the decaying

TABLE I. Angular correlation and atomic shell.

Isotope	Cd^{111}	Hg^{197}	Pb^{204}	Mg^{24}	Sr^{88}	Pd^{104}	Ba^{134}
Cascade	$\gamma-\gamma$	$\delta^--\delta^-$	$\gamma-\gamma$	$\gamma-\gamma$	$\gamma-\gamma$	$\gamma-\gamma$	$\gamma-\gamma$
Lifetime of the intermediate state in sec.	8×10^{-8}	7×10^{-9}	3×10^{-7}	—	—	—	—
Anisotropy $[K(180°)/K(90°)]-1$	−0.06	+0.24	+0.22	+0.17	−0.06	+0.50	+0.12
Ground state of the atom	$^1S_0$	$^1S_0$	$^3P_0$	$^1S_0$	$^1S_0$	$^1S_0$	$^1S_0$
Magnetic moment in Bohr magnetons	0	0	0	0	0	0	0
References	a, b	a	d	a	a	a	a

[a] F. Boehm and M. Walter, Helv. Phys. Acta **22**, 378 (1949).
[b] Reference 4. [c] Reference 7. [d] Reference 3. [e] Reference 2.

atom is, for a time comparable with the lifetime of the intermediate nuclear level, in a state with an appreciable magnetic moment. This occurs for the elements of Table I, if the atom is suitably excited (e.g., Cd $^1P_1$, $^3P_1$) or suitably ionized (e.g., Cd^+, Cd^{+++}). Therefore, it should be possible to reduce the angular correlation by exciting or ionizing the decaying atom and preventing it for a sufficiently long time from being de-excited or neutralized. Most of the nuclear events are accompanied by processes which may lead to excitation or ionization (e.g., beta-decay or K-capture with subsequent rearrangement of the shell,[5] internal conversion, Auger effect after K-capture or internal conversion, recoil after the decay).

We consider first the case of excitation. If the decaying atom is embedded in a metal, the transition from the excited to the ground state is very fast[6] compared with the lifetime of the intermediate nuclear level, and we may assume that the measured correlation is "true." But if the atom forms a lattice defect in an ionic crystal or a semiconductor, the lifetime of the excited state may be so long that its associated magnetic moment may partially destroy the angular correlation.

A similar consideration may be valid for ionized atoms. The free electrons of a metal neutralize the ion in a very short time. In an insulator, however, the time for the neutralization may be long compared with the half-life of the nuclear level.

Thus, there may be a possibility of observing an influence of the atomic shell by comparing the angular correlation of metal sources with that of ionic crystal sources.

Usually, angular correlation is measured with the radioactive element in a chemical compound. This is not very suitable for the investigation of the mentioned effects, because it is very difficult to avoid contaminations. Furthermore, it is not possible to vary the type of binding and the nature of the surroundings to a very large extent.

An excellent method for varying the environment of the atom is through the use of evaporated "double stream" sources.[7,8] The substance of the second vapor stream may be varied for different sources from metal to ionic and molecular crystal. Such evaporated sources would give perhaps the best approximation to the ideal arrangement of isolated atoms or ions in a homogeneous medium.

A second proposal for embedding the source in a suitable medium might be the thermal diffusion of the radioactive isotope into the medium.

Experiments of this type should also give insight into the mechanism of the rearrangement after the decay.

[1] G. Goertzel, Phys. Rev. **70**, 897 (1946).
[2] E. L. Brady and M. Deutsch, Phys. Rev. **78**, 558 (1950).
[3] Sunyar, Alburger, Friedlander, Goldhaber, and Scharff-Goldhaber, Phys. Rev. **79**, 181 (1950).
[4] D. M. Roberts and R. M. Steffen, Phys. Rev. **82**, June 1 (1951).
[5] E. P. Cooper, Phys. Rev. **61**, 1 (1942).
[6] F. Seitz, *The Modern Theory of Solids* (1940), Chapter XVII.
[7] Frauenfelder, Walter, and Zünti, Phys. Rev. **77**, 557 (1950).
[8] H. Frauenfelder, Helv. Phys. Acta **23**, 347 (1950).

Influence of the Atomic Shell on Nuclear Angular Correlation in Cd^{111}

H. Aeppli, A. S. Bishop,* H. Frauenfelder, M. Walter, and W. Zünti
Swiss Federal Institute of Technology, Zurich, Switzerland
(Received April 5, 1951)

THE previous letter[1] discusses possibilities of influencing the angular correlation of successive nuclear radiations. We have succeeded in establishing a definite effect upon the angular correlation of the γ-rays in Cd^{111}. Cd^{111} results from the K-capture of In^{111}, and seemed especially promising because of the long lifetime of the intermediate state and the properties of the electron shell.[1]

The resolving time of the coincidence circuit† (2.2×10^{-7} sec) was so great that practically all transitions were measured regardless of the lifetime of the intermediate level. Both crystals were shielded with lead against scattered quanta.

The sources were prepared with a "double stream" method.[2] The cadmium, containing the radioactive In^{111} (from bombardment by 7-Mev protons), was placed in a carbon crucible. By slowly heating the crucible in a vacuum, all cadmium was evaporated away, most of the radioactive indium remaining in the crucible. Finally, the crucible was heated to 900°C for 1 minute and the (carrier-free) indium, accompanied by an intense vapor stream from a second crucible, was evaporated onto a thin aluminum foil. As a result of this procedure In^{111} was embedded free from contaminations within a suitable medium. After the evaporation the foil was rolled and placed in a small tube with very thin walls, so that the scattering of the γ-rays in the whole source was negligible. Four to six different sources were prepared in this way from each cyclotron irradiation.

The anisotropy was determined by measuring the coincidence rate at 90° and 180° alternatingly. The different sources were frequently interchanged. The different measurements were always consistent statistically. All results were corrected for the finite angular resolution.

The results for Cd^{111} are summarized in Table I. These values provide two important conclusions:

1. We have to assume that the value for "thick" metal sources ($>10^3$A) is the best approximation to the true angular correlation for the atom in the ground state. Therefore our new value, $A=-0.16\pm0.01$, is considerably higher than the hitherto reported values[3,4] $A=-0.07\pm0.04$ and $A=-0.06\pm0.02$.

It seems possible that the values found for the anisotropy in several other cases (e.g., Sr^{85}, Pd^{106}, Te^{124}) may similarly be in error and should be remeasured with a metallic embedding medium. In addition, several $\beta-\gamma$-correlations (e.g., Cd^{115}), which until now have shown an isotropic distribution, may become anisotropic when the source is embedded in a suitable medium. The wide discrepancy in the measured anisotropy of Rb^{86} may also be due to the way in which the source was prepared.

TABLE I. Angular correlation of Cd^{111} in different media.

Embedding medium	Approx. thickness in A	$A=\frac{K(180°)}{K(90°)}-1$, in %	Mean statistical error, in %
LiF	10^5	+1.6	±2.6
AgCl	5×10^4	+0.9	±1.4
SiO 1	10^5	−1.1	±1.9
SiO 2	5×10^4	+0.3	±2.0
Se (red)[a]	10^5	−5.8	±2.2
Au 1	$<10^5$	−5.8	±2.2
Au 2	$<10^5$	−6.5	±1.7
Ag 1	$<10^5$	−5.0	±2.1
Ag 2	$<10^5$	−10.6	±1.9
Ag 3	$\sim10^5$	−17.6	±1.3
Ag 4	3×10^5	−16.8	±2.1
Ag 5	5×10^5	−15.7	±2.3
Ag 6	10^4	−15.6	±1.7
Ag 7	10^4	−17.0	±1.4
Ag 8	2×10^4	−14.0	±1.2
Chemical compound $In(OH)_3$, 4 different sources		−3.0 to −7.5	±2.0

[a] P. K. Weimer, Phys. Rev. **79**, 171 (1950).

2. A variation of the correlation with the thickness of the metal film is obvious from Table I. This is not surprising, because very thin metal films show strong anomalies in their electric and magnetic behavior. One is therefore required to use relatively thick metal sources in order to obtain the "true" angular correlation. In measurements involving low energy electrons, the scattering in the source will thus necessarily be large.

We thank Professor P. Scherrer for his continued interest, and H. Albers-Schönberg and H. Huber for their assistance during the measurements.

* Postdoctoral Research Fellow, Institute of International Education.
[1] H. Frauenfelder, Phys. Rev. **82**, 549 (1951).
† Each anthracene crystal was viewed by two multipliers in coincidence, in order to reduce the background. We are indebted to Mr. F. Humbel for the design and construction of the electronic equipment.
[2] H. Frauenfelder, Helv. Phys. Acta **23**, 347 (1950).
[3] F. Boehm and M. Walter, Helv. Phys. Acta **22**, 378 (1949).
[4] D. M. Roberts and R. M. Steffen, Phys. Rev. **82**, 332 (1951).

Energy Level Perturbation of a Particle in a Spheroidal Potential Well

S. GALLONE AND C. SALVETTI
Istituto di fisica dell'Università e Laboratori C.I.S.E., Milan, Italy
(Received April 5, 1951)

RECENT papers[1-3] have drawn attention to the problem of the motion of a nucleon in a spheroidal potential well. Since so far this problem has been treated for P_2 deformations, i.e., for an ellipsoidal well, it may be of some interest to point out a method which is applicable to spheroidal deformations of a more general type:

$$R(\mu)=R_0[1+\sum_{i=1}^{\infty}\alpha_i P_i(\mu)], \quad (1)$$

μ being the direction cosine of the nucleon position vector, relative to the core symmetry axis, and R_0 the renormalized radius of the core.

The spheroidal potential well of depth D may be represented in the following way:

$$U(r,\mu)=D\mathbf{1}[r-R(\mu)]\simeq D\mathbf{1}(r-R_0)-D\delta(r-R_0)\Delta R(\mu), \quad (2)$$

where

$$\Delta R(\mu)=R_0\sum_i \alpha_i P_i(\mu)$$

and

$$\mathbf{1}(r-R_0)=\begin{cases}0 & \text{for } r\leqslant R_0\\ 1 & \text{for } r>R_0\end{cases}.$$

In spite of the singular character of the perturbation energy term $-D\delta(r-R_0)\Delta R(\mu)$, standard perturbation methods yield correct results as far as small deformations are concerned.

The energy shift relative to the unperturbed eigenvalue $E_{n,l,m}$ is given by:

$$\Delta E_{n,l,m}=-DR_0^3|\rho_{n,l}(R_0)|^2\sum_i \alpha_i\int|Y_{l,m}(\mu,\varphi)|^2P_i(\mu)d\mu d\varphi, \quad (3)$$

where $\rho_{n,l}$ and $Y_{l,m}$ are the normalized radial and angular parts of the unperturbed eigenfunctions.

The integral in formula (3), which we denote by $I_{l,m,i}$, has the following values in the cases $i=2$ and $i=4$:

$$I_{l,m,2}=\frac{l(l+1)-3m^2}{(2l-1)(2l+3)}, \quad (4)$$

$$I_{l,m,4}=\frac{3}{4}\frac{35m^4+5[5-6l(l+1)]m^2+3l(l-1)(l+2)}{(2l-3)(2l-1)(2l+3)(2l+5)}. \quad (5)$$

Formula (3) is in agreement with Feenberg and Hammack's particular result; in fact, for an ellipsoidal deformation ($\Delta R=R_0\alpha_2P_2(\mu)$) we have $\alpha_2=\frac{1}{3}\epsilon$, where ϵ is the eccentricity introduced by these authors.

The case of an impenetrable spheroidal box is obtained by evaluation of the limit:

$$\lim_{D\to\infty}D|\rho_{n,l}(R_0)|^2=\hbar^2x_{n,l}^2/MR_0^2,$$

where $x_{n,l}$ is sth zero of a bessel function of order $l+\frac{1}{2}$.

Formulas (3) and (5) together with the well-known expression of the surface and electrostatic deformation energy may be used for a variational calculation of the P_4 contribution to the total energy shift. The equilibrium shape of the nucleus up to P_4 deformations may be calculated in the same way; an equatorial neck may thus possibly appear in some cases.

Formula (5) shows that the P_4 degree of freedom remains unexcited for s and p states of the nucleon.

A more detailed discussion will soon be published in *Nuovo Cimento*.

[1] J. Rainwater, Phys. Rev. **79**, 432 (1950).
[2] A. Bohr, Phys. Rev. **81**, 134 (1951).
[3] E. Feenberg and K. C. Hammack, Phys. Rev. **81**, 285 (1951).

The Production and Detection of a Non-Equilibrium Number of Vacancies in a Metal*

A. S. NOWICK
Institute for the Study of Metals, University of Chicago, Chicago, Illinois
(Received April 2, 1951)

THE mechanism of diffusion in substitutional alloys and of self-diffusion in metals has never been determined satisfactorily. The experiments described below seem to be the most direct evidence, to date, that diffusion in close-packed metals occurs, predominantly, through the movement of vacancies.

It has been found[1,2] that anelastic effects occur in alloys when the two components differ in size. These effects, first observed in the case of brass,[1] have been attributed[2] to stress-induced reorientation of pairs of solute atoms. Inasmuch as the mechanism of this reorientation must be the same as that responsible for macroscopic diffusion, the writer[3] has begun a series of investigations to utilize this effect in the study of atomic mobility in alloys. In contrast to diffusion experiments, the time required for a measurement of the relaxation effects is of the order of magnitude of the mean time of stay of an atom. The alloys used are α solid solutions of Ag-Zn; it has been found, for example, that the total relaxation in an alloy of 29 atomic percent Zn is about 0.18.

If the mechanism of atomic movement is predominantly through the movement of vacancies, it should be possible to quench a non-equilibrium number of vacancies into a specimen; the presence of the excess of vacancies may be detected by the effect they have in lowering the relaxation time of the specimen at any given temperature. Such effects have been found. A specimen in the form of a wire 0.03 inch in diameter, is held at 400°C in a N_2 atmosphere for several minutes and then rapidly quenched into water at room temperature. Subsequent measurements of elastic aftereffect at 50°C, in which the wire is twisted for 15 minutes, then released, shows an initial time of relaxation of about 15 minutes (the first curve of Fig. 1). The magnitude of the relaxation is in agreement

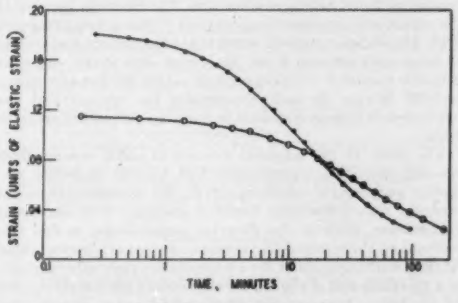

FIG. 1. Elastic aftereffect at 50°C of a 29 atomic percent Ag-Zn wire quenched from 400°C. Curve 2 follows curve 1 directly; each curve was obtained after a 15-minute twist of the wire.

with that obtained under equilibrium conditions at higher temperatures. However, under equilibrium conditions, the time of relaxation at 50°C, as obtained by extrapolating the data from higher temperatures, is about 3.4×10^8 minutes. The time of relaxation of the quenched specimen slowly increases, as shown by the second curve of Fig. 1, which indicates that the number of vacancies is gradually approaching the equilibrium number. None of the effects described appear when the same specimen is slowly cooled from 400°C.

The only alternate possibility to the explanation of these experiments in terms of vacancies is to assume that the observed relaxation effects result from quenching strains in the wire. In view of the small diameter of the specimen and the fairly rapid

disappearance of the effects at 50°C, this explanation is unlikely. By way of more positive verification, however, a specimen containing 14 atomic percent Zn was similarly studied. The pair-reorientation effect in such a specimen has been found to be 6 times smaller than that for the above specimen; the plastic properties of the two specimens should be approximately the same. The quenching experiments on these specimens show effects considerably smaller than on the original specimens. It therefore seems as if this alternate explanation has been discounted.

In terms of the vacancy mechanism, the heat of activation in diffusion or pair-reorientation experiments should be $H=H_1+H_2$, where H_1 is the heat of activation for the formation of a vacancy and H_2 for its movement. In the present alloy, $H=32.9$ kcal/mole. Inasmuch as the concentration of vacancies responsible for the relaxation in the quenched specimen is that which would be in equilibrium at 400°C or a lower temperature, it is readily calculated, as a preliminary estimate, that $H_1 \geqq 12.5$ and $H_2 \leqq 20.4$ kcal/mole. Further results will be reported in a forthcoming publication.

The writer wishes to thank Mr. R. Sladek for taking the measurements.

* This research was supported in part by the ONR.

[1] C. Zener, Trans. A.I.M.E. **152**, 122 (1943).
[2] A. S. Nowick, Phys. Rev. **82**, 340 (A) (1951).
[3] C. Zener, Phys. Rev. **71**, 34 (1947).

On Antiferromagnetism in a Single Crystal

N. J. Poulis, J. van den Handel, J. Ubbink, J. A. Poulis, and C. J. Gorter
Kamerlingh Onnes Laboratorium, Leiden, Netherlands
(Received March 27, 1951)

HYDRATED copper chloride $CuCl_2 \cdot 2H_2O$ apparently becomes antiferromagnetic at a temperature slightly above the boiling point of liquid helium. Single crystals of this substance have been investigated by three different magnetic methods at a number of liquid helium temperatures. The magnetic moment of the crystal was measured as a function of the external magnetic field. The nuclear magnetic resonance of the protons was studied at frequencies between 8 and 38 Mc/sec. And finally, electronic magnetic resonance of the copper ions was observed at a frequency of 9400 Mc/sec. In each investigation the external field was orientated in various directions in the plane perpendicular to the c-axis.

The study of the magnetic moment in small external fields revealed that, in agreement with Van Vleck's[1] theoretical prediction and Stout's[2] results on MnF_2, the susceptibility in one direction (the x-direction) vanishes gradually with decreasing temperature, while in the direction perpendicular to that (the y-direction) the susceptibility remains constant at a normal value. At the lower temperatures the x-susceptibility rises rather abruptly at a threshold field of about 7000 oersteds to a normal value, while at the higher temperatures the threshold region extends from about 7000 to about 8500 oersteds. The y-susceptibility is very little influenced by the magnitude of the field.

In the investigations on nuclear magnetic resonance the contribution of the copper ions to the average local magnetic field acting on the different protons is directly detected. In the antiferromagnetic state the dependence of this field on the temperature and on the external field has a very different character[3] from that observed in the paramagnetic $CuSO_4 \cdot 5H_2O$ crystals[4] and in $CuCl_2 \cdot 2H_2O$ at liquid hydrogen temperatures. A striking symmetry of the resonance diagram indicates that, in each orientation of the external field, to every contribution to the field at one proton there occurs an exactly opposite contribution at another proton. The threshold region is also quite marked.

When the external field is orientated in the x-direction two electronic resonance bands have been observed at 9400 Mc/sec. near the threshold region. They approach each other when the temperature is lowered. They are of unequal polarization and the dispersion in their neighborhood is of opposite sign. In the y-direction a band is observed in low external fields which vanishes rapidly when the temperature decreases.

In the threshold region the orientation of the two systems of antiparallel spins is apparently decoupled from the preferred x-axis in such a way that it places itself perpendicular to an external field above the threshold value.[5] A simple extension of the phenomenological treatment of Neël,[6] Bitter,[7] and Van Vleck[1] to high field strengths in an anisotropic crystal leads to the expectation of such a decoupling. In particular, the results on the proton magnetic resonance follow the decoupling in detail.

The symmetry of the resonance diagram appears to suggest the existence of two spin systems with antiparallel orientations which interchange their directions only slowly.

Though the general picture seems clear, it is, however, not yet possible to explain in detail the many data collected. They will be published and discussed in *Physica* and in the Leiden Communications.

[1] J. H. Van Vleck, J. Chem. Phys. **9**, 85 (1941).
[2] J. W. Stout and M. Griffel, Phys. Rev. **76**, 144 (1949).
[3] N. Poulis, Leiden Comm. 283a.
[4] N. Bloembergen, Leiden Comm. 280c; Physica **16**, 95 (1950).
[5] C. G. B. Garrett, Proc. Phys. Soc. (London) **63**, 1042 (1950), observed somewhat similar phenomena in a crystal of cobalt ammonium Tuttonsalt at still lower temperatures.
[6] L. Neël, Ann. de Phys. X **18**, 5 (1932); XI **5**, 232 (1936).
[7] F. Bitter, Phys. Rev. **54**, 97 (1938).

Beta-Decay of 7.5-Day Ag^{111} to a 0.1-Microsecond Excited State of Cd^{111}

D. Engelkemeir
Argonne National Laboratory, Chicago, Illinois
(Received March 29, 1951)

IN the decay scheme of Ag^{111} proposed by Johansson[1] (Fig. 1) 8 percent of the disintegrations lead to a 340-kev level and one percent to a 243-kev level of Cd^{111}. Johansson postulates that

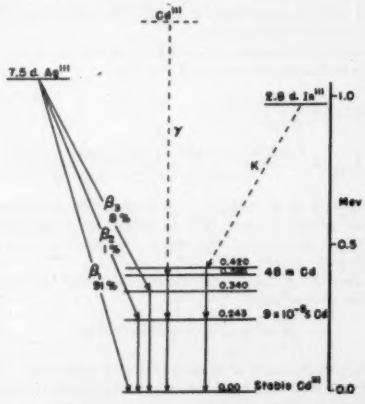

FIG. 1. Disintegration schemes of Ag^{111}, Cd^{111m}, and In^{111}.

the 243-kev level is identical with the 0.09-μsec level observed in the K-capture decay of In^{111} and in the 48-min isomeric transition[2,3] of Cd^{111*}. McGowan[3] did not observe the 0.09-μsec level of Cd^{111} in the beta-decay of Ag^{111}.

Since it was felt that McGowan may have missed the 0.09-μsec level because of its low occurrence in the beta-decay of Ag^{111}, a careful search for delayed coincidences in Ag^{111} was made at this laboratory.

Stilbene scintillation counters with 1P21 photomultipliers cooled

with liquid nitrogen were employed to detect the radiations. The beta-crystal was so thin (*ca* 20 mg/cm²) that its efficiency for gamma-rays was negligible. The coincidence circuit employed blocking oscillator pulse shaping and a 6BN6 mixing stage. Various lengths of terminated RG 65/U cable were used to introduce the delays.

A plot of the coincidence rate *versus* delay time is shown in Fig. 2. The dotted curve is that of Co^{60} and is typical of substances

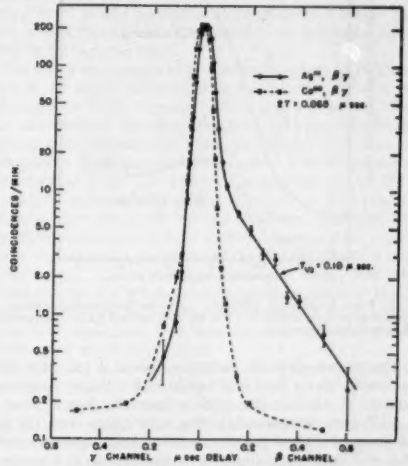

FIG. 2. Delayed coincidences in 7.5-day Ag^{111}.

showing no measurable gamma-delay. The solid curve is that observed with a purified source[4] of Ag^{111}. The main body of the transitions shows no delay greater than 0.02 μsec. A small fraction of the transitions are delayed with a half-life of 0.10±0.02 μsec. Since nearly equal counting efficiencies for the two gammas are expected, it may be calculated that the ratio of the undelayed to delayed transitions is about 6:1. This agrees well with the ratio of 8:1 for the 340-kev to 243-kev transitions found by Johansson.

The identification of the 243-kev level in Cd^{111} formed by beta-decay of Ag^{111} with the 0.09-μsec level observed in the *K*-capture decay of In^{111} and in the 48-min isomeric transition of Cd^{111*} thus appears to be justified.

[1] Stig Johansson, Phys. Rev. **79**, 896 (1950).
[2] M. Deutsch and D. T. Stevenson, Phys. Rev. **76**, 184(A) (1949).
[3] F. K. McGowan, ORNL-366, 34 (August 12, 1949) (unpublished).
[4] Obtained through the courtesy of the Isotopes Division of the Oak Ridge National Laboratory.

The Thermal Neutron Capture Cross Section of Co^{59}

L. YAFFE, R. C. HAWKINGS, W. F. MERRITT, AND J. H. CRAVEN
Atomic Energy Project, National Research Council of Canada, Chalk River, Ontario, Canada
(Received April 2, 1951)

A DISCREPANCY has existed in the values published for the thermal neutron capture cross section of Co^{59}. The activation method used by Seren, Friedlander, and Turkel[1] yielded a value of 21.7±4.3 barns. The "pile oscillator" or "danger coefficient" method gave values of 34.3±0.7 barns,[2] 34.2±3.4 barns,[3] and 38.2±3.0 barns.[4] This discrepancy suggested either an error in the pile activation determination or possibly a short-lived isomer of Co^{60} that had not been detected.

We have determined the activation cross section of Co^{59} for thermal neutrons, using the NRX heavy-water reactor. The thermal neutron cross section of Au—93 barns—was used as a standard.[5] The Au and Co were irradiated simultaneously in a position where the neutron distribution was known to be predominantly thermal. The contribution of epi-cadmium neutrons was determined by an irradiation under cadmium and small corrections were made for this (2.2 percent for Au and 0.2 percent for Co).

The Co metal (99.92 percent pure) was irradiated as a weighed disk 0.3 mm thick. A disk was cut out of a sheet of gold leaf of known weight and area, floated on water, and lifted onto an aluminum backing. The water was then evaporated, and the area of the disk, and hence its weight, was determined under a microscope.

After a measured irradiation period of about 20 hours the Co and Au samples were dissolved in *aqua regia* and made up to standard volumes. From these solutions known aliquots were withdrawn and activity measurements made several hours later. The absolute disintegration rates of these aliquots were measured by 4π proportional counting and by coincidence counting techniques. The relative values were confirmed by an end window counter.

Half-lives of 5.26 years[6] and 2.69 days[6] for Co^{60} and Au^{198}, respectively, were used in making corrections for decay and for lack of saturation of bombardment.

The thermal neutron capture cross section for Co^{59} leading to the formation of 5.26 year Co^{60} was found to be 34.2±1.4 barns. This result is the mean of 6 activations. A large proportion of the probable error is introduced by variations in the thickness of the gold leaf used. The cross section leading to the formation of the 10.7-minute isomer is 0.66 barns,[1] and thus only about 2 percent of the thermal neutron captures lead to the short-lived isomer. Of this, less than 10 percent[7] decays independently to Ni^{60}, leaving a maximum of only 0.2 percent not included in the ultimate production of 5.26 year Co^{60}. The cross section as measured can then be taken equal to the total absorption cross section of Co^{59}, with an error of less than 0.07 barns.

It will be noted that the activation cross section is now in excellent agreement with the results obtained by the "pile oscillator" method.

When this work was completed Dr. B. W. Sargent kindly drew our attention to an unpublished report by Jones, *et al.*,[8] which gives a value of 33 barns for Co^{59} obtained by the activation method. Agreement with our value is satisfactory.

[1] Seren, Friedlander, and Turkel, Phys. Rev. **72**, 888 (1947).
[2] Harris, Muehlhause, and Thomas, Phys. Rev. **79**, 11 (1950).
[3] H. S. Pomerance, private communication.
[4] F. C. W. Colmer and D. J. Littler, Proc. Phys. Soc. (London) **A63**, 1175 (1950).
[5] G. L. Brownell and C. J. Maletskos, Phys. Rev. **80**, 1102 (1950).
[6] Nuclear Data, National Bureau of Standards Circular No. 499.
[7] Deutsch, Elliott, and Roberts, Phys. Rev. **68**, 193 (1945).
[8] Jones, Clark, and Overman, MonC 398 (unpublished).

The Excitation Functions for $B^{10}(d, \alpha)Be^8$

W. D. WHITEHEAD
*Bartol Research Foundation of the Franklin Institute, Swarthmore, Pennsylvania**
(Received March 29, 1951)

THE excitation functions for the ground-state group and the first excited state group for $B^{10}(d, \alpha)Be^8$ have been determined by bombarding thin targets (375 μg/cm²) of isotopically enriched boron (96 percent B^{10}) and of normal boron with deuterons from the Bartol van de graaff generator, and observing the reaction α-particles with an argon-filled proportional counter, biased to count the α's at the end of their range, at 90° to the incident beam. The isotopic assignment of groups was first made by observing the α-particle groups from the target of 96 percent B^{10} (Fig. 1) and from a normal boron target (Fig. 2) bombarded with 1.20-Mev deuterons and noting the change in intensity with change in isotopic ratio. As seen in the curves, groups 1, 2, and 3 are due to the B^{10} reaction, and group 4 is due to B^{11}. This confirms

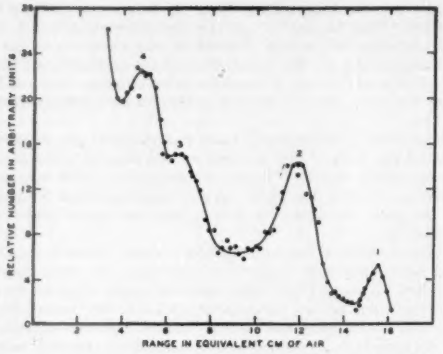

FIG. 1. Number of α-particles *vs* range in equivalent cm of air for B(d, α)Be with a target of 96 percent B^{10} and a bombarding energy of 1.20 Mev.

the work of Smith and Murrell[1] and shows that their tentative assignment of the group with a Q value of 4.90 Mev to the Li contamination is probably correct, for there is no evidence of a group between groups 2 and 3 on either curve.

The ranges of the α-particles were measured using aluminum absorbing foils and a movable proportional counter; the gross range changes were made with foils and the fine changes by moving the counter in air. The energy of the α-particles was determined from the range to the peak of the group, using the procedure of Holloway and Moore[2] for converting from the range to the peak to the mean range, and using the Brookhaven[3] range tables to determine the energy. The Q values determined from these energies are 17.92±0.15 Mev for the ground state, and 15.19±0.15 Mev for the first excited state which is thus 2.73±0.20 Mev above the ground state. Using the ground-state Q value from this reaction, the masses of B^{10} and d from Tollestrop *et al.*,[4] and the mass of the α-particle from Whaling and Li,[5] the mass of Be^8 is 8.00780±0.0016 MU and is unstable to α-emission by 0.110±0.150 Mev. Assuming that the width in range at half-maximum for the excited state is $(\sigma_x^2+\sigma_n^2)^{\frac{1}{2}}$, where σ_x is the experimental half-width due to range straggling and angular straggling, and σ_n is the spread in range due to the natural width of the level, the width of the first excited level in Be^8 is 0.95±0.20 Mev.

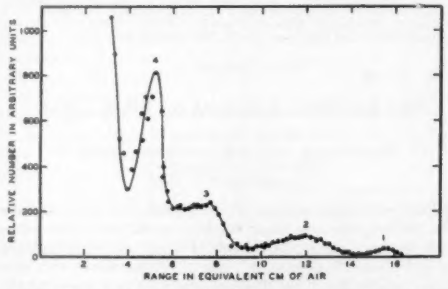

FIG. 2. Number of α-particles *vs* range in equivalent cm of air for B(d, α)Be with a target of normal boron (80 percent B^{11}) and a bombarding energy of 1.20 Mev.

The excitation functions were determined by measuring the peak heights as the bombarding energy was varied from 0.50 Mev to 1.60 Mev in 0.1-Mev intervals (Fig. 3). The ratio of the peak heights of the two groups is not equal to the ratio of the intensities; but the ratio of the areas under the peaks is, and at 1.20 Mev

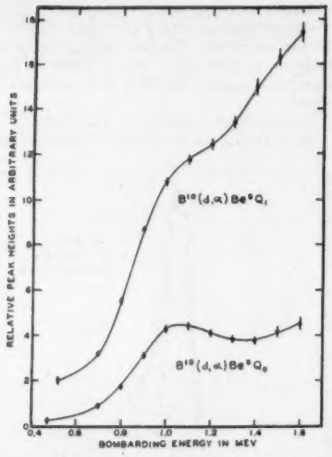

FIG. 3. Peak heights in arbitrary units *vs* bombarding energy for $B^{10}(d, \alpha)Be^8$ ground state and $B^{10}(d, \alpha)Be^8$ first excited state. The statistical errors are less than 2 percent.

is 7.1. The resonances in the excitation curves at 1.05-Mev bombarding energy give a level in C^{13} at 26.1 Mev. Since the ground-state group of α's and the protons from the ground state of $C^{12}(d, p)C^{13}$ have approximately the same range, and the first excited group of α's and the protons from the ground state group of $O^{16}(d, p)O^{17}$ have approximately the same range, at a bombarding energy of 1.05 Mev, the possibility that the resonance is due to piling up of the protons and alphas has to be considered. The protons are not counted directly because their maximum pulse height is 16 volts, and a bias of 30 volts was used in the discriminator; also, the number of counts per microcoulomb was independent of current as the current was changed by a factor of six, so that the piling up is negligible.

* Assisted by the joint program of the ONR and AEC.

[1] Smith and Murrell, Proc. Cambridge Phil. Soc. **35**, 298 (1939).
[2] M. G. Holloway and B. L. Moore, Phys. Rev. **58**, 847 (1940).
[3] H. A. Bethe, "The properties of atomic nuclei II," Brookhaven National Laboratory BNL-T-7 (unpublished).
[4] Tollestrop, Fowler, and Lauritsen, Phys. Rev. **78**, 372 (1950).
[5] W. Whaling and C. W. Li, Phys. Rev. **81**, 150 (1951).

Erratum: The Cathode Field in Diodes under Partial Space-Charge Conditions with Initial Velocities

[Phys. Rev. **81**, 274 (1951)]

A. O. BARUT
Department of Applied Physics, Swiss Federal Institute of Technology, Zurich, Switzerland

(Received March 28, 1951)

IN the formulas for $f(0)$ and for the saturation current I_{sa}, the letter ϑ should read $(2e)$, where e is the charge of the electron.

The Ratio of Proton and Electron Masses

FRIEDRICH LENZ
Düsseldorf, Germany

(Received April 5, 1951)

THE most exact value at present[1] for the ratio of proton to electron mass is 1836.12±0.05. It may be of interest to note that this number coincides with $6\pi^5=1836.12$.

[1] Sommer, Thomas, and Hipple, Phys. Rev. **80**, 487 (1950).

Ferromagnetism in the Manganese-Indium System

WALTER V. GOEDDEL* AND DON M. YOST
Gates and Crellin Laboratories of Chemistry, California Institute of Technology, Pasadena, California
(Received March 26, 1951)

WE recently undertook an investigation of the phase equilibria in the previously unreported manganese-indium system. About twenty-five alloys, varying in manganese content from 3 to 91 weight percent in steps of about 4 weight percent, have been prepared, and over half of these specimens have been found to be ferromagnetic.

The alloys were prepared by melting 40-gram to 70-gram mixtures of the metals under argon in an induction furnace, using a Westinghouse 10-kw rf generator as a source of power. "Triangle RR recrystallized alumina" crucibles (Morgan, England) and alumina-silica thermocouple protective tubes, sealed off at one end with packed magnesia, were used. Indium of 99.97 percent purity was obtained from the Indium Corporation of America and electrolytic manganese of purity greater than 99.9 percent was obtained from the U. S. Bureau of Mines. Chemical analysis showed both materials to be at least 99.9 percent pure. A chromel-alumel thermocouple, calibrated at the freezing points of tin, zinc, silver, copper, and copper-silver eutectic alloy, was used in conjunction with a Brown recording potentiometer to obtain the cooling curves of the alloys. All specimens were chemically analyzed to make sure that they were homogeneous and to determine their exact composition.

The existence of ferromagnetism in this system was suggested by Hames and Eppelsheimer, but no data were given.[1] While we have made only qualitative magnetic measurements with a small Alnico magnet, the intensity of magnetization appears to increase regularly from 3 to about 50 weight percent manganese, and then to die out completely. An alloy containing 53.2 percent manganese is strongly ferromagnetic, while one containing 59.4 percent manganese is unaffected by the magnet, as are the subsequent alloys of increasing manganese content. The same range of ferromagnetism holds for alloys annealed and quenched from temperatures between 850 and 950°C. On the basis of these, plus incomplete thermal and metallographic data, we believe the ferromagnetism is due to a single phase, the compound Mn_3In. The alloys containing up to 49 percent manganese appear to be composed of indium plus Mn_3In, no eutectic mixture being formed (the solidus is at the freezing point of indium, 157.5°C).

In a private communication, Dr. R. M. Bozorth has pointed out to us that there are now definitely known about sixteen binary systems, containing no ferromagnetic elements, which show ferromagnetism. Of these binary systems, both components are metals in eight cases. The manganese-indium system described here provides a new additional case.

Thermal and metallographic measurements are being continued, as a thorough knowledge of the phase relations is needed before proceeding to further measurements of magnetic and other properties.

The authors gratefully acknowledge a grant from the Research Corporation which aided this investigation.

* Present address: Atomic Energy Research Department, North American Aviation, Inc., Downey, California.

[1] F. A. Hames and D. S. Eppelsheimer, Nature 162, 968 (1948). See also R. R. Grinstead and D. M. Yost, Phys. Rev. 75, 984 (1949) on ferromagnetism in the Mn-Cu-In system.

Erratum: The $Li^6(n,\alpha)H^3$ Reaction Spectrum

[Phys. Rev. 81, 475 (1951)]

UGO FACCHINI, EMILIO GATTI, AND ELIO GERMAGNOLI
Laboratori C.I.S.E., Pissnale Cimitero Monumentale, Milan, Italy

THE sentence on lines 10 and 11 of the right-hand side of page 476 in the above article should read, "Deviations from ideal behavior of the whole apparatus are in any case less than 0.3 percent."

Least-Squares Adjusted Values of the Atomic Constants as of December, 1950

JESSE W. M. DUMOND
California Institute of Technology, Pasadena, California
AND
E. RICHARD COHEN
North American Aviation Inc., Downey, California
(Received March 8, 1951)

AS part of the work of the National Research Council Committee on Constants and Conversion Factors of Physics and at the request of its chairman, E. U. Condon, we have prepared a report,[1] dated December, 1950, giving a complete re-evaluation of the atomic constants in the light of the wealth of important new and very accurate data obtained since our previous study of January, 1948. As input data we have used the most recent results of Kusch and Prodell[2] on the hydrogen hyperfine shift; of Hipple and his N.B.S. associates[3] and also of Bloch and Jefferies of Stanford[4] on the proton cyclotron frequency; of Gardner and Purcell[5] on the electron cyclotron frequency; of Craig and Hoffman[6] (N.B.S.) on the faraday by electrolysis of sodium oxalate; of Bearden and associates[7] on h/e (which latter have recently also been verified at 25 kv at this Institute by the work[8] of Gaelen Felt and John Harris); of Birge[9] on λ_e/λ_s and on N obtained in 1945 from a study of all experimental evidence; of the four independent sources, Hansen and Bol,[10] Bergstrand,[11] Aslakson,[12] and Essen,[13] on the velocity of light; and of Cohen[14] on a re-evaluation of R_∞ in the light of the Lamb shift.

As a result of making a number of trial adjustments, we soon discovered that the new data are likely to lead to observational equations whose observed numerics are not independent but are observationally correlated. If such correlations are ignored, a serious error of method is committed and wrong results[15] are obtained, because the error (or the weight) to attach to each equation cannot then be described by a single number. Instead an error matrix must be used to describe the error situation with all the intercorrelations between equations. The classical procedure for forming the normal equations of least squares no longer applies, but one of us has shown[16] how a generalization in matrix algebra can be used.

A simpler method may be, as we have shown in our report, to recast the equations so as to diagonalize the error and weight matrices,[17] thus removing the correlations between equations. To do this completely, it may be (and in this case was) necessary to transfer some of the observational data from the category of fixed auxiliary constants to that of the unknowns to be adjusted. For this and other more involved reasons discussed in the above report we finally concluded that a solution in the following six unknowns was required: N, e, m, h, c, and λ_e/λ_s. The present data permit of setting up, with a diagonalized error matrix, nine observational equations in these six unknowns (including equations for the direct observations on c and λ_e/λ_s) so that the overdetermination is sufficient to yield an index of the presence or absence of systematic errors in the data from a study of the residues. The consistency of the data, so adjusted, is excellent. The somewhat abridged Table I gives the resulting adjusted values of the six primary unknowns and of other useful quantities which can be computed from them, the probable errors being all computed by the ellipsoid method. The adjusted value of λ_e/λ_s turns out to be a little lower than our input value, while that for c is a little higher.

These values must still be regarded as tentative, partly because not all of the input data are as yet quite finally settled, and also because the theoretical formula,[18] connecting the hydrogen fine structure shift with Sommerfeld's α, is not yet known, as regards certain correction terms,[19,18] with the accuracy which the observational data warrant. The Bethe-Longmire correction terms give only "orders of magnitude" and *may*, according to H. Bethe, have to be modified by many parts in 10^3. (See Γ-coefficients in Table I). We are also suspicious regarding the magnitude of the higher order corrections[19] giving the electron moment in Bohr magnetons for hydrogen. This ratio is probably Z-dependent, and we are informed

TABLE I. Least-squares adjusted values of atomic constants and conversion factors, December, 1950. (Each quantity is accompanied with a Γ-coefficient giving the change in ppm which may later be made in that quantity for each ppm change in the constant G^2 of the equation $\Delta\nu_H = \alpha^2(\mu_p/\mu_0)R_\infty G^{-2}$ as later advances in our theoretical knowledge may require. The present values are based on $G^2 = 0.004751364$. The physical scale of atomic weights is used here exclusively, since Nier has shown that the definition of the chemical scale in terms of "natural abundance ratios" is ambiguous to presently accessible accuracy).

N	Avogadro's number $(6.02544 \pm 0.00011) \times 10^{23}$ g-mole^{-1} (phys.)	(-1.241Γ)
c	Velocity of light (299790.2 ± 0.9) km sec^{-1}	(0.023Γ)
e	Electronic charge $(4.80223 \pm 0.00007) \times 10^{-10}$ esu	(1.291Γ)
m	Electron rest mass $(9.10721 \pm 0.00025) \times 10^{-28}$ g	(1.077Γ)
h	Planck's constant $(6.62377 \pm 0.00018) \times 10^{-27}$ erg sec	(2.073Γ)
$\lambda_\delta/\lambda_\alpha$	Conversion factor from Siegbahn x-units to milliangstroms (1.002020 ± 0.000011)	(0.349Γ)
$F' = Ne/c$	Faraday constant (9651.94 ± 0.07) emu g-mole^{-1} (phys.)	(0.027Γ)
h/e	$(1.379311 \pm 0.000018) \times 10^{-17}$ erg sec esu^{-1}	(0.782Γ)
e/mc	Specific charge of the electron $(1.758897 \pm 0.000032) \times 10^{7}$ emu g^{-1}	(0.191Γ)
h/m	(7.27311 ± 0.00009) cm^2 sec^{-1} or erg sec g^{-1}	(0.966Γ)
$\alpha = 2\pi e^2 h^{-1} c^{-1}$	Fine structure constant $(7.29698 \pm 0.00005) \times 10^{-3}$	(0.486Γ)
α^{-1}	137.0429 ± 0.0009	(-0.486Γ)
$\lambda_{e0} = hm^{-1}c^{-1}$	Compton wavelength of the electron $(2.426067 \pm 0.000032) \times 10^{-10}$ cm	(0.973Γ)
Nm	Atomic wt. (electron) $(5.48749 \pm 0.00010) \times 10^{-4}$ (phys.)	(-0.164Γ)
$a_0 = h^2(4\pi^2 me^2)^{-1}$	Firat Bohr radius $(5.29151 \pm 0.00003) \times 10^{-9}$ cm	(0.487Γ)
$r_0 = e^2 m^{-1} c^{-2}$	Classical radius of the electron $(2.81751 \pm 0.00006) \times 10^{-13}$ cm	(1.459Γ)
H	Atomic wt. of hydrogen 1.0081284 ± 0.0000030 (phys.)	
$H^+ = H - Nm$	Atomic wt. of proton 1.0075797 ± 0.0000030 (phys.)	$(8.94 \times 10^{-3}\Gamma)$
H^+/Nm	Ratio proton mass to electron mass 1836.139 ± 0.034	(0.164Γ)
R_∞	Rydberg for infinite mass (109737.323 ± 0.010) cm^{-1}	
$R_H = (1 - Nm/H)R_\infty$	Rydberg for hydrogen (109677.591 ± 0.010) cm^{-1}	$(8.94 \times 10^{-3}\Gamma)$
$\mu = mH^+/H$	Reduced mass of electron in hydrogen atom $(9.10225 \pm 0.00024) \times 10^{-28}$ g	(1.077Γ)
$\sigma = 2\pi^5 R_0^4/(15c^2h^3N^4)$	Stefan-Boltzmann constant $(5.6699 \pm 0.0009) \times 10^{-5}$ erg cm^{-2} deg^{-4} sec^{-1}	(-1.301Γ)
$c_1 = 8\pi hc$	First radiation constant $(4.99071 \pm 0.00014) \times 10^{-15}$ erg cm	(2.096Γ)
$c_2 = hcNR_0^{-1}$	Second radiation constant (1.43868 ± 0.00006) cm deg	(0.855Γ)
c_2/c	Atomic specific heat constant $(4.79894 \pm 0.00021) \times 10^{-11}$ sec deg	(0.832Γ)
$k = R_0 N^{-1}$	Boltzmann's constant $(1.38026 \pm 0.00006) \times 10^{-16}$ erg deg^{-1}	(1.241Γ)
$\lambda_{max}T = chN/(4.965114R_0) = 0.2014052c_2$	Wien's displacement law constant (0.289757 ± 0.000012) cm deg	(0.855Γ)

TABLE I.—*Continued.*

$\mu_0 = he'/(4\pi m)$	Bohr magneton $(0.927120 \pm 0.000022) \times 10^{-20}$ erg gauss^{-1}	(2.264Γ)
$(3k/N)^{\frac{1}{2}} = (3R_0/N^3)^{\frac{1}{2}}$	Multiplier of (Curie const.)$^{\frac{1}{2}}$ to give magnetic moment per molecule $(2.62148 \pm 0.00007) \times 10^{-20}$ (erg mole deg^{-1})$^{\frac{1}{2}}$ (phys.)	(1.241Γ)
$E_0 = c^2 F'^{-1} 10^{-14}$	Conversion factor from atomic mass units to Mev (931.152 ± 0.008) Mev (amu)$^{-1}$ (phys.)	(0.019Γ)
$E_g = c^2 e'^{-1} 10^{-14}$	Conversion factor from grams to Mev $(5.61060 \pm 0.00009) \times 10^{26}$ Mev g^{-1}	(-1.222Γ)
$E_e = c^2 (e'/m)^{-1} 10^{-14}$	Energy equiv. of electron mass in Mev (0.510969 ± 0.000010) Mev electron-mass^{-1}	(-0.145Γ)
$E_p = E_e H^+/Nm$	Energy equiv. of proton mass in Mev (938.210 ± 0.008) Mev proton^{-1}	(0.019Γ)
$\lambda_{cp} = \lambda_{c0} Nm/H^+$	Compton wavelength of the proton $(1.321287 \pm 0.000017) \times 10^{-13}$ cm	(0.809Γ)
$\lambda_\delta = (hc^2 e^{-1}) 10^{-8}$	Wavelength associated with 1 ev $(12396.44 \pm 0.17) \times 10^{-8}$ cm	(0.828Γ)
$\tilde{\nu}_\delta = 10^8 ch^{-1} c^{-1}$	Wave number associated with 1 ev (8066.83 ± 0.11) cm^{-1}	(-0.828Γ)
$e10^8/c$	Energy associated with 1 ev $(1.601864 \pm 0.000024) \times 10^{-12}$ erg	(1.268Γ)
$(F'/R_0)10^8$	"Temperature" associated with 1 ev (11605.6 ± 0.5) deg Kelvin	(0.027Γ)
$n_0 = N/V_0$	Loschmidt's number $(2.68744 \pm 0.00007) \times 10^{19}$ cm^{-3}	(-1.241Γ)
$S_0/R_0 = \ln\{(2\pi k)^{\frac{1}{2}}(2.71828)^{5/2} h^{-3} N^{-5/2}\}$	Sakur-Tetrode constant (-5.57305 ± 0.00007)	(0.225Γ)
S_0	$(-4.634907 \pm 0.000036) \times 10^3$ erg mole^{-1} deg^{-1} (phys.)	(0.225Γ)

that it may soon be settled (for hydrogen) by direct measurements now in progress at Columbia University.

[1] For costs of printing of this report the N.R.C. was assisted by the Office of Naval Research. A limited number of copies are still available upon request from R. C. Gibbs of the NRC, Washington, D. C., or from the authors.

[2] P. Kusch and Prodell, Phys. Rev. **79**, 1009 (1950).

[3] Hipple, Sommer, and Thomas, Phys. Rev. **80**, 487 (1950); Thomas, Driscoll, and Hipple, N.B.S., R.P. 2104, Vol. 44, June, 1950; Phys. Rev. **78**, 787 (1950).

[4] F. Bloch and C. D. Jefferies, Phys. Rev. **80**, 487 (1950).

[5] J. H. Gardner and E. M. Purcell, Phys. Rev. **76**, 1262 (1949).

[6] D. N. Craig and J. I. Hoffman, Phys. Rev. **80**, 487 (1950).

[7] J. A. Bearden and G. Schwarz, Phys. Rev. **79**, 674 (1950); Bearden, Johnson, and Watts, NORD 8036, July 31, 1950; Phys. Rev. **81**, 70 (1951).

[8] G. Felt and J. Harris. As yet unpublished, this constituted G. Felt's doctorate thesis. Available on library loan.

[9] R. T. Birge, Am. J. Phys. **13**, 63 (1945).

[10] Kees Bol, Phys. Rev. **80**, 298 (1950).

[11] L. E. Bergstrand, Arkiv. Mat. Astron. Fysik, A **36**, paper 20 (1949); Nature **165**, 405 (1950).

[12] Aslakson, Nature **164**, 711 (1949).

[13] L. Essen and Gordon-Smith, Proc. Roy. Soc. (London) **A194**, 348 (1948); L. Essen, Nature **165**, 582 (1950).

[14] E. R. Cohen, as yet unpublished. May be obtained from author upon request.

[15] This is illustrated in certain earlier versions of Bearden and Watts' recent adjustments of the atomic constants. They have since corrected their error of method in part, but have nevertheless still overlooked (Phys. Rev. **81**, 73 (1951)) an important correlation entering, because they have used $\lambda_\delta/\lambda_\alpha$ (which they still treat as a fixed auxiliary constant) in computing the numerics for two of their observational equations (their Eqs. (1) and (6), Table V).

[16] E. R. Cohen, Phys. Rev. **81**, 162 (1951). Appendix III of the December, 1950 DuMond and Cohen report gives the theory of the matrix method of least squares, and Part IV illustrates its application.

[17] This obvious alternative, which we have been using since June, 1950, has recently also been applied by Bearden and Watts, Phys. Rev. **81**, 160 (1951), but they avoid the difficulty (which we met by increasing the number of our variables) by the simple device of ignoring two important basic equations, (i) the equation (reference 9) relating Avogadro's number N with $\lambda_\delta/\lambda_\alpha$ and the x-ray and other physical constants of crystals, (ii) the equation (reference 6) relating the new N.B.S. results on the faraday with N, e, and c.

[18] H. A. Bethe and C. Longmire, Phys. Rev. **75**, 306 (1949).

[19] R. Karplus and N. M. Kroll, Phys. Rev. **77**, 536 (1950).

Darling's Theory and the Mass of the π-Meson

P. R. ZILSEL
University of Connecticut, Storrs, Connecticut
(Received March 26, 1951)

IN Darling's theory of elementary particles[1] the Dirac equation for a free electron

$$(\gamma_\nu\partial/\partial x_\nu+k)\psi=0, \tag{1}$$

with $k=mc/\hbar$, is replaced by the infinite order equation

$$\{[8J_3(z)/z^3]\gamma_\nu\partial/\partial x_\nu+k2J_1(z)/z\}\psi=0, \tag{2}$$

in which the operator z, which occurs only in even powers, is defined by $z^2=4\omega^2\Box^2$. The fundamental length ω is chosen as

$$\omega=\beta e^2/mc^2, \quad \beta=1.610. \tag{3}$$

The relation between (2) and the Dirac equation is of a correspondence principle character, in that (2) reduces to (1) in the limit $\omega\to 0$. A ψ representing a free particle of mass μ satisfies the Klein-Gordon equation $[z^2-(2\omega\mu c/\hbar)^2]\psi=0$, so that Eq. (2) gives a mass spectrum for spin $\frac{1}{2}$ particles, the allowed mass values being the roots of

$$\mu_n c/\hbar=z_n/2\omega=kz_nJ_1(z_n)/[4J_3(z_n)]. \tag{4}$$

With the choice (3) for ω, this mass spectrum includes the μ-meson and the proton mass to great accuracy. The smallest positive root of (4) (electron mass) is[1]

$$\mu_0\simeq m[1-\beta^2(e^2/\hbar c)^2/6]\simeq m, \tag{5}$$

i.e., almost exactly the mass of the particle described by the Dirac equation (1), to which (2) reduces in the correspondence principle limit.

This correspondence does not hold for an arbitrary value of k^{-1}, such as, e.g., the Compton wavelength of the proton or the μ-meson. In fact the correspondence requirement that the particle described by the Dirac equation (1) be itself one of the family of particles described by (2) restricts the possible values of k to $k_i=\mu_i c/\hbar=z_i/2\omega$, where, from Eq. (4), the z_i are the roots of

$$z_i/4=J_2(z_i)/J_1(z_i). \tag{6}$$

The first two roots of (6) are $z_0=0$, $z_1=6.3801$. The near equality (5) is thus due to the near equality between the smallest positive root of (4) (with $k=mc/\hbar$), i.e., $z_0=0.0235$, and the root $z_0=0$ of (6). One surmises that the shift of this root from zero, i.e., the nonzero mass of the electron and thus the nonzero value of k in Eqs. (1) and (2), may be due to the electromagnetic self-energy correction to the intrinsic mass.

Kemmer[2] has shown that the field equations for spin one and zero may be written in the form (1) with suitable redefinitions of the γ_ν. Since the transition from (1) to (2) in Darling's theory does not depend on the spin character of the equation, Eq. (2) (with redefined γ_ν's) will also describe boson fields, and Eq. (4), with suitable values of k, will give the corresponding mass spectra. The value of k belonging to the root z_1 of (6) is $k_1=6.3801/2\omega=271.5mc/\hbar$, the corresponding mass being

$$\mu_1=271.5m. \tag{7}$$

The latest experimental value of the charged π-meson mass[3] is $275\pm 2m$. Both k_1 and μ_1 are presumably subject to a small upward correction for electromagnetic self energy. The correction in the mass (7) may be expected to be of the order $e^2/\omega c^2\simeq m$, which would make the agreement with the observed pion mass even better. It is suggested, therefore, that Eq. (2) with $k=k_1+(\sim mc/\hbar)$ may be the correct equation for the family of particles having the spin character of the charged π-meson. With this value of k, Eq. (4) has one positive root lower than μ_1: $\mu_0\simeq 132m$. Thus, the theory would predict the existence of a π-type meson of this mass.

I want to express my gratitude to Professor Darling for extensive discussions of his theory.

[1] B. T. Darling, Phys. Rev. **80**, 460 (1950).
[2] N. Kemmer, Proc. Roy. Soc. (London) **A173**, 91 (1939).
[3] R. E. Marshak, private communication.

Energy Spectrum of the Electrons from μ^+ Meson Decay

RYOKICHI SAGANE,* WILLIAM L. GARDNER, AND HARMON W. HUBBARD
Radiation Laboratory, Department of Physics, University of California, Berkeley, California
(Received April 2, 1951)

DECAY electrons of μ-mesons have been studied for several years in cosmic-ray work. From theoretical studies, the process of $\mu^\pm\to e^\pm+2\nu$ is indicated to be the most likely one out of four or five possibilities.[1] Results of the calculations along this line have been given by Tiomno, Wheeler, and Rau.[2]

An attempt to measure the electron energy spectrum is now being made with the use of artificial mesons produced by the proton beam from the 184-in. cyclotron.

The experimental set up for this attempt is shown schematically in Fig. 1. The electrically deflected proton beam from the cyclotron

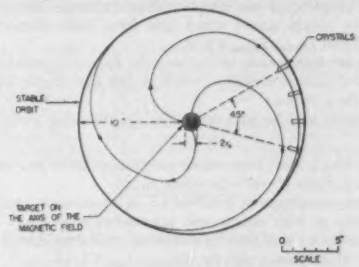

FIG. 1. Experimental arrangement (spiral orbit spectrometer).

was collimated by a 1½-in. hole on the axis of the iron pole pieces of the magnet. The pole pieces are 20 in. in diameter. π^+ mesons are produced by proton bombardment at the target located in between the pole pieces. The targets used are rods: Be, 1½ in.×3 in.; C, ¾ in.×3 in.; Al, 1½ in.×3 in. A considerable part of the π^+ mesons thus produced are expected to remain in the target due to absorption and also partly due to the effect of the applied magnetic field. Then these π^+ mesons are expected to produce μ^+ mesons due to the $\pi\to\mu$ decay process, and again most of the μ^+ mesons are also expected to remain inside of the target because of their low initial energies.

The energy loss for electrons passing through matter is comparatively small when the electron energy is over several million volts. So one can expect a fairly good yield of μ decay electrons coming out of the target.

Electrons of all momenta are produced at the target on the axis of the magnetic field. As shown in Fig. 1, electrons of a certain momentum are focused close to the so-called "stable orbit." This method of focusing has been studied and developed at Tokyo University since 1941 and is entitled the "spiral orbit spectrometer."[3]

Four thin anthracene crystals are used for counting the electrons. They are placed close to the "stable orbit" and are separated by a central angle of 15 degrees from each other. High energy electrons focused close to the orbit will go through all of the crystals and are capable of producing quadruple coincidences. Because of the large number of background pulses, especially immediately after the proton beam pulse, counting has been started usually with a delay of 3 to 5 μsec after each of the beam pulses and continued for the duration of 6 to 10 μsec.

The energy spectrum obtained so far is shown in Fig. 2. The data have been corrected for the resolution curve of the spectrometer which is now being checked.

This curve indicates the closest similarity to the one given by Tiomno, Wheeler, and Rau for the assumption of $\mu^+\to e^++2\nu$ where $m_\nu\simeq 0$ and with tensor coupling in the anti-symmetrical

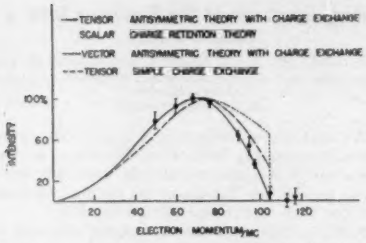

FIG. 2. Observed energy spectrum, and comparison with theory.

theory with charge exchange. However,[4] by using an appropriate linear combination (e.g., vector and pseudovector) of the various forms of coupling in the simple charge exchange theory, it is possible to obtain curves which also have their maximum at $p/mc=70$ and $IE_{max}/II_{max}<1/10$.

Efforts are being made to improve the accuracy, especially for the value of maximum energy, which in turn should give the mass value of the μ-meson.

Our results may be summarized in the following three major points:

1. $E_{max}=53\pm2$ Mev, from which we get $m_\mu=212\pm5m_e$ with the assumptions $\mu^+\to e^++2\nu$ where $m_\nu\cong0$.
2. Intensity maximum at $p=70mc\pm3$ on a momentum scale.
3. Intensity at high energy end approaches zero. That is, the intensity at this limit is indicated to be less than 1/10 of that at $p=70mc$—namely, $IE_{max}/II_{max}<1/10$.

The authors are grateful to Dr. W. Powell for the use of the magnet, and to Dr. W. Barkas for his continuous interest and help throughout the work. Thanks are also due to the crew members of the cyclotron. One of the authors extends his thanks to Professor Lawrence for the privilege of visiting and working at the Radiation Laboratory.

* On leave from Tokyo University, Tokyo, Japan.
[1] B. Pontecorvo, Conference on Elementary Particles, Edinburgh, Nov. 14–16, 1949.
[2] Tiomno, Wheeler, and Rau, Revs. Modern Phys. 21, 144 (1949).
[3] G. Miyamoto, Proc. Phys. Math. Soc. Japan 24, 676 (1942); Proc. Phys. Soc. Japan 17, 587 (1943); M. Sakai, J. Phys. Soc. Japan 5, 178 (1950); R. Sagane and P. C. Giles, Phys. Rev. 81, 653 (1951).
[4] T. A. Green, private communication.

Thermal Neutron Fission of Am^{241}

B. B. CUNNINGHAM AND A. GHIORSO
*Radiation Laboratory and Department of Chemistry, University of California, Berkeley, California**
(Received March 26, 1951)

MEASUREMENTS first performed in 1946 with microgram amounts of Am^{241} indicated a small but definite fission cross section with thermal (i.e., cadmium absorbable) neutrons. These earlier attempts to measure the cross section were inconclusive, because of the small amounts of material available and the inadequate sensitivity of the fission pulse measuring apparatus. Upon the accumulation of larger amounts of Am^{241} and improvement of the fission counting apparatus[1], it became possible in 1947 to measure the cross section more accurately. Since the Am^{241} is produced as the decay product of Pu^{241} in pile plutonium, it is associated initially with a relatively large amount of Pu^{239} and requires very stringent purification.

The purification procedure used by us consisted of the following steps: (a) separation of the bulk of the plutonium by a precipitation process, leaving americium in the supernatant liquid; (b) separation of trace amounts of plutonium by oxidation[2] with argentic oxide to the hexapositive "fluoride soluble" state and precipitation of the americium with lanthanum fluoride carrier; and (c) separation from lanthanum on a cation exchange column, using Dowex 50 and 0.25M citric acid-ammonium citrate solution[3] of pH 3.2.

Half-microgram to one-microgram samples of the purified americium were spread as thin uniform deposits on one-inch diameter platinum disks for fission measurements. These measurements were carried out in the thermal neutron column of the Argonne National Laboratory's heavy water uranium pile at Chicago. The cross sections were measured relative to that of Pu^{239}. In several instances samples were removed from the plates after the first measurements, repurified, and remeasured. No significant differences in the apparent cross section were noted following repurification. The mean value of the cross section, as computed from several measurements, was 3.0 ± 0.2 barns, consistent within the experimental error of the measurements themselves.

We wish to express our appreciation to Dr. W. H. Zinn, who made available to us the facilities of the Argonne heavy water pile, and to Dr. W. M. Manning for permission to utilize the facilities of the Chemistry Division laboratories of the Argonne National Laboratory.

We are particularly grateful to Professor G. T. Seaborg for suggesting the problem and for his interest and advice in connection with the measurements.

* This work was done under the auspices of the AEC.
[1] A. Ghiorso and W. C. Bentley, National Nuclear Energy Series, Plutonium Project Record, Vol. 14B, *The Transuranium Elements: Research Papers*, Paper No. 22.29 (McGraw-Hill Book Company, Inc., New York, 1949).
[2] G. T. Seaborg and A. C. Wahl, J. Am. Chem. Soc. 70, 1128 (1948).
[3] K. Street, Jr., and G. T. Seaborg, J. Am. Chem. Soc. 72, 2790 (1950). The general technique of separation of actinide and lanthanide elements by cation exchange columns is discussed in this paper, but without specific reference to lanthanum–americium separations.

The Uranium Isotope U^{236}

A. GHIORSO,* J. W. BRITTAIN, W. M. MANNING, AND G. T. SEABORG†
Argonne National Laboratory,‡ Chicago, Illinois
(Received April 2, 1951)

FOLLOWING the early observation[1] that U^{235} captures slow neutrons to an appreciable extent in competition with the fission reaction, an attempt was made to detect the expected alpha-particles from the resultant U^{236}, and the negative result led to the placement of a lower limit of 3×10^8 years for this half-life.[2] A little later the isotope U^{236} was detected with the mass spectrograph[3] in a sample of enriched U^{235} which had been irradiated with slow neutrons in the uranium chain reacting pile.

In the summer of 1945 a sample of enriched U^{235} which had been strongly irradiated with slow neutrons became available for measurements of the alpha-radiation. Measurements with the alpha-pulse analyzer apparatus[4] on the chemically purified uranium indicated alpha-particle activity of energy about 4.5 Mev (i.e., slightly greater than that of the main group of U^{238} alpha-particles) with intensity about half as great as that of the U^{235}. This corresponded to an alpha-half-life for U^{236} of about 2×10^7 years. Measurements, a little later, on another sample similarly prepared, containing a different concentration of U^{235}, led to the same result.

This alpha-particle energy corresponds very well with that expected for U^{236} from the systematics of alpha-radioactivity.[5] The half-life is just that expected for a nucleus of atomic number 92 of the even-even type, in which case the decay is not hindered. The isotope U^{236} is, of course, expected to be beta-stable.

* Present address: Radiation Laboratory, University of California, Berkeley, California.
† Work performed under auspices of Manhattan District in 1945 at the then Metallurgical Laboratory (now Argonne National Laboratory).
[1] Wilson, Williams, Segrè, and co-workers, unpublished work at the Los Alamos Scientific Laboratory (1943).
[2] H. Anderson and D. Nagle, Manhattan Project Metallurgical Laboratory Report CP-1389, (February, 1944), p. 10 (unpublished).
[3] D. Williams and P. Yuster, Los Alamos Scientific Laboratory Report LAMS-195 (January, 1945) (unpublished).
[4] Ghiorso, Jaffey, Robinson, and Weissbourd, National Nuclear Energy Series, Plutonium Project Record, Vol. 14B, "The transuranium elements: research papers," Paper No. 16.8 (McGraw-Hill Book Company, Inc., New York, 1949).
[5] Perlman, Ghiorso, and Seaborg, Phys. Rev. 77, 26 (1950).

Water Vapor Absorption Lines in the Solar Spectrum between 8μ and 13μ*

J. H. SHAW AND H. H. CLAASSEN
Ohio State University, Columbus, Ohio
(Received March 26, 1951)

A GRATING map of the solar spectrum from 7 to 14 microns has been published by Adel[1] in which bands of carbon dioxide, ozone, nitrous oxide, water vapor, and HDO were identified. Besides these well-defined bands, other lines of medium and strong intensity occur with no apparent regularity throughout the entire region. Adel[2,3] has suggested that some of these lines are due to atomic transitions, and he has tentatively identified several with transitions between high energy levels of NaI and KI, finding fairly good frequency agreement. Benedict[4] has also found that many of these lines coincide with predicted lines in the water vapor spectrum.

This region of the solar spectrum has recently been remapped at Columbus, Ohio, using a 3600-line/inch grating, and a Perkin-Elmer thermocouple and a thirteen-cycle-per-second amplifier. An improved resolution has been obtained and many new lines discovered, although the main structure closely resembles that observed in the earlier work of Adel. In particular, the intense irregularly spaced lines were again a prominent feature. However, by comparison with a laboratory absorption spectrum, obtained with the same spectrograph, of an eight-meter path of steam at 110°C and near atmospheric pressure, it has now been possible to assign most of these lines definitely to water vapor. This assignment has been further verified by observing that the intensities of the lines in the solar spectrum vary with the amount of water vapor in the atmosphere, being much weaker on cold winter days than during the summer months.

The water vapor lines in this region are too weak to be observed with the absorption path lengths ordinarily used for laboratory spectra. They are intense in the solar spectrum because of the large amount of water vapor in the atmosphere. Most of them are undoubtedly lines arising from transitions between levels of high J values; most of those lying beyond about ten microns are probably pure rotational lines, while those at shorter wavelengths are lines of the ν_2 fundamental at 6.3μ.

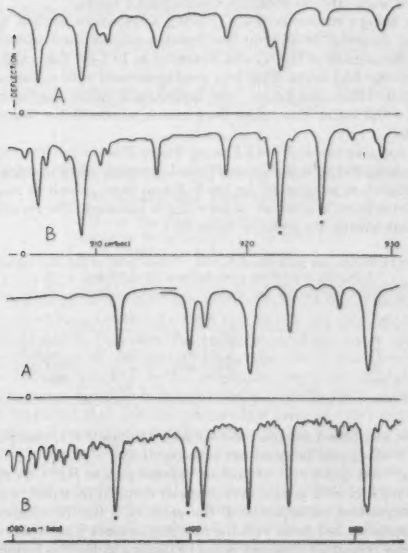

FIG. 1. Portions of the spectrum of an eight-meter path of steam at 110°C and corresponding portions of the solar spectrum. A. Water vapor spectrum. B. Solar spectrum.

In Fig. 1 two portions of these spectra are shown. The upper curves are parts of the laboratory spectrum of steam, and the lower curves are parts of the solar spectrum of the same regions. The lines which Adel tentatively identified as atomic in origin are marked with dots. The relative intensities of the water lines in the two spectra are sometimes different, and the lines are sharper in the solar spectrum. This is to be expected, since the steam was at 110°C which is considerably higher than the average temperature of the water vapor in the atmosphere.

With the identification of these water vapor lines in the solar spectrum, it is now believed that all the structure in the 8–13μ region of this spectrum, with the possible exception of some weak lines, is due to the known atmospheric gases, water vapor, carbon dioxide, ozone, methane, and nitrous oxide.

A more complete description of both the solar spectrum and the water vapor spectrum between 7μ and 13μ is being prepared for publication.

* This work was supported in part by a contract between the U. S. Air Force and the Ohio State University Research Foundation, through sponsorship of the Geophysical Research Directorate of the Air Force Cambridge Research Laboratories.

[1] A. Adel, Astrophys. J. 94, 451 (1941).
[2] A. Adel, Astrophys. J. 94, 449 (1941).
[3] A. Adel, *The Atmospheres of the Earth and Planets* (University of Chicago Press, Chicago, Illinois, 1949), p. 269, edited by G. P. Kuiper.
[4] W. S. Benedict, Symposium on Molecular Structure and Spectroscopy, The Ohio State University, Columbus, Ohio, June, 1950.

Evidence for an Excited State of He[5]*

WALLACE T. LELAND AND HAROLD M. AGNEW
Los Alamos Scientific Laboratory, Los Alamos, New Mexico
(Received April 5, 1951)

A RECENT investigation of the energy spectrum of neutrons produced in the reaction of tritons with tritons has revealed two distinct groups of neutrons. These neutron groups are most reasonably accounted for by the assumption they arise from the reactions:

(a) $T+T \rightarrow He^5+n+10.53$ Mev;
(b) $T+T \rightarrow He^{5*}+n+7.9$ Mev.

The experiment consisted of bombarding tritium gas with tritons accelerated by the Los Alamos 2.5-Mev electrostatic generator. The neutrons were detected at 0° by means of 200-micron, Ilford C-2 photographic plates. The triton energy in the gas target varied from 906 kev to 426 kev due to target thickness. Recoil proton tracks within a cone of 10° centered around 0° were measured in the photographic emulsion. The neutron energy distribution shown in Fig. 1 was obtained after applying the known range-energy relationships in this type of emulsion and the $(n-p)$ cross section. A correction was made for the range dependence of the number of tracks which leave the emulsion. Although plotted every 250 kev, the points actually are computed on the basis of the relative number of neutrons per 500-kev

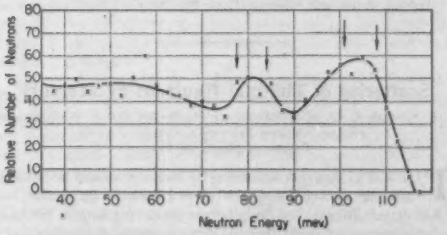

FIG. 1. Energy spectrum of neutrons from T+T reaction.

interval. The statistical uncertainty is about 15 percent. A background plate, obtained under identical conditions by accelerating tritons into the same target filled with He^4, indicated that the number of background neutrons over the complete spectrum was less than 1 percent.

One notices in Fig. 1 that two broad peaks appear at 10.4 and 8.1 Mev. We attribute these peaks to reactions (a) and (b), respectively. The corresponding ground state peak (a) has also been observed in the neutron spectrum obtained by Sanders, *et al.*[1] Although the variation of the incident triton energy was large, the high Q of the reaction greatly reduces the effect of the energy variation on the peak widths. The lines bracketing the peaks in Fig. 1 indicate the extent of peak broadening to be expected from the spread of incident triton energy. The remainder of the peak width is readily attributed to the finite resolution of the neutron detection system. The remainder of the neutrons are presumed to arise from various other possible reactions such as:

(c) $T+T \rightarrow He^4+n+n+11.4$ Mev;
(d) $T+T \rightarrow He^4+n^2+Q$;
(e) $He^5 \rightarrow He^4+n+0.87$ Mev;
(f) $He^{5*} \rightarrow He^4+n+3.5$ Mev.

Reactions (e) and (f) represent the disintegration of the unstable He^5 formed in reactions (a) and (b). The occurrence of special interactions in the three particle disintegration could conceivably produce energy groups in the neutron spectrum. However, we feel that this possibility is a considerably less likely source of groups than the reactions (a) and (b). The greatest neutron energy expected from reactions (d), (e), and (f) occurs in reaction (f) and is less than 6.2 Mev. Consequently, these reactions would not contribute to the observed neutron energy groups at 10.4 Mev and 8.4 Mev.

The idea of He^5 having an excited state in the vicinity of 2.6 Mev above its ground state is not new nor inconsistent with previous results. As suggested by Goldstein,[2] a $P_{1/2}$ level above a $P_{3/2}$ ground state could provide satisfactory agreement between theory and the existing data on the low lying levels of He^5 as obtained from n-He^4 scattering.[3-6] Adair[7] reports that his analysis of the n-He^4 total cross-section measurements of Bashkin *et al.*[8] indicates the existence of a widely spaced inverted doublet in He^5.

The authors wish to express their appreciation for the advice given to them by Dr. Louis Rosen and for the analysis of the photographic plates by Dr. Alice Armstrong and Mrs. May Bergstresser.

* Work performed under the auspices of the AEC.

[1] Sanders, Allen, Almquist, Dewan, and Pepper, Phys. Rev. **79**, 238 (1950).
[2] H. Goldstein, Phys. Rev. **79**, 740 (1950).
[3] H. Staub and H. Tatel, Phys. Rev. **58**, 820 (1940).
[4] H. H. Barschall and M. H. Kanner, Phys. Rev. **58**, 590 (1940).
[5] T. A. Hall and P. R. Koontz, Phys. Rev. **72**, 196 (1947).
[6] T. A. Hall, Phys. Rev. **77**, 411 (1950).
[7] R. K. Adair, private communication.
[8] Bashkin, Petrie, and Mooring, Phys. Rev. **82**, 378 (1951).

Scattering of Thermal Neutrons by Mercury

C. T. Hibdon, C. O. Muehlhause, G. R. Ringo, and T. R. Robillard
Argonne National Laboratory, Chicago, Illinois
(Received March 26, 1951)

THERMAL neutron scattering by mercury should be strongly affected by the resonance[1] at -2.0 ev. In particular, one would expect a large positive coherent scattering length. We have recently measured three thermal cross sections of mercury: σ_{coh} (coherent scattering), $\sigma_{th\text{-}s}$ (total scattering), and $\sigma_{th\text{-}a}$ (absorption). In addition, we have measured the potential scattering cross section, σ_p, near thermal (19.5 ev). These data have been used to calculate the -2.0 ev resonance parameters in Hg^{199} in an attempt to assign a compound angular momentum value (J) to the capturing level.

The coherent scattering cross section is not easily measured by crystal diffraction schemes because of the high thermal absorption cross section (370b). Instead, it was measured by finding the critical wavelength for reflection of a beam of thermal neutrons incident on a surface of liquid mercury at a given angle. Observations were made at two angles, using a time-of-flight velocity selector.[2] An additional observation was made at a third, larger angle by comparison of intensities with the first two angles. The critical wavelength and the angle determine the index of refraction, which in turn determines the coherent scattering amplitude.[3] Results are given in Table I. From this it can be seen that mercury

TABLE I. Observed coherent scattering cross section of Hg for thermal neutrons.

Angle (min)	Wavelength (angstroms)	σ_{coh} (barns)
8.29	1.84	22.1
12.25	2.63	24.8
20.22	4.70	18.4
		av 21.5 ± 2

makes a particularly good neutron mirror. The surface is easy to prepare and is stable for at least several days with only ordinary care.

It is appropriate to take an average value of σ_{coh} since no energy dependence is to be expected, and none is observed.

Measurement of $\sigma_{th\text{-}s}$ was done with the use of a 4π-annular neutron scattering counter.[4] The counter is provided with an axial hole through which a neutron beam from the pile may pass. A scattering material is placed transverse to the beam on the axial center of the counter. Known thicknesses of gold-mercury amalgam and vanadium metal foil were placed separately in the counter, and their counting rates compared. The effect of gold scattering was subtracted after observing the counting rate from a gold foil of the same thickness as that used in the Au-Hg amalgam. Vanadium was chosen as a standard ($\sigma_{th\text{-}s} = \sigma_{inc} = 5.00$ barns) since thermal neutron scattering from vanadium is almost entirely incoherent.[5] This and the mercury amalgam minimize diffraction effects. $\sigma_{th\text{-}s}$ (Hg) so obtained was 26.5 ± 0.1 barns.

By using a resonance beam, placing a resonance neutron scattering detector[6] of W^{186} in the annular counter, and observing the transmission of Hg, σ_p was measured at 19.5 ev. The value obtained was 13.3 barns. This is in good agreement with σ_p measurements at 120 ev and 350 ev.[7] The thermal absorption cross section, $\sigma_{th\text{-}a} = 370$ barns, was taken from recent pile-oscillator measurements.[8]

If one assumes $4\pi R^2 = 13.3$ barns where R is the nuclear radius (spin independent and identical for all isotopes), one can calculate the resonance parameters for the -2.0-ev level as well as σ_{coh}. A one-level Breit-Wigner set of formulas is assumed. The results of this calculation are given in Table II.

TABLE II. Resonance parameters for the -2.0-ev level of Hg, and calculated coherent scattering cross section, for $J=0$ and $J=1$.

	$J=0$	$J=1$
Γ_n	0.053 ev	0.027
Γ_γ	0.225 ev	0.149
Γ	0.278 ev	0.176
σ_{coh}	17.1	20.0

One sees here a definite preference for the case $J=1$, though the case $J=0$ cannot be ruled out with certainty.

Hg^{199} has spin $\frac{1}{2}$ and on neutron capture goes to Hg^{200}, an even-even nucleus with ground-state angular momentum equal to zero. An interesting consequence of the value of J for the compound capture state had to do with the resulting cascade γ-ray spectrum. A γ-ray transition of energy equal to binding in Hg^{200} is forbidden for $J=0$ and allowed for $J=1$. Furthermore, the first transition in the cascade is usually of sufficient energy that no other γ-ray will

be likely to be confused with the total transition. B. Hamermesh reports no structure in the high energy end of the capture γ-ray spectrum of mercury.[9] This would indicate $J=0$ for the capture state, since in cases where the total transition is allowed, it is observed to be 10 to 20 percent of the total intensity. The present work, however, favors $J=1$.

[1] W. W. Havens and J. Rainwater, Phys. Rev. 70, 154 (1946).
[2] T. Brill and H. V. Lichtenberger, Phys. Rev. 72, 585 (1947).
[3] E. Fermi and L. Marshall, Phys. Rev. 71, 666 (1947).
[4] Harris, Langadorf, and Seidl, Phys. Rev. 72, 866 (1947).
[5] M. Hamermesh and C. O. Muehlhause, Phys. Rev. 78, 175 (1950).
[6] Harris, Muehlhause, and Thomas, Phys. Rev. 79, 11 (1950).
[7] C. T. Hibdon and C. O. Muehlhause, Phys. Rev. 76, 100 (1950).
[8] Harris, Muehlhause, Rasmussen, Schroeder, and Thomas, Phys. Rev. 80, 342 (1950).
[9] B. Hamermesh, Phys. Rev. 80, 415 (1950).

On the Viscosity of Gaseous He^3

OTTO HALPERN
University of Southern California, Los Angeles, California
(Received April 4, 1951)

THE effect of the similarity of particles on their gas-kinetic properties was studied[1] some time ago and in particular, attention was drawn to the influence exerted by the presence of nuclear spins. Since then, the discovery of He^3 has offered an opportunity to apply these theoretical concepts (with proper modifications) to a case in which sizable effects may well be observed rather conveniently.

If we denote collision cross sections for particles with symmetric or antisymmetric wave functions of their relative motion by σ_S and σ_A, respectively, and the corresponding cross section for the collision of two otherwise equivalent but *dissimilar* particles by σ_D, then one can easily show that $\sigma_S+\sigma_A=2\sigma_D$. In the case of He^3, the cross section for the collision of two atoms is, obviously,

$$\tfrac{1}{4}\sigma_S+\tfrac{1}{4}\sigma_A=\sigma_D-\tfrac{1}{2}(\sigma_S-\sigma_D).$$

Since[2] $\sigma_S>\sigma_D$ we find that the nuclear spin of He^3 raises the viscosity of He^3 with respect to He^4 very appreciably (quite apart from the influence of the masses).

We shall present the quantitative details of this effect and some related phenomena in a following paper.[3]

[1] O. Halpern and E. Gwathmey, Phys. Rev. 52, 944 (1937).
[2] Mott and Massey, *Theory of Atomic Collisions* (Oxford University Press, London, 1933), p. 231.
[3] Figure 1 on p. 951 of reference 1 was based on the assumption, since discarded, that a nucleus of even (odd) Z follows Bose (Fermi) statistics, and has therefore to be replaced by a different diagram.

Further Evidence for a Two Quantum Transition in Molecular Spectroscopy*

LUDWIG GRABNER AND VERNON HUGHES
Columbia University, New York, New York
(Received March 27, 1951)

IT has been pointed out[1] that an extra line group was observed in a study by the molecular beam electric resonance method of transitions between the electrical quadrupole hyperfine structure levels of $Rb^{85}F$. This extra line group occurred exactly at one-half the frequency of the normal transition $(J=1,\ F_1=\frac{3}{2})\rightarrow(J=1,\ F_1=7/2)$, in which $\mathbf{J}$ is the molecular rotational angular momentum and $\mathbf{F}_1=\mathbf{I}_1+\mathbf{J}$, $\mathbf{I}_1$ being the spin of the Rb^{85} nucleus. It was suggested that this line group might arise as a two quantum transition in which two half-frequency quanta supply the energy for the transition. The theory of this two quantum transition was presented as a second-order time-dependent perturbation.

A simple extension of this theory indicates that the two quantum transition should be observed if two separate frequencies (f_1 and f_2) are applied, provided $f_1+f_2=\Delta E/h$, in which ΔE is the energy difference associated with the normal transition. We arranged experimentally to apply two frequencies in the C-field region and did indeed observe the peak of the zeroth vibrational line to occur as predicted. The pairs of frequencies at which this transition occurred are indicated in Table I. The rf field intensity associated both with f_1 and f_2 was ~4 volts/cm. A weak static C-field of ~14.2 volts/cm was applied. The frequency for the normal transition is 6.328 Mc/sec and for the extra line 3.160 Mc/sec.

TABLE I.

f_1 Mc/sec	f_2 Mc/sec	f_1+f_2 Mc/sec
3.928	2.400	6.328
3.828	2.500	6.328
3.628	2.700	6.328
3.528	2.800	6.328

It was observed further that, with $f_1=3.528$ Mc/sec and $f_2=2.800$ Mc/sec and the rf field intensities as above, the line intensity increased by a factor of two when the static field was reduced from 14.2 volts/cm to 2.0 volts/cm, and the line was present at the higher intensity when no static field was applied. This increase in line intensity is in qualitative agreement with the theory; no adequate quantitative theory of line intensities has been worked out. Also, the presence of the line at zero applied static field, which we were not able to observe previously, is strong evidence in support of the two quantum theory. No known change was made in the apparatus which would account for our present success in observing the line at zero static field; it is likely that whether or not the line is present at zero static field depends critically upon interfield conditions because of nonadiabatic transitions, and these conditions are not easily controllable.

It is still not understood why other half-frequency lines are not observed. Further search was made with higher rf field intensities (from 5 to 15 volts/cm) at static fields from 0 to 8 volts/cm for half-frequency lines in the spectrum of $Rb^{85}F$, $Rb^{87}F$, and $K^{39}F$, but with negative results.

* This research has been supported in part by the ONR.
[1] V. Hughes and L. Grabner, Phys. Rev. 79, 314 (1950); V. Hughes and L. Grabner, Phys. Rev. 79, 829 (1950).

Threshold for Photoneutron Reaction in U^{238}

J. R. HUIZENGA, L. B. MAGNUSSON, P. R. FIELDS, AND M. H. STUDIER
Argonne National Laboratory, Chicago, Illinois
AND
R. B. DUFFIELD
Physics Research Laboratory, University of Illinois, Champaign, Illinois*
(Received April 3, 1951)

RECENT experimental neutron binding energy measurements[1] in the region of lead give energy differences between the radioactive series. Additional binding energy measurements to bridge the radioactive series in the region of uranium would serve as valuable checks in closing energy cycles. The binding energy of a neutron in U^{238} is of particular interest, since some uncertainty exists in the energy difference between the $4n+1$ and $4n+2$ radioactive series.[2]

X-rays produced by the 22-Mev betatron at the University of Illinois were used to measure the threshold for the photoneutron reaction $U^{238}(\gamma, n)U^{237}$. The energy scale is determined relative to the threshold for the 10-minute activity from the $Cu^{63}(\gamma, n)Cu^{62}$ reaction which is taken as 10.9 Mev. The experimental arrangements are similar to those described elsewhere.[3]

Five 150-mg samples of uranium oxide were bombarded at different energies in a probe inside the x-ray donut for periods of time ranging from four to thirty-four hours. The uranium was depleted in U^{234} and U^{235} to decrease neutron fission activity and to reduce the growth of the 25-hour UY activity after chemical purification. The bombarded uranium was chemically purified to constant specific activity. Fifty-mg samples of U_3O_8 were prepared for counting by repeatedly painting and igniting many small portions of an organic uranium solution. The U^{237} activity was measured with a thin-window helium-filled Geiger tube with

sufficient aluminum absorber to cut out the uranium alpha-particles. The U^{237} counting rate was determined by using the least squares method to extrapolate the linear growth curve of the uranium daughters to an accurately controlled zero time (time of chemical purification). Such extrapolations with similar unirradiated uranium gave a background of 2 c/min (above counter background). The counting rate of U^{237} for each sample varied from 6 to 100 c/min. This activity decayed with a 6.6-day half-life.

The excitation function could be approximated by a parabola; hence it was possible to estimate the threshold from a linear extrapolation of the square root of the U^{237} yield plotted as a function of x-ray energy. The results are shown in Fig. 1, where

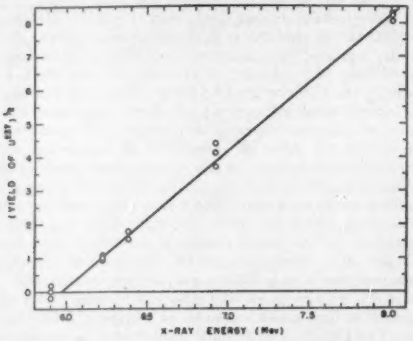

FIG. 1. Square root of the U^{237} yield plotted as a function of x-ray energy.

the yield is expressed in c/min of U^{237} for 50 mg of U_3O_8 given constant bombardment. Analysis of the data gives a threshold of 5.97 ± 0.10 Mev for the $U^{238}(\gamma, n)U^{237}$ reaction.

British workers[4] obtained a neutron emission threshold of 5.85 ± 0.15 Mev for natural uranium by an indirect measurement of the neutrons produced in photodisintegration. As Parsons and Collie[4] point out, their method of measurement does not yield a clearly defined threshold since the end product is not identified, and the source of the neutrons is uncertain. However, the close agreement between the two values leads one to believe that they were measuring the neutrons from the $U^{238}(\gamma, n)U^{237}$ reaction.

* This work was supported in part by the joint program of the AEC and ONR.

[1] J. A. Harvey, Phys. Rev. **79**, 241 (1950); H. Palevsky and A. O. Hanson, Phys. Rev. **79**, 242 (1950); Kinsey, Bartholomew, and Walker, Phys. Rev. **78**, 77 (1950).

[2] Huizenga, Magnusson, Simpson, and Winslow, Phys. Rev. **79**, 908 (1950).

[3] McElhinney, Hanson, Becker, Duffield, and Diven, Phys. Rev. **75**, 542 (1949).

[4] R. W. Parsons and C. H. Collie, Proc. Phys. Soc. (London) **63A**, 839 (1950).

Lithium Ammonium Tartrate Monohydrate, A New Ferroelectric Crystal*

WALTER J. MERZ
Department of Physics, Pennsylvania State College, State College, Pennsylvania

(Received March 26, 1951)

IN an investigation of the electrical properties of a series of tartrates we have found that $LiNH_4C_4H_4O_6 \cdot H_2O$ is ferroelectric. (In a private communication to the author, Matthias has reported his parallel discovery of the ferroelectric behavior of this crystal.[1]) It appears that isomorphous salts such as LiRb- and LiTl-tartrate·H_2O are also ferroelectric. The electrical behavior of the $LiNH_4$ salt is reported in the present letter.

The crystals are orthorhombic, and the dielectric constants in all three axial directions are small (between 8 and 10) at room temperature. Upon lowering the temperature, ϵ_a and ϵ_c remain essentially constant, whereas ϵ_b shows a sudden and sharp peak at about 106°K (Fig. 1). Below this temperature we find a spontaneous electric polarization which establishes this transition as a Curie point (Θ).

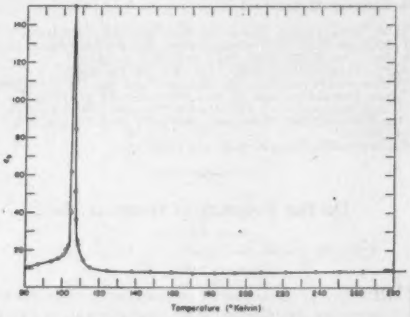

FIG. 1. Dielectric constant ϵ_b *versus* temperature.

The hysteresis loops (Fig. 2) show the onset of a spontaneous

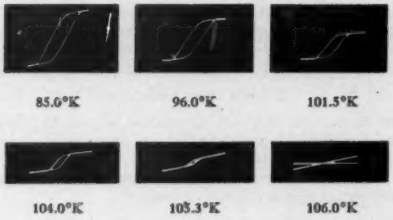

FIG. 2. Hysteresis loops *versus* temperature.

polarization P_s at the Curie point and its increase when the temperature is lowered. The saturated value at low temperatures is about $P_s = 0.21\times10^{-6}$ coulomb/cm².

The crystal is strongly piezoelectric, with a modulus d_{25} of about 20×10^{-8} cgs at room temperature. The piezoelectric resonance frequencies show the usual sharp minimum at the Curie point (Fig. 3). Using these measurements of the dielectric constant

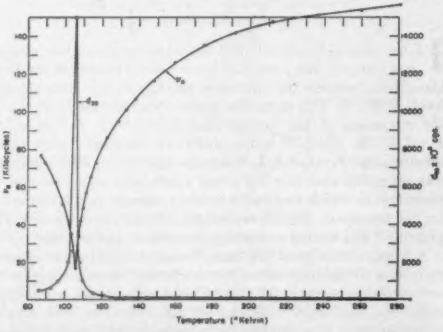

FIG. 3. Resonance frequency and piezo constant d_{25} *versus* temperature.

ϵ_0 and the resonance frequency ν_R, the calculations for the piezoelectric modulus d_{25} show a sharp increase at low temperature, with a peak value at Θ of about 10,000 to 20,000$\times 10^{-8}$ cgs (Fig. 3).

Though $LiNH_4C_4H_4O_6 \cdot H_2O$ is related crystallographically and chemically to rochelle salt ($KNaC_4H_4O_6 \cdot 4H_2O$) and shows typical ferroelectric properties, we observe the following principal differences. The ferroelectric direction is along the b-axis in the $LiNH_4$ salt, whereas in rochelle salt it is along the a-axis. There is just one molecule of water of crystallization, instead of the four as in rochelle salt. It appears that there is no lower Curie point in the $LiNH_4$ salt, again in contrast with the behavior of rochelle salt.

An x-ray analysis of the $LiNH_4$ salt is in progress, in order to establish the dependence of the ferroelectric direction upon the molecular arrangement, the position and role of the water molecule, and if possible the nature of the structural transition at the Curie point. Crystallographic and electrical properties of other members of this group of tartrates are also under examination.

The author wishes to thank Professor Ray Pepinsky and members of his solid-state group for support of this program.

* This investigation is part of a program supported by the Office of Air Research.

[1] B. T. Matthias and J. K. Hulm, Phys. Rev. 82, June 1 (1951).

Energy Levels of a Vector Particle in a Pure Coulomb Field*

K. M. Case† and A. M. L. Messiah
University of Rochester, Rochester, New York
(Received April 5, 1951)

In a recent paper[1] one of the authors showed that the Schrödinger equation for a hamiltonian with a singular potential can be made to yield a complete orthonormal set of solutions. In addition to the usual condition of quadratic integrability, the wave function is required to have a fixed behavior at the origin. This behavior is conveniently described by prescribing a phase β. Since the choice of β is rather arbitrary, it is of interest to know how sensitively the resulting spectrum depends on this parameter.

In a relativistic problem there is always some value of β which will give a bound state corresponding to any fixed energy between $\pm mc^2$. One really wants to know if it is only for a small range of phases that the spectrum varies considerably. This has been found true[1] for Dirac and Klein-Gordon particles in fields such that $\alpha Z \gtrsim 1$ or $\frac{1}{2}$, respectively. To investigate this further we have considered the energy levels for a vector particle in a pure coulomb field. It has been shown[1] that the phase method does apply to this problem.

Since the exact numerical determination of the energy levels for a given β would be extremely difficult in the vector case, we have attempted to obtain approximate values for the deepest levels and their dependence on phase by means of the variation principle

$$\delta M = 0; \quad M = (\Psi|\tau_3 H|\Psi)/(\Psi|\tau_3|\Psi). \tag{1}$$

We will use the same notation and units as in the paper referred to above. The stationary values of M are the desired eigenvalues. While the method has only been used for a weak coulomb field ($\alpha Z \ll 1$), no practical restriction results since the finite size of the nucleus will certainly eliminate the singularity for any other case. The best trial functions independent of β were found to be:

$$F_1 = (q+1)r^s \exp(-\tfrac{1}{2}\rho r), \quad G_2 = (q-1)r^s \exp(-\tfrac{1}{2}\rho r),$$
$$F_2 = \frac{(\epsilon^2+\alpha Z r)F_1 - rG_2'}{1+r^2/j(j+1)}, \quad G_2 = \frac{(\epsilon^2+\alpha Z r)G_2 - rF_1' - F_1}{1+r^2/j(j+1)}, \tag{2}$$

depending on the parameters ϵ, ρ, s, q.

Varying with respect to ϵ gives $\epsilon = M$. Assuming ρ to be of order αZ and expanding M in powers of αZ makes it possible to extremise with respect to ρ, s, q.

It was found that there are two values of q for which M is extremal. Denoting these by $q_{\min}$ and $q_{\max}$ the results may be expressed as:

$$q_{\min} = 2j(j+1) - (2j+1); \quad s = j; \quad \rho = 2\alpha Z/j;$$
$$M_{\min} \cong 1 - (\alpha Z)^2/2j^2, \tag{3}$$
$$q_{\max} = 2j(j+1) + (2j+1); \quad s = j+2; \quad \rho = 2\alpha Z/(j+2);$$
$$M_{\max} \cong 1 - (\alpha Z)^2/2(j+2)^2. \tag{4}$$

Comparing with the behavior of the exact wave function we see,

(a) Since $\epsilon = M$, the connection of F_2, G_1, with F_1, G_2 is correct.

(b) The exponential decrease $[\exp -(1-M^2)^{\frac{1}{2}}r]$ at infinity is correct.

(c) The behavior at the origin is wrong since the exact wave function is either strongly vanishing ($\sim\psi = \exp[-\lambda/r^k]$) or strongly oscillatory ($\sim\varphi = \cos[\lambda/r^k + \beta]$).

Improving the wave function by inserting a factor of ψ or φ into the expression for F_1 and G_2 gave: (1) with ψ the same result (3) and (4) as above; (2) with φ the same result (3) and (4) as above, except for $\beta = \pi/2 + O(\alpha Z)$. For $\beta = \pi/2$, deeper levels were obtained.

These results seem to indicate that, except for a small range of β of order αZ, the energy levels of a vector particle in a coulomb field are to order αZ the same as those given by the nonrelativistic theory. The shift of levels due to magnetic and relativistic effects is of higher order[2] in αZ just as in the case of spin 0 and $\frac{1}{2}$ particles.

To check these conclusions the relative amounts of $l = j+1$ and $l = j-1$ states present in the bound states were computed. With the above trial functions the lowest state corresponding to $M_{\min}$ was found to be almost entirely $l = j-1$, while $M_{\max}$ corresponded to a predominant $l = j+1$ state.

* This work was supported by the joint program of the ONR and AEC for one of the authors (K.M.C.) and by the Direction des Mines et de la Siderurgie (Paris) for the other (A.M.L.M.).

† Now at the Randall Laboratory of Physics, University of Michigan, Ann Arbor, Michigan.

[1] K. M. Case, Phys. Rev. 80, 797 (1950).
[2] Compare with A. Simon, Phys. Rev. 76, 1877 (1949).

On the Phase Transition of Tungsten Trioxide

Ryuzo Ueda and Takeo Ichinokawa
Department of Applied Physics, Waseda University, Tokyo, Japan
(Received March 26, 1951)

In a previous letter,[1] we described the optical and x-ray studies on the domain structure of tungsten trioxide, WO_3. Although WO_3 behaves like a ferroelectric, having high dielectric constants and domain structure similar to that of $BaTiO_3$, it was unknown at that time whether WO_3 shows a ferroelectric transition at a certain temperature (the Curie point) or not.

The present authors proceeded with the x-ray study on the lattice transformation of this crystal at higher temperatures, and found that it transforms into the tetragonal lattice from the orthorhombic one between 700°C and 750°C (Fig. 1). This

Fig. 1. X-ray powder photographs of WO_3 using Cu K_α radiation. (a) Orthorhombic lattice at 700°C; (b) tetragonal lattice at 750°C.

transformation seems to correspond to the disappearance of the domain patterns at nearly the same temperature, which were recently observed microscopically by Sawada.[2]

The lattice constants of WO_3 calculated from Debye lines are plotted in Fig. 2, in which it is seen that a and b expand linearly with temperature in the orthorhombic region up to about 700°C, where an abrupt phase change occurs and the crystal becomes tetragonal, resulting in $a=b$. The lattice constant c shows a similar linearity in both phases, accompanying a discontinuous

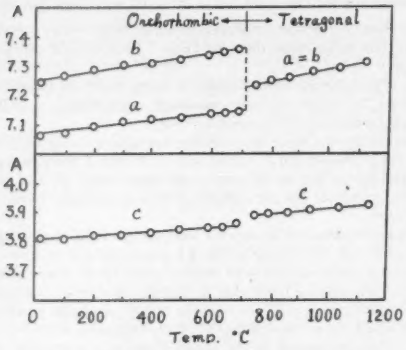

FIG. 2. Lattice constants vs temperature curve of WO_3.

change at the transition temperature, which is, however, considerably smaller than the others. Above the transition temperature, the tetragonal lattice persists up to about 1100°C. It is uncertain at the present stage, however, whether or not WO_3 has another phase change (tetragonal⇄cubic) above this temperature.

It has been observed, by the dilatometer and specific heat measurements recently performed by us, that there exists a sharp contraction in volume and a fairly large energy change at about 720°C. Detailed x-ray studies to detect the minute change in the neighborhood of the transitional region by means of a back reflection method are now in progress.

The disappearance of the domain patterns at about 700°C when viewed parallel to the c-axis under the microscope may be explained easily by considering that twinning planes {110} disappear, since the lattice parameters a and b coincide with each other. Dielectric studies will be required to reveal the ferroelectric transition of this crystal at about 720°C, but they will be exceedingly difficult on account of its semiconductive properties at higher temperatures.

The details of the investigation will be published elsewhere.

The authors wish to express their sincere thanks to Professor S. Miyake for his encouragement in the course of the study, and also to Mr. S. Sawada for his kind information.

[1] R. Ueda and T. Ichinokawa, Phys. Rev. **80**, 1106 (1950).
[2] S. Sawada (unpublished).

Cloud-Chamber Analysis of Stopped Particles in the Sea-Level Cosmic Radiation*

G. M. NONNEMAKER AND J. C. STREET
Lyman Laboratory of Physics, Harvard University, Cambridge, Massachusetts
(Received March 26, 1951)

A WILSON cloud chamber beneath a filter of 119 g cm^{-2} lead plus 21 g cm^{-2} lead-equivalent and above an absorber of 81 g cm^{-2} lead plus 7 g cm^{-2} lead-equivalent was expanded by an anticoincidence arrangement which selected particles stopping in the absorber (see Fig. 1). The momentum was determined from the track curvature in a magnetic field of about 4300 gauss. The specific ionization was estimated from the density of droplets along the track as compared with minimum ionization tracks. From these two quantities, particles occurring singly were identified as electrons, mesons, or protons. Although pi-mesons were indistinguishable from mu-mesons in this experiment, as is seen

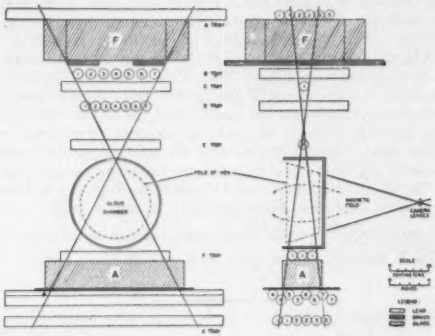

FIG. 1. Experimental arrangement. The cloud chamber was expanded by the event $(A\ B_a\ C\ D_a\ E\ F\text{-}X)$.

below, the momentum cutoff indicates that the mesons are predominantly mu-mesons, as is expected.

A total of 348 pictures were taken at an average rate of 0.0159 count/min. Of these, 227 were mu-mesons, 10 were dense tracks with momenta greater than 250 Mev/c, 23 were energetic particles which failed to trigger the anticoincidence tray beneath the absorber, 15 were single electrons with momenta less than 70 Mev/c, and 73 were other electronic events such as showers and knock-on processes which triggered the proper sequence of counters.

By assuming that the telescope counting rate of (0.503 ± 0.003) count/min is due entirely to the hard component,[1] the absolute intensity of mesons stopping within the differential range interval of this experiment was found to be $(3.26\pm0.23)\times10^{-6}$ g^{-1} sec^{-1} sterad^{-1} (air-equivalent) for mesons with a range of 115 g cm^{-2} (air-equivalent).[2,3] The intensity has been corrected by +7 percent for mesons lost by scattering and magnetic deflection, by +3 percent for the difference in angular distribution between the hard component and the slow mesons,[2] by −10 percent for the effective increase of the lead absorber as a result of multiple scattering,[4] and by −8 percent for the inclusion of single electrons which could not be distinguished from mu-mesons in the momentum interval 70 Mev/c to 160 Mev/c.

The ratio of positive to negative mesons stopping in the absorber was 0.94 ± 0.07.

The observed differential distribution in momentum of the stopped mesons (see Fig. 2) had a low intensity tail extending beyond the expected vertical cutoff of 216 Mev/c to about 400 Mev/c probably as a result of multiple scattering in the absorber. The upper cutoff in momentum as determined from this distribution gave a meson mass of 220 ± 12 electron masses. A mass determination was not made from the lower cutoff in momentum because the thickness of material penetrated was not known to better than 10 percent.

The 10 particles which formed dense tracks were all positively charged. One of them was identified as an alpha-particle (or heavier nucleus). The remaining nine particles had mass values which ranged from 900 to 2000 electron masses. However, since the

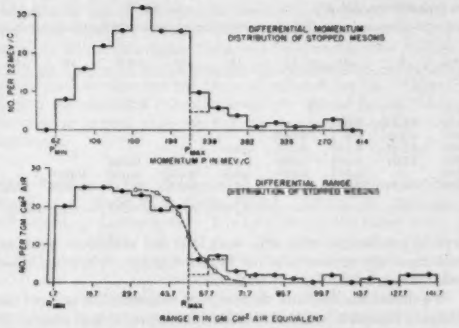
DIFFERENTIAL MOMENTUM DISTRIBUTION OF STOPPED MESONS
NO. PER 23 MEV/C
MOMENTUM P IN MEV/C
DIFFERENTIAL RANGE DISTRIBUTION OF STOPPED MESONS
NO. PER 10M GM/CM² AIR
RANGE R IN GM/CM² AIR EQUIVALENT

FIG. 2. Momentum and range distribution of stopped mesons. The range distribution was obtained by transforming the momentum distribution under the assumption of a mu-meson mass of 216 electron masses.

errors were difficult to evaluate, all that can be said at present is that they are probably protons. If the technique can be significantly improved, a similar experiment will be undertaken in order to obtain more accurate mass determinations.

*This work was supported in part by the joint program of the ONR and AEC.

[1] B. Rossi, Revs. Modern Phys. **20**, 537 (1948).
[2] W. L. Kraushaar, Phys. Rev. **76**, 1045 (1949).
[3] L. Germain, Phys. Rev. **80**, 616 (1950).
[4] H. P. Koenig, Phys. Rev. **69**, 590 (1946).

Theory of Antiferromagnetic Resonance

C. KITTEL
Bell Telephone Laboratories, Murray Hill, New Jersey
(Received April 2, 1951)

WE calculate the frequencies associated with magnetic dipole transitions in an antiferromagnetic crystal, extending to dynamic effects the Van Vleck theory of antiferromagnetism, which works remarkably well for static effects. The model is that of two sublattices of magnetization $\mathbf{M}_1$, $\mathbf{M}_2$ oppositely directed and each of magnitude M_s. The calculation given here is classical; a quantum calculation following the method used by Van Vleck[1] in ferromagnetic resonance has been made and will be discussed in a subsequent publication.

The exchange forces are treated as molecular fields $\mathbf{H}_1=-\lambda\mathbf{M}_2$, $\mathbf{H}_2=-\lambda\mathbf{M}_1$ acting on the sublattices 1 and 2. It is known that there are preferred directions of orientation in antiferromagnetic crystals, and in analogy to ferromagnetism we introduce an anisotropy energy density constant K to describe the energy involved in turning both spin systems together relative to the crystal lattice. We may then, for small deflections, say that there is an anisotropy field $H_A=K/M_s$ acting on each sublattice. We take the static field H_0 and the preferred axis to be in the z-direction. We suppose that the crystal consists of a single domain and is spherical in shape, so that demagnetizing effects do not enter.

The equations of motion with a transverse rf field are

$$d\mathbf{M}_1/dt=\gamma\mathbf{M}_1\times[(H^x-\lambda M_2{}^x)\mathbf{i}+(H^y-\lambda M_2{}^y)\mathbf{j}+(H_0+H_A+H_E)\mathbf{k}];$$

$$d\mathbf{M}_2/dt=\gamma\mathbf{M}_2\times[(H^x-\lambda M_1{}^x)\mathbf{i}+(H^y-\lambda M_1{}^y)\mathbf{j}+(H_0-H_A-H_E)\mathbf{k}];$$

here $H_E=\lambda M_s=\lambda M_1{}^z=-\lambda M_2{}^z$. Defining $M^-=M_x-jM_y$, $H^-=H_x-jH_y$, we solve for the susceptibility:

$$\chi^-=M^-/H^-=2\gamma^2M_sH_A/(\omega-\omega_0)^2;$$
$$\omega_0/\gamma=H_0\pm[H_A(H_A+2H_E)]^{\frac{1}{2}}. \quad (1)$$

Note that H_E enters only if $H_A\neq0$. For $H_0=0$ and $H_A\ll H_E$, the zero field splitting is $\omega_0\cong\gamma(2H_AH_E)^{\frac{1}{2}}=\gamma(2K\lambda)^{\frac{1}{2}}$. The two frequencies in Eq. (1) correspond to different directions of circular polarization, and a linearly polarized rf field will excite both precessional modes. In polycrystalline specimens the line widths will be at least of the order of H_0, as only the component of the static field parallel to the domain axis is fully effective.

In the common antiferromagnetics such as MnO, MnF_2, FeO, and Cr_2O_3, we may estimate $H_A\sim10^3$ oersteds and $H_E\sim10^6$ oersteds. Then $(2H_AH_E)^{\frac{1}{2}}\sim5\times10^4$ oersteds and $\omega_0\sim5$ cm^{-1}, which is higher than the experimental frequency 0.3 cm^{-1} used by Maxwell[2] *et al.* and Hutchison.[3] The low experimental frequency is the reason we suggest to explain the observed extinction of the spin resonance absorption lines in antiferromagnetic crystals on cooling below the Curie temperature. It would be valuable to work in intense magnetic fields to pull one of the frequencies into the usual range, or else to work at millimeter wavelengths.

We note that the anisotropy energy may be quite high even in cubic antiferromagnetics containing Mn^{++} ions in a ^6S ground state. Consider a simple-minded model: the Kramers superexchange interaction[4] connecting Mn ions in MnO depends on the overlap of the wave functions of electrons on the Mn and O ions. With an admixture of orbital moment the overlap depends on the spin direction. The order of magnitude of the anisotropy energy per ion on this model may be estimated as $\sim|g-2|k\Theta$; for $\Delta g\sim10^{-2}$ and $k\Theta\sim5\times10^3$ cm^{-1} the anisotropy field can be as high as 10^4 oersteds.

With ferrite-type ferromagnetism, according to the Néel theory, we may set $M_1{}^z=M_s$; $M_2{}^z=-(1-\eta)M_s$. The observed saturation magnetization is $M_1{}^z+M_2{}^z=\eta M_s$. We let $H_E=\lambda M_s$, and suppose for simplicity that H_A has the same value for both sublattices. We find

$$\omega/\gamma=H_0-(\eta H_E/2)\pm[(\eta H_E/2)^2+H_EH_A(2-\eta)+H_A{}^2]^{\frac{1}{2}}.$$

The over-all anisotropy field deduced from static deflections at small angles will differ in ferrites from that deduced from microwave resonance experiments by a fractional amount $\propto H_A/H_E\eta$, which may usually be neglected. The difference should be detectable in weakly magnetic zinc ferrites.

[1] J. H. Van Vleck, Phys. Rev. **78**, 266 (1950).
[2] Trounson, Bleil, and Maxwell, Phys. Rev. **79**, 226 (1950); L. R. Maxwell, talk at Pittsburgh meeting APS, March 1951.
[3] C. A. Hutchison, private communication.
[4] P. W. Anderson, Phys. Rev. **79**, 350 (1950). Because of superexchange the value of g used may refer to an excited Mn^+ state.

Fractional Transition Probabilities of the First Positive Band System ($B^3\Pi\rightarrow A^3\Sigma$) of Molecular Nitrogen

C. E. MONTGOMERY AND R. W. NICHOLLS
Department of Physics, University of Western Ontario, London, Ontario, Canada
(Received March 12, 1951)

AS part of a computational program of fractional vibrational transition probabilities for molecular band systems occurring in upper atmospheric radiations, the results for the first positive system of molecular nitrogen are here presented in Table I.

The method of calculation employed is similar to that used in previously reported results,[1] and involves a computation of the overlap integral of suitably modified hermite wave functions.[2] It will be noted that the fractional transitional probability $f(v', v'')$ is so defined that in any v' progression

$$\sum_{v''} f(v', v'')=1.$$

From a 3-dimensional presentation of Table I it will also be noted that what was formerly thought of as the primary Condon parabola in the (v', v'') array of reported intensities of the first positive bands[3] is in fact the limbs corresponding to the smaller v'' values of the primary and a subsidiary parabola. The limb of the

TABLE I. Fractional transition probabilities, $f(v', v'')$.

v' \ v''	0	1	2	3	4	5	6	7	8	9	10	11	12	13	14	15	16
0	0.385	0.338	0.158	0.077	0.031	0.007											
1	0.479	—	0.125	0.139	0.106	0.095	0.048	0.004									
2	0.228	0.265	0.091	0.037	0.075	0.074	0.108	0.098	0.021								
3	0.037	0.416	0.046	0.160	—	0.033	0.043	0.083	0.136	0.039	0.004						
4	—	0.149	0.383	—	0.151	0.015	0.007	0.012	0.057	0.141	0.071	0.008					
5	—	0.006	0.268	0.285	0.023	0.098	0.021	0.001	0.002	0.027	0.104	0.131	0.029				
6	—	—	0.023	0.376	0.190	0.066	0.031	0.023	0.001	0.001	0.005	0.093	0.139	0.041	0.006		
7	—	0.001	0.003	0.047	0.411	0.084	0.076	0.012	0.068	—	0.013	0.004	0.060	0.152	0.053	0.009	
8	—	—	—	0.012	0.111	0.435	0.022	0.092	0.007	0.024	0.002	0.012	0.018	0.031	0.123	0.076	0.017

primary parabola lying at higher v'' values will include unreported bands in the near infrared which are at the moment being investigated experimentally. The fuller significance of such three-dimensional $f(v', v'')$ surfaces is also being sought.

Although the question as to whether bands of the first positive system may be identified in the spectrum of the upper atmosphere is by no means settled,[4] the results presented above may be useful in discussing this topic.

The results are also of importance in considerations of mechanisms of population of $A^3\Sigma$ as a prelude to the emission of the Vegard-Kaplan system. The sensitivity of the first positive systems to the presence of contaminants, particularly oxygen, has been discussed elsewhere.[5]

A careful experimental determination of the relative intensity of bands of the first positive system is at present in progress, and it was in connection with this work and an associated problem relating to the excitation of the Vegard-Kaplan system that these calculations were originally initiated.

We should like to thank the National Research Council and the Defence Research Board of Canada for interest in and support of this work.

[1] R. W. Nicholls, Phys. Rev. **77**, 421 (1950). R. G. Turner and R. W. Nicholls, Phys. Rev. **82**, 290 (1951).
[2] R. W. B. Pearse and A. G. Gaydon, Proc. Roy. Soc. (London) **A173**, 37 (1939). M. E. Pillow, Proc. Phys. Soc. (London) **62**, 237 (1949); **63A**, 940 (1950).
[3] R. W. B. Pearse and A. G. Gaydon, *The Identification of Molecular Spectra*, 2nd Ed. (John Wiley & Sons, Inc., New York, 1950), p. 168.
[4] G. P. Kuiper, *The Atmospheres of the Earth and Planets* (University of Chicago Press, Chicago, 1949), p. 198 (paper by P. Swings). D. R. Bates, Proc. Roy. Soc. (London) **A196**, 217 (1949).
[5] R. W. Nicholls, J. Chem. Phys. **19**, 250 (1951).

PHYSICAL REVIEW VOLUME 82, NUMBER 4 MAY 15, 1951

Proceedings of the American Physical Society

MEETING OF THE CONFERENCE ON GASEOUS ELECTRONICS, SPONSORED BY THE DIVISION OF ELECTRON PHYSICS OF THE AMERICAN PHYSICAL SOCIETY, AT NEW YORK ON OCTOBER 19–21, 1950

THE third annual Conference on Gaseous Electronics, sponsored on this occasion by our Division of Electron Physics, was held on October 19, 20, and 21, 1950, in the Barbizon-Plaza Hotel, New York City. Following are the abstracts of some of the papers presented at this meeting. The Secretary of the American Physical Society expresses great regret that these abstracts appear so belatedly. Apparently the original copies of this material, duly forwarded in December, 1950, to the office of the American Physical Society, were mislaid and have never since been traced. Mr. J. A. Hornbeck has thus been obliged to prepare a second copy, which is printed hereunder.

A1. Electron Removal Processes in Hydrogen, Argon, and Krypton.* R. B. HOLT, JOHN M. RICHARDSON, AND A. REDFIELD, *Harvard University*.—Previously described techniques[1] for the measurement of electron densities in and light emission from pulsed discharge afterglows have been applied to hydrogen, argon, and krypton. Electron densities were measured by observing the shift in resonant frequency of a microwave cavity containing the discharge. The spectrum of the light emitted was observed *vs* time by means of pulsed photomultipliers and by a spectrograph and high speed mechanical shutter. In argon, recombination-type electron removal was observed in the moderate pressure range (1–30 mm) with a coefficient which depends on pressure and also on the degree of excitation of the ions produced initially. The total light emitted indicated that the electron removal process was partially radiative and partially nonradiative. In hydrogen at moderate pressures, nonradiative (in the optical region, at least) recombination accounts for the removal of most of the electrons. The recombination coefficient was a function of pressure. Recombination-type electron removal was also observed in krypton, with the amount of light emitted strongly dependent on minute amounts of impurities (particularly xenon).

* This work was assisted by the ONR.
[1] Holt, Richardson, Howland, and McClure, Phys. Rev. **77**, 239 (1950).

A3. Ionization by Metastable Atoms in Pure Helium and in Neon. MANFRED A. BIONDI, *Westinghouse Research Laboratories*.—Microwave techniques have been used to study the electron density variation in He and Ne afterglows. An initial *increase* in density is observed lasting for approximately one millisecond after the maintaining field is removed from the discharge. This delayed ionization evidently results from the collision of pairs of metastable atoms. Analysis of the initial rise permits an evaluation of the diffusion and volume loss of the metastable atoms. The results are given in the following table:

Gas	$D_m p$ (cm²/sec)(mm Hg)	Volume destruction cross section, σ_v cm³ × 10^{28}
Airco reagent He	530 ± 30	5.8 ± 0.5
Purified He	565 ± 30	2.9 ± 0.6
Airco reagent Ne	200 ± 20	30 ± 3

The volume loss of Ne metastables can be explained by collisions with normal Ne atoms which raise the metastable to a radiating stage. This explanation fails for He where the nearest radiating level is 0.7 volt above the metastable level. To assure that impurities were not the cause of this volume loss, reagent He was liquefied and re-evaporated into special flasks. From the table it is seen that the volume loss is reduced but not eliminated.

A4. Studies of the Lifetimes of Metastable Atoms in the Afterglow of Rare Gas Discharges.* ARTHUR V. PHELPS, *Bell Telephone Laboratories.*—The lifetimes of the lower metastable states of Ne, He, and A in the afterglow of a pulsed discharge have been measured as a function of pressure, p, at 300°K and 77°K. The lifetimes were determined by passing light of an appropriate wavelength through the gas and measuring the time constant of decay of the absorption at low percentage absorption. In neon at 300°K and high p the probabilities of decay of the lower metastable state and the nearby radiating state are equal and directly proportional to p. Thus, the metastable destruction process appears to be one of excitation to the radiating state by collision with normal atoms. At 77°K the volume destruction is much lower and is proportional to p^3. In helium at high p the destruction is proportional to p^2 and about 60 times as probable at 300°K as at 77°K. In argon the volume loss approaches a p^2 law at 300°K and 77°K and is roughly independent of temperature. The variation in the metastable diffusion coefficients is between T^1 and T at constant gas density.

* The method and apparatus were developed by Dr. J. P. Molnar of the Bell Telephone Laboratories and used by the author at the Laboratories during the summer of 1950 while on leave from the Research Laboratory of Electronics, Massachusetts Institute of Technology.

B2. Mass Spectrometric Studies of Molecular Ions in the Rare Gases. J. P. MOLNAR AND JOHN A. HORNBECK, *Bell Telephone Laboratories.*—Molecular ions of the rare gases (He_2^+, Ne_2^+, A_2^+, Kr_2^+, and Xe_2^+) produced by electron impact at gas pressures from 10^{-4} to 10^{-2} mm Hg were detected with a small mass spectrometer. The ion intensity increased linearly with electron current and with the square of the gas pressure. The form of the ionization *vs* electron energy curves resembles closely curves of excitation probability. The onset (appearance) voltages for the molecular ions were less than those for the atomic ions by 1.4 (+0.7, −0.2) volts for He, 0.7 (+0.7, −0.3) volt for Ne, 0.7 (+0.7, −0.2) volt for A, 0.7 (+0.7, −0.3) volt for Kr. These results can be interpreted, we believe, only by assuming that the method of formation of the molecular ions observed in this experiment is, using helium as an example, first by electron impact $He+e+K.E.\rightarrow He^*+e$ followed by the collision process $He^*+He\rightarrow He_2^++e$, where He^* stands for a helium atom raised to a high-lying excited state. Arnot and M'Ewen[1] proposed a similar interpretation of their mass spectrometric studies of helium, except that they reported onset voltages low enough to permit metastable atoms to form molecular ions.

[1] F. L. Arnot and M. B. M'Ewen, Proc. Roy. Soc. (London) **A171**, 106 (1939).

B3. Mobilities of Rare Gas Atomic and Molecular Ions. JOHN A. HORNBECK, *Bell Telephone Laboratories.* [See Phys. Rev. **80**, 297 (1950).]

B4. Mobilities of Positive Ions in Gases. T. HOLSTEIN, *Westinghouse Research Laboratories.*—The mobilities of Ne^+ and A^+ in their parent gases have been calculated by a procedure similar to that employed by Massey and Mohr[1] for He^+ and He. The results are 4.2 and 1.64 cm/sec per volt/cm, respectively, under conditions of standard gas density (2.69×10^{19}/cc), and $T=293$°K. A crucial step in the procedure is the computation of the "resonance" or charge-exchange component of the total ion-atom interaction. In the present paper, this step is achieved by a new method whose sole requirement is a knowledge of the Hartree-Fock wave function of the outermost atomic shell. The resonance interaction curves so obtained differ somewhat from those given by Massey and Mohr's perturbation treatment. The mobility theory in its present form is strictly valid only for ions whose electronic angular momentum is zero. However, preliminary estimates show that the error incurred in its application to Ne^+ and A^+ (whose ground states are either $^2P_{1/2}$ or $^2P_{3/2}$) is <10 percent.

[1] H. S. W. Massey and C. B. O. Mohr, Proc. Roy. Soc. (London) **A144**, 188 (1934).

B5. Diffusion of Ions in a Strong Electric Field. GREGORY H. WANNIER, *Bell Telephone Laboratories.*—When gaseous ions move with appreciable drift velocity in a strong electric field, the diffusion concept can be salvaged: there exists a diffusion tensor in the frame of reference moving with the ion drift velocity. The tensor has two components D_{ss} and D_{nn}, which are, respectively, diffusion coefficients longitudinal and transverse to the field. They depend on the field strength E; for high field, $D\sim E^1$ for constant mean free path and $D\sim E^0$ for constant mean free time. In the latter case explicit expressions for the coefficients can be derived:

$$D_{ss}=(M+m)\tau\langle c_s^2\rangle_{hl}[M(1-\cos\chi)_{hl}]^{-1};$$
$$D_{nn}=(M+m)\tau[\langle c_s^2\rangle_{hl}-\langle c_s\rangle_{hl}^2][M(1-\cos\chi)_{hl}]^{-1};$$

where M and m are the masses of the gas molecules and ions, respectively, χ the angle of scattering, and $\langle c_s^2\rangle_{hl}$, $\langle c_s^2\rangle_{hl}$, $\langle c_s\rangle_{hl}$ are velocity averages communicated earlier.[1] Einstein's relation can be generalized to read $eD_{nn}=2$ (ion mobility) (random energy in the direction n). Since this relation contains no model parameters and holds dimensionally in the high field range, it may apply more generally than just to the mean-free-time case for which it was derived.

[1] M.I.T. Conference Report on Physical Electronics, March 30, 1950, p. 65.

B6. Further Studies in Mercury Band Fluorescence. A. O. MCCOUBREY, D. ALPERT, AND T. HOLSTEIN, *Westinghouse Research Laboratories.*—Previous researches on the persistence of band fluorescence in mercury vapor[1,2] have been continued. Shot fluctuations, which limited the accuracy of earlier measurements, have been greatly reduced by time sampling techniques involving the use of a gated photomultiplier tube. Improved measurements of the time decay of band fluorescence as a function of temperature and vapor density have been carried out down to densities as low as 6×10^{16}/cc. At this limit, and with a fluorescence tube of radius 0.65 cm, diffusion of the metastable entities to the walls is found to be the predominant removal mechanism. With a second tube of radius 2.3 cm, in which the diffusion was cut down by a factor of 12.5, and at $T=200$°C, a decay time of seven milliseconds is observed. This time constant is essentially independent of density over the range 0.9×10^{16}/cc to 2×10^{16}/cc. The density independence indicates that the decay process is radiative and hence suggests that the metastable entity is molecular. At higher densities (4×10^{16}/cc), a composite decay curve, indicative of the presence of a second metastable "reservoir," is observed.

[1] Holstein, Alpert, and McCoubrey, Phys. Rev. **76**, 1259 (1949).
[2] McCoubrey, Alpert, and Holstein, Report on Conference on Gaseous Electronics, November 3, 4, and 5, 1949, Paper D1.

B7. Isotope Effect in the Imprisonment of Resonance Radiation. D. ALPERT, A. O. MCCOUBREY, AND T. HOLSTEIN, *Westinghouse Research Laboratories.*—On theoretical grounds[1] it is expected that the decay time of imprisoned resonance

radiation in the vapor of a single even isotope of mercury should be from five to six times larger than that observed with the natural samples of mixed isotopic constitution. To investigate this effect experimentally, decay measurements[1] were carried out with a sample of Hg_{198} (3.1 percent contamination of Hg_{199}) kindly loaned to us by the Bureau of Standards. For vapor densities below 3×10^{15} atoms/cc, the predicted effect was verified; e.g., at $N=2\times10^{15}$/cc, the decay time T_{198} is equal to sixteen microseconds, whereas T_{mixed} is three microseconds. For N greater than 3×10^{15}/cc, the ratio T_{198}/T_{mixed} diminishes; this secondary effect can be interpreted in terms of a transfer of excitation from Hg_{198} to Hg_{199} by collisions of the second kind. A rough estimate of the cross section for this process gives a value of 5×10^{-16} cm^2, ten times the gas kinetic cross section and in order-of-magnitude agreement with theoretical expectations.

[1] T. Holstein, Phys. Rev. **72**, 1212 (1947); and subsequent unpublished calculations.
[2] Alpert, McCoubrey, and Holstein, Phys. Rev. **76** 1257 (1949).

C2. Breakdown in Hydrogen at 100-mc Frequency.* SANBORN C. BROWN, *Massachusetts Institute of Technology*.—Previous studies of microwave breakdown in hydrogen have led to a very successful theoretical explanation for the behavior of the phenomenon of ac breakdown. The theory was applied not only to the microwave region but also to longer wavelength measurements. The 100-mc experiment was designed to extend the range of experimental observations beyond the range of the previous theory in the direction of higher pressure. A new theory has been developed for the radiofrequency breakdown in hydrogen which is applicable to higher pressure phenomena. At higher pressures the energy per mean free path which the electrons gain in the field is low, and the electrons make very few ionizing collisions compared to elastic and exciting collisions. A much simpler theory has been developed for this case which is applicable also to high pressure breakdown at lower frequencies calculated by the previous theory, so that the two theories can be shown to overlap. The experimental methods of observation will be outlined, and good agreement will be shown between theory and experiment.

* This work has been supported in part by the Signal Corps, the Air Materiel Command, and ONR.

C3. Maintaining Electric Fields in a Steady-State Microwave Discharge.* DAVID J. ROSE, *Massachusetts Institute of Technology*.—The microwave field required to maintain a discharge at various electron densities in hydrogen has been measured. The experimental methods are summarized. The electron velocity distribution in the hydrogen plasma is derived from the Boltzmann transport equation, taking account of the dc space charge field. From this distribution, the ionization rate per electron, the diffusion coefficient, and the mobility are calculated by standard formulas. In the steady state, a relation exists between these three quantities and the space charge field. The resulting equation is solved to yield the rate of electron flow out of the discharge and the average electron energy, in terms of the applied microwave field, its frequency, the cavity size, and gas pressure. The spatial distributions of ions and electrons in the plasma also yield an equation for the rate of flow in terms of the diffusion and mobility coefficients of the charged particles and the electron density. The electric field required to maintain the discharge is calculated as a function of electron density, cavity size, and frequency, using the fundamental properties of the gas. Theory and experiment are compared.

* This work has been supported in part by the Signal Corps, the Air Materiel Command, and ONR.

C4. Electron Recombination and Cross-Section Measurements in Decaying Hydrogen Plasma.* LAWRENCE J. VARNERIN, JR., *Sylvania Electric Products, Inc., Boston, Massachusetts*.—A method is described by which the impedance of a decaying plasma in a section of wave guide may be determined as a function of time by use of transient standing wave detection equipment. From the impedance, both real and imaginary components of the complex dielectric constant of the plasma may be obtained. The density can then be determined and, as a result, the mode of decay of electron density established. In addition, the resistive component is related to the collision cross section of electrons. This measurement affords a means of determining the energy dependence of the mean free path of electrons. Data for hydrogen are presented.

* This work was made possible by S. C. Proj. No. 27-3238-2.

C5. A Microwave Method for Measuring P_c at Thermal Energies.* O. T. FUNDINGSLAND, *AF Cambridge Research Laboratories*.—The ratio σ_r/σ_i of the real to the imaginary part of the complex conductivity of an ionized gas in a microwave resonant cavity can be measured during the post-discharge plasma decay by transient standing wave techniques. The solutions for constant collision frequency ($P_c \propto v^{-1}$) and for constant P_c differ in that σ_r/σ_i is inversely proportional to the pressure p in the first case, but not strictly so in the latter. This distinction is small, but it implies that an experimental plot of $1/p(\sigma_r/\sigma_i)$ *versus* either p or σ_r/σ_i should give some indication of the velocity dependence of P_c. Further evidence concerning $P_c(v)$ can be obtained by noting how the measurements are affected when the average electron energy is raised slightly by increasing the intensity of the probing signal. Measurements at room temperature will be reported for helium, hydrogen, and neon. The values calculated by assuming constant P_c agree satisfactorily with extrapolations of Brode's collision probability curves.

* Performed at M.I.T., R.L.E., supported in part by the Signal Corps, the Air Materiel Command, and ONR.

C6. Dielectric Coefficient of Ionized Gases. DONALD E. KERR, *The Johns Hopkins University*.—The formula for the conductivity or dielectric constant of an ionized gas has been a subject of some controversy, chiefly because of the possible existence of a Lorentz polarization term. Using the single-electron approach in a manner due essentially to Darwin, it is found that Lorentz polarization and positive ion collision forces just cancel in an electrically neutral plasma, but local differences in electron and positive ion densities introduce a correction and also modify the local plasma-resonance frequency. The effects of mixed ac and dc fields and of diffusion are best expressed through the electron energy distribution function and the Boltzmann transport equation. The spherically symmetrical part of the distribution function, F_0, is customarily considered to be independent of time. This is not true, however, when both ac and dc electric fields are present, and the electron current depends upon both the steady and alternating components of F_0 as well as those of the electric field. This fact, coupled with the effects of diffusion in a bounded discharge, renders quantitative measurements difficult. A discussion will be given of the theoretical and experimental problems that are encountered.

C8. The High Frequency Discharge in Helium-Argon Mixtures. C. S. CLAY AND J. G. WINANS, *University of Wisconsin*.—High frequency breakdown and extinction field strengths were measured for argon, helium, and helium-argon mixtures. The excitation frequency was 527 mc. The discharge chamber was a cylinder, 13 mm diameter and 110 mm long. With increase in pressure the breakdown and extinction field strengths passed through a minimum. The pressure for minimum break-

down field strength was less for argon and argon-helium mixtures than for pure helium. The pressure at which the extinction field strength was minimum was less than the pressure at which breakdown field strength was minimum. In mixtures of argon and helium, the spectra of argon was more strongly excited, relative to helium, by high frequency than by low frequency excitation. Under high frequency excitation the source was brightest when the gas pressure was that for minimum extinction field strength. The spectrum of mercury was photographed under pulsed and continuous wave excitation at a carrier frequency of 527 mc. Pulsed excitation gave spectral lines of Hg I, Hg II, as well as Hg_2^+, bands. Continuous wave excitation gave Hg I lines only. The theory of Brown, Herlin, and MacDonald described all observations.[1]

[1] Brown, Herlin, and MacDonald, Phys. Rev. 75, 411 (1948).

D1. Formative Time Lags of Spark Breakdown in Nitrogen and Argon.* G. A. KACHICKAS AND L. H. FISHER, *New York University*.—Formative time lag measurements of spark breakdown in air[1] and oxygen[2] have been extended to nitrogen and argon. The results in nitrogen and air are almost identical, the time lags in both gases being independent of pressure and increasing with increasing gap separation. In argon, the formative time lags at overvoltages above a few percent are many orders of magnitude longer than the corresponding times in nitrogen and air. The time lag *vs* percent overvoltage (o.v.) curve varies much more slowly in argon than in nitrogen. For example, at a tmospheric pressure and a gap separation of 1 cm, the time lags are 100 μsec at 10 percent o.v. and decrease to 1 μsec at 100 percent o.v. In argon, the time lag *vs* percent o.v. curve is not independent of pressure, the curves for low pressures lying below those for high pressures. The time lags for argon increase with increasing gap separation. Interpretation of the results will be given.

* Supported by the ONR and the Research Corporation.
[1] L. H. Fisher and B. Bederson, Phys. Rev. 78, 331 (1950).
[2] G. A. Kachickas and L. H. Fisher, Phys. Rev. 79, 232 (1950).

D2. Ion Pulses in the Positive Ion Space Charge Detector.* NATHAN WAINFAN AND G. L. WEISSLER, *University of Southern California*.—Using a Kingdon cage space charge detector,[1] pulses were observed due to individual positive ions generated in the residual gas by emission electrons. The pulse shape was essentially independent of the number of pulses; they disappeared when operating the detector in the saturation region. The average pulse duration was of the same order as ion lifetimes found by Kingdon.[1] The pulse number decreased with decreasing pressure, with no pulses in a very high vacuum. However, dry, pure He does not increase the pulse number until the anode voltage is raised to the He ionization potential. Using a Kunsman ion source external to the detector, no induced pulses were observed, in agreement with calculations on electron shot noise and ion pulse heights. An internal ion source produced pulses with very low efficiencies. Differential counting rates will be presented for various instrument parameters and pulse heights. These results were in agreement with expectations. Under certain conditions of electrode potentials and geometry sustained sinusoidal ion oscillations were observed. It will be shown that they are analogous to electron Barkhausen oscillations. The ion oscillation periods are in good agreement with calculated ion transit times.

* Sponsored by the ONR.
[1] K. H. Kingdon, Phys. Rev. 21, 408 (1923).

D3. Further Results on Absorption Coefficients of N_2 in the Vacuum Ultraviolet.* PO LEE AND G. L. WEISSLER, *University of Southern California*.—Quantitative results of N_2 absorption coefficients have been obtained with a line spectrum source, and the absorption law $I_x = I_0 \exp(-k_\lambda x)$ has been verified for 26 lines. In contrast to our Lyman source work, general scattering or fluorescence in the absorbing gas did not obscure the results. Values of the coefficients between 1300A and 1050A are generally small, 10 cm^{-1} or less. In the N_2 band region from 1050A to 800A, the coefficients oscillate rapidly attaining maximum values of about 350 cm^{-1}, in approximate agreement with Schneider[1] and Clark.[2] They must be regarded with caution due to blending of source lines and absorption bands. From 800A to 500A, k_λ is nearly constant at about 600 cm^{-1}, indicating a decrease toward shorter wavelengths. At 303A, $k_\lambda = 120$ cm^{-1}. Very strong absorption was observed on several plates at 775.9A with a k_λ of at least 2200 cm^{-1} ($N_2^+ = 795.8$A). Agreement between the results presented and Wulf's predictions from N_2 dispersion[3] is fair.

* Supported by the ONR.
[1] E. G. Schneider, J. Opt. Soc. Am. 30, 128 (1940).
[2] K. C. Clark, Phys. Rev. 73, 1250A (1948); private communication.
[3] O. R. Wulf and L. S. Deming, Terr. Magn. Atmos. Elect. 43, 283 (1938).

D5. Time Studies in Positive Point-to-Plane Corona.* M. MENES, *New York University*.—Since the positive point-to-plane corona was of fundamental importance in establishing the streamer theory of sparking, it seemed desirable to study the formative time lags of the various types of discharges encountered with positive points. Tungsten points ranging from about 0.1 to 0.5 mm in radius were used with gaps of the order of 1 cm. Continuous ultraviolet illumination of the cathode provided initiating electrons. An approach voltage well below onset was used and an additional voltage step applied. The time lags were measured from the application of this step by means of an amplifier and synchroscope. The gases studied were air, oxygen, and nitrogen at pressures from atmospheric down to a few mm of Hg. At higher pressures, formative time lags were found to be well defined only for nitrogen. In air and especially in oxygen, a large scatter in the times exists. This scatter (which decreases with increasing illumination) has been tentatively ascribed to electron attachment by oxygen molecules. At higher pressures, the formative time lags for prebreakdown pulses in nitrogen have been found to be of the order of a microsecond or less very near threshold (overvoltages of the order of 0.1 percent).

* Supported by the ONR and the Research Corporation.

D7. Experiments upon the Initiation of an Electric Arc. L. H. GERMER, *Bell Telephone Laboratories*.—When a condenser charged to a potential of the order of 50 volts is discharged by bringing two electrodes together, field emission current flows before contact is made. Whether or not an arc is initiated by this current depends upon the nature of the electrode surfaces and upon the circuit voltage and inductance. For clean noble metal electrodes, an arc occurs only if the quotient of the voltage and inductance exceeds about 10^7 amperes per second. For carbon surfaces an arc is struck if this quotient is greater than about 5×10^4. Noble metal surfaces contaminated by very thin carbonaceous films or grease, or by very thin insulating films, or by insulating particles such as magnesia powder, behave much as do carbon surfaces. When an arc occurs the potential across it is characteristic of the electrode material and independent of the nature of the film, if any, by which the arc was initiated, and independent also of the current except during the first 2×10^{-8} second of the arc's duration. The characteristic voltages for silver, copper, gold, palladium, platinum, and carbon are, respectively, 11, 12, 12, 14, 15, and 20–30. The arc voltage is much higher during the first 2×10^{-8} second.

D8. On the Production of Extreme Temperatures by Electrical Discharges. LOUIS GOLD, *Watertown, Massachusetts*.—Recently, stellar temperatures have been identified with

nuclear explosions.[1] In the face of literature which attests both mechanical and electrical means for producing such high temperatures, it has been improperly adduced that the above represents our only known approach.[2] Indeed, Anderson[3] resorted to the exploding wire in simulating the excitation presumed to originate by meteors plunging into the sun. Appropriate analysis of the temperatures in such sparks must take cognizance of two facets: (1) collision and radiative processes involving particle-wave interactions, and (2) the circuitry question. Item (1) concerns the opacity in a variable star and is so grossly complicated that it is expedient to deal initially with the circuitry aspect, assuming negligible radiative losses during the energy build-up stage, an assumption for which there is reasonable experimental justification.[4] The circuitry influence is contained in an energy-time function which permits suitable evaluation of the salient features of energy build-up in discharges and on which basis one can show that temperatures of millions of degrees are attainable.

[1] P. Caldirola, J. Chem. Phys. **18**, 846 (1948).
[2] R. F. Bacher, Sci. American **182**, 11 (1950).
[3] J. A. Anderson, Astrophys. J. **51**, 37 (1920).
[4] J. D. Craggs and W. Hopwood, Proc. Phys. Soc. (London) **59**, 771 (1946).

E1. Motion of an "Anchored" Arc Impelled by a Magnetic Field. C. G. SMITH, *Raytheon Manufacturing Company.*—A cylinder 2 cm in diameter of polished molybdenum or such, with axis vertical, projects well above a surface of mercury in an evacuated tube. The anode is above and radially larger than the cylinder. An arc anchors along the circle where the mercury wets the molybdenum. A magnetic field of 1000 to 10,000 oersteds applied vertically is parallel to the arc stream except for a few thousandths of a cm where the arc current is radial to the molybdenum. The cathode spot races around on the cylinder in the retrograde direction. Observations were made through a rotating toothed wheel, and with photocell and oscillograph, and with radial probe and oscillograph. The velocity does not change from retrograde to proper for any field strength but usually approaches asymptotically to approximately 120 meters per sec. Current density is greatest at the leading edge of the spot. Spot may be single or a unified flock of two or more equal segments separated by darker regions. A mode of one, two, or more, once established is stable.

E4. Exceptionally Low Voltage Drops in Hot Cathode Gas Diodes. GUSTAV MEDICUS AND GOTTFRIED WEHNER, *Wright Field, Dayton, Ohio.*—The potential, plasma density and electron temperature distribution in Xe low voltage arcs without oscillations and with voltage drops lower than the lowest excitation potential of Xe (8.3 v) were measured. Minimum arc drops of about 1.5 v in the amp range were obtained without an indication of this being a lower limit. The findings of Compton and Eckart[1] and of Druyvesteyn,[2] namely, potential and plasma density maxima near the hot cathode and decreasing electron temperature with increasing distance from the anode, were confirmed, provided the discharge—which normally confines itself to regions of preference, especially of lowest work function of the anode—was prevented from shunning the region of the movable probe. Otherwise, under cylindrically or spherically uniform geometrical conditions no maxima were found, in spite of their doubtless existence in regions not covered by the probe. By artificially increasing the plasma density near its "natural" maximum by means of an auxiliary discharge with fast electrons being extracted from a saturated cathode, the arc drop could be considerably decreased.

[1] K. T. Compton and C. Eckart, Phys. Rev. **25**, 139 (1925).
[2] M. J. Druyvesteyn, Z. Physik **64**, 782 (1930).

E5. Experimental Techniques for the Measurement of Thyratron Breakdown. HANNS J. WETZSTEIN, *Cambridge, Massachusetts.*—Throughout all tests the anode of the thyratron is connected to the vertical deflection plates of a cathode-ray oscilloscope. A sinusoidal voltage of normal operating frequency is applied to it through a series load impedance of any desired value. (1) A dc voltage varied about once a second over the control range desired is applied to the grid and the horizontal deflection plates simultaneously. The upper edge of the pattern resulting on the screen is the grid control characteristic. (2) A fixed value of dc voltage is applied to the grid (through the usual *RC* network), and the horizontal deflection plates are connected directly to the grid. The complex pattern gives the grid-anode voltage relationship at all times, including breakdown. (3) The grid is made to fire using dc and some synchronizing voltage. A sinusoidal voltage of anode supply frequency in series with a suitable rf voltage is applied to the horizontal deflection plates. A Lissajous figure is obtained with a straight vertical line (breakdown) on which there is superimposed the rf sine wave, thus allowing accurate measurement of breakdown times. The relative ease and simplicity of the techniques allows close investigation of the influence of all parameters under operating conditions.

E8. Improved Potential-Probe Measurements in Carbon Arcs. WOLFGANG FINKELNBURG, *Fort Belvoir, Virginia.*—The potential distribution along the arc-stream axis, in the potential drop regions close to the electrodes, and in certain boundary layers of carbon arcs has been studied, despite arc temperatures up to 12,000°K, by means of fast moving potential probes. Tungsten wires covered by insulating glass or quartz, except for a small tip, were whipped through the arc stream, or pneumatically shot against and retracted from the electrodes, while the probe potential with reference to one of the electrodes, the total arc voltage, the arc current, and the position of the probe's tip with respect to the electrode surface were simultaneously recorded by a Hathaway oscillograph. Tungsten probes plated with different metals were used for checking a possible influence of oxide formation, differences of work function, etc. However, the results proved to be independent of the probe material and, in a fairly wide range, of the probe speed. Results concerning potential distribution and potential drops in different regions of carbon arcs at low and high current density will be discussed, together with possible sources of error and their elimination.

E9. Oscillations in Direct Current Arcs.* T. B. JONES AND B. H. LIST, *The Johns Hopkins University.*—Two types of oscillations have been discovered in dc carbon arcs in air. One type, consisting of low audiofrequency oscillations of 100 to 400 cycles/sec, occurs in a narrow current range just below the hissing point. Simultaneous oscillations of voltage, current, light, and sound have been observed. High speed motion pictures show that these so-called "quiet" oscillations are the result of the rotation of the anode spot around the anode crater circumference. The voltage oscillations are a result of the varying arc length as the spot rotates. Their frequency was found to be dependent on the material, size, and separation of the electrodes and the arc current. The second type of oscillations begins when the arc enters the hissing stage. They occur in the rf spectrum in definite bands up to at least ninety megacycles. Their frequency appears to be independent of electrode material, arc length, or current but dependent on the atmosphere. Both types of oscillations are independent of any external inductance or capacitance in the arc circuit. Oscillations are present in materials other than carbon, e.g., W, Al, and Cu. However, the "quiet" oscillations in these materials are very unstable due to melting of electrodes.

* This work was supported by the ONR.

E10. Characteristics of the Helium-Tungsten Arc with High Currents.* T. B. JONES AND MERRILL SKOLNIK, *The Johns Hopkins University.*—Properties of the electric arc are investigated for tungsten rod electrodes in He at a pressure slightly above one atmosphere and for currents ranging from 15 to 80 amperes. The arc properties studied include voltage-current and voltage-arc length characteristics, physical appearance, and starting phenomena. The helium-tungsten arc may exist as the cold-cathode arc, or the thermionic arc. The cold-cathode arc always appears on starting and may last a few seconds before extinguishing. If the current exceeds 70 amperes (approximately), the cold-cathode arc will change quickly to the stable thermionic arc. The voltage-current curves are similar in appearance to the usual *V-I* characteristics for the arc except that in most cases two different curves, displaced by several volts, may be obtained for the same arc length. The arc voltage usually follows the upper of these two curves for low currents and transfers to the lower curve for high currents. This transition is accompanied by a change in arc appearance and is believed to be caused by vaporization of the cathode material. For short electrode separations and higher values of current, the arc voltage approaches 20 volts, which is near the first resonance potential of helium.

* This work was supported by the ONR.

F1. Probe Technique for the Measurement of Electron Temperature. M. A. EASLEY, *General Electric Company, Nela Park.*—A study has been made of the characteristics of the positive column of the low pressure mercury arc in the presence of one to 3.5 mm pure argon or krypton gas. Under some conditions, nonlinear probe characteristics were found, similar to those reported by others for discharges in pure mercury. This discontinuity in the slope of the $\log i_p - V_p$ plots for wire probes was eliminated in many cases by heating the probe by electron bombardment before each reading. With this technique, linear probe characteristics over the measurable range of electron current (i.e., over a 10,000-fold range in probe current) were obtained for discharges in 0.5 to 46μ-mercury vapor mixed with one to 3.5 mm pure krypton or argon gas, provided the discharge was free of oscillations. Nonlinear plots were obtained for discharges with striations and for gas contaminated by a fraction of a micron of CO or CO_2. The linear probe characteristics lead to the conclusion that in the discharges with no oscillations, the electron velocity distribution followed the maxwell distribution law, at least to 10 or 11 volts from space potential. The report will include typical probe plots and electron temperature measurements illustrating the results described.

F2. Gas Temperatures and Elastic Losses in Low Pressure Mercury Argon Discharges. C. KENTY, M. A. EASLEY, AND B. T. BARNES, *General Electric Company, Nela Park.*—The increase ΔT in average gas temperature for ac and dc has been determined from measurements of the increase in pressure. A small McLeod gauge was used. Wall temperature was regulated. Corrections for end effects were made by comparing results for long and short tubes of 3.6 cm diameter. Assuming the radial variation of heat input to be parabolic, the temperature distribution was calculated using published values of heat conductivity K. From the results the heat input P_m per centimeter length was calculated. This value was compared with the elastic loss P_e computed from electron temperature T_e and number of electrons N_e per centimeter column, taking into account the variation of mean free path with electron velocity. The table indicates the good agreement obtained.

t_{Hg}	Amp	p_A mm	ΔT	T_e	$N_e \times 10^{-12}$	P_m	P_e
17°	0.42	3.5	42.7	15,000	2.5	$0.16W$	$0.19W$
60	0.42	3.5	15.8	9,800	2.65	0.061	0.064
42	0.20	3.5	13.1	11,900	1.15	0.047	0.047
42	0.60	3.5	27.1	10,800	3.3	0.107	0.104
42	0.42	1.7	10.0			0.037	
42	0.42	5.1	30.3			0.12	

F3. Characteristics of Moving Striations in a Mercury-Krypton Mixture. H. L. STEELE, JR., *Westinghouse Electric Corporation.*—This paper supplements that presented before the 1949 Conference on Gaseous Electronics. The discharge is photographed with a shutterless camera which moves the film at right angles to the discharge. At low currents and pressures, bright regions (striations) move from anode toward cathode at thousands of centimeters per second with a frequency of hundreds per second. The characteristic mercury color is maintained with or without striations. As the mercury pressure is increased the voltage per striation decreases to about 4 volts, and the distance between striations decreases to 5 centimeters before the positive column becomes homogeneous. The bright regions first disappear from the cathode end of the positive column. The striation spacing changes discontinuously so that an integral number of bright regions exist. This is explained by a synchronization of these striations with an oscillatory phenomenon at the anode, and near the cathode with high speed striations associated with the anode oscillations. When the discharge is pulsed the bright regions are created near the cathode, later ones at constant spacings toward the anode. If a second pulse is applied within 8 milliseconds, striations also carry-over from those in the first pulse. This is evidence of slow diffusion of ions.

F4. Moving Striations in H_2 and D_2 Glow Discharges.* T. M. DONAHUE, *The Johns Hopkins University.*—A study of glows in hydrogen by means of photomultiplier tubes connected to an oscillograph[1] has revealed that such "dc" discharges can exist in both oscillatory and non-oscillatory states. The oscillations found generally have a frequency of a few times 10^4 sec^{-1}. Two regimes for these discharges will be discussed. (1) Low pressure, low current (below 0.2 mm and 1.0 ma): The positive column appears homogeneous, but there exist in it moving striations. The most prominent of these travel toward the cathode at a speed higher than 5×10^7 cm/sec. The frequency of oscillation increases linearly with current and decreases with pressure. (2) Higher pressure and current: Stationary striations begin to appear in the column. Oscillations do not usually exist, but they may appear. Generally this occurs when there are a few standing striations at the head of a homogeneous column. In the homogeneous column, then, moving striations are found, all of which *move toward the anode.* The light intensity in the stationary striations also oscillates. When deuterium glows were studied under identical conditions, no essential differences were noted. Thus, the prominent oscillation parameters are independent of the positive ion mass.

* Work supported through an ONR contract under the direction of G. H. Dieke.
[1] T. Donahue and G. H. Dieke, Phys. Rev. 81, 248 (1951).

F5. Electrode Reactions in the Glow Discharge. F. E. HAWORTH, *Bell Telephone Laboratories.*—The reactions which occur at silver electrodes in a *normal* glow discharge in air have been determined. These are: (1) formation of $AgNO_3$ and some Ag_2O at the anode at the rate of 3.4 μg/coulomb; (2) loss of metal from the cathode by chemical action at the rate of 3.5 μg/coulomb (probably the same reaction as (1) with subsequent loss of the reaction products by the greater heating of the cathode, but this hypothesis has not been established); and (3) normal sputtering loss at the cathode at the rate of 0.4 μg/coulomb. These processes result in building

a conducting layer on the anode. If the electrode separation is so small that the anode extends into the region of the cathode fall, then the high electric field pulls the newly formed and not very coherent growth upon the anode across into a bridge between the electrodes.

F6. Dynamic Characteristics of Glow Discharges in the Rare Gases at Ultrasonic Frequencies.* W. D. PARKINSON, *The Johns Hopkins University.*—A systematic study has been made of the dynamic characteristics of rare gas glow discharges in the frequency range 10 to 300 kc. This region is approximately free from the influence of voltage and current fluctuations associated with moving striations, which play a dominant part at lower frequencies. The peak voltage is always well below the sparking voltage except at the lowest pressures. To a first approximation the glow discharge, especially in He, behaves as a linear resistance at these frequencies. In the heavier gases there is a tendency for the discharge to have a lower conductance while the voltage and current are increasing. During this phase of the cycle there is a brief period in which the current is higher than would be expected. This effect is slight in Ne and much more marked in A and Kr. This is interpreted as due to the low cross section for elastic collision of low energy electrons with rare gas atoms. This is supported by the fact that phototube observations of the positive column during this period show practically no light output in the case of A and Kr, indicating a lack of excitation in spite of the high current.

* This work was supported through an ONR contract under the direction of G. H. Dieke.

F7. Decimeter Oscillations in Mercury Plasmas, Experiments and Considerations.* L. BRENNAN, J. SALOOM, AND R. WELLINGER, *University of Illinois.*—A three-electrode oscillator, as described by G. Wehner,[1] has been investigated extensively. It is shown that this structure displays the same behavior as some gas diode oscillators enclosed in glass, thus establishing a close relation between the diode-type oscillators and the particular Wehner structure. A systematic set of data shows the variation of wavelength with each of the parameters involved in the oscillation. These experimental results disagree with the majority of the formulas published to date. The system oscillates in different modes, and as the cathode current is increased continuously, the frequency remains constant except for discrete jumps. Further, the transit time of the beam electrons between two electrodes is always an integer plus one-quarter times the period of oscillation. A theory similar to Wehner's, based on the model of the double gap klystron oscillator, should describe the oscillations satisfactorily. However, this model implies the questionable assumption that within each dark space there exists a layer with marked resonant properties.

* This work was supported by the Air Materiel Command, Dayton, Ohio.

[1] G. Wehner, J. Appl. Phys. 21, 62 (1950).

F9. Momentary Intensification of the Electron Beam Obtained from a High Voltage Cold-Cathode Discharge. JOHN H. PARK, *National Bureau of Standards.*—A method for obtaining a 10- to 50-fold momentary increase in the intensity of the electron beam obtained from a high voltage cold-cathode discharge tube has been developed. Its application for increasing the recording speed of a high voltage cathode-ray oscillograph is described. Oscillograms have been obtained in which the trace speed is about three-fourths the velocity of light. The intensification is caused by superposing a steeply rising voltage pulse on the normal steady voltage across the electrodes of the discharge tube serving as the electron beam source. The voltage pulse momentarily disrupts equilibrium conditions in the discharge and produces an intense discharge that lasts for about 2 microseconds. Measurements of the magnitude and duration of the superposed pulse and of the changes in discharge current have been made. A tentative explanation of the mechanism of intensification based on these measurements is given.

Author Index to Papers

Alpert, D., A. O. McCoubrey, and T. Holstein—No. B7
Biondi, Manfred A.—No. A3
Brennan, L., J. Saloom, and R. Wellinger—No. F7
Brown, Sanborn C.—No. C2
Clay, C. S. and J. G. Winans—No. C8
Donahue, Thomas M.—No. F4
Easley, M. A.—No. F1
Finkelnburg, W.—No. E8
Fundingsland, O. T.—No. C5
Germer, L. H.—No. D7
Gold, Louis—No. D8
Haworth, F. E.—No. F5
Holstein, T.—No. B4
Holt, R. B., John M. Richardson, and A. Redfield—No. A1
Hornbeck, John A.—No. B3
Jones, T. B. and B. H. List—No. E9
Jones, T. B. and Merrill Skolnick—No. E10
Kachickas, G. A. and L. H. Fisher—No. D1
Kenty, C., M. A. Easley, and B. T. Barnes—No. F2
Kerr, Donald E.—No. C6
Lee, Po and G. L. Weissler—No. D3
McCoubrey, A. O., D. Alpert, and T. Holstein—No. B6
Medicus, G. and G. Wehner—No. E4
Menes, M.—No. D5
Molnar, J. P. and John A. Hornbeck—No. B2
Park, John H.—No. F9
Parkinson, W. D.—No. F6
Phelps, Arthur V.—No. A4
Rose, David J.—No. C3
Smith, C. G.—No. E1
Steele, Howard—No. F3
Varnerin, Lawrence J.—No. C4
Wainfan, Nathan and G. L. Weissler—No. D2
Wannier, Gregory H.—No. B5
Wetzstein, Hanns J.—No. E5

MEETING OF THE DIVISION OF ELECTRON PHYSICS AT THE COLLEGE OF THE CITY OF NEW YORK ON JANUARY 30–31, 1951

(Joint Meeting with the Panel on Electron Tubes of the Research and Development Board)

Invited Papers

Energy Levels in BaO, J. A. KRUMHANSL, *Cornell University*

Cathode Interface Effects in Oxide-Coated Cathode Tubes, L. S. NERGAARD, *RCA Laboratories*

Ejection of Electrons from a Metal by Positive Ion Impact, H. D. HAGSTRUM, *Bell Telephone Laboratories*

Production and Measurement of Ultra High Vacua, DANIEL ALPERT, *Westinghouse Research Laboratory*

Life of Secondary Electron Emitters at High Current Densities, D. A. JENNY, *RCA Laboratories*

Application of Electron Counting to Emission Problems, A. S. EISENSTEIN, *University of Missouri*

Contributed Papers

EP1. Pulse Emission and Life Test Data on *L* Cathode. J. BABAKIAN, *Air Force Cambridge Research Laboratories* (Introduced by A. LEDERMAN).—Philips results on dc emission were verified using high vacuum diodes. Activation phenomena was observed and compared with oxide-coated cathodes. Peak emission measurements at 1050°C to 1200°C brightness gave from 30 to 80 amp/cm². These tests involving four tubes were conducted at pulse lengths from ½ to 3 μsec, and voltage from 1200 to 2500. Low duty cycle tests were made at pulse lengths up to 80 μsec. Normal and high duty cycle tests (0.001–0.01) were made at 40 μsec. Under none of these conditions was there any droop in the pulse shape such as occurs with oxide-coated cathodes. The life test was set up at 2250 volts 500 pps 1-μsec pulse length with the cathode at 1100°C brightness. Under these conditions the peak emission was 40 to 50 amp/cm². One tube has been on life test for 400 hours. Another tube has 200 hours on life at 2200 volts, 2.2-μsec pulse length, 1250 pps and 46 peak amperes. A fair amount of barium evaporation was noticeable in the 400-hour tube. It was considered tolerable for possible use in switch tubes. Under prolonged sparking induced by long pulse lengths (50 μsec) and high voltage (2800 volts), the peak emission recovered rapidly and remained unimpaired.

EP2. Concerning the Mechanism of Operation of the "*L*-Cathode." F. K. DU PRÉ AND E. S. RITTNER, *Philips Laboratories.*—Emission is considered to come from the tungsten, the work function of which is lowered by a surface double layer of barium on oxygen. The unactivated cathode is believed to have a chemisorbed layer of oxygen on the tungsten and the activation process supplies the required barium to the external surface via the following steps: (a) chemical reduction of BaO by W, yielding Ba vapor of low partial pressure at the bottom of the porous tungsten plug, (b) transport of barium through the plug by means of Knudsen flow through the pores and by means of surface diffusion over the pore walls, (c) diffusion over the external emitting surface. Barium is slowly lost from the cathode by evaporation from this surface and by pore flow. Termination of life appears to be associated with the exhaustion of the barium supply.

EP3. Thermionic Properties of Uncoated and Thoria-Coated Rhodium and Iridium Cathodes. O. A. WEINREICH, *Bartol Research Foundation.*—Richardson plots of rhodium and iridium, cleaned by prolonged heating in high vacuum, were made in temperature ranges from 1550°K to 1950°K for Rh and from 1700°K to 2200°K for Ir. The A constant for Rh was ~100 amp/cm² deg², and $\varphi = 4.9$ ev. Previously published values are $A = 33$ amp/cm² deg², $\varphi = 4.8$ ev. For iridium the measured constants were $A \cong 100$ amp/cm² deg², and $\varphi = 5.3$ ev. A search in the literature yielded no published values of the thermionic constants for Ir. Cleaned rhodium and iridium filaments were coated with purified thoria and the electron emission measured in vacuum and in oxygen at different pressures. At an O_2 equilibrium pressure of 10^{-3} mm Hg, thoria on iridium yielded $A = 6 \times 10^7$ amp/cm² deg², and $\varphi = 6.2$e v. It is believed that these data represent a state in which all thorium donors are destroyed. Thoria-coated iridium cathodes can be used in ionization gauges. They are not damaged when exposed hot to open air, and continuous pressure readings in O_2 up to 10^{-2} mm Hg are possible.

EP4. Dc and Pulse Emission of Several Rare Earth Oxides. E. N. WYLER AND F. C. TODD, *Battelle Memorial Institute.*—Techniques and equipment have been developed and employed for reproducible determinations of the dc and pulse emission constants for oxides. A platinum-coated and water-cooled anode is employed to minimize contamination of the emitting surface by metal from the anode. The anode surface was thoroughly cleaned prior to insertion of each new cathode. The heater for the oxides is a sintered, conducting sleeve of 18 to 20 percent powdered molybdenum and 82 to 80 percent of powdered thoria. The oxide for investigation is coated on this sleeve in a layer of two to four mils thickness. For comparison with published measurements, the emission current and voltage at saturation are employed for evaluation of the constants. The techniques and equipment were checked by measuring the dc and pulse emission constants of thoria, and values were found which agree well with those of Wright.* After checks on the reproducibility, measurements were made and will be given for lanthanum oxide and for the following oxides in the *4f* series of rare earths: cerium, praseodymium, neodymium, samarium, europium, gadolinium, dyprosium, and ytterbium.

* D. A. Wright, Nature **160**, 129 (1947). Project for Evans Signal Laboratory and Wright-Patterson Air Force Base.

EP5. Boride Cathodes. J. M. LAFFERTY, *General Electric Company.*—The thermionic emission properties of the borides of the alkaline-earth and rare-earth metals and thorium have been investigated. These compounds all have the same formula MB_6 and the same crystal structure, consisting of a

three-dimensional boron framework in whose interlattice spaces the metal atoms are embedded. The valence electrons of the metal atoms are not accepted by the B_6 complex, thus giving rise to the presence of free electrons, which impart a metallic character to these compounds. This, together with the strong bonds between the boron atoms in the framework, produces a series of compounds which have high electrical conductivities and high thermal and chemical stabilities—ideal properties for a cathode material. When this structure is heated to sufficiently high temperature, the metal atoms at the surface evaporate away. They are, however, immediately replaced by diffusion of metal atoms from the underlying cells. The boron framework does not evaporate but remains intact. This process gives a mechanism for constantly maintaining an active cathode surface. Thermionic emission measurements made on these materials show the rare-earth metal borides to be superior to the others. The highest emission was obtained from lanthanum boride. Its emission constants for the Dushman equation were $\Phi = 2.66$ v and $A = 29$ amp/cm²/deg K².

EP6. The Adsorption of Sr Metal on Tungsten. H. W. ALLISON, AND GEORGE E. MOORE, *Bell Telephone Laboratories.*—Monatomic films of Sr metal were deposited on clean tungsten ribbons by producing the Sr in a controlled chemical reaction between SrO and tungsten in an adjacent filament. X-ray tests have shown that the (100) crystal face is predominantly exposed on the flat surface of these rolled ribbons. By combining radioactive tracer and thermionic techniques, the amount of Sr in a monolayer was measured directly. The amount found, 0.073 ± 0.010 microgram cm^{-2} agrees with the value predicted for a (100) tungsten surface (lattice spacing $= 3.15$A) populated on alternate lattice sites with Sr atoms. This determination, along with thermionic measurements of the work function of the monolayer, indicated an effective dipole moment per adsorbed Sr atom in a monolayer of 1.22×10^{-18} esu. From the relative average rates of evaporation at different temperatures the use of the Clapeyron equation indicates an approximate heat of adsorption of 86,000 cal/mole or 3.74 ev/atom for coverage between 1 layer and 0.5 layer. The heat of adsorption increases as the surface density of Sr decreases.

EP7. Conductivity and Hall Effect in Barium Oxide Films. D. A. WRIGHT, *M. O. Valve Company at the G.E.C. Research Laboratories, Wembley, England.*—Measurements have been made of the conductivity and Hall effect in BaO films of thickness about 10^{-5} mm, formed by evaporating barium onto a magnesia base, and heating in 5×10^{-5} mm oxygen at 500°C. The conductivity σ in vacuum was 10^{-4} ohm^{-1} cm^{-1} at 1000°K; the Hall coefficient was 10^{5} cm³/coulomb. The plot of $\log\sigma$ against $1/T$ was linear from 600 to 1100°K, with slope 2 to 2.5 ev. After evaporating Ba onto the oxide, heating to 750 to 800°K established a state with $\sigma = 2.5 \times 10^{-3}$ at 800°K, and slopes of 0.2 ev below 800°K, and 0.7 ev above 800°K. The low slope conductivity is attributable to residual surface Ba. It was destroyed at 850 to 900°K; here σ fell slightly, and on cooling, the slope was 0.7 ev down to 530°K. The Hall coefficient was 2.5×10^{4} cm³/coulomb at 800°K, indicating 3×10^{14} electrons/cm³, which denotes a donor concentration near 10^{18} centers/cm³. The mobility was 65 cm²/volt-sec, and the free path 1.5×10^{-4} cm. Raising the temperature above 950°K caused a gradual loss of donor centers, σ falling to its initial value 10^{-4} at 1000°K, with the high slope. The whole cycle was repeated many times, with good reproducibility. The results are considered free from confusion by emission processes.

EP8. Diffusion of Barium in Barium Oxide. R. W. REDINGTON, *Cornell University.*—The diffusion of barium in barium oxide was measured to provide the information necessary to determine the role of barium in conductivity and activation in barium oxide. Barium 140, a radioactive isotope, in the form of barium oxide was evaporated onto the surface of a crystal of barium oxide. The distribution of radioactive barium in the crystal after heat treatment was determined by sectioning the crystal with a microtome. In the temperature range from 1350° to 1500°K and in quenched crystals, two diffusion mechanisms were present, one of which transported charge. In this temperature range from 1350° to 1500°K, the diffusion constant for the neutral process was about 20 times the diffusion constant for the charge transporting process, and varied from 10^{-11} to more than 10^{-8} cm²/sec. In the temperature range from 600° to 1300°K, in annealed crystals only the neutral process was detected, and this diffusion constant varied from 10^{-13} to 10^{-11} cm²/sec. In quenched crystals, the charge transporting process also appeared, with a similar temperature dependence. In these quenched crystals, the magnitudes of both diffusion constants depended on the temperature from which the crystal had been quenched.

EP9. Diffusion of Magnesium Through Nickel. G. F. ROUSE AND R. FORMAN, *National Bureau of Standards.*—By means of an evaporation apparatus, operating under very good vacuum conditions, a magnesium nickel system is formed consisting of a thin layer of magnesium sandwiched between a relatively thick sheet of pure electrolytic nickel and a much thinner layer of the same nickel. When this system is held at a temperature above the melting point of magnesium, the magnesium diffuses through the thin nickel layer and evaporates from its surface. Thus, a zero magnesium concentration is maintained at the surface. This behavior, together with the known initial concentration distribution of magnesium, makes it possible to describe the process mathematically with the diffusion constant as a parameter. The fractional amount of magnesium evaporated and the corresponding time appear in the equation and are measurable quantities. Properly distributed experimental values of these latter quantities make it possible to establish a value for the diffusion constant. Preliminary data indicate that the diffusion constant for a temperature of 720°C is greater than 10^{-9} cm²/sec. Steps to acquire sufficient data to fix the value of the constant more exactly are underway.

EP10. Initial Emission and Life of a Planar-Type Diode as Related to the Effective Reducing Agent Content of the Cathode Nickel. H. E. KERN AND R. T. LYNCH, *Bell Telephone Laboratories* (Introduced by J. A. BURTON).—A description of the Bell Laboratories planar-type diode will be given, as well as a brief outline of the method of determining cathode emission and the conditions of life testing the diode. A method will be described for calculating the effective reducing agent content of a cathode nickel based on the following factors: 1. The chemical composition of the nickel. 2. The equations of the chemical reactions between the reducing agents in the nickel and the oxide coating. 3. The thickness of the nickel directly beneath the oxide coating. A correlation will be shown to exist between this effective reducing agent figure and both initial cathode emission and tube life. In general, as the effective reducing agent content of the nickel is increased the initial emission also increases, but not without limit. Increase of the reducing agent content above a certain level causes no further increase in initial emission. The relationship between tube life and effective reducing agent content indicates that a maximum tube life is obtained over a very narrow range of effective reducing agent values and that this maximum is apparently limited to a region in which the effective reducing agent content is approximately chemically equivalent to the total oxide coating content.

EP11. Thermionic Emission from Zirconium with Gases in Solution. ARTHUR WAHL, *Princeton University** (Intro-

duced by G. E. MOORE).—In 1945, Rentschler and Henry reported† that the gases oxygen, nitrogen, and hydrogen in solution in the element zirconium caused its photoelectric threshold to shift toward the longer wavelengths. Thermionic investigation of these phenomena showed that nitrogen has no significant effect, but oxygen, in solution in quantities of from ten to twenty atom percent, approximately doubles the magnitude of the emission at the high filament temperatures and increases the emission by ten times or more at lower temperatures. This increase in emission is not destroyed by positive ion bombardment. Pure zirconium with no gas in solution and cleaned by standard procedures before and during tube evacuation was found to have a work function of 4.21 volts and an A coefficient of 1260. After this, zirconium was also cleaned by bombardment of positive ions of an inert gas such as argon, the work function became 3.78 volts and the A coefficient 120. Zirconium with about 17 atom percent of oxygen and cleaned by standard procedures plus bombardment showed a thermionic work function of 3.57 volts and an A coefficient of 40. Emission efficiencies at practical operating temperatures are quite low.

* Now with Bell Telephone Laboratories.
† J. Electrochem. Soc. **87**, 289–298 (1945).

EP12. Electron Emission from Alkaline-Earth Metals. C. H. KILLIAN, *Brooklyn, New York.*—Ives and Stillwell (J. Opt. Soc. Am. **28**, 223 (1938)) reported that high speed hydrogen canal rays showed displacements, for certain accelerating voltages, which were not in accord with the usual theory. These discordances were attributed to perturbation shifts by spectral lines of molecular hydrogen. Irregularities in the progression of the spectral lines of recognized chief series of mercury, copper, aluminum, the alkali metals, and the alkaline-earth metals are known; and these irregularities are commonly explained, by modern theories, as mutual perturbations by terms of closely related spectral series. The most marked irregularities appear in the spectra of the alkaline-earth metals, aluminum, and copper. These are the metals used extensively in rectifiers, electrolytic condensers, and oxide cathodes. The mentioned perturbations are commonly explained as a sort of resonance phenomenon and are an indication of the storing of energy which can be released by the phenomenon of "auto-ionization" (Wentzel and Shenstone, Phys. Rev. **38**, 873 (1931)), or by radiation. This view of energy storage and emission appears to be experimentally confirmed by Stillwell and Ives, and hence is a valuable viewpoint for explaining the copious emission of electrons by the alkaline-earth oxide cathode, and perhaps also for explaining rectification.

EP13. High Voltage Breakdown due to Field Emission Processes.* DANIEL H. GOODMAN AND DAVID H. SLOAN, *University of California* (Introduced by L. C. MARSHALL).—The fields at which breakdown occurs between coplanar cold metal surfaces in vacua have been studied. The experiments were performed with a 200-ohm, 200-kilovolt, 1-microsecond pulse line, and with copper, aluminum, molybdenum, nickel, and stainless steel electrodes. The results indicate that field-emitted electrons are the initiating factor in breakdown and that the field required for breakdown is proportional to the square root of the resistivity of the metal. A considerable mass of metal was transferred from the anode to the cathode. It is proposed that breakdown is dependent on the occurrence of four distinct processes: (1) emission of pure field electrons from the cathode; (2) production of ions from gas atoms or anode surface film due to bombardment by high velocity electrons; (3) further extraction of electrons from the cathode by (a) production of many secondary electrons by ion bombardment, (b) atomically close approach of an ion to the cathode, (c) fields about atoms which are splashed out of the cathode and are intermittently ionized and neutralized without traveling far; (4) liberation of atoms by tremendous currents that heat the anode, which may be ionized as they leave the anode surface, leading to breakdown into a metallic arc.

* This work was supported by the Air Materiel Command, U. S. Air Force, Contract No. W-33-038 ac-16649.

EP14. Field Electron Emission from Sodium Chloride. R. T. K. MURRAY AND ALEXANDER MACKENZIE, *Long Island University.*—The field electron emission from dielectrics previously reported* has been extended to single crystal sodium chloride. The cathode consisting of a 3.5-mm plane parallel plate of sodium chloride ground and polished in the (1, 0, 0) plane was supported from above by a brass plate and placed over the aperture of a counter. For a given gap distance linear log current against reciprocal potential characteristics were obtained for currents up to 100 electrons per second. From the experimental current-potential curves from the same emitting surface taken at different gap distances identical values of the field for the same current could be obtained only if calculated from an expression that allows for a steady-state negative surface charge less than the equilibrium polarization one. This decrease in the negative surface charge has the effect of increasing the field in the dielectric and decreasing the field at the surface in order that in the steady state the conduction current will equal the emission current. Assigning values for the parameters of sodium chloride in Poole's law and the Fowler-Nordheim equation, a connection between the dielectric and surface fields is obtained.

* R. T. K. Murray and A. Mackenzie, Phys. Rev. **78**, 350 (1950).

EP15. High Density Field Emission from Single Tungsten Crystals.* W. P. DYKE AND J. K. TROLAN, *Linfield College.*—Field emission of large current densities from single tungsten crystals has been studied, using pulse techniques. Observed current densities agree within an order of magnitude with values predicted by the image force corrected theory of Fowler and Nordheim, up to a current density of 10^8 amp/cm^2 and an electric field of 10^8 v/cm. The vacuum arc occurs at a slightly higher value of the electric field under the conditions which follow. Field currents of 0.1 amp, with potentials up to 17 kv at pulse lengths of a few microseconds, have been drawn from electrolytically etched emitters whose surface approximated a hemisphere of radius of the order of 10^{-5} cm. Emitters were pulsed in a Müller projection tube; emission patterns for each pulse were recorded photographically. Current density, electric field, and emitting area were calculated with the help of emitter geometry obtained from its shadow cast in a conventional electron microscope. The work function was taken as the accepted value for clean tungsten. The variation of the current density across the emitting area was obtained by photometric methods. Emission patterns from clean tungsten at high current densities are similar to patterns observed previously at low densities.

* Sponsored by the ONR and by Research Corporation.

EP16. Migration of W Atoms on the Surface of a W Single Crystal as a Function of Temperature and Electric Field Strength. J. A. BECKER, *Bell Telephone Laboratories.*—A field-emission electron microscope is used to observe the density of field-emission electrons from an approximately hemispherical surface of a W single crystal at the end of a W point.* If the point is flashed at 2400°K, a reproducible pattern is observed. This pattern shows that 15 percent of the surface consists of (110), (211), and (100) planes. Glowing below 1000°K produces no changes. At 1000°K the pattern changes slowly: (211) planes enlarge and (111) zones form step structures. At 1200°K changes occur more rapidly and

(100) planes enlarge; when a steady state prevails the areas of (211) and (100) planes are four times as large as originally. At still higher temperatures the rates are higher. When electric fields of 45 million volts/cm are applied while the point is at 1000°K, changes occur more rapidly and are more pronounced than without the field. At 1400°K and 41 million volts/cm, pronounced changes occur in 1 minute; in 20 minutes, (211) planes grow until they meet (110) planes. Subsequent glowing at 1000°K or higher with zero field decreases the area of (211) and (110) planes.

* Mueller, Z. Physik **126**, 642–665 (1949).

EP17. High Speed Ten-Volt Effect. R. M. MATHESON AND L. S. NERGAARD, *RCA Laboratories.*—In 1935, H. Nelson* observed that tubes with oxide-coated cathodes operating under space-charge limited conditions show a small deviation from the Child-Langmuir law for anode voltages exceeding ten volts. Recent measurements confirm his observations. The effect is stable and is independent of frequency for all frequencies for which the electron transit time may be neglected. Measurements made on triodes, rotating anode diodes, and diodes with cathode probes indicate that the effect is not caused directly by the cathode. Observations on diodes in which the anode temperature could be varied associate the effect with the anode. It is shown that an increase of space charge by secondary and reflected electrons from the anode can account for the deviation. The required secondary emission ratios are in substantial agreement with those reported for BaO.

* H. Nelson, unpublished research.

EP18. Origin of Bombardment-Enhanced Thermionic Current. J. B. JOHNSON, *Bell Telephone Laboratories.*—Cathodes of (BaSr)O, bombarded by electrons, emit three categories of electron current: thermionic electrons, secondary electrons, and a component that on a microsecond scale rises during and persists after the bombardment.* The last has been considered of thermionic origin and called bombardment-enhanced thermionic emission. Measurements now show the initial energies of the enhanced component resemble those of the thermionic current, not the much higher ones of secondary electrons, adding proof of the thermionic origin. Calculations support the view that this current arises from increased concentration of free electrons in the emitter. Reasonable assumptions are made that primary electrons create an electron-hole pair for each 10 ev of their initial energy with mobility of the carriers $\mu=1$ cm²/volt sec. Experimental evidence points to lifetime of the carriers of the order $\tau=10$ μsec. Neglecting surface recombination, the density of holes and electrons within the diffusion distance from the surface should, on this simple basis, rise during the pulse by a calculable amount. This exceeds by a factor of the order 10 the amount obtained from the observed enhancement and reasonable estimates of the original density. The assumed mechanism could therefore account amply for the enhancement.

* J. B. Johnson, Phys. Rev. **73**, 1058 (1948).

EP19. Extension of Wooldridge's Theory of Secondary Emission.* A. VAN DER ZIEL, *University of Minnesota.*—Wooldridge's[1] formula (32) for the rate of increase of the number of secondary electrons with time can be rewritten as

$$\frac{1}{\Omega}\frac{dN_\rho}{dt}=4\pi\epsilon^4\rho_1(k)J_\rho\frac{|b_\rho(k)|^2(2R_0/K)\rho}{|E(k')-E(k)|^2}.$$

This formula is more general than Wooldridge's, for it can be shown that it also holds for insulators. The formula may be applied to the calculation of the most probable energy loss of the primary electrons in the collision process. The result fits closely with *Ruthemann's*[2] and *Lang's*[3] experimental data, but differs considerably from Wooldridge's average energy loss E_0.

* Work being supported by the United States Signal Corps.
[1] D. E. Wooldridge, Phys. Rev. **56**, 562 (1939).
[2] G. Ruthemann, Ann. Physik Leipzig. 6th Series **2**, 113 (1948).
[3] W. Lang, Optik **3**, 233 (1948).

EP20. Optical Interference Effects in the Photoelectric Emission from *F*-Centers in RbBr. E. TAFT AND L. APKER, *General Electric Research Laboratory.*—Photoelectric emission from *F*-centers in RbBr was measured by methods previously used on KI.* (RbBr is of interest because it is transparent throughout the easily accessible ultraviolet.) When salt films of sufficient uniformity were deposited on metal mirrors, optical interference produced pronounced fluctuations in the frequency variation of the photoelectric yield. In a typical case, a film ~4000A thick exhibited four maxima between $\lambda=4500$ and $\lambda=2300$A. The yields at these points were four times higher than at the intermediate minima. The phase shift on reflection at the metal surface appeared to be ~170° instead of 180°. The data indicate that the photoelectrons originate within 10^{-6} cm of the surface or less, a result consistent with Hebb's calculations.† Electron bombardment appears to roughen the films, as noticed previously by I. Estermann. The possibility of these interference effects must be recognized in the interpretation of photoelectric data on transparent materials.

* L. Apker and E. Taft, Phys. Rev. **79**, 964 (1950).
† Malcolm H. Hebb, Phys. Rev. **81**, 321 (1951).

EP21. The Enhanced Photoelectric Emission Effect in Barium Oxide Cathodes. B. D. MCNARY, *University of Missouri.*—An enhanced activation of BaO cathodes for photoelectric emission has been accomplished by prolonged irradiation with wavelengths from 2537 to 7000A. The photoelectric response is increased for all wavelengths with the greater increase in response in the long wavelength region. Increases in yield of a thousandfold have been produced. This increase in response decays with time and is temperature dependent. The rate of decay also depends upon the wavelength used in studying the decay, the rate being higher for the longer wavelengths at which the greater enhancement was produced. No simple first- or second-order reaction law has been found to fit the complete decay curves, but the assumption that the initial decay depends on a Boltzman factor yields an activation energy of about 1 ev.

EP22. Photoconductivity of Composite Photoemissive Surfaces. S. PAKSWER AND W. O. REED, *Rauland Corporation.*—It is still questionable whether photoelectrons in composite photoemissive surfaces are emitted from alkali metal atoms adsorbed on the surface, whether they are formed in the top layers of the sensitized coating, or whether they are produced as a volume effect inside the coating. To contribute to the problem of the mechanism of photoemission, measurements of photoconductivity in semitransparent cathodes with Ag–Cs_xO–Cs, Sb–Cs and caesiated Pb–O–S layers were attempted. It was observed that most of the current between the conductivity strips was due to "skimming" electrons, and this current was reduced in our experiments by the introduction of ½ atmos of He. The spectral distribution of the remaining very small conduction current shows a shift to longer wavelengths in the case of Sb–Cs coating as compared to remaining photoemissive current. Nonphotoemissive Pb–O–S cells having infrared photoconductivity lose photoconductivity and acquire photoemissivity to short wave radiation. Some effects suggesting quenching by short wave radiation were observed on Ag–Cs_xO–Cs cathodes.

Supplementary Program

EPS1. Interface Potentials and Ion Migration. C. H. KILLIAN, *Brooklyn, New York.*—The observed forms of diode characteristics can be very closely represented either by *titration* types of curves or by *interface potential* types of curves. The latter are preferred because of the establishment of an orthosilicate interface between the oxide coating and the cathode sleeve. Application of the reasoning of R. W. Gurney (Proc. Roy. Soc. (London) **A136**, 378 (1932)) leads to the following equation for the interface potential:

$$\frac{eV}{kT}=\frac{U_e-U_e'}{kT}+\log\left\{C_e\beta_e+C_{Ba}\beta_{Ba}\exp\left[\frac{U_{Ba}-U_{Ba}'-U_e+U_e'}{kT}\right]+C_{Si}\beta_{Si}\exp\left[\frac{U_{Si}-U_{Si}'-U_e+U_e'}{kT}\right]+C_{Sr}\beta_{Sr}\exp\left[\frac{U_{Sr}-U_{Sr}'-U_e+U_e'}{kT}\right]+\cdots\right\},$$

where U' is the lowest energy level of the ion identified by an appropriate subscript at the interface, C is the ionic concentration of the ion identified by the subscript, U is the energy level of the ion identified by the subscript, β is the ratio of the probabilities of an ion emission to an ion deposition, and all other symbols have their usual significance. (Ba = barium, Si = silicon, Sr = strontium.)

MINUTES OF THE 1951 SPRING MEETING OF THE OHIO SECTION OF THE AMERICAN PHYSICAL SOCIETY AT MIAMI UNIVERSITY, OXFORD, OHIO, APRIL 6–7, 1951

THE regular spring meeting of the Ohio Section of the American Physical Society was held jointly with the Ohio Academy of Science at Miami University, Oxford, Ohio, on April 6–7, 1951. The attendance was very good. There were fifty in the room at the beginning and thirty-five when the final paper was finished.

The officers chosen for the year 1951–1952 are as follows: Chairman, Dr. Forrest G. Tucker, Oberlin College; Vice-chairman, Dr. John E. Edwards, Ohio University, Athens, Ohio; Secretary-Treasurer, Leon E. Smith, Denison University, Granville, Ohio.

The programme follows:

Friday, April 6th: Contributed papers, "The formation of meteor craters," Lloyd Wylie, Wittenberg College; "Probes in an oscillating glow discharge," Albert B. Stewart, Antioch College; "Experimental study of sliding friction," Charles A. Maney, Defiance College. SYMPOSIUM—Physical Methods in Qualitative and Quantitative Analysis: A. Emission Spectroscopy, E. R. Vance, Timken Roller Bearing Company, Canton, Ohio; B. Absorption Spectroscopy, D. L. Timma, Mound Laboratory, Monsanto Chemical Company, Miamisburg, Ohio; C. Infrared Analysis, Robert Oetjen, The Ohio State University; D. Nonradioactive Isotopes-Mass Spectrometer, D. R. Lawler, The B. F. Goodrich Research Center, Brecksville, Ohio; E. Radioactive Isotopes—Tracer Techniques, George D. Calkins, Battelle Memorial Institute, Columbus, Ohio; F. X-Ray Applications, Charles H. Shaw, The Ohio State University.

Saturday, April 7th: SYMPOSIUM—The Undergraduate Physics Curriculum: A. In the Liberal Arts College, Thomas D. Phillips, Marietta College; B. In the Engineering College, Dudley Williams, The Ohio State University; C. From the Point of View of Industry, Mound Laboratory, The Monsanto Chemical Company, Miamisburg, Ohio; D. As a Preparation for Graduate Study, R. L. Edwards, Miami University, Oxford, Ohio. The contributed papers were: "A jet propulsion apparatus," James Dueker, Wittenberg College; "A laboratory current balance," Albert Paschkis and Albert Stewart, Antioch College; "The effect of small diameter tubes in loudspeaker damping," V. B. Yeich, Wittenberg College; "Recurrent misunderstandings of Einstein's General Theory," Frank Estabrook, Miami University; "The contributions of physics in a liberal arts curriculum," Harold Loudin, Kent State University, Kent, Ohio; "Engineering aspects of sound," Andrew Weber, University of Dayton; "An advanced undergraduate laboratory experiment on coupled oscillators," Franklin Miller, Kenyon College, Gambier, Ohio.

LEON E. SMITH, *Secretary*
Ohio Section
American Physical Society
Denison University
Granville, Ohio

THE AMERICAN INSTITUTE OF PHYSICS

INCORPORATED

57 East 55 Street, New York 22, N.Y.

MEMBER SOCIETIES

American Physical Society
[illegible], Secretary, College of the City of New York 31, New York

Optical Society of America
[illegible], Secretary, Massachusetts Institute of Technology, Cambridge, Massachusetts

American Association of Physics Teachers
[illegible], Secretary, Hofstra College, Hempstead, New York

Society of Rheology
[illegible], Secretary, North American Rayon Corporation, Inc., P. O. Box [illegible], Elizabeth

American Association of Physicists in Medicine
[illegible], Secretary, University of Illinois, Urbana, Illinois

AFFILIATE SOCIETIES

American Crystallographic Association
Electrochemical Society of America
Physical Society of Pittsburgh
Physics Club of Chicago
Physics Club of Philadelphia
Chemical Physics Society
Physical Society of the District of Columbia

ASSOCIATES

Over [illegible] industrial [illegible] other institutions which [illegible] the support of Physics

JOURNALS

The Physical Review
S. [illegible], Editor, Brookhaven National Laboratory, Upton, Long Island, New York

Reviews of Modern Physics
[illegible], Editor, University of Minnesota, Minneapolis, Minnesota

Journal of the Optical Society of America
[illegible], Editor, National Bureau of Standards, Washington 25, D. C.

The Review of Scientific Instruments
[illegible], Editor, 57 East 55 Street, New York 22, New York

American Journal of Physics
[illegible], Editor, Middlesex County College, East Lansing, Michigan

The Physics of Fluids
[illegible], Editor, Graduate Laboratory of Physics, University of Pennsylvania, Philadelphia, Pennsylvania

The Journal of Chemical Physics
[illegible], Editor, Institute for Nuclear Studies, University of Chicago, Chicago 37, Illinois

Journal of Rheology
[illegible], Editor, Columbia University, Department of Chemistry, Chemical Engineering and Metallurgy, New York 27, New York

Physics Today
[illegible], Editorial Director, R. DAVIS, Physics Department, American Institute of Physics, 57 East 55 Street, New York 22, New York

OFFICERS

George B. [illegible], Chairman
Massachusetts Institute of Technology

George B. [illegible], Treasurer
Columbia University

GOVERNING BOARD

J. W. [illegible]
C. P. [illegible]
Walter [illegible]
W. H. [illegible]
S. A. [illegible]
G. P. [illegible]
[illegible]
F. V. [illegible]
Ruben [illegible]
Paul [illegible]
F. W. [illegible]
R. C. [illegible]
[illegible]
L. E. [illegible]
Detlev [illegible]
Harold [illegible]
Percy [illegible]
Frank [illegible]
John [illegible]
[illegible]
[illegible]

ADMINISTRATIVE STAFF

Henry A. [illegible], Director
Walter [illegible]
[illegible]
Thomas [illegible]
Administrative Assistant and Assistant Secretary
Ruth [illegible]
Public [illegible]
Betty [illegible]
Assistant Secretary
Ellen [illegible]
Circulation Manager
Katherine [illegible]
Assistant

THE American Institute of Physics was established in 1931 as a federation of leading societies in the field of physics. It combines into one operating agency those functions of common interest to all of physics which can best be administered by the Societies jointly. Its purpose is the advancement and diffusion of physics and its application to human welfare. To this end it publishes for itself and other societies the principal journals in physics, promotes relations and interchange of effort among physicists who are interested in physics in numerous fields, provides certain common services for physicists and to the public, and maintains with governmental and other national associations, with institutions, technical societies, and others in such manner as to further the opportunities and the responsibilities of physics as an important and constructive human activity